SLIDING MODE CONTROL
OF
POWER CONVERTERS

Thesis by
Ramanarayanan. Venkataramanan

in Partial Fulfillment of the Requirements
for the Degree of
Doctor of Philosophy

California Institute of Technology
Pasadena, California

1986
(submitted May 6, 1986)

ACKNOWLEDGEMENTS

I thank my advisors, Professors S. M. Ćuk and R. D. Middlebrook for providing me with an opportunity to work in the field of Power Electronics. I am grateful for their generous support, guidance, and constructive engagement during the course of my stay at Caltech.

I am grateful to Professor A. Sabanović of Energoinvest of Yugoslavia, Visiting Professor of Electrical Engineering at Caltech 1983-85. He exposed the exciting field of sliding mode control to me, and offered me constant support and encouragement.

I thank Caltech for the various Graduate Fellowship, Teaching Assistantships, and Research Assistantships that made my stay at Caltech possible.

I owe a great deal to my colleagues at the Power Electronics Group at Caltech for the many enlightening interactions, which made my work possible and pleasant. My particular thanks are due to R. Mahadevan, and Z. Zhang, who developed the software for the graphics used in this thesis.

ABSTRACT

Switched mode power converters are being used extensively for the purpose of efficient power conversion. Such converters are nonlinear, time variant systems. In the past such converters were being modelled using the state space averaging method. The theory of variable structure systems (VSS), and sliding mode control form a mutually complementary analysis and design tools for the control of switched mode power converters. The application of sliding mode control is presented for dc-to-dc converters and electrical motor drives in this thesis. The concept of sliding mode control is brought out through exhaustive examples of second order systems. The equivalent control, an analysis method of VSS, is applied to obtain transfer function description of dc-to-dc power converters. The sliding mode control is applied to the control problem of dc-to-dc power converters and speed controlled electrical drives to develop practical design techniques. The practical design methods are confirmed through experimental results.

TABLE OF CONTENTS

CHAPTER 1

INTRODUCTION

This thesis deals with the principles of sliding mode control and their application to power converters. The power converters that are taken up for the application are dc-to-dc electrical power converters, and electromechanical power converters.

In power converters a high premium is placed on the efficiency of power conversion, besides the steady state and dynamic performance requirements. As a result the topologies used in power conversion applications rely on high speed switches for efficient operation. Chapter 2 contrasts the power conversion topologies with signal processing systems, and brings out the most important feature of power converters, namely dynamic structural changes brought about because of their switching nature. Such systems are nonlinear and time variant. The switching property makes the power converters prime candidates for the application of the theory of Variable Structure Systems (VSS).

VSS theory results in a time domain description of switching converters. Sliding mode control complements VSS as an effective analysis and design tool. The concept of sliding mode control relies on a firm understanding of the system in terms of system states and the state space or the phase space. In order to appreciate

thoroughly the basic principles involved, Chapter 3 treats simple second order systems exhaustively, and brings out the relevant features of sliding mode control. These concepts are then extended to general higher order systems.

In the past the switching converters had been analyzed using the technique of state space averaging. State space averaging method essentially developed linear, small signal, frequency domain models of the nonlinear power converters. Chapter 4 briefly reviews the state space averaging method. The power converters are then analyzed using the theory of VSS. The sliding mode control principles are then applied to develop practical design criteria for the control of dc-to-dc converters. Experimental results are then presented.

Another major area of power processing application is the electromechanical power conversion. Such systems consist of switching power converter and electromechanical actuators (dc or ac motor). In the past such systems have been analyzed separately – a model for the power converter and a model for the motor. Sliding mode control can be used as an integrated control approach for such composite systems. Chapter 5 reviews the general theory of electrical machines. It is seen that all electrical machines can be described as qualitatively identical systems. Chapter 6 goes on to apply the sliding mode control to two representative machines, namely the dc motor and the permanent magnet synchronous motor. Practical design criteria for the speed control of these machines are developed. Experimental results verifying the design strategy are presented.

Chapter 7 discusses the extension of the sliding mode control to synchronous motors. The possibility of loss optimization under different operating conditions is then presented.

CHAPTER 2

VARIABLE STRUCTURE SYSTEMS

In this chapter some of the characteristics definining variable structure systems (VSS) are explained. This is done by contrasting the natures of power processing systems and signal processing systems. Examples of a few of the VSS often encountered in power processing requirements are highlighted.

2.1 Power Processing Vs Signal Processing

The essential features of signal processing systems and power processing systems are shown in Fig.2.1 [1].

Figure 2.1(a) shows a signal processing system. The input is analog or digital information and so is the output. The system carries out one or more of the signal processing functions. The various processing functions include amplification, coding, decoding, analog to digital, and digital to analog conversion. The most important concern during the processing is to preserve the integrity of the information content. Classical concepts of linear control theory, sampled data control, etc., provide the necessary tools for the design of signal processing systems. The power required to process the signals is incidental (This statement, though strong, is justified because one can think of at least a couple of signal processing functions that do not require external power.) and

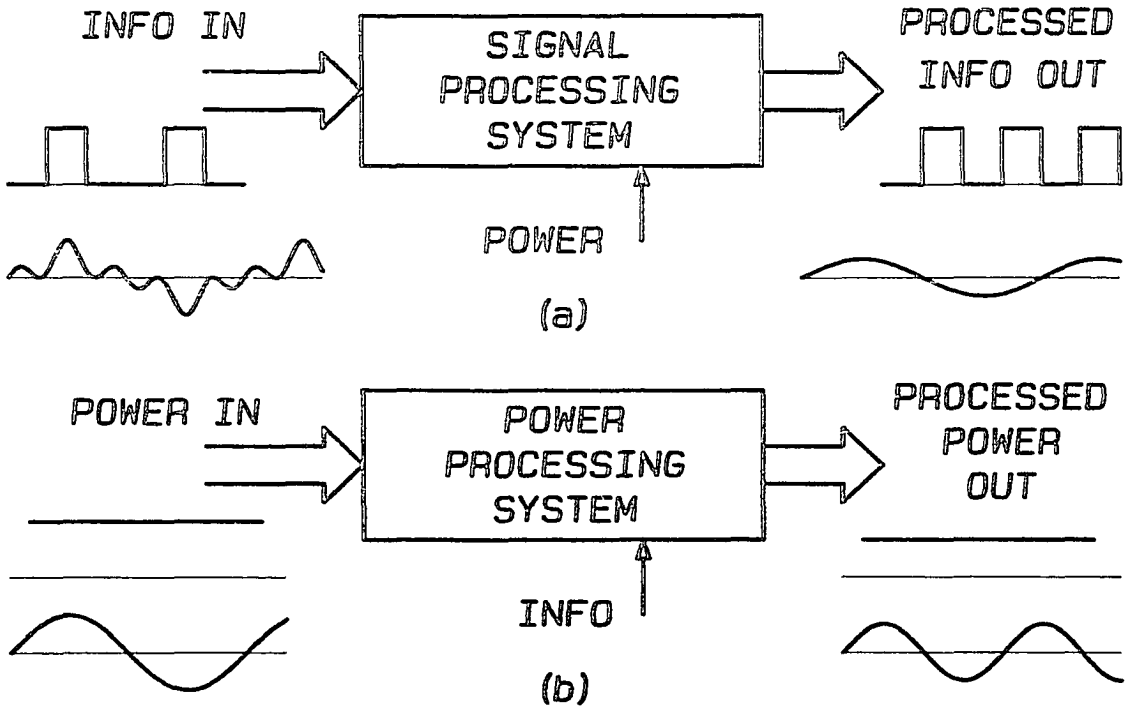

Fig. 2.1 A signal processing system (a), contrasted with a power processing system (b).

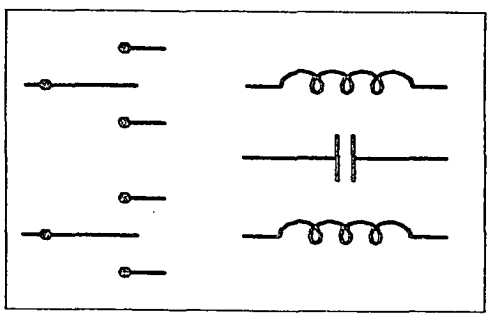

Fig. 2.2 Contents of a typical power processing system. The components are limited to switches, and lossless reactive elements in order to process power efficiently.

considerations of efficiency rarely become critical. Size, cost and the consequent demand to integrate large signal processing functions into ever smaller packages lead the choice of system components limited to resistors, active devices, and occasionally capacitors. Magnetic elements are, as a rule, avoided.

Figure 2.1(b) shows a power processing system. In comparison to the signal processing system, the "power" and "information" inputs are interchanged. The objective is to process power under readily available conditions at the input, and deliver it at the output under conditions suitable for convenient utilization. Typical electrical power processing functions are controlled rectification (conversion of ac power to dc power), inversion (conversion of dc power to ac power), cycloconversion (conversion of ac power at one frequency to ac power at a different frequency), and so on. Frequently power processing systems also include appropriate actuators to convert electrical power into other forms of power, namely mechanical, thermal, and hydraulic. The major concern during power processing is to conserve the total power from input to output. This preoccupation with efficiency limits the choice of the system components to switches and lossless reactive elements. There is one more major difference between the two systems: whereas the power required for a signal processing system is only incidental, the information required – or the control strategy to be adopted – is crucial for the performance of the power processing system.

Figure 2.2 shows the contents of a typical electrical power processing system. It consists of inductors, capacitors and switches. With the elements of the system so limited, it is not hard to see that the only way of achieving the power processing objectives is to dynamically vary the structure of the system in an intelligent way. In order to develop proper control strategies for the power processing systems, it is neccesary to understand, analyze, and develop models for the purpose. Such dynamically varying structures result in nonlinear and timevariant description. The theory of VSS [2] provides a mathematical framework to define such systems and are well suited to define, analyze and to develop control strategies for power processing systems. It may be mentioned here that there are also other tools available for this purpose such as state space averaging [3], and describing equations [4].

2.2 Variable Structure systems (VSS)

VSS are systems whose physical structure or network topology is changed intentionally during the transient in accordance with a preset structure control law [5]. The instants of time, at which the control action of changing the structure occurs, are not determined by a fixed program, but in accordance with the current state of the system. This property distinguishes VSS from programmed controllers. However, as will be seen in some later sections, programmed controllers may be considered as a subset of VSS, by suitable mathematical manipulations.

In general we may state that VSS consist of a number of well defined elements, linear or nonlinear. Under control action the elements may be configured into a number of possible well defined substructures. Out of the total number of all such well defined substructures, there will be a minimum set of independent substructures. This minimum number of independent substructures available in the system is considered as the number of control inputs to the system. The theory of VSS provides a systematic method of defining such systems using discontinuous variables – known as switching variables – and selecting a rational control law to pick out the substructure used at any instant in order to achieve the control objective. Before we go on to see these aspects of VSS in the following chapter, two examples – a single input VSS and a multiple input VSS – of VSS encountered in power conversion application are presented now.

2.3 Some Examples of VSS

Figure 2.3(a) shows a flyback dc-to-dc converter consisting of a single pole double throw switch S, an inductor L, and a capacitor C. The two substructures of the system are shown in Fig. 2.3(b) and 2.3(c). When the system is connected as in Fig. 2.3(b), energy is absorbed into the inductor from the input battery. When the system is connected as in Fig. 2.3(c), part of the energy from the inductor is transferred to the load R. Although there are two substructures available, the presence of the inductor on the pole of the switch forces the throws of the switch to be mutually dependent.

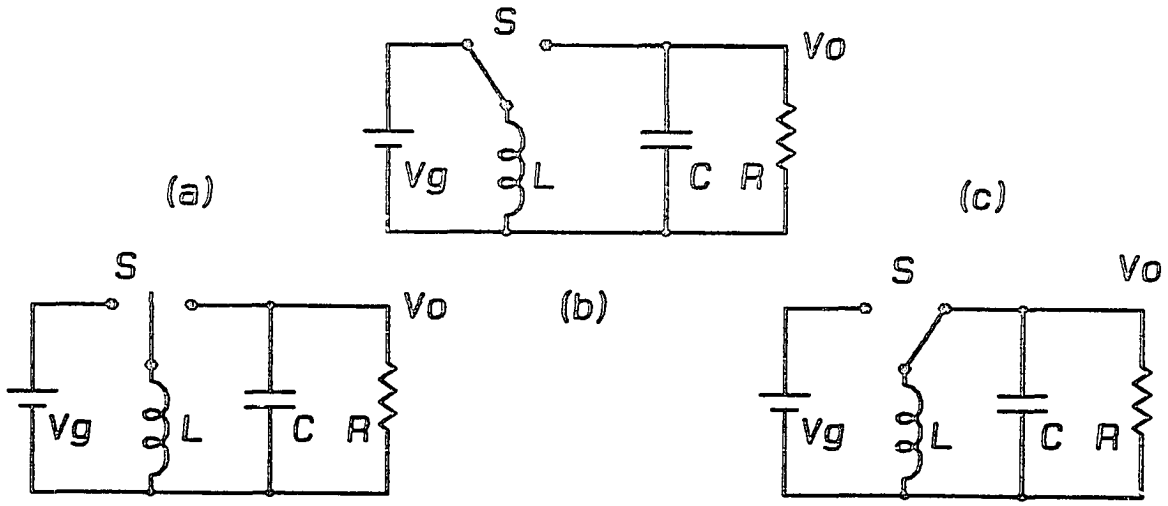

Fig. 2.3 An example of a single control input variable structure system.

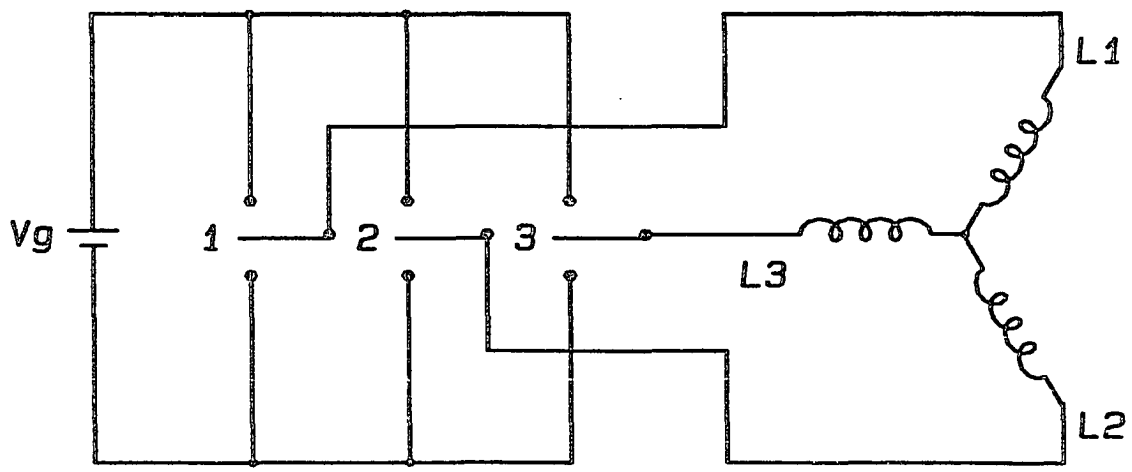

Fig. 2.4 An example of a multiple control input variable structure system.

This is an example of a single input VSS.

Figure 2.4 shows an induction motor drive – an application of electrical to mechanical power conversion. Electrical power from the battery is switched sequentially into the three phase windings of the induction motor in order to produce mechanical torque at the shaft of the motor. This is an example of a three input VSS as is evident from the three single pole double throw switches present in the system.

CHAPTER 3

SLIDING MODE CONTROL

The theory of Variable Structure Systems (VSS) is the analysis and synthesis of systems, whose structures are changed intentionally during the transient, according to a preset structure-control law, to achieve the control objectives. The utilization of control hardware is most effective in such systems. Furthermore, it is possible in VSS to obtain overall system properties that are qualitatively different from the constituent substructures. These aspects of VSS are best seen through the phase plane description of the constituent substructures. Section 3.1 explains the phase plane description of systems and describes the different types of phase trajectories encountered in second order systems.

On the foundation of the phase trajectories described for simple second order systems in Section 3.1, the important features of sliding mode control are built up in Section 3.2. The concept of sliding regimes is formally defined.

Graphical visualization of phase trajectories is tedious, if not impossible, for higher order systems. In such instances it is necessary to resort to formal mathematical methods. The mathematical description of a general dynamic VSS of order n is given in Section 3.3 along with the scope of the theory of VSS.

The analysis problem of VSS consists of tests for the existence of sliding regimes, system description under sliding mode control, and the performance of the overall system. These aspects are dealt with in detail in Sections 3.4 through 3.6. The second aspect of the theory of VSS, namely the design methods, are described in Section 3.7. At the end in Sections 3.8 and 3.9, other applications of sliding mode control such as state estimation and static optimization are indicated.

3.1 Phase Plane Description of Systems

The control action in VSS is the change of the system structure following a preset structure-control law. As a result, VSS are time varying systems. In order to study such systems, it is advantageous to select a system description where time information is suppressed or implicit [6]. The phase plane description satisfies this condition and provides valuable insight into the various aspects pertaining to VSS. The phase plane description is very handy for second order systems and brings out the features of sliding mode control remarkably well. For systems of order higher than two, the phase plane description is clumsy if not impossible. In those instances, the graphical ideas obtained for second order systems are extended mathematically.

The phase plane description is used widely to characterize second order systems. The axes of the phase plane are the system states. The instantaneous state of the system is represented on the phase plane by a Representative Point (RP) whose coordinates on the

phase plane are the present states of the system. The study of the system involves the motion of the RP on the phase plane under different input and initial conditions. The evolution of the system states with respect to time on the phase plane, referred to as the phase trajectories or the state trajectories, represent the dynamic properties of the system. For a given system, the phase trajectories are a family of curves satisfying the dynamic properties of the system. The axes of the phase plane are the system states and hence, the time information is implicit in the state trajectories.

In the case of VSS, the phase plane description consists of a set of a family of phase trajectories, one for each of the substructures used. The analysis problem of VSS is to study the overall system behavior under a given structure-control law. The design problem in VSS is to develop a rationale to synthesize a structure-control law in order to achive the performance objectives of the overall system.

3.1.1 Properties of Phase Trajectories

The study of VSS, and the techniques of sliding mode control for dynamic systems, are intimately related with the phase plane description of the system. The concept of sliding regimes introduced subsequently relies on the phase plane description to get a good intuitive grasp. Therefore it is worthwhile to study the phase trajectories for simple second order systems and become fully familiar with these ideas.

Consider a second order system described by the following homogeneous differential equation.

$$\frac{d^2x}{dt^2}+2\zeta\omega_0\frac{dx}{dt}+\omega_0^2x = 0 \tag{3.1}$$

The above equation may be normalized to obtain

$$\frac{d^2x}{d\tau^2}+2\zeta\frac{dx}{d\tau}+x = 0 \tag{3.2}$$

By defining $x_1 = x$ and $x_2 = dx/d\tau$, the above equation may be written as a set of first order differential equations.

$$\begin{aligned}\frac{dx_1}{d\tau} &= x_2\\ \frac{dx_2}{d\tau} &= -2\zeta x_2 - x_1\end{aligned} \tag{3.3}$$

Let q_1 and q_2 be the characteristic roots of the Eq. (3.2). Then

$$\begin{aligned}q_1+q_2 &= -2\zeta\\ q_1q_2 &= 1\end{aligned}$$

x_1 and x_2 are the dynamic states of the system and are the axes of the phase plane. The differential equation between x_1 and x_2 dictating the properties of the phase trajectories is obtained from Eq. (3.3).

$$\frac{dx_2}{dx_1} = m = -\frac{x_1+2\zeta x_2}{x_2} \tag{3.4}$$

m is the slope of the phase trajectory passing through the point (x_1,x_2). x_1 and x_2 are related to the slope by

$$x_2 = -\frac{1}{m+2\zeta}x_1 \tag{3.5}$$

The phase trajectories are constructed satisfying Eq. (3.4) in the phase plane. The following properties of the phase trajectories are

used to construct them.

i) The straight lines $x_2 = q_1 x_1$ and $x_2 = q_2 x_1$, when they exist, are phase trajectories. This property is seen by substituting $m = q_1$ and $m = q_2$ in Eq. (3.5).

$$x_2 = -\frac{1}{q_1 + 2\zeta} x_1 = \frac{1}{q_2} x_1 = q_1 x_1$$

$$x_2 = -\frac{1}{q_2 + 2\zeta} x_1 = \frac{1}{q_1} x_1 = q_2 x_1$$

The straight lines $x_2 = q_1 x_1$ and $x_2 = q_2 x_1$, exist only when q_1 and q_2 are real.

ii) The phase trajectories intersect the x_2 axis with a slope of -2ζ.

$$\left[\frac{dx_2}{dx_1}\right]_{x_1 = 0} = -2\zeta$$

iii) The phase trajectories intersect the x_1 axis at right angles.

$$\left[\frac{dx_2}{dx_1}\right]_{x_2 = 0} = \infty$$

iv) The zero slope of the phase trajectories occurs along the straight line $x_2 = -(1/2\zeta)x_1$. This property is found by solving for $m = 0$ in Eq. (3.5).

v) The trajectories converge for stable systems (eigenvalues with negative real parts), and diverge for unstable systems (eigenvalues with positive real parts). For marginally stable systems (purely imaginary eigen values), the trajectories are closed curves.

vi) Individual phase trajectories do not cross each other. This property is owing to the fact that, the present state uniquely determines the past history of the system.

All free second order systems exhibit the above properties in their phase trajectories. Depending on the nature of the eigenvalues q_1 and q_2, the phase trajectories have qualitatively different shapes.

3.1.2 Stable Systems with Negative Real Eigenvalues

The eigenvalues q_1 and q_2 being real, the straight lines with slopes q_1 and q_2 are phase trajectories. Other representative trajectories are constructed with the properties given in the last Section. The phase trajectories in the parametric form are given by

$$x_1 = \frac{1}{q_2-q_1}[(q_2x_{10}-x_{20})e^{q_1\tau}-(q_1x_{10}-x_{20})e^{q_2\tau}]$$

$$x_2 = \frac{1}{q_2-q_1}[(x_{10}-q_1x_{20})e^{q_1\tau}-(x_{10}-q_2x_{20})e^{q_2\tau}]$$

x_{10} and x_{20} are the coordinates of any point on a given trajectory. q_1 and q_2 are negative. As τ tends to $+\infty$, x_1 and x_2 tend to zero. Therefore the equilibrium point for all the trajectories is the origin. Figure 3.1 shows the phase trajectories for this class of systems with distinct, negative, and real eigenvalues. In the case of negative, real, repeated eigenvalues the phase trajectories in the parametric form are given by

$$x_1 = x_{10}e^{q\tau}+(x_{20}+x_{10})\tau e^{q\tau}$$

$$x_2 = x_{20}e^{q\tau}-(x_{20}+x_{10})\tau e^{q\tau}$$

x_{10} and x_{20} are the coordinates of any point on a given trajectory. q is equal to -1. As τ tends to $+\infty$, x_1 and x_2 tend to zero. Therefore

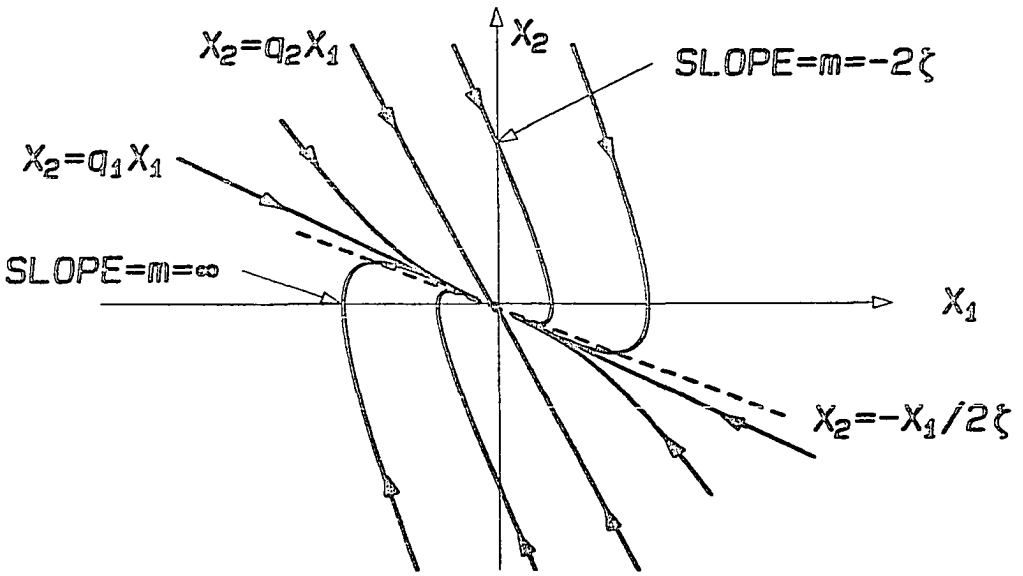

Fig. 3.1 The phase trajectories of a normalized ($q_1 = -0.5, q_2 = -2, \zeta = 1.25$) *second order system with distinct, negative real eigenvalues. The system is stable and all the trajectories converge to the origin.*

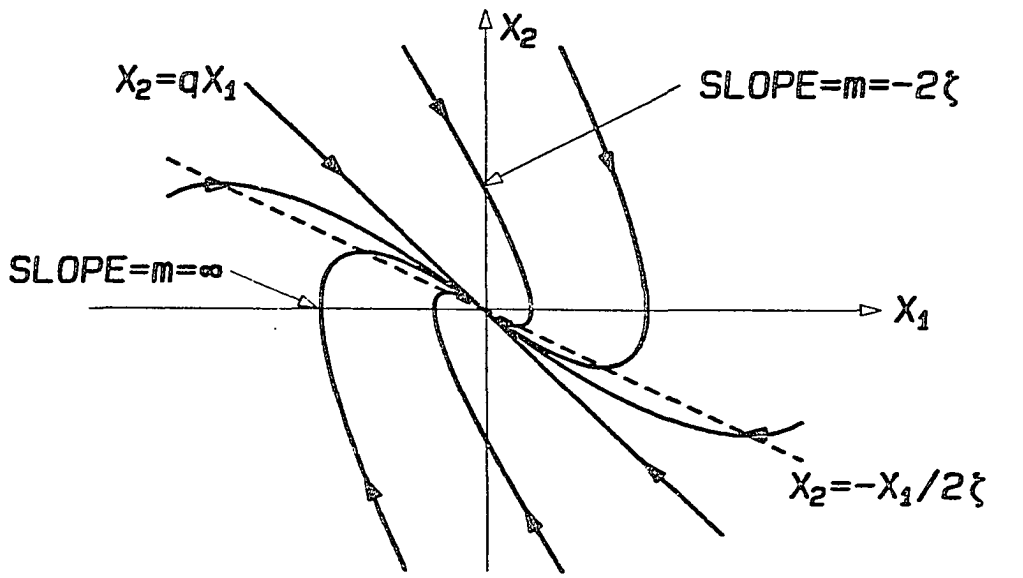

Fig. 3.2 The phase trajectories of a normalized ($q_1 = q_2 = q = -1, \zeta = 1$) *second order system with repeated, negative real eigenvalues. The system is stable and all the trajectories converge to the origin.*

the equilibrium point for all the trajectories is the origin. Figure 3.2 shows the phase trajectories when the eigenvalues are real, negative, and repeated.

3.1.3 Stable Systems with Complex Eigenvalues

The eigenvalues q_1 and q_2 are complex conjugates. There are no straight line trajectories. All the other properties of the trajectories hold. The system may be solved to obtain the phase trajectories in the following parametric form.

$$x_1 = e^{-\zeta\tau}[x_{10}\cos\Omega\tau + \frac{\zeta x_{10}+x_{20}}{\Omega}\sin\Omega\tau]$$

$$x_2 = e^{-\zeta\tau}[x_{20}\cos\Omega\tau - \frac{\zeta x_{20}+x_{10}}{\Omega}\sin\Omega\tau]$$

$$\Omega = \sqrt{1-\zeta^2}$$

x_{10} and x_{20} are the coordinates of any point on a given trajectory. As τ tends to $+\infty$, x_1 and x_2 tend to zero. The trajectories all therefore converge towards the origin, which is the equilibrium point. Figure 3.3 shows typical trajectories for this class of systems. They have the shape of converging logarithmic spirals.

3.1.4 Marginally Stable Systems

Marginally stable systems do not have any damping ($\zeta = 0$). The eigenvalues are purely imaginary. The system is conservative and the phase trajectories are closed circles of radius r.

$$r = \sqrt{x_{10}^2+x_{20}^2}$$

x_{10} and x_{20} are the coordinates of any point on a given trajectory. The system is asymptotically stable and has no equilibrium point.

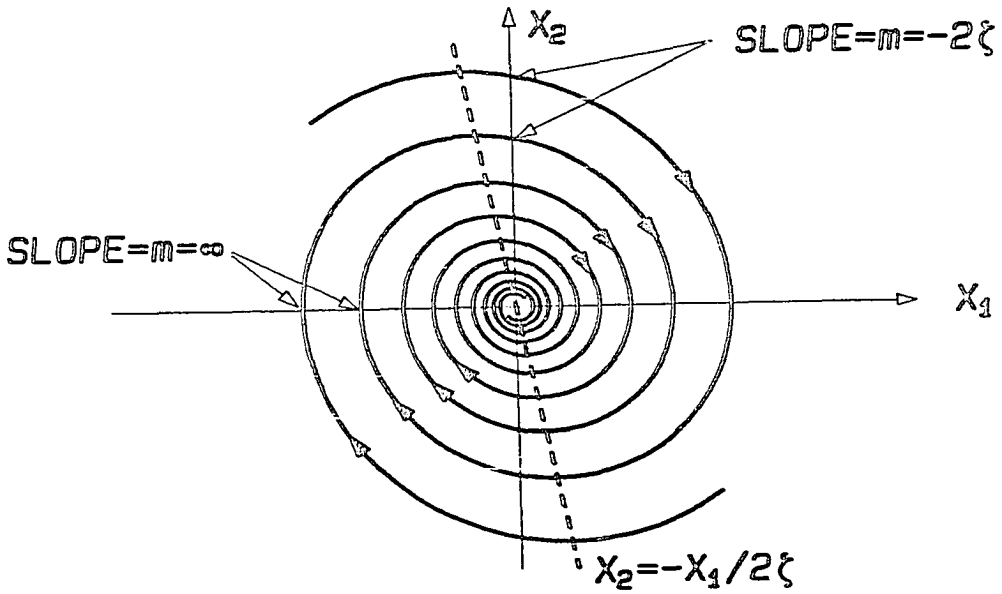

Fig. 3.3 The phase trajectories of a normalized ($q_1q_2 = 1, q_1+q_2 = -2\zeta = -0.4$) *second order system with stable, complex conjugate eigenvalues. The system is stable and the trajectories are converging logarithmic spirals.*

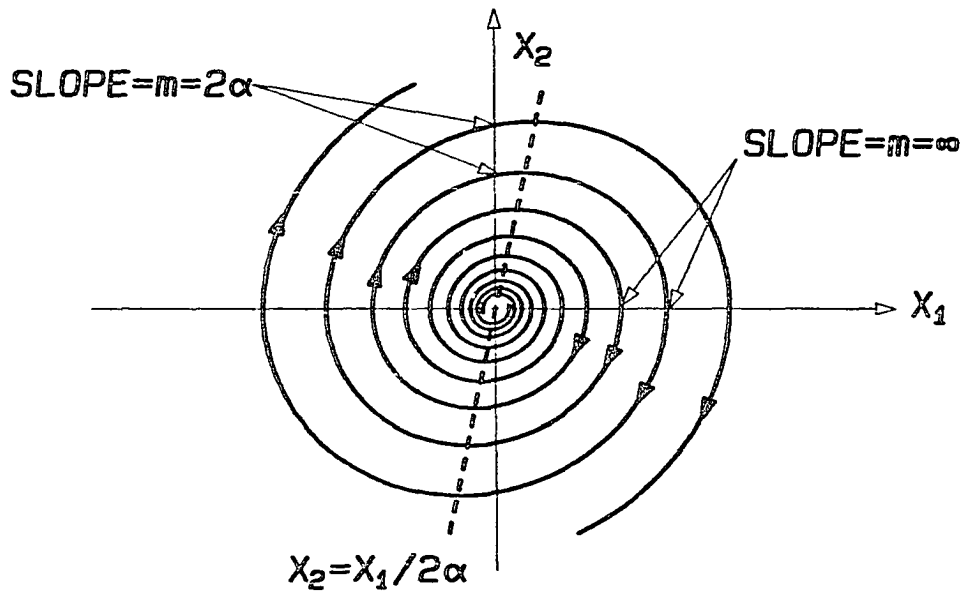

Fig. 3.4 The phase trajectories of a normalized ($q_1q_2 = 1, q_1+q_2 = -2\zeta = 0.4$) *second order system with unstable, complex conjugate eigenvalues. The system is unstable and the trajectories are diverging logarithmic spirals.*

3.1.5 Unstable Systems with Complex Eigenvalues

The eigenvalues are complex conjugates with positive real parts. The phase trajectory is given by the following parametric equations.

$$x_1 = e^{\alpha\tau}[x_{10}\cos\Omega\tau + \frac{x_{20}-\alpha x_{10}}{\Omega}\sin\Omega\tau]$$

$$x_2 = e^{\alpha\tau}[x_{20}\cos\Omega\tau + \frac{\alpha x_{20}-x_{10}}{\Omega}\sin\Omega\tau]$$

$$\Omega = \sqrt{1-\zeta^2}\ ;\ \alpha = -\zeta$$

x_{10} and x_{20} are the coordinates of any point on a given trajectory. As τ is traced back in time to $-\infty$, x_1 and x_2 are zero. Therefore all the trajectories emerge from the origin and diverge towards ∞ as time evolves. The phase trajectories for this class of systems are shown in Fig. 3.4. They are diverging logarithmic spirals.

3.1.6 Unstable Systems with Positive Real Eigenvalues

The eigenvalues are real. The straight lines with slopes q_1 and q_2 are also phase trajectories. The phase trajectories in parametric form are given by

$$x_1 = \frac{1}{q_2-q_1}[(q_2x_{10}-x_{20})e^{q_1\tau}-(q_1x_{10}-x_{20})e^{q_2\tau}]$$

$$x_2 = \frac{1}{q_2-q_1}[(x_{10}-q_1x_{20})e^{q_1\tau}-(x_{10}-q_2x_{20})e^{q_2\tau}]$$

x_{10} and x_{20} are the coordinates of any point on a given trajectory. q_1 and q_2 are positive. As τ is traced back in time to $-\infty$, x_1 and x_2 tend to zero. Therefore all the trajectories emerge from the origin and grow with time. Figure 3.5 shows representative phase trajectories.

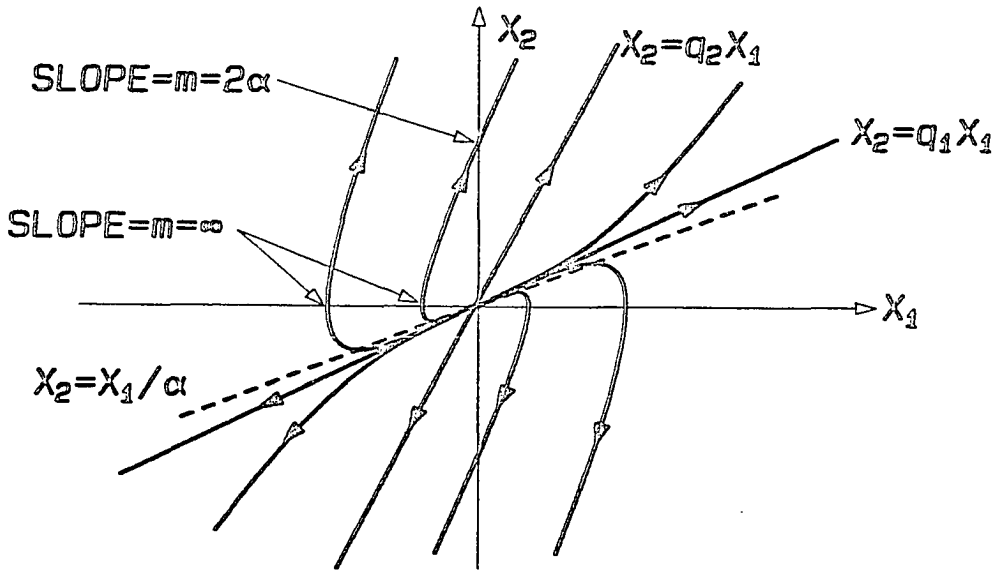

Fig. 3.5 The phase trajectories of a normalized ($q_1 = 0.5, q_2 = 2, \zeta = -1.25$) *second order system with distinct, positive real eigenvalues. The system is unstable and all the trajectories diverge to* ∞.

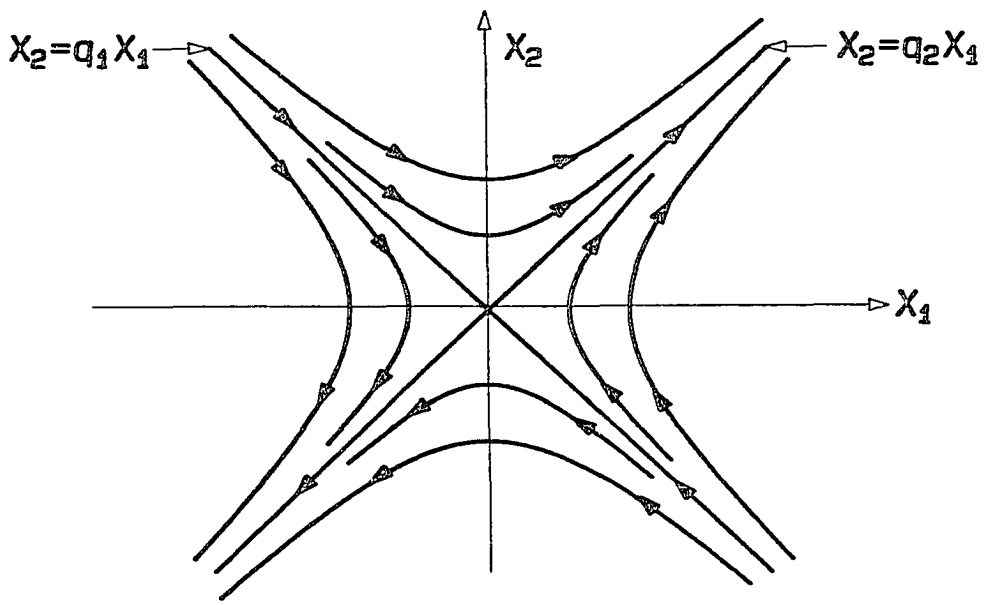

Fig. 3.6 The phase trajectories of a normalized ($q_1 = 1, q_2 = -1, \zeta = 0$) *second order systems with distinct eigenvalues of unlike polarity. The trajectories eventually diverge to* ∞.

They diverge indicating unstable eigenvalues and are the mirror image of the trajectories obtained for systems with negative, real eigenvalues.

3.1.7 Unstable Systems with Eigenvalues Real and Unlike Sign

The eigenvalues are real. The straight lines of slopes q_1 and q_2 are also phase trajectories. The phase trajectories in parametric form are given by

$$x_1 = \frac{1}{q_2-q_1}[(q_2x_{10}-x_{20})e^{q_1\tau}-(q_1x_{10}-x_{20})e^{q_2\tau}]$$

$$x_2 = \frac{1}{q_2-q_1}[(x_{10}-q_1x_{20})e^{q_1\tau}-(x_{10}-q_2x_{20})e^{q_2\tau}]$$

x_{10} and x_{20} are the coordinates of any point on a given trajectory. q_1 and q_2 are of unlike polarity. Therefore the phase trajectories are not uniformly divergent. They emerge from ∞ and evolve towards ∞. Figure 3.6 shows typical trajectories. The overall behavior is divergent.

The nature of the phase trajectories for free second order systems given by Eq. (3.1) is consolidated in Fig. 3.7. It is plotted between damping factor ζ and natural frequency ω_0^2. The different regions are numbered and typical trajectories hinted. Some of these trajectories are used in the following section to highlight the properties of VSS and the concept of sliding regimes.

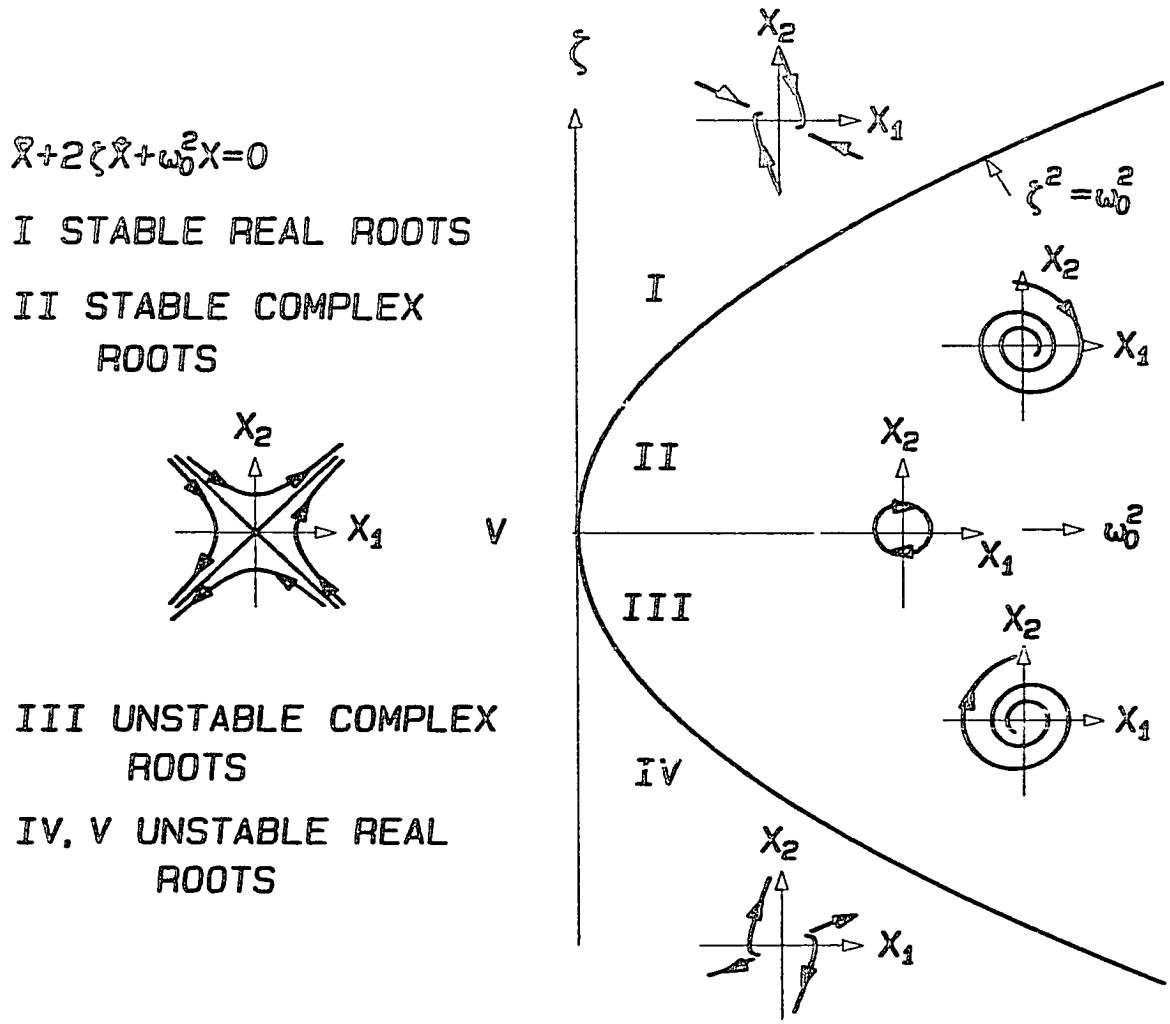

Fig. 3.7 The qualitative difference in the phase trajectories of a second order system as a function of the natural frequency ω_0 and damping ζ. Systems located in region I and II in the ω_0, ζ plane are stable systems. Systems located in regions III, IV, and V are unstable systems. Systems located on the positive ω_0 axis do not have damping and are conservative systems.

3.2 Sliding Regimes in VSS

It was asserted that, in the case of VSS, phase trajectories that are qualitatively different from those of the substructures can be obtained. This point and other features of VSS are now illustrated. Consider the following two substructures (from Section 3.1.5 and 3.1.7 respectively).

Substructure I is given by

$$\dot{x}_1 = x_2$$
$$\dot{x}_2 = -2\zeta x_2 - x_1 \qquad -1 < \zeta < 0$$

The eigenvalues of substructure I are complex with positive real parts. The phase trajectories of this substructure are shown in Fig. 3.8a and is the same as shown in Fig. 3.4. The trajectories are diverging logarithmic spirals and the substructure I is unstable.

Substructure II is given by

$$\dot{x}_1 = x_2$$
$$\dot{x}_2 = -2\zeta x_2 + x_1 \qquad q_1 = -\zeta + \sqrt{1+\zeta^2}\ ;\ q_2 = -\zeta - \sqrt{1+\zeta^2}$$

The eigenvalues of substructure II are real and of unlike polarity. The phase trajectories of substructure II are given in Fig. 3.8b. They diverge to ∞ indicating instability and are the same as shown earlier in Fig. 3.6.

3.2.1 Simple VSS

It may be observed that the trajectories of substructure I are bounded in every quadrant. The trajectories of substructure II are bounded in quadrants 2 and 4. A VSS may be synthesized

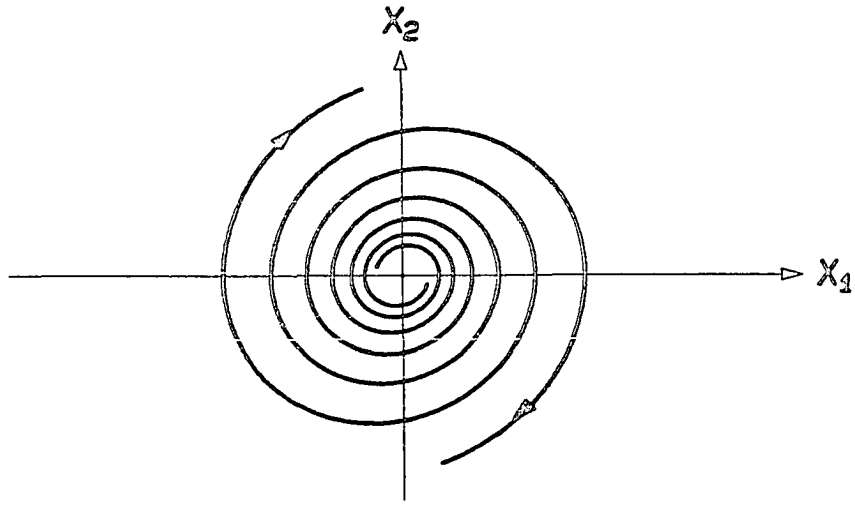

(a) SUBSTRUCTURE I

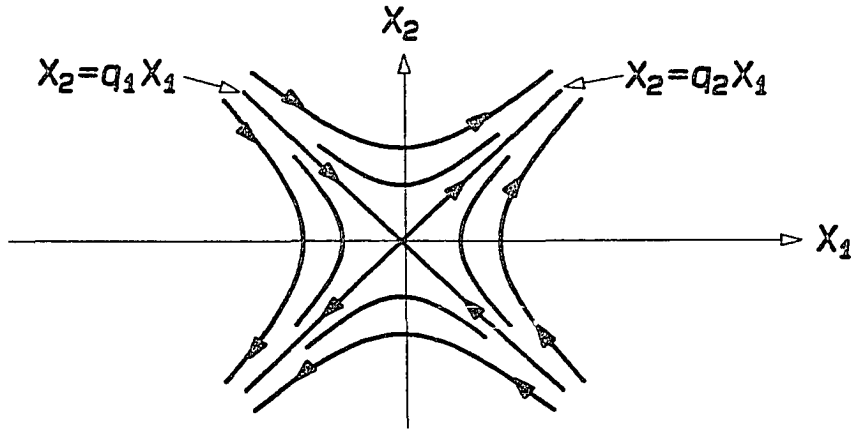

(b) SUBSTRUCTURE II

Fig. 3.8 The phase trajectories of two second order subsystems employed to illustrate Variable Structure Systems (VSS). Subsystem I is an unstable system with complex eigenvalues (a). Subsystem II is also an unstable system with real eigenvalues of unlike polarity (b).

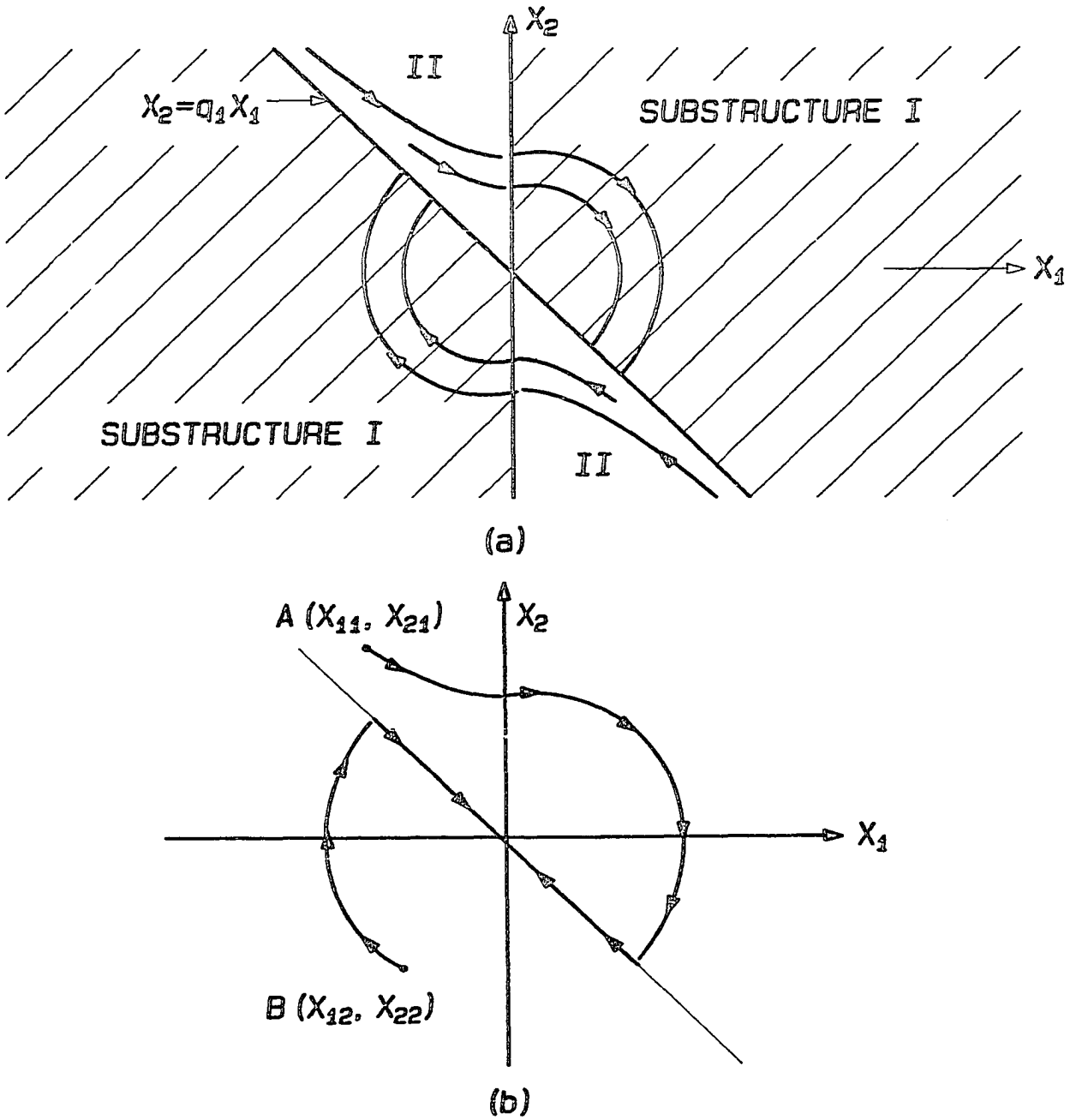

Fig. 3.9 A simple VSS made up of the two substructures given earlier in Fig. 3.8. The substructures active in the different regions of the phase plane are shown. The resultant overall trajectory of the overall VSS is shown in (a). Typical trajectories starting from arbitrary initial conditions $A(x_{11},x_{21})$ and $B(x_{12},x_{22})$ are shown in (b). The VSS made up of unstable substructures is seen to be stable.

composing of these desirable portions of the trajectories of the substructures I and II. The structure-control law may be stated as

Substructure I holds for $x_1(x_2-q_1x_1) > 0$

Substructure II holds for $x_1(x_2-q_1x_1) < 0$

According to the structure-control law the phase plane is divided into several regions, as shown in Fig. 3.9a. The substructures active in each of these regions are labeled. The overall phase trajectory is composed of the trajectories of each of the substructures in the appropriate regions. The phase trajectories for the composite VSS are shown in Fig. 3.9a. The trajectories of the system starting from arbitrary initial conditions $A(x_{11},x_{21})$ and $B(x_{12},x_{22})$ are shown in Fig. 3.9b. Starting from any initial condition the states of the VSS converge to zero and so the overall system is stable.

In the above example it was assumed that the structure-control law was realized perfectly. In other words the change of structure from one substructure to the other acted whenever the system RP crossed the boundaries set up by the structure-control law. In practice such perfect sensing of the location of the RP with respect to the various boundaries is impossible. There will always be nonidealities such as delay, hysteresis etc, inherent in physical hardware used for changing the structure. We now see the effect of such nonideal realization of the structure-control law. Let the real structure-control law be

Substructure I holds for $x_1(x_2-q_1x_1) > \Delta$

Substructure II holds for $x_1(x_2-q_1x_1) < \Delta$

Δ is a small positive quantity introduced to reflect the nonidealities

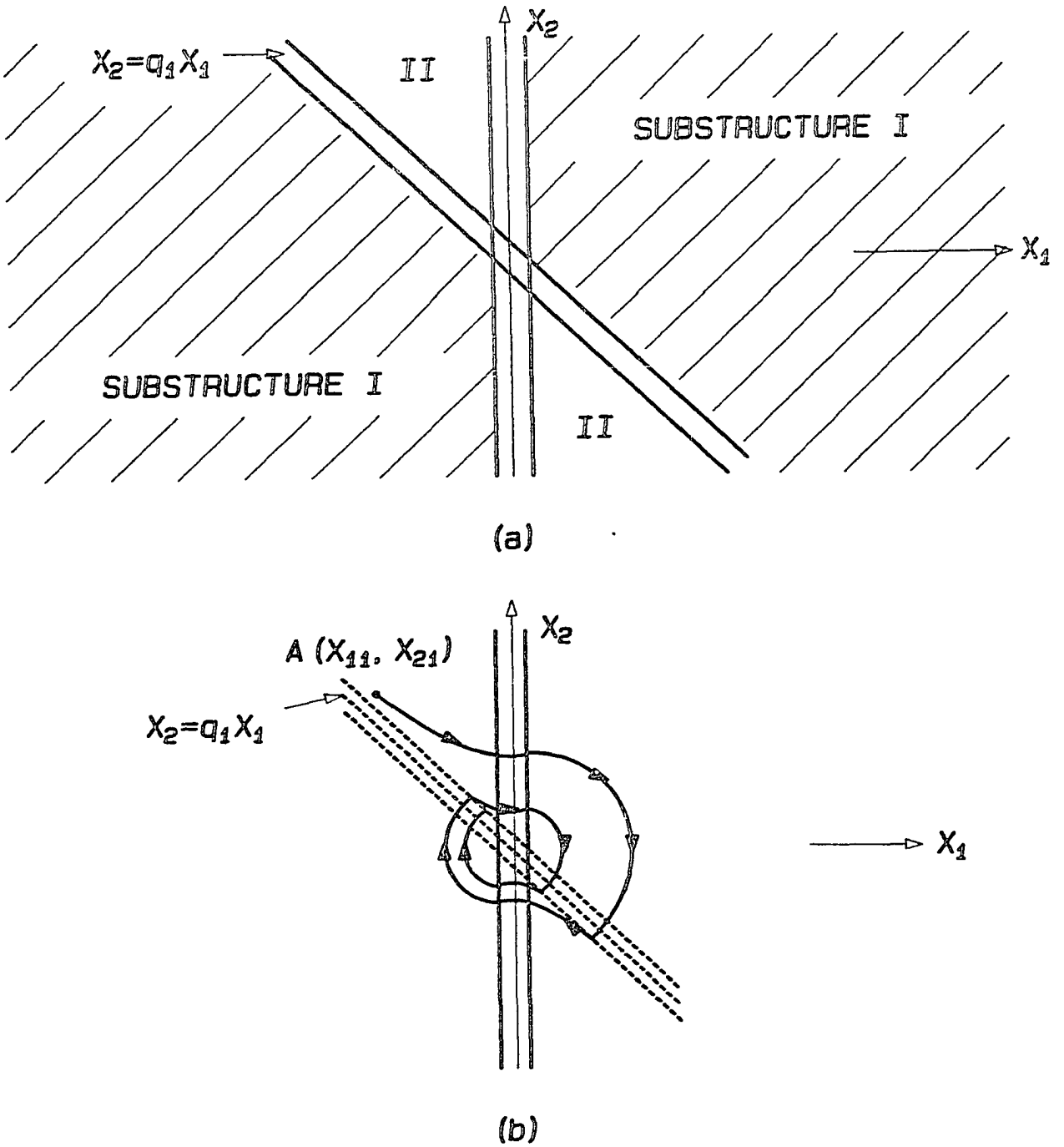

Fig. 3.10 Switching boundaries in a real VSS (a). The boundaries extend over a small Δ neighbourhood of the switching lines. The effect of the nonideal switching boundary on the overall trajectory (b) is seen to be sensitive to the hysteresis in the switching boundary.

of the VSS hardware and goes to zero as these nonidealities vanish. Figure 3.10a shows the partitioning of the phase plane into various regions and the substructures that are active in each of these regions according to the structure-control law. The switching boundaries are shown extended to include the hysteresis zone. System trajectories starting from an arbitrary initial condition $A(x_{11},x_{21})$ are shown in Fig. 3.10b. The effect of the switching nonidealities results in trajectories that are different from the ideal case. However the overall system continues to be stable. It may also be observed that as Δ approaches zero, the real trajectory approaches the ideal trajectory.

3.2.2 Sliding Modes in VSS

In the above examples, desirable sections of the phase trajectories of unsatisfactory systems are pieced together to obtain a VSS with a desirable property (stability in these examples). A more fundamental aspect of VSS is the possibility to obtain resultant phase trajectories that are not inherent in any of the substructures used. This aspect is brought out in the extension of the same example.

Consider the VSS that consists of the same substructures I and II as before. The structure-control law is now modified.

Substructure I holds for $x_1(x_2+c\,x_1) > \Delta$

Substructure II holds for $x_1(x_2+c\,x_1) < \Delta$

$c > 0$; $|c| < |q_1|$

The idealized switching boundaries, the substructures active in the various regions of the phase plane, and the trajectories in each of

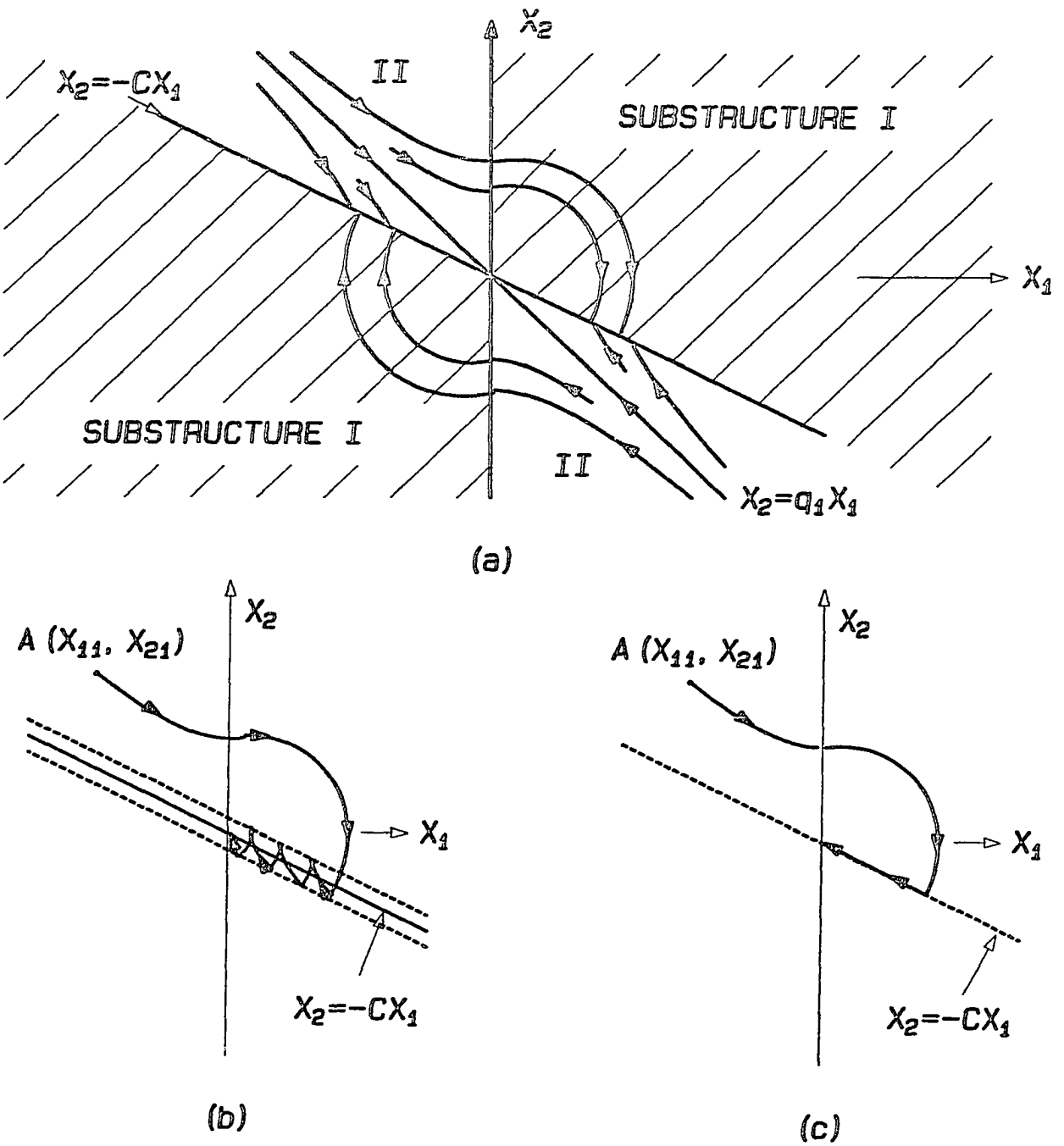

Fig. 3.11 Sliding regime in VSS (a). The switching line $x_2+cx_1 = 0$ is such that the trajectories of the substructures on either side of the switching line are directed towards the switching line. The resultant overall trajectory (b) is seen to be confined within the hysteresis bounds of the switching line. The ideal overall trajectory (c) is seen to be different from, and independent of the substructures used.

the regions of the phase planes are all shown in Fig. 3.11a. The switching boundaries are the x_2 axis and the straight line $x_2+cx_1 = 0$. The line $x_2+cx_1 = 0$ is the switching line. The structure changes whenever the Representative Point (RP) enters a region defined by the switching boundaries. The important property of the phase trajectories of the substructures is that, in the vicinity of the switching line, the phase trajectories converge to the switching line. The immediate consequence of this property is that, once the RP hits the switching line the structure-control law ensures that the RP does not move away from the switching line. Figure 3.11b shows a typical trajectory starting from an arbitrary initial condition $A(x_{11},x_{21})$. The resultant trajectory is seen to be confined along the switching boundary $x_2+cx_1 = \Delta$. Figure 3.11c shows the same trajectory as in Fig. 3.11b, when the nonidealities of the switching boundaries approach zero ($\Delta = 0$). In the case of ideal switching it may be seen that once the RP moves onto the switching line $x_2+cx_1 = 0$, the system motion is then along the switching line. The switching line $x_2+cx_1 = 0$ is defined by the structure-control law and is not part of the trajectories of any of the substructures of the VSS. *This motion of the system RP along a trajectory, on which the structure of the system changes, and that is not part of any of the substructure trajectories, is called the sliding mode*. This property is one of the strongest features of VSS. When sliding modes exist, and are exploited, the resultant system performance is independent of the properties of the substructures employed and depends only on the preset structure-control law (in this example the boundary

$x_2+cx_1 = 0$ on which the overall system trajectories are confined.)

3.2.3 Stability of Sliding Modes

Another example of VSS is now synthesized to illustrate the aspect of stability of the system operating in a sliding mode. The VSS considered here also is composed of the same substructures I and II as in the previous examples. The structure-control law is now given as

Substructure I holds for $x_1(x_2+cx_1) > \Delta$

Substructure II holds for $x_1(x_2+cx_1) < \Delta$

$c < 0$; $|c| < |q_2|$

The idealized switching boundaries, the substructures active in the various regions of the phase plane, and the trajectories in each of the regions of the phase planes are all shown in Fig. 3.12a. The switching boundaries are the x_2 axis and the straight line $x_2+cx_1 = 0$. The structure changes whenever the Representative Point (RP) enters a region defined by the switching boundaries. As in the previous example the phase trajectories of the substructures in the vicinity of the boundary $x_2+cx_1 = 0$, converge to the boundary $x_2+cx_1 = 0$. Figure 3.12b shows a typical trajectory starting from an arbitrary initial condition $A(x_{11},x_{21})$. The resultant trajectory is seen confined along the switching boundary $x_2+cx_1 = \Delta$. Figure 3.12c shows the same trajectory as in Fig. 3.12b, when the nonidealities of the switching boundaries approach zero ($\Delta = 0$). In the ideal case the system motion, as in the previous example, is along the switching line $x_2+cx_1 = 0$. However unlike the previous example, the system

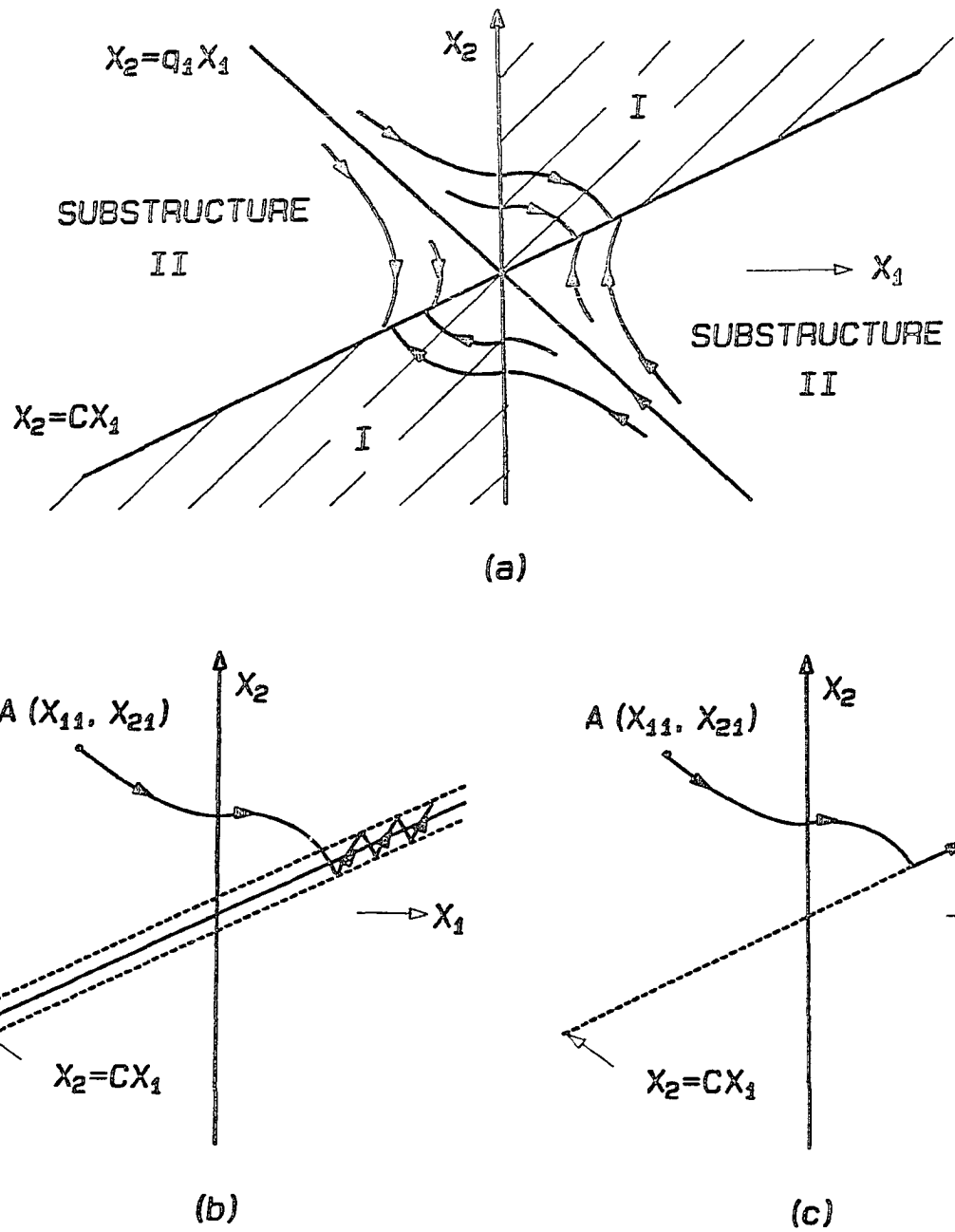

Fig. 3.12 An unstable sliding regime in VSS (a). The switching line $x_2+cx_1 = 0$ is a sliding regime. Resultant overall trajectory (b) and ideal trajectory (c) are confined to the switching line, but unstable.

motion is forever away from the origin and is unstable. The important point made through this example is that, when sliding modes exist, analysis of the stability of the overall system is done simply by examining if the trajectories on the switching boundaries lead to a stable operating point or not.

3.2.4 A Practical Example

The examples considered in the previous sections were all free second order systems . They brought out the various features of the sliding modes in VSS. To reinforce the concepts illustrated by the previous examples, a practical example of a dc-to-dc electrical power converter is presented, before we go on to generalize these concepts for general dynamic systems.

Consider the dc-to-dc converter circuit shown in Fig. 3.13a. Depending on the position of the single pole double throw (SPDT) switch, the system consists of two substructures. The switching variable u is related to the SPDT position. $u = 1$ when the inductor is connected to V_g. $u = 0$ when the inductor is connected to ground. The substructures 0 and 1 are the resultant circuits for $u = 0$ and $u = 1$ respectively, and are shown in Fig. 3.13b, and Fig. 3.13c. The dynamic equations of the system are,

$$C\frac{dv_0}{dt} = i - \frac{v_0}{R}$$

$$L\frac{di}{dt} = V_g u - v_0$$

The same equations represent both substructures 0 and 1 depending on the value taken by the switching variable u. The system equations

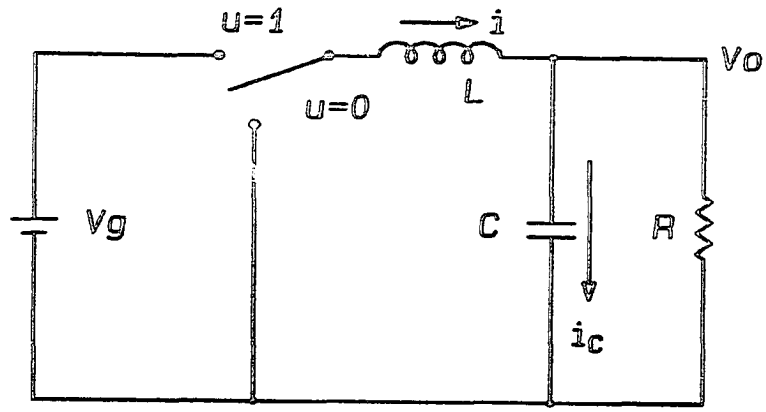

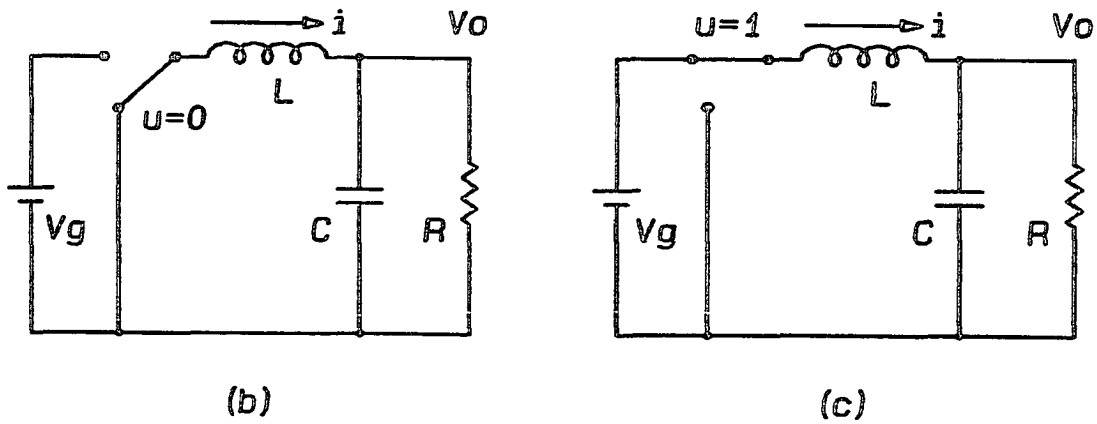

Fig. 3.13 The example of a buck converter (a) as a VSS. The substructures (b) and (c) are the effective circuits during the active and nonactive periods of the operation of the converter. Both (a) and (b) are second order systems.

may be put in the following form.

$$\frac{d^2v_0}{dt^2} = -\frac{1}{LC}v_0 - \frac{1}{RC}\frac{dv_0}{dt} + \frac{V_g}{LC}u$$

With the definition of $v_0 = x_1$; $dv_0/dt = x_2$; $1/LC = \omega_0^2$; $2\zeta\omega_0 = 1/RC$, the following representation is obtained.

$$\dot{x_1} = x_2$$
$$\dot{x_2} = -\omega_0^2 x_1 - 2\zeta\omega_0 x_2 + \omega_0^2 V_g u$$

In normal converters the damping factor ζ is less than 1, resulting in complex conjugate eigenvalues with negative real parts.

For substructure 0, $u = 0$ and the system equations are identical to those given in Section 3.1.3. The equilibrium point is given by $v_0 = dv_0/dt = 0$. The phase trajectories for the substructure 0 are shown in Fig. 3.14. For substructure 1, $u = 1$ and the system equations have an extra forcing term $\omega_0^2 V_g$. The equilibrium point is then $v_0 = V_g$. The eigenvalues being complex with negative real parts, the phase trajectories are similar to those given in Section 3.1.3, and are also shown in Fig. 3.14.

We now synthesize a control law given by

Substructure 0 *holds* for $(v_0 - V_0^*) + \tau\frac{dv_0}{dt} > 0$

Substructure 1 *holds* for $(v_0 - V_0^*) + \tau\frac{dv_0}{dt} < 0$

The switching boundary established by the above control law, and part of the trajectories valid in the two regions defined by the switching boundaries are shown in Fig. 3.15. The consequences of the above structure-control law are as follows.

i) The phase trajectories everywhere in the phase plane are

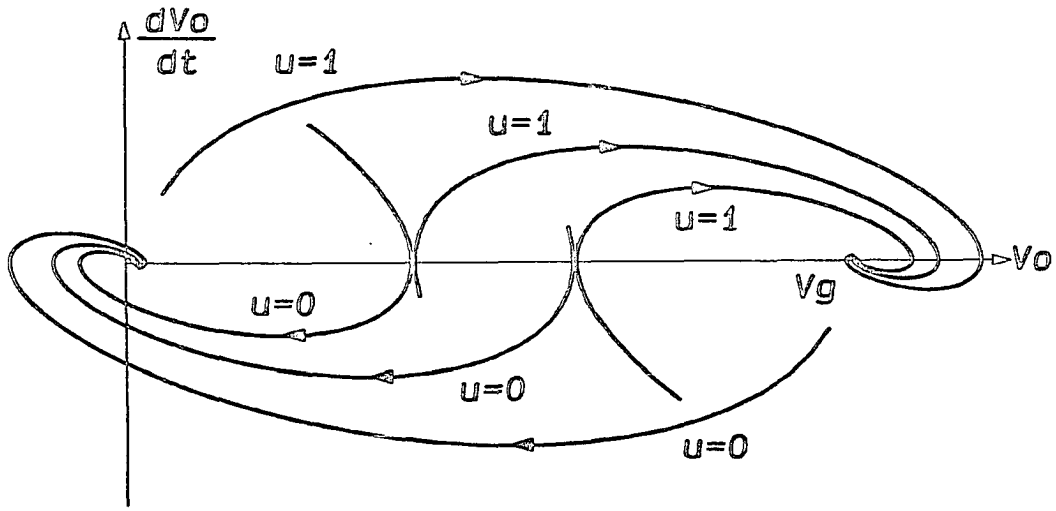

Fig. 3.14 The trajectories of the substructures involved in the buck converter. The trajectories marked u = 0, and u = 1 correspond to the active and nonactive substructures of the buck converter repectively.

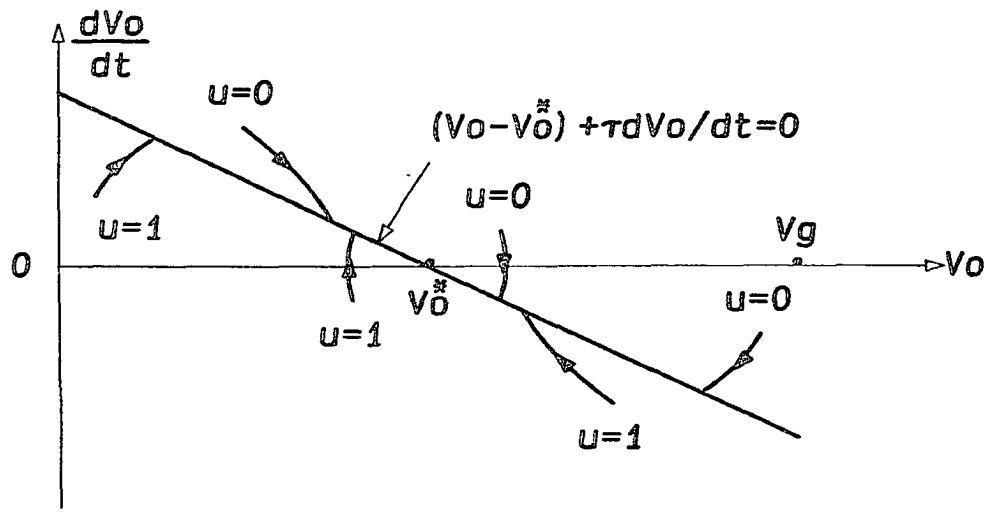

Fig. 3.15 The desired response of the buck converter $(v_0-v_0^*)+\tau\frac{dv_0}{dt}$ *is seen to be a sliding regime. The trajectories on either side of the sliding line are directed towards the sliding line.*

directed towards the switching boundary.

ii) When the switching boundary is considered as a trajectory, there exists a stable operating point given by $v_0 = V_0^*$.

The steady state operating point defined by the switching boundary is different from those of either of the substructures. Starting from zero initial conditions, the system motion is shown in Fig. 3.16. The overall system motion consists of two parts. The first part is the motion from any arbitrary initial condition on the phase plane till the RP reaches the switching boundary or the sliding line. The time taken for this part of the motion depends on the system parameters and will be a small fraction of the total response time in a well designed system. The second part of the motion is from where the RP hits the sliding line, to the steady state operating point on the sliding line. In this example this motion is with a time constant of τ, and is independent of the system parameters.

3.2.5 Equations of Motion on the Switching Boundary

The same example shown in the previous section is now studied for the equations of motion of the system RP along the switching boundary. It was seen that the resultant motion of the RP, in the case of ideal switching, is directed along the switching boundary. One may then take the equation of the sliding boundary to represent the system motion. Alternatively, the actual system motion taking into account the nonidealities in switching may be computed and the resultant motion arrived at by the process of taking the nonidealities to the limit of zero. This method of arriving at the

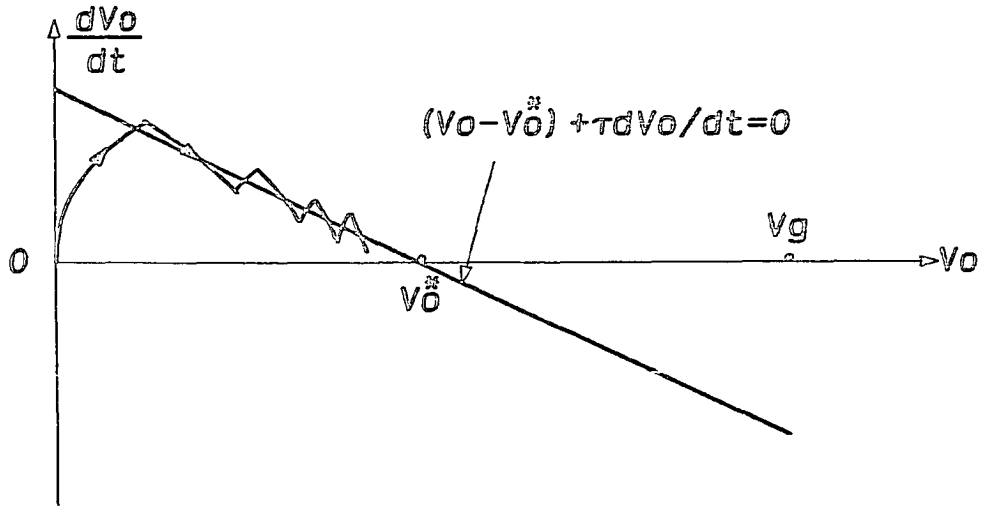

Fig. 3.16 Typical starting transient of the buck converter seen on the phase plane. The steady state operating point is $v_0 = V_0^*$.

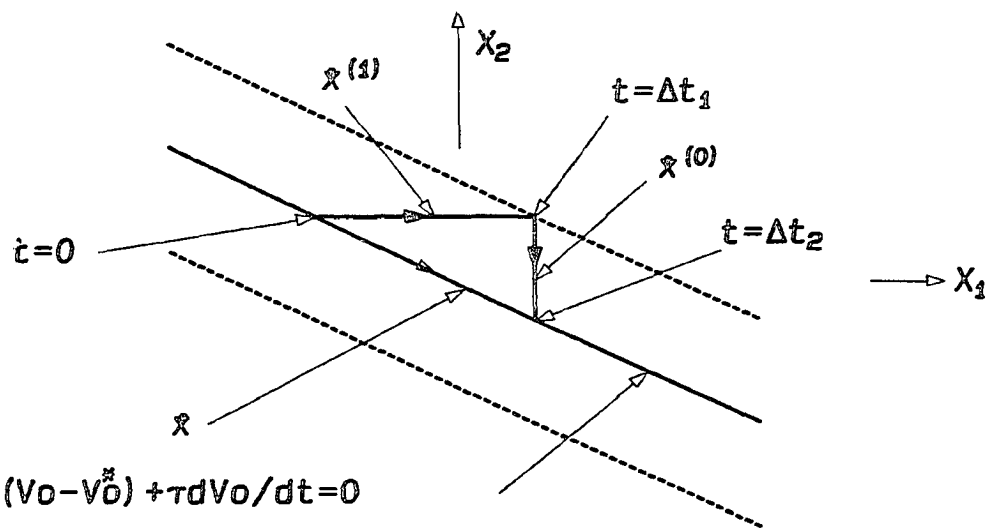

Fig. 3.17 The equivalent trajectory along the sliding line consists of a series of trajectories corresponding to the individual substructure trajectories. The average trajectory along the sliding line is the average of the individual trajectories.

equivalent system description is called the Filippov's method, and is illustrated for this example here. The sliding line, the Δ vicinity as a result of real switching, and the actual motion of the RP starting on the sliding line at time $t = 0$ are shown in Fig. 3.17. $\dot{x}^{(1)}$ and $\dot{x}^{(0)}$ are the state velocity vectors for $u = 1$ and $u = 0$ respectively in the narrow Δ vicinity of the sliding line. The time taken for the system RP to reach the edge of the switching boundary and back to the sliding line are finite and equal to Δt_1 and Δt_2 respectively. Suppose that the hysteresis region is small. Then the state velocity vectors $\dot{x}^{(1)}$ and $\dot{x}^{(0)}$ are constants in the region considered. Then as $\Delta \to 0$

$$\dot{x} = \frac{\dot{x}^{(1)}\Delta t_1 + \dot{x}^{(0)}(\Delta t_2 - \Delta t_1)}{\Delta t_2}$$

$$\dot{x} = \dot{x}^{(1)}\mu + \dot{x}^{(0)}(1-\mu) \; ; \quad \mu = \frac{\Delta t_1}{\Delta t_2}$$

In words then, the resultant motion of the system on the sliding boundary is the weighted average of the motions of the substructures on either side of the sliding boundary. In this example it is seen that the weights are the relative duration of each substructure in a cycle to the total duration of the cycle. The higher the frequency of switching, the better is this approximation. In a real sliding mode system the finite switching frequency of the system is caused by the various nonidealities and is not constant. In such instances, the method followed to get equivalent description of the overall system is given in Section 3.5.

The examples given in this section, though simple, illustrated several important aspects of sliding modes in VSS. Before these concepts are generalized, several features of the general problem are highlighted. For a general system of order higher than two, the phase space is of dimension higher than two. The existence of sliding modes is difficult to visualize for such systems. It is then required to prove the existence of sliding modes through more abstract mathematical means. The phase plane for the second order system was set up in terms of the output variable and its derivative. For higher order systems, not only that higher order derivatives are difficult to measure, but could prove to be discontinuous as well. Therefore sliding regimes in a phase space made up of states which are measurable, physical, and continuous variables would be desired. Further, the system may have more than two substructures indicating multiple control inputs. These aspects are dealt with in detail in the following sections.

Having seen the above examples, certain aspects of VSS are now recapitulated [2]. The control laws developed in the theory of VSS usually provide for changes in the structure of the system, whenever the RP crosses certain surfaces in the phase space of the system. These surfaces across which the system structure changes are called the sliding surfaces. Once the RP of the system moves onto these sliding surfaces, the control action is such that the RP stays on these surfaces. The form of the sliding surfaces depends on the type of the system and the desired performance of the overall system. Essentially the theory of VSS is the study of the properties

of such regimes of operation in VSS, selecting rational sliding surfaces appropriate for the type of response desired, and selecting the appropriate substructures of the VSS to ensure the desired performance.

3.3 General Dynamic System

A general dynamic system in the state space is described mathematically as follows.

$$\dot{x} = f(x,t,u) \; ; \quad x \in R^n \; ; \; f \in F^n \; ; \; u \in R^m.$$

x is a column vector which represents the state of the system. f is a vector function. u is a control input vector.

$$x = [x_1 \;\; x_2 \;\; \ldots \;\; x_n]^T$$
$$f = [f_1 \;\; f_2 \;\; \ldots \;\; f_n]^T$$
$$u = [u_1 \;\; u_2 \;\; \ldots \;\; u_n]^T$$

The case of x, f, and u, all being continuous functions leads to the class of continuous dynamic systems.

In the case of VSS, the control at any instant is dependent on the location of the RP in the state space at that instant. These are mathematically described as

$$u_i = \begin{cases} u_i^+(x,t) & \text{for } S_i(x) > 0 \\ u_i^-(x,t) & \text{for } S_i(x) < 0 \end{cases} \quad i = 1,2, \ldots ,m$$

The equation $S_i(x) = 0$ represents a boundary in the state space, across which the i^{th} control undergoes discontinuity ($u_i^+ \neq u_i^-$). Away from this boundary $S_i(x) = 0$, i^{th} control input is either u_i^+ or u_i^-, both of which are continuous functions.

In the general class of VSS, $u_i^+(x,t)$ and $u_i^-(x,t)$ are both continuous functions of the state. The properties of this class of systems have been the focus of extensive study in the literature [2] [5], and a whole range of results on the existence, reachability, and stability of such systems exist. The subclass of VSS where $u_i^+(x,t)$ and $u_i^-(x,t)$ take on only fixed values u_i^+ and u_i^-, is classified as relay control VSS. This class of systems arises in the study of on-off systems. Most of the VSS encountered in power control applications belong to this category. The scope of the present work is limited to this subclass of VSS, namely relay control VSS.

The general problem of VSS, just like any other control problem, has two aspects namely analysis and synthesis. In the case of the analysis problem, the substructures and the structure-control law are given. It is required to find out the conditions for the existence of sliding mode, conditions that the system RP will eventually reach the sliding regime, the stability of the system under sliding control, etc. The synthesis or the design problem is the reverse of this. From the desired performance specifications, suitable boundaries ($S_i(x) = 0$) defining the sliding regime are to be established. Then the discontinuous control inputs u_i^+ and u_i^- are to be determined such that existence of sliding mode is guaranteed at every point on the boundary $S_i(x) = 0$. Finally the control must be able to steer the system towards and onto the intersection of the sliding boundaries $S_i(x) = 0$.

In the case of the second order system considered in Section 3.2, it was seen that sliding mode exists if the phase trajectories in the vicinity of the sliding line $x_2+cx_1 = 0$, are directed towards the sliding line. In the following section this idea is generalized to obtain conditions for the existence of sliding regime in general.

3.4 Conditions for Existence of Sliding Regime

Consider the general dynamic VSS given by

$$\dot{x} = f(x,t,u) \; ; \quad x \in R^n \; ; \quad f \in F^n \; ; \quad u \in R^m. \tag{3.6}$$

$$u_i = \begin{cases} u_i^+(x,t) & \text{for } S_i(x) > 0 \\ u_i^-(x,t) & \text{for } S_i(x) < 0 \end{cases} \quad i = 1,2, \quad ,m \tag{3.7}$$

The control inputs $u_i (i = 1,2, \quad ,m)$ are defined by the location of the RP in the state space with reference to the structure-control boundaries $S_i(x) = 0$. When sliding regime exists the system RP eventually moves onto the intersection of all $S_i(x) = 0$ $(i = 1,2, \quad m)$. The hypersurface defined by the intersection of the m switching boundaries $S_i(x)=0$ is called the sliding surface $\sigma(x) = 0$. The sliding surface $\sigma(x) = 0$, being the intersection of m switching boundaries $S_i(x) = 0$, is an $(n-m)$ dimensional hypersurface in the state space. The structure-control law is active on the switching boundaries, and so the right hand side of Eq. (3.6) is discontinuous on the hypersurface $\sigma = 0$ in the state space R^n. At all other points in the state space, away from the switching boundaries, the state velocity function given by Eq. (3.6) is continuous. Therefore the limits of the

functions $f(x,t,u)$ exist as the RP approaches the sliding hypersurface from either side. Let these limits be represented by

$$\lim_{\sigma = 0^+} f(x,t,u^{\circ +}) = f^+(x,t)$$

$$\lim_{\sigma = 0^+} f(x,t,u^{\circ -}) = f^-(x,t)$$

$u^{\circ +}$ and $u^{\circ -}$ are the input vectors for $\sigma = 0^+$ and $\sigma = 0^-$ respectively. In general $f^+(x,t) \neq f^-(x,t)$. We now inspect the trajectory of the RP on either side of the boundary defined by $\sigma = 0$.

$$\frac{d\sigma}{dt} = \sum_{i=1}^{n} \frac{\partial \sigma}{\partial x_i} \frac{dx_i}{dt} = \sum_{i=1}^{n} \frac{\partial \sigma}{\partial x_i} f_i = f \ \ grad \ \sigma$$

$$\lim_{\sigma=0^-} \frac{d\sigma}{dt} = f^- \ \ grad \ \sigma$$

$$\lim_{\sigma=0^+} \frac{d\sigma}{dt} = f^+ \ \ grad \ \sigma$$

At every point in the neighbourhood of $\sigma = 0$ the signs of these limits satisfy any one of the following nine relations.

$$\lim_{\sigma = 0^-} \frac{d\sigma}{dt} > 0 < \lim_{\sigma = 0^+} \frac{d\sigma}{dt} \tag{3.8}$$

$$\lim_{\sigma = 0^-} \frac{d\sigma}{dt} < 0 > \lim_{\sigma = 0^+} \frac{d\sigma}{dt} \tag{3.9}$$

$$\lim_{\sigma = 0^-} \frac{d\sigma}{dt} < 0 < \lim_{\sigma = 0^+} \frac{d\sigma}{dt} \tag{3.10}$$

$$\lim_{\sigma = 0^-} \frac{d\sigma}{dt} = 0 < \lim_{\sigma = 0^+} \frac{d\sigma}{dt} \tag{3.11}$$

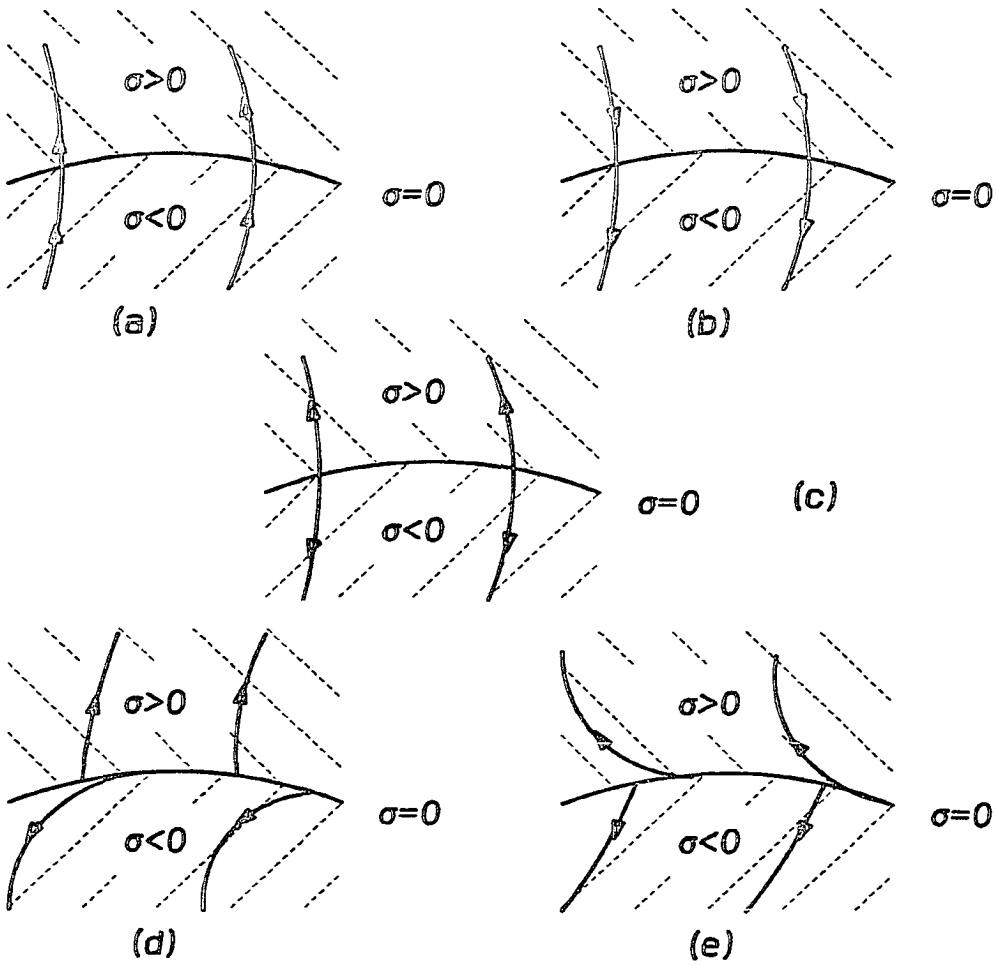

Fig. 3.18 Phase trajectories of VSS where no sliding regime exists. In all the examples (a) through (e), the trajectories on either side of the switching boundary move away from the switching boundary.

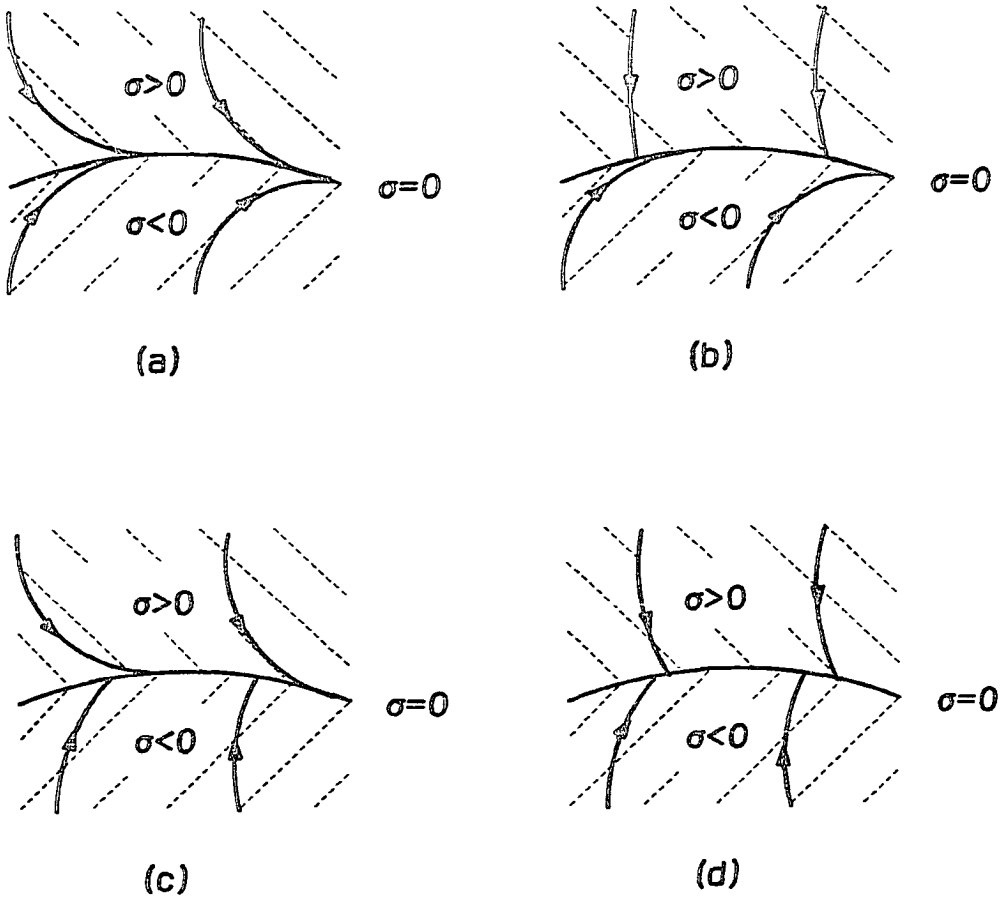

Fig. 3.19 Phase trajectories of VSS where sliding regime exists. In all the examples (a) through (d), the trajectories on either side of the switching boundary are towards the switching boundary.

$$\lim_{\sigma = 0^-} \frac{d\sigma}{dt} < 0 = \lim_{\sigma = 0^+} \frac{d\sigma}{dt} \tag{3.12}$$

$$\lim_{\sigma = 0^-} \frac{d\sigma}{dt} = 0 = \lim_{\sigma = 0^+} \frac{d\sigma}{dt} \tag{3.13}$$

$$\lim_{\sigma = 0^-} \frac{d\sigma}{dt} = 0 > \lim_{\sigma = 0^+} \frac{d\sigma}{dt} \tag{3.14}$$

$$\lim_{\sigma = 0^-} \frac{d\sigma}{dt} > 0 = \lim_{\sigma = 0^+} \frac{d\sigma}{dt} \tag{3.15}$$

$$\lim_{\sigma = 0^-} \frac{d\sigma}{dt} > 0 > \lim_{\sigma = 0^+} \frac{d\sigma}{dt} \tag{3.16}$$

These relations are illustrated in Fig. 3.18 and 3.19. The Eqs. (3.8) and (3.9) correspond to the RP moving freely across the switching hypersurface. Equations (3.10), (3.11) and (3.12) show the RP diverging away from the switching hypersurface on one or both sides of the surface. Equation (3.16) is the case of the ideal sliding regime on the hypersurface $\sigma = 0$. The RP is forced to remain within an infinitismal neighbourhood of the hypersurface and oscillating about $\sigma = 0$ at infinite frequency. This provides the necessary condition for the existence of sliding regime. Equations (3.13), (3.14) and (3.15) are also essentially similar to Eq. (3.16). In those instances too, if the RP is on the hypersurface $\sigma = 0$, then it cannot leave an infinitesimal neighborhood of the hypersurface. The RP again oscillates about $\sigma = 0$. Inequality (3.16) was first suggested as the necessary and sufficient condition for the existence of sliding regime[1]. More recently [5] cases of Eqs. (3.13), (3.14), (3.15) and (3.16) are all combined together and stated as any one of the

following equivalent conditions.

$$\lim_{\sigma \to 0^+} \frac{d\sigma}{dt} \leq 0 \leq \lim_{\sigma \to 0^-} \frac{d\sigma}{dt} \tag{3.17a}$$

$$\lim_{\sigma \to 0} \sigma \frac{d\sigma}{dt} \leq 0 \tag{3.17b}$$

$$\lim_{\sigma \to 0} \frac{d(\sigma^2)}{dt} \leq 0 \tag{3.17c}$$

Any one of the above conditions may be used as the necessary and sufficient condition for the existence of sliding regime.

When the inequality given by Eq. (3.16) holds in the entire half space,

$$\left[\frac{d\sigma}{dt}\right]_{\sigma>0} < 0 < \left[\frac{d\sigma}{dt}\right]_{\sigma<0}$$

it provides a sufficient condition that the system will reach the sliding hypersurface.

A direct consequence of the above result, when applied to relay control VSS, leads to the following simple test for reaching conditions for sliding mode.

Theorem:

Let

$$\dot{x} = f(x,t,u) \; ; \quad x \in R^n \; ; \quad f \in F^n \; ; \quad u \in R^m.$$

$$u_i = \begin{cases} u_i^+ & \text{for} \quad S_i(x) > 0 \\ u_i^- & \text{for} \quad S_i(x) < 0 \end{cases}$$

be a general VSS made up of stable substructures. Let the set $\{x^{i+}\}$

and the set $\{x^{i-}\}$ be the set of steady state RPs corresponding to the inputs u^{i+} and u^{i-}, where

$$u^{i+} = [u_1 \ . \ . \ u_i^+ \ . \ u_m]^T$$

$$u^{i-} = [u_1 \ . \ . \ u_i^- \ . \ u_m]^T$$

Then a sufficient condition for reaching of the sliding regime is given by

$$\begin{aligned} x^{i+} &\in S_i(x)<0 \\ x^{i-} &\in S_i(x)>0 \end{aligned} \qquad \text{for } \textit{all } i = 1,2, \quad ,m$$

Proof:

The number of control inputs is m. Therefore the sets $\{x^{i+}\}$ and $\{x^{i-}\}$ each consists of 2^{m-1} elements, each of which represents a steady state operating point in the n dimensional state space. Consider an element of the set $\{x^{i+}\}$.

$$x^{i+} \in S_i(x) < 0$$

Therefore

$$u_i = u_i^- \quad ; \quad S_i(x^{i+}) = -K$$

K is a positive real number. Under this control input the steady state operating point is x^{i-}.

$$\lim_{t \to T} S_i(x) = S_i(x^{i-}) = M$$

M is a positive real number, and T is the settling time.

$$\left[\frac{dS_i(x)}{dt}\right]_{average} = \frac{M+K}{T} > 0$$

$$\left[\frac{dS_i(x)}{dt}\right]_{S_i(x)<0} > 0$$

In a similar way starting from any point x^{i-}, we get

$$\left[\frac{dS_i(x)}{dt}\right]_{S_i(x)>0} < 0$$

The above theorem may be stated in words as follows. If the steady state operating point of a substructure effective in any region of the state space in a VSS does not belong to the same region in the state space, then the system RP eventually reaches the switching boundary. The existence of sliding mode may then be examined by studying the state velocity vectors in the neighborhood of the sliding surface.

Having seen the existence and reaching conditions of sliding regimes in VSS, the next focus of interest in the analysis of VSS is, the behavior of the system operating in a sliding regime. The next section deals with this aspect of VSS.

3.5 Equivalent Control

Equivalent control is an analytical tool of VSS theory to study the behaviour of the system under sliding mode control. The method is due to Utkin [2] and is described first for a general case and then applied for a variety of particular classes of VSS.

Consider the general dynamic VSS,

$$\dot{x} = f(x,t,u) \; ; \quad x \in R^n \; ; \quad f \in F^n \; ; \quad u \in R^m. \tag{3.18a}$$

$$u_i = \begin{cases} u_i^+(x,t) & \text{for} \quad S_i(x) > 0 \\ u_i^-(x,t) & \text{for} \quad S_i(x) < 0 \end{cases} \qquad i = 1,2, \quad ,m \tag{3.18b}$$

The control inputs u_i^+, u_i^-, f and the system states are all continuous functions of time. The individual switching boundaries defining the structure-control laws are all continuous functions of the system states. The sliding regime is on the hypersurface $\sigma = 0$, which is the intersection of all the individual switching boundaries.

$$\sigma = 0 = [S_1 \quad S_2 \qquad S_m]^T \tag{3.19}$$

Away from the sliding hypersurface $\sigma = 0$, the equations of motion of the RP of the system are well defined and continuous. On the switching boundaries the control inputs u_i undergo discontinuity and the equations of motion of the RP given by Eq. (3.18a) are undefined. When sliding regime exists, the system RP eventually reaches the switching hypersurface $\sigma = 0$ and hence the equation of motion of the RP as given by Eq. (3.18a) is undefined and cannot be of any help in studying the behavior of the system under sliding mode control. An alternative method is then required to define the equations of motion of the system, in terms of the equations of motion away from the discontinuity surfaces and the equations of the discontiuity surfaces themselves. The formal method of achieving this objective is the equivalent control method.

The application of equivalent control method is as follows. Time derivatives of the switching functions $S_i(x)$ are determined using Eq. (3.18). Under ideal sliding mode the system RP stays on the sliding hypersurface $\sigma = 0$ and hence the time derivatives of $S_i(x)$ are zero. This fact is used along with Eq. (3.18) to solve for the components of the control vector. The vector thus obtained is called equivalent control u_{eq}. This equivalent control vector u_{eq} is then substituted into Eq. (3.18a) to obtain the equations of motion of the system under ideal sliding mode. In the case of real sliding mode, the RP makes oscillatory motion about the switching hypersurface in a small but finite neighborhood of the sliding hypersurface. This difference between ideal sliding mode and real sliding mode arises out of nonidealities in the switching hardware such as hysteresis, delay, etc. These nonidealities are ignored for the moment. These nonidealities and their effect on the ideal sliding motion are discussed in Section 3.5.5. In the following sections the method of equivalent control are applied to a few particular classes of VSS.

3.5.1 Linear Systems with Scalar Control

We consider here a class of VSS that are linear with a single control input.

$$\dot{x} = A(t)x + b(t)u \tag{3.20}$$

$x \in R^n$; $A(t) \in F^n$ *by* F^n ; $b(t) \in F^n$; $u \in R^1$

$$u = \begin{cases} u^+ & \text{for } S(x) > 0 \\ u^- & \text{for } S(x) < 0 \end{cases}$$

The control is scalar and the switching boundary is given by the following function.

$$S(x) = g.x = [g_1 \quad g_2 \qquad g_n].[x_1 \quad x_2 \qquad x_n]^T$$

Under sliding mode control, the RP of the system eventually moves onto and stays on the switching surface $S(x) = 0$.

$$\frac{dS}{dt} = g.\dot{x} = 0 \tag{3.21}$$

Combining Eq. (3.20) and Eq. (3.21), we get

$$gA + gbu_{eq} = 0$$
$$u_{eq} = -[gb]^{-1}gAx \tag{3.22}$$

Replacing the discontinuous control input u by the equivalent continuous control input u_{eq} in Eq. (3.20), under the assumption that $[gb]^{-1}$ exists, we get

$$\dot{x} = [A - b(gb)^{-1}gA]x = [I - b(gb)^{-1}g]Ax \tag{3.23}$$

The equation of motion of the RP described by Eq. (3.23) is continuous and is the equation of motion of the system under ideal sliding mode control. The rank of $[I - b(gb)^{-1}g]$ is less than full. The equivalent system is therefore of reduced order. This same fact may be seen in the following way. Under sliding mode control the system trajectories stay on the switching boundary $S = 0$ in the state space. $S = gx = 0$ represents a surface of dimension $(n-1)$ in the state space. The system states may be reassigned to give the following equivalent description of the system.

$$\dot{x}_1 = x_2$$
$$\dot{x}_2 = x_3$$
$$\cdot \quad \cdot$$
$$\dot{x}_{n-1} = x_n = -\frac{1}{g_n}(g_1x_1+g_2x_2+ \quad g_{n-1}x_{n-1}) \tag{3.24}$$

Equations (3.23) and (3.24) describe the same system in two different ways and the order of the system is seen to be $(n-1)$ from Eq. (3.24).

3.5.2 Linear system with Vector Control

Consider the linear dynamic system described by

$$\dot{x} = A(t)x+B(t)u \tag{3.25a}$$

$x \in R^n$; $A(t) \in F^n$ by F^n ; $B(t) \in F^n$ by F^m ; $u \in R^n$

$$u = \begin{cases} u_i^+ & \text{for } S_i(x) > 0 \\ u_i^- & \text{for } S_i(x) < 0 \end{cases} \quad i = 1,2, \quad ,m \tag{3.25b}$$

The elements of $A(t)$,$b(t)$ are all continuous functions. u_i^+ and u_i^- are constants away from the switching boundaries $S_i(x) = 0$. The switching boundaries are also continuous functions of the system states. In the vector case the sliding hypersurface is the intersection of the individual switching boundaries. The system RP eventually moves onto and stays on the sliding hypersurface under sliding control. The intersection of the individual switching boundaries is given by,

$$\sigma = 0 = [S_1 \quad S_2 \quad S_m]^T \tag{3.26}$$

Under sliding mode control, the system trajectories stay on the sliding surface and so $d\sigma/dt = 0$.

$$\frac{dS_j}{dt} = \sum_{i=1}^{n} \frac{\partial S_j}{\partial x_i} \frac{dx_i}{dt}$$

$$\frac{d\sigma}{dt} = G\dot{x} = 0 \; ; \quad G = [g_{ij}] \; ; \quad g_{ij} = \frac{\partial S_i}{\partial x_j} \tag{3.27}$$

G is an m by n matrix whose rows are the gradient vectors of $S_i(x)$. Under the assumption that $[GB]^{-1}$ exists Eqs. (3.25a) and (3.27) may be combined to obtain the equivalent control input u_{eq}.

$$GAx + GBu_{eq} = 0$$
$$u_{eq} = -[GB]^{-1}GAx \tag{3.28}$$

Substitution of u_{eq} into Eq. (3.25a) leads to

$$\dot{x} = (I - B[GB]^{-1}G)Ax \tag{3.29}$$

Equation (3.29) describes the system motion under sliding control. The matrix $(I - B[GB]^{-1}G)$ is less than full rank. The system motion is constrained to be on the intersection of the m switching boundaries given by $S_i(x) = 0$. Each of these switching boundaries is an $n-1$ dimensional surface in the state space. Therefore the sliding surface is described by an $n-m$ dimensional surface in the state space. Therefore the equivalent system description is of order $n-m$.

3.5.3 Systems Linear in Control

Equivalent control method is also applicable to systems that may be nonlinear but are linear with respect to control. Consider the dynamic VSS described by

$$\dot{x} = f(x,t) + B(x,t)u$$

$x \in R^n$; $f \in F^n$ by F^n ; $B \in F^n$ by F^m ; $u \in R^m$

$$u = \begin{cases} u_i^+ & \text{for } S_i(x) > 0 \\ u_i^- & \text{for } S_i(x) < 0 \end{cases} \quad i = 1,2, \quad ,m$$

f and B are continuous functions. The individual switching boundaries are continuous functions of the state and are described by $S_i(x) = 0$. The sliding hypersurface is represented by $\sigma = 0$.

$$\sigma = 0 = [S_1 \quad S_2 \qquad S_m]^T$$

Under sliding control,

$$\frac{d\sigma}{dt} = G\dot{x} = 0$$

G is an m by n matrix whose rows are the gradient vectors of $S_i(x)$. When $[GB]^{-1}$ exists, u_{eq} may be computed.

$$Gf + GBu_{eq} = 0$$
$$u_{eq} = -[GB]^{-1}Gf$$

The continuous equivalent system under sliding control is given by

$$\dot{x} = (I - B[GB]^{-1}G)f$$

As before, the overall system dynamics are determined by the nature of the sliding hypersurface and is independent of the parameters of the substructures. The equivalent control input u_{eq} is also independent of the individual control inputs u^+ and u^- for the class of systems that are linear in control.

3.5.4 Nonlinear Systems

Consider the general system

$$\dot{x} = f(x,t,u) \tag{3.30a}$$

$$u = \begin{cases} u_i^+ & \text{for } S_i(x) > 0 \\ u_i^- & \text{for } S_i(x) < 0 \end{cases} \quad i = 1,2, \quad ,m \tag{3.30b}$$

Equation (3.30a) may be put in the following form.

$$\dot{x} = f^+ + u^\circ (f^- - f^+)$$

$$u^\circ = \begin{cases} 0 & \text{for } \sigma(x) > 0 \\ 1 & \text{for } \sigma(x) < 0 \end{cases}$$

u° is a new control function also having discontinuities on the sliding hypersurface. f^+ and f^- are the state velocity vectors on either side of the sliding hypersurface. Finding such a decomposition is always possible when u_i^+ and u_i^- are constants [2]. In other words for relay control systems the state equations can always be manipulated and expressed linear in control. With respect to u° equivalent control method can be conveniently applied.

3.5.5 Physical Meaning of Equivalent Control

It was assumed that in ideal sliding mode control, the control u_i is capable of changing at an infinite rate and that the system RP stays always on the sliding hypersurface. In the ideal case the system trajectories are always directed along the sliding surface. In reality the hardware used to realize sliding control (finite switching time of the switches used, hysteresis involved in sensing

the crossover of switching boundaries), introduces nonidealities such as hysteresis and delay in the real sliding motion. As a result in a real sliding control, the control inputs change at a finite rate alternately taking on the values u_i^+ and u_i^-, and the system RP stays in a finite Δ vicinity of the sliding surface.

$$\|\sigma\| \leq \Delta$$

Consider the general system linear with respect to control.

$$\dot{x} = f(x,t) + B(x,t)\mathcal{U}$$

where $\mathcal{U}$ is the discontinuous control input which keeps the system motion within a Δ vicinity of the ideal sliding surface.

$$\dot{\sigma} = Gf + GB\mathcal{U}$$
$$\mathcal{U} = -[GB]^{-1}Gf + [GB]^{-1}\dot{\sigma}$$

As before G is an m *by* n matrix whose rows are the gradient vectors of $S_i(x)$ and $[GB]^{-1}$ exists.

$$\mathcal{U} = u_{eq} + [GB]^{-1}\dot{\sigma}$$

What is known about $\mathcal{U}$ is that it keeps the system RP in a finite Δ vicinity of the ideal sliding surface, and that as the nonidealities tend to zero, Δ vanishes. The system motion is forever bounded within the Δ vicinity of $\sigma = 0$. Therefore the average value of $\dot{\sigma} = 0$. Taking averages

$$\mathcal{U}_{ave} = [u_{eq}]_{ave}$$

Thus physically the equivalent control input is the average value of the input control signal, continuous or discontinuous, that will maintain the system on the sliding surface. Alternatively it may be

viewed as a fictitious continuous input which will keep the system, with initial conditions on the sliding surface, to remain on the sliding surface.

3.6 Stability of Motion in the Sliding Regime

The final step involved in the analysis of VSS is the stability of the system in sliding mode. This step is much simpler than one would imagine. The existence of sliding regime and the condition for reaching the sliding regime guarantee that the system motion is confined to remain on the sliding surface. As a result the answer to the stability question rests solely on the nature of the trajectories on the sliding surface. If the phase trajectories on the sliding surface all converge to a unique steady state operating point, then the system is stable. The sliding surface is normally expressed as a linear combination of the states being equal to zero. The obvious advantage then is the ability to apply the theory of linear differential equations to study the stability of the trajectories on the sliding surface.

3.7 Design Methods

The design process in VSS consists of two steps. The first step is to select appropriate switching boundaries in the state space. The system motion under sliding control is at all times on the sliding surface, and consequently the overall system dynamics is dictated by the nature of the switching boundaries employed in the structure-control law. The criteria in selecting the switching boundaries are

that the trajectories on the sliding hypersurface must converge to the desired operating point, and that transients in the course of reaching the operating point must satisfy the requirements of overshoot and settling time in the various states. The second step in design is to select appropriate substructures active in the various regions of the state space defined by the switching boundaries. This selection is done in order to satisfy the conditions for the existence and reaching of the sliding mode.

The switching boundaries are usually selected as one given by $S_i = 0$, where S_i is a linear combination of the states of the system. The reason for this choice is two-fold. It enables analytic solution to the overall system behavior through the application of equivalent control method. Besides, since stability involves essentially the study of the stability of the trajectories on the sliding surface, it enables the application of linear system theory for the study of stability. The state assignment to a system is not unique. It is seen in subsequent sections that the desirable state assignment is the output error and its derivatives. These states are called the controllable states or phase variable states. Then the desired operating point is the origin in the state space and the stability study reduces to output zeroeing problem. The second aspect of design, namely the selection of control inputs to satisfy the existence, and reaching conditions of sliding mode, is achieved through the application of the inequalities stated in Section 3.2.

3.7.1 Transformations in State Space

It was mentioned that the desirable way of assigning states in VSS is output error and its successive derivatives. This desirable assignment is not always feasible, the reason being discontinuous control as in the case of VSS invariably leads to discontinuities in the higher order derivatives of the output. Besides, all higher order derivatives of output may not be physically accessible for measurement in the system. In such instances, it is necessary to define the system through alternative states which are continuous and accessible. The switching boundaries also then necessarily have to be a linear combination of these physical states. It was seen in Section 3.5, that the method of equivalent control provides an equivalent continuous system description. This property is used to transform the actual sliding equations in physical coordinates into a fictitious continuous system states of output error and its successive derivatives. Such a transformation enables simple stability analysis even though the actual sliding surfaces are defined through the physical states of the system.

Consider the system

$$\dot{y} = f(y,t) + B(y,t)u$$

$$u_i = \begin{cases} u_i^+ & \text{for } S_i(y) > 0 \\ u_i^- & \text{for } S_i(y) < 0 \end{cases} \qquad i = 1,2, \quad ,m$$

$$\sigma = 0 = [S_1 \quad S_2 \qquad S_m]^T = Gy$$

G is an m by n matrix whose rows are the gradient vectors of $S_i(y)$. Under sliding mode control applying equivalent control, we get

$$\dot{y} = (I - B[GB]^{-1}G)f \tag{3.31}$$

Equation (3.31) represents an equivalent continuous system and may be used to obtain the relationship between the physical states and the phase variable states.

$$y = \Omega(x,t)x$$

The sliding equation may now be transformed to phase variable form.

$$\sigma = Gy = [G\Omega]x = G^*x \tag{3.32}$$

The system motion is now given by $G^*x = 0$. The sliding equation is now in terms of output error and its successive derivatives, and hence the study of stability is simpler than otherwise. However, Eq. (3.32) is in general nonlinear and dependent on the system parameters implicitly through the transformation matrix $\Omega(x,t)$. In the following sections the design methods for a few particular classes of VSS are indicated.

3.7.2 Linear Systems with Scalar Control

We consider now a limited class of VSS, which is linear, with single input, and which may be expressed in the phase variable canonical form.

$$\dot{x} = A(t)x + bu \; ; \quad x = \left[x_0 \quad \frac{dx_0}{dt} \quad \frac{d^{n-2}x_0}{dt^{n-2}} \quad \frac{d^{n-1}x_0}{dt^{n-1}}\right]^T$$

(3.33a)

$$u = \begin{cases} u^+ & \text{for} S(x) > 0 \\ u^- & \text{for} S(x) < 0 \end{cases} \tag{3.33b}$$

The system states are defined as the output error and its successive derivatives. It is also known that the system order being n and number of controls being 1, it is possible to obtain an overall system response of order $n-1$ under sliding control. The steady state and dynamic requirements may be expressed as a homogeneous differential equation of order $n-1$, whose eigenvalues are the desired eigenvalues of the overall system. Let

$$\sigma = g_{n-1}\frac{d^{n-1}x_0}{dt^{n-1}} + \ . \ + \ . \ + g_1\frac{dx_0}{dt} + x_0 = gx = 0 \tag{3.34}$$

The steady state solution of Eq. (3.34) is $x_0 = 0$, leading to output error being zero under steady state. The transient response during error recovery depends on the eigenvalues of Eq. (3.34). In this class of VSS the system dynamics are entirely determined by the eigenvalues of the switching boundary $\sigma = 0$ and are totally independent of the system parameters.

The condition for the existence of sliding regime is

$$\lim_{\sigma=0^+} \dot{\sigma} < 0 < \lim_{\sigma=0^-} \dot{\sigma}$$

$$\lim_{\sigma=0^+} gAx + gbu^+ < 0 < \lim_{\sigma=0^-} gAx + gbu^-$$

The condition for reaching the sliding regime is given by

$$\lim_{\sigma>0} \dot{\sigma} < 0 < \lim_{\sigma<0} \dot{\sigma}$$

$$gAx + gbu^{+} < 0 < gAx + gbu^{-}$$

3.7.3 Systems Linear in Scalar Control

The class of system described here is linear in control. The system states are output error and other continuous, physically accessible variables in the system.

$$\dot{y} = f(y,t) + bu \; ; \; y = [y_0 \;\; y_1 \;\; \cdots \;\; y_{n-2} \;\; y_{n-1}]^T \tag{3.35a}$$

$$u = \begin{cases} u^{+} & \text{for} S(y) > 0 \\ u^{-} & \text{for} S(y) < 0 \end{cases} \tag{3.35b}$$

As before, the desired system response may be expressed as a differential equation of order $n-1$. Let

$$\sigma(y) = g_{n-1}y_{n-1} + \cdots + g_1 y_1 + y_0 = gy = 0 \tag{3.36}$$

Under sliding mode control, applying equivalent control method

$$\dot{y} = [I - b(gb)^{-1}g]f \tag{3.37}$$

From Eq. (3.37) the relationship between the physical states and the output and its derivatives are computed.

$$y = \Omega x \; ; \; x = [\, y_0 \;\; \frac{dy_0}{dt} \;\; \frac{d^{n-1}y_0}{dt^{n-1}} \,]^T \tag{3.38}$$

where x represents the vector whose elements are output error and its derivatives. The sliding equation in the phase variable form is now given by,

$$\sigma(x) = g\Omega x = 0 \tag{3.39}$$

Equation (3.39) determines the stability of the trajectories on the sliding surface. The condition for reaching the sliding regime is,

$$gf + gbu^+ < 0 < gf + gbu^-$$

3.7.4 Systems Linear in Vector Control

In the case of vector control of a system of order n with m control inputs, it was seen that under sliding control the overall system order may be reduced to one of order $n-m$. As a result the dynamic requirements of the overall system may be represented by a differential equation of order $n-m$. This requirement of $\sigma(x) = 0$ (of order $n-m$) may be written down as the intersection of m sliding surfaces $S_i(x) = 0$ each of order $n-1$. Therefore, to begin with we see that there is freedom available in selecting the m individual switching boundaries in order to achieve the same overall response. Let the sliding hypersurface be

$$\sigma(x) = 0 = [S_1 \quad S_2 \qquad S_m]^T = Gx$$

G is the m *by* n matrix whose rows are the gradient vectors of the individual switching functions. The only condition in synthesizing G is that the intersection of the various switching boundaries is the sliding hypersurface $\sigma = 0$ of dimension $n-m$. In the vector case there is no general method that can be used to solve the second aspect of the design process, namely selecting u_i^+ and u_i^- to satisfy the requirement of reaching the sliding regime. Of a few methods that exist, the simplest and most useful method is the diagonalization

method. It consists of transforming the original set of inputs u into a new set of inputs u^* such that the individual components decouple the motion of the system with respect to one of the switching boundaries.

Consider

$$\dot{x} = f(x,t) + B(t)u$$

Let the original set of inputs u be transformed to u^*.

$$u^* = Q^{-1}[GB]u$$

where Q is an arbitrary diagonal m by m matrix and $[GB]^{-1}$ exists.

$$\dot{x} = f(x,t) + B[GB]^{-1}Qu^*$$
$$\dot{\sigma} = Gf + Qu^*$$

Q being a diagonal matrix, the motion with respect to each of the surfaces, is coupled only to the respective inputs. The control law then is chosen as

$$u_i^* = \begin{cases} u_i^+ & \text{for } S_i(x) > 0 \\ u_i^- & \text{for } S_i(x) < 0 \end{cases}$$

In the case of relay control systems, where u^+ and u^- are constrained to be constants, the diagonalization method is applicable when B is a constant matrix [1].

The condition for the reaching of the sliding regime turns out to be m decoupled conditions as a result of the diagonalization.

$$q_{ii}u_i^+ < -\,grad\ S_i(x)f(x,t) < q_{ii}u_i^-$$

where q_{ii} is the i^{th} diagonal element of Q.

3.8 State Estimation

Another area of application of the sliding mode control is state estimation in systems. It was seen in the design of sliding mode control that, the robustness of the response against parameter uncertainties is available only when the states are assigned to be the output error and its successive derivatives (the controllable states), and the sliding surfaces are designed to be a linear combination of these states. This important advantage of sliding modes is lost whenever the state assignment is other than the output error and its derivatives. In those instances a need arises to estimate the controllable states of the system when they are not directly accessible in the plant. Besides, in many physical systems only a few of the states are available for convenient measurement. In linear control theory there exists a method of designing observers to reconstruct all the states of the system from the available states and inputs [7]. Similar to these observers in linear control, sliding mode principles may be used to reconstruct the system states from the inputs, and other available states. Unlike linear observers, sliding mode observers may be applied to nonlinear systems as well, the only constraint being the plant observed is itself stable.

It was mentioned in Section 3.2 that under sliding mode control, the overall response of an n^{th} order system with m control inputs will be of order $n-m$. A particular case of interest in case of state estimation is a first order system with one control. The overall response obtainable in this case is of order zero. The sliding surface in this case is of dimension 0. The structure-control law reduces

effectively to bang-bang control. Consider the simple first order system with one control input, where it is required to get an estimate of $\dot{x}$.

$$\dot{y} = u$$

$$u = \begin{cases} -K & \text{for } x-y < 0 \\ +K & \text{for } x-y > 0 \end{cases}$$

The block diagram of the scheme is given in Fig. 3.20. The sliding point is represented by the equation $\sigma = x-y = 0$. Under sliding control, $\sigma = \dot{\sigma} = 0$.

$$\dot{\sigma} = \dot{x}-\dot{y} = 0$$
$$\dot{x} = \dot{y}$$

The equivalent continuous signal u_{eq} represents the average value of $\dot{y}$ and equals $\dot{x}$. u_{eq} may be derived by passing u through a low pass filter. The condition for the existence of sliding mode is given by

$$\dot{\sigma} = \dot{x}-\dot{y} = \dot{x}-u \begin{cases} < 0 & \text{for } \sigma > 0 \\ > 0 & \text{for } \sigma < 0 \end{cases}$$

$$k > |\dot{x}|$$

The nonideality of hysteresis in the comparator makes, in the real sliding control, the switching frequency to be finite. The low pass filter corner frequency is decided by the switching frequency. Therefore, the useful range of frequencies up to those for which satisfactory estimation of $\dot{x}$ may be done, depends on the filter corner and in turn on the nonidealities in the comparator. With high slew rate integrators and fast switching comparators, such state estimation circuits may be cascaded to obtain estimates of higher

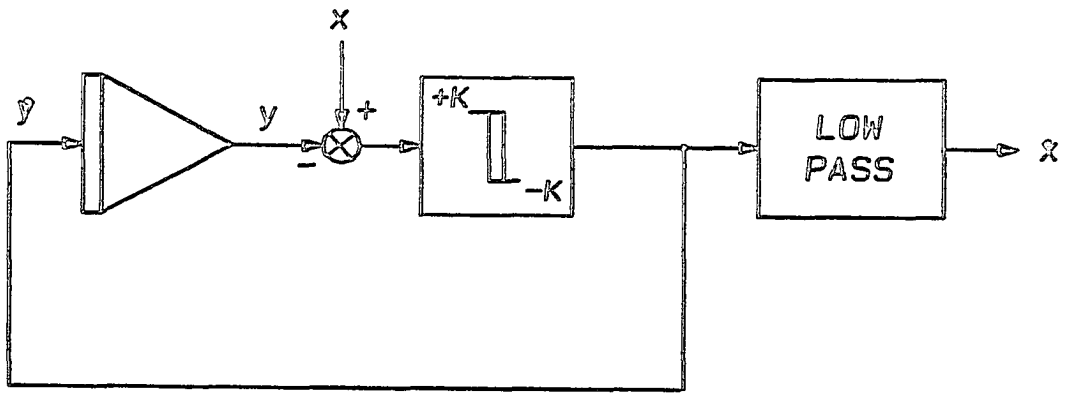

Fig. 3.20 A phase variable state estimator employing sliding mode control. The output from the low-pass filter is an estimate of the derivative of the input x.

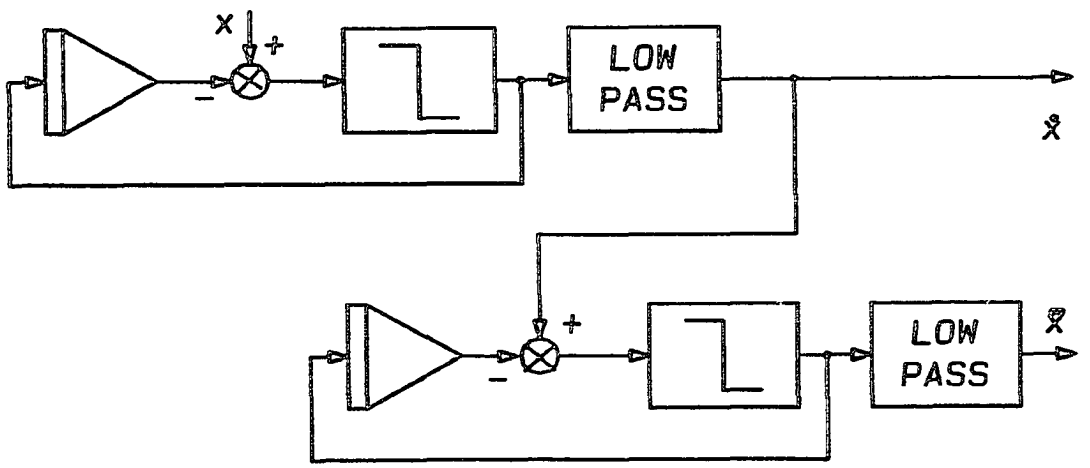

Fig. 3.21 A cascaded phase variable state estimator to obtain the first and second derivative of the input function x.

derivatives of x as well. It must be mentioned that the finite switching frequency of practical circuits causes considerable deterioration in the useful bandwidth of such estimators. Figure 3.21 shows two such circuits cascaded to obtain estimates of $\dot{x}$ and $\ddot{x}$.

3.9 Static Optimization

It was mentioned in Chapter 2 that in all power converters one of the major concerns is to process power with minimum losses within the converter. This is normally done by avoiding dissipative elements in the converter, and by using near ideal reactive elements, and switches. In practical power converters, power dissipation due to the nonideal nature of the reactive elements is inevitable. One of the questions that arise in this context is, whether one is able to select the operating point of the converter to minimize the losses within the converter. This is essentially a static optimization problem. It was also seen that, in sliding mode control, the dynamic response obtainable depends upon the order of the substructures used and the number of control inputs available. Clearly one can foresee applications where more controls are available than are required to achieve the dynamic requirements of the system. In these instances, the extra controls available may be used to achieve optimization of the operating point of the system. Or static optimization could also be a stand-alone application of sliding control.

We illustrate here the simple example of a one dimensional optimization problem. Consider the plant input x and the performance function $f(x)$ which is to be minimized. The plant is

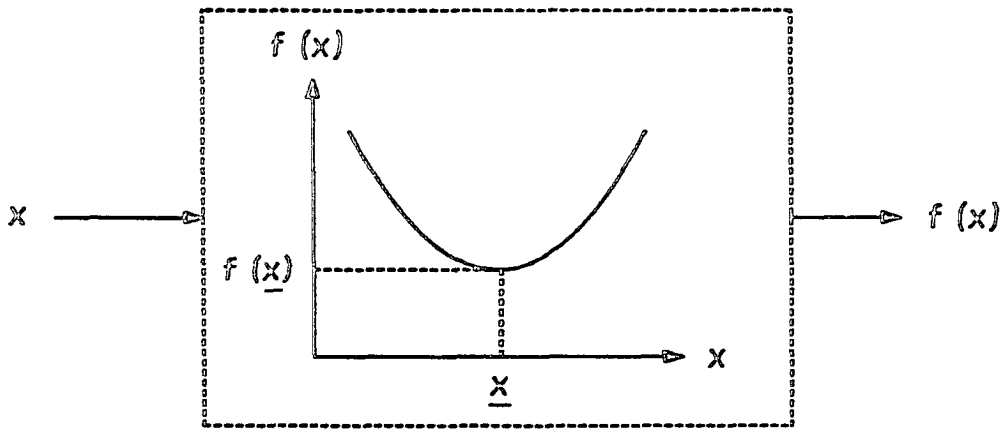

Fig. 3.22 The relationship between the plant input and the performance index $f(x)$ of a plant. Sliding mode control can be used to minimize (or maximize) the performance index in such plants.

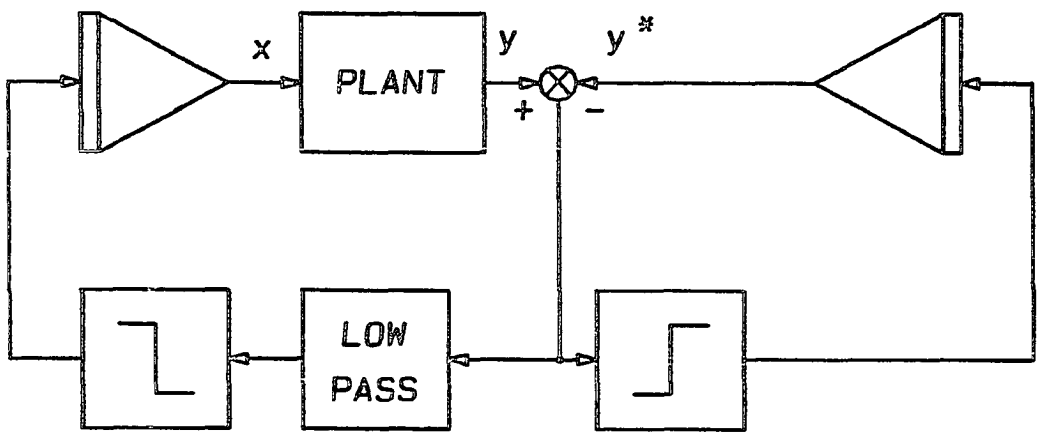

Fig. 3.23 Sliding mode controller to minimize the performance index $f(x)$ of the plant shown in Fig. 3.22.

shown in Fig. 3.22. The control objective is to drive the parameter x, that is input to the plant, such that $f(x)$ is minimized.

$$y = f(x) \; ; \; [f(x)]_{min} = f(\underline{x})$$

Suppose that there are no local minimums and that $f(x)$ on either side of $\underline{x}$ is a monotonically increasing function. The principle involved is an extension of the estimation of the derivative of $f(x)$. The sliding mode controller to achieve this objective is shown in Fig. 3.23. The input x is supplied with a time varying function. $\dot{f}(x)$ is estimated. The polarity of $\dot{f}(x)$ is the switching boundary which decides the rate of change of the input variable x.

CHAPTER 4

DC-TO-DC CONVERTERS

A major area of application of electrical power processing is the conversion of power from one voltage level to another. In the case of ac power, conversion from one voltage level to another is done efficiently with transformers. The transformer consists of two windings – a primary and a secondary – electrically isolated from each other, and magnetically coupled to each other through a common magnetic circuit. The primary, excited by the ac source, sets up an ac flux in the magnetic circuit. The secondary winding linked to the common magnetic circuit experiences an induced electromotive force (emf) across it, which is used to power the load connected to the secondary. The primary emf and the secondary emf are related to each other by the ratio of the respective number of turns. Conversion from one voltage level to another is achieved by suitable turns ratio between the primary and the secondary windings. Ideally the transformer is lossless. Electromagnetic voltage conversion depends on the rate of change of intermediate magnetic flux, and is not applicable for dc voltage conversion.

Efficient dc-to-dc power conversion is done by switched mode power converters. As has been explained in Chapter 2, such switched mode power converters consist of reactive elements and

switches. The principle employed is to alternately draw energy from the source to charge up reactive (energy storage) elements, such as capacitors and inductors, and then to deliver the stored energy to the load. When the frequency of such energy packets delivered to the load is large, the load experiences practically uninterrupted dc power. Satisfactory operation of such converters depends on suitable configuration of reactive elements, and appropriate method of controlling the switches to obtain efficient power conversion.

Switched mode dc-todc converters are nonlinear and time variant systems, and do not lend themselves to the application of linear control theory. In the past, the method of state space averaging had been successfully applied to characterize dc-to-dc converters [3]. The basic converter topologies and the method of state space averaging, leading to small signal transfer function description of dc-to-dc converters, are reviewed in Section 4.1. The variable structure system (VSS) description of the dc-to-dc converters, explained in Section 4.2, is an alternative method of characterizing the dc-to-dc converters in the time domain. The control problem associated with the dc-to-dc converters is also presented in the same Section.

Equivalent control method of analysis of VSS provides a simple equivalent description of switched mode converters under sliding mode control. In Section 4.3 duty ratio controlled dc-to-dc converters are described in the sliding mode control format. The equivalent control method is then applied to obtain small signal models. It is shown that the equivalent control method and the state

space averaging method of analysis both, though they follow different mathematical formalism, arrive at essentially the same low frequency characterization of the converters. One of the design methods, namely transfer function description and classical control concepts such as loop-shaping, opens up to solve the control problem then onwards.

In chapter 3, it was mentioned that the most important feature of VSS is the ability to achieve responses that are independent of the system parameters through the application of sliding regimes. It is therefore more fruitful to apply the concept of sliding regimes to the control problem of dc-to-dc converters, in contrast to the transfer function characterization and frequency domain design techniques. The buck dc-to-dc converter is ideally suited for this application, since its controllable states (output and its derivative) are all continuous and accessible for measurement. The application of sliding mode control is explained in Section 4.4. The conditions for the existence and reaching of sliding regime are derived. Suitable protection features needed for practical converters are indicated alongwith the design criterion. The design method used for the buck dc-to-dc converters is not applicable to boost and buck-boost converters. Section 4.4 also indicates the features associated with boost and buck-boost converters leading to the difficulties.

An alternative method of control of all three dc-to-dc converters is the control of the inductor current. Section 4.5 describes the current controlled dc-to-dc converters. Application of

equivalent control leads to the small signal description, as well as time domain relationship between the inductor current and the controllable states of the converters (output voltage and its time derivative). Equipped with the relationship between the inductor current and the output voltage, it becomes possible to set up the sliding mode control to all the converters in terms of physical, continuous states of the system, namely the inductor current and the output voltage. Section 4.6 illustrates this method exhaustively for the example of a boost converter. Conditions for the existence and reaching of sliding mode, small signal and large signal stability are established. Practical considerations and design criterion are highlighted and test results for the boost dc-to-dc converter are presented. Similar design criteria for the buck and the buck-boost converters are presented.

4.1 Dc-to-Dc Converter topologies

In this section, the different power converter topologies and their operation are briefly reviewed. For simplicity the operation is shown with constant switching frequency. Figure 4.1 shows the basic power converters and their inductor current waveforms. Each of the above converters consists of one inductor (L), one capacitor (C), and a single pole double throw (SPDT) switch. The purpose of the converter is to take in power that is available at the source with a voltage v_g, and to deliver power to the load (R) at a voltage v_0. The SPDT switch is operated at a constant switching frequency ($1/T_s$). During a fraction d (duty ratio) of the switching period, the SPDT

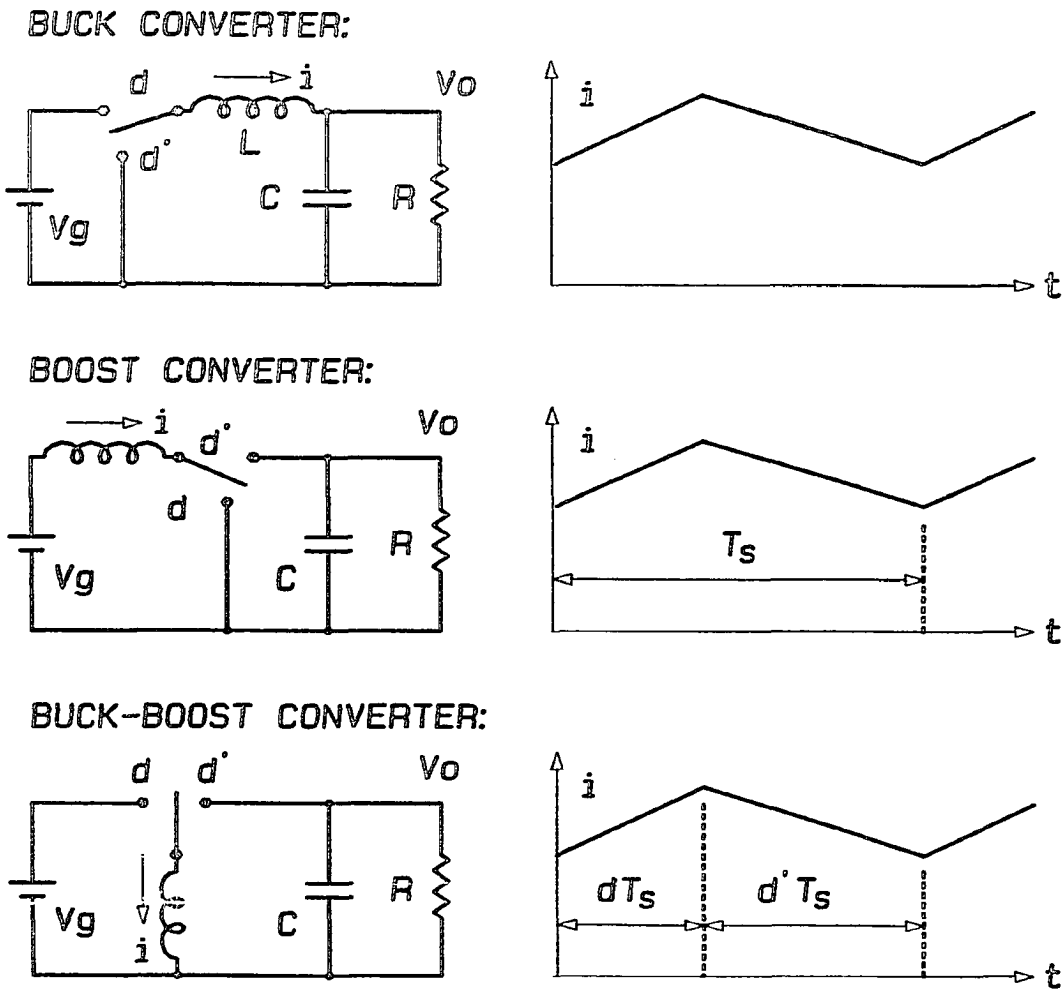

Fig. 4.1 The three basic dc-to-dc converters. During the active period dT_s, energy is drawn from the source (seen from the increasing inductor current). During the nonactive period $d'T_s$, excess energy from the reactive elements is supplied to the load.

switch is thrown to the active position. During this period energy is drawn from the source v_g to charge up the inductor (seen by the rising inductor current). During the fraction d' of the switching period, the switch is thrown to the nonactive position. During this period part of the energy from the inductor is transferred to the capacitor and the load. The active and nonactive period of the switch are complementary to each other ($d = 1-d'$). The average voltage at which power is delivered to the load is a function of the duty ratio (d). The voltage conversion is efficient, since no resistive elements are used in the converter.

4.1.1 Voltage Conversion Ratios

The above converters are named on the basis of the obtainable voltage conversion ratios from each of them. The average voltage conversion ratios for each of the converters may be computed from the fact that, under steady state, the flux (the volt-second integral) in the inductor is conserved from cycle to cycle. The following are the average voltage conversion ratios of the converters.

Buck Converter: $V_0/V_g = D$

Boost Converter: $V_0/V_g = 1/(1-D)$

Buck-Boost Converter: $V_0/V_g = D/(1-D)$

where V_0 is the average load voltage, V_g is the average source voltage and D is the average duty ratio. The buck converter is capable of providing voltage conversion ratios of 0 to 1. The boost converter provides voltage conversion ratios of 1 and above. The

buck-boost converter can give voltage conversion ratios of 0 through 1 and above.

4.1.2 Dynamic Model – State Space Averaging

One of the widely used methods of controlling the output voltage of dc-to-dc converters is by means of closed loop control of the duty ratio (d). In order to design such closed loop controllers, it is necessary to obtain a dynamic model of the duty ratio controlled converters. State space averaging is an analytical method to obtain the dynamic model of the dc-to-dc converters, and is done as follows. The dynamic model (state space description) of the converter in each of the different periods making up the complete switching cycle is written down. The overall dynamic model is then the weighted average of the constituent dynamic models over one complete switching cycle. The weightage factor for each constituent dynamic model is the duration for which the respective circuits are active in each cycle. The method is illustrated here for a two switched network boost converter.

Figure 4.2a shows the boost converter. The two different circuits resulting from the two different positions of the SPDT switch are shown in Fig. 4.2b and 4.2c. The dynamic model of the converter when the switch is in active position ($kT_s < t < (k+d)T_s$) is given by

$$\dot{x} = A_1 x + b_1 v_g \; ; \quad y = c_1^T x$$

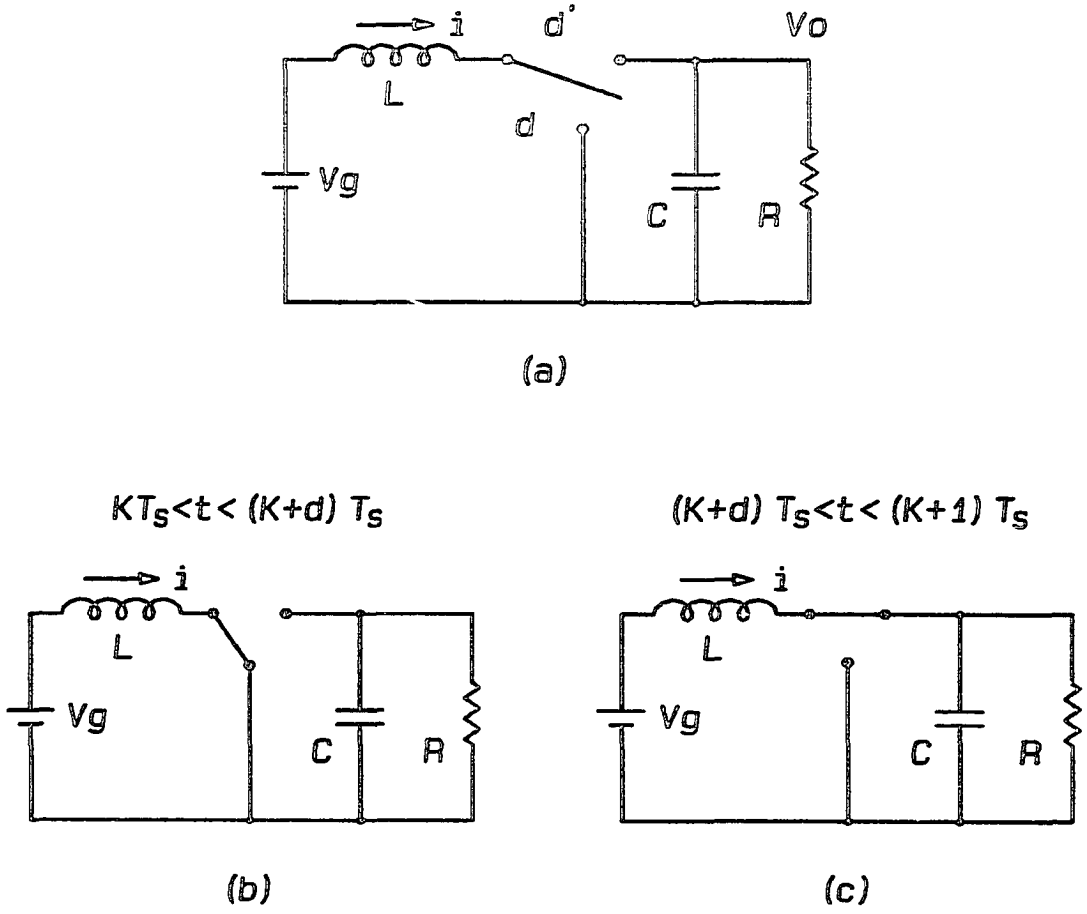

Fig. 4.2 The boost converter (a), and the linear equivalent circuits of the converter during the active period (b) and nonactive period (c).

$$x = \begin{bmatrix} i \\ v_0 \end{bmatrix}; \quad b_1 = \begin{bmatrix} 1/L \\ 0 \end{bmatrix}; \quad A_1 = \begin{bmatrix} 0 & 0 \\ 0 & -1/RC \end{bmatrix}$$

$$y = v_o; \quad c_1 = [0 \quad 1]^T$$

The dynamic model of the converter when the SPDT switch is in the nonactive position $((k+d)T_s < t < (k+1)T_s)$ is given by

$$\dot{x} = A_2 x + b_2 v_g; \quad y = c_2{}^T x$$

$$x = \begin{bmatrix} i \\ v_0 \end{bmatrix}; \quad b_2 = \begin{bmatrix} 1/L \\ 0 \end{bmatrix}; \quad A_2 = \begin{bmatrix} 0 & -1/L \\ 1/C & -1/RC \end{bmatrix}$$

$$y = v_o; \quad c_2 = [0 \quad 1]^T$$

The overall dynamic model is given by

$$\dot{x} = [dA_1 + (1-d)A_2]x + [db_1 + (1-d)b_2]v_g = Ax + bv_g \tag{4.1}$$

$$y = [dc_1 + (1-d)c_2]^T x = c^T x \tag{4.2}$$

Equations (4.1) and (4.2) describe a continuous model of the converter which is equivalent to the duty ratio controlled switching converter.

4.1.3 Transfer Function Description of the System

The averaged dynamic model described by Eq. (4.1) and (4.2) can be applied to any two switched network converters. The control in all such converters is by means of duty ratio modulation. The above dynamic model can be used to find the transfer function description of the converter between output voltage and the duty ratio modulation [3]. Suppose that the duty ratio is $d(t) = D + \hat{d}$,

where D is the steady state duty ratio and $\hat{d}$ is the superimposed perturbation. With the corresponding perturbations $x = X+\hat{x}$, $y = Y+\hat{y}$, and $v_g = V_g+\hat{v}_g$,

$$\dot{X} = AX+bV_g \quad (\textit{Steady state solution})$$

$$\dot{\hat{x}} = A\hat{x}+b\hat{v}_g+[(A_1-A_2)X+(b_1-b_2)V_g]\hat{d}+[(A_1-A_2)\hat{x}+(b_1-b_2)\hat{v}_g]\hat{d}$$
$$\textit{linear terms} \qquad + \qquad \textit{nonlinear terms}$$

$$Y = c^TX \quad \textit{Steady state solution}$$

$$\hat{y} = c^T\hat{x}+(c_1{}^T-c_2{}^T)X\hat{d}+(c_1{}^T-c_2{}^T)\hat{x}\hat{d}$$
$$\textit{linear terms} \quad + \quad \textit{nonlinear terms}$$

Under the assumption that the perturbations are small ($\frac{\hat{v}_g}{V_g} \ll 1$, $\frac{\hat{d}}{D} \ll 1$, $\frac{\hat{x}}{X} \ll 1$), the nonlinear terms may be dropped to obtain,

Steady state model:

$$X = -A^{-1}bV_g \; ; \quad Y = -c^TA^{-1}bV_g$$

Dynamic model:

$$\dot{\hat{x}} = A\hat{x}+b\hat{v}_g+[(A_1-A_2)X+(b_1-b_2)V_g]\hat{d} \tag{4.3}$$

$$\hat{y} = c^T\hat{x}+(c_1{}^T-c_2{}^T)X\hat{d} \tag{4.4}$$

Equations (4.3) and (4.4) represent the small signal dynamic model of the converters, and may be used to obtain the following transfer functions:

$$\frac{\hat{x}(s)}{\hat{v}_g(s)} = (sI-A)^{-1}b \tag{4.5}$$

$$\frac{\hat{y}(s)}{\hat{v}_g(s)} = c^T(sI-A)^{-1}b \tag{4.6}$$

$$\frac{\hat{x}(s)}{\hat{d}(s)} = (sI-A)^{-1}[(A_1-A_2)X+(b_1-b_2)V_g] \tag{4.7}$$

$$\frac{\hat{y}(s)}{\hat{d}(s)} = [c_1{}^T-c_2{}^T]X+c^T(sI-A)^{-1}[(A_1-A_2)X+(b_1-b_2)V_g] \tag{4.8}$$

Equations (4.5) through (4.8) describe the small signal low frequency model of the duty ratio controlled two switched network dc-to-dc converters, in the frequency domain. The various transfer functions for the different converters are given in Table 4.1.

4.2 Dc-to-dc Converters as VSS

In the state space averaging method, the dynamic equations of the system are arrived at by averaging the dynamic equations of the constituent circuits over a complete cycle. The resulting overall system is a continuous equivalent model of the actual converters. In the VSS description of the system, the dynamic equations are written as a single set consisting of some discontinuous switching functions as well. Different values valid for the discontinuous switching variables lead to the different substructures involved in the VSS. In this section, VSS description of the three basic dc-to-dc converters are given. The analysis and design problem associated with the dc-to-dc converters is then indicated.

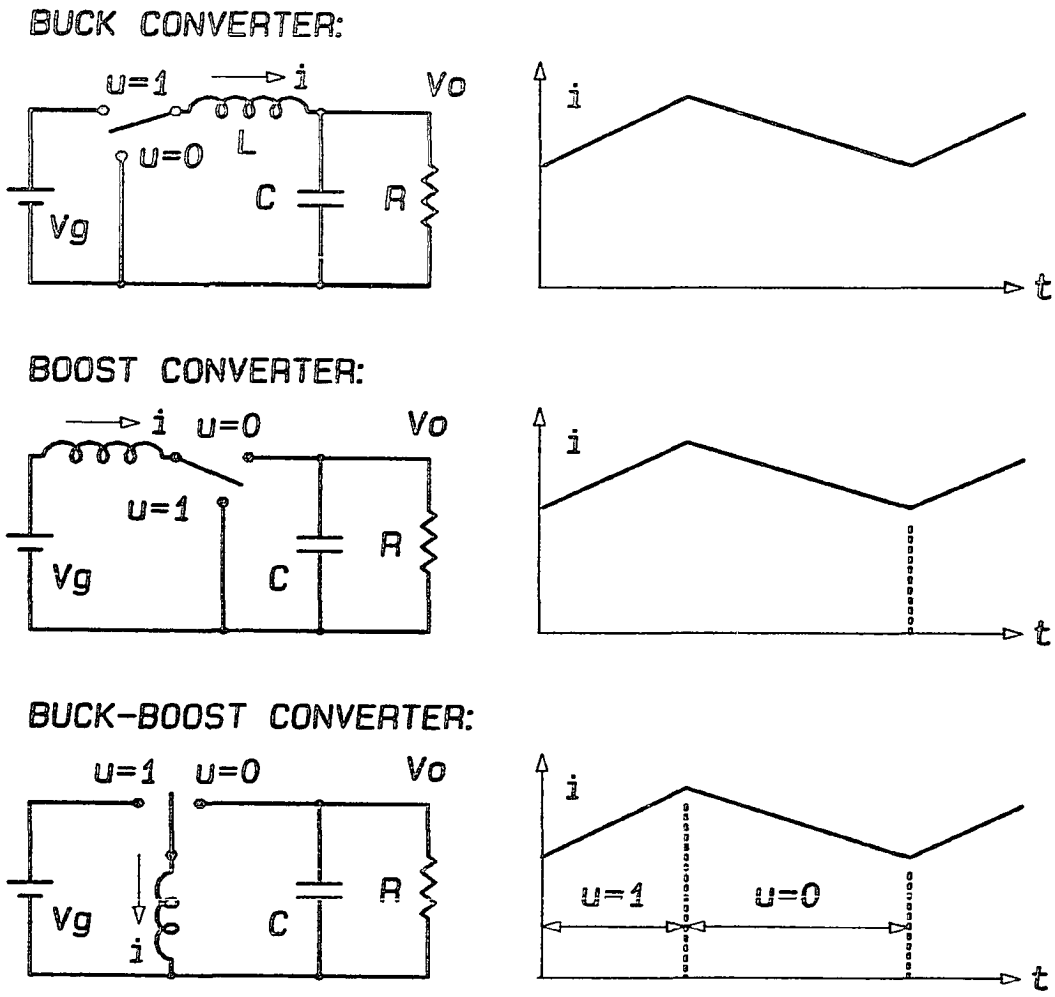

Fig. 4.3 The three basic dc-to-dc converters defined through the switching variable u. During the active and nonactive periods, the switching variable u is assigned values 1 *and* 0 *respectively.*

4.2.1 System Description

Figure 4.3 shows the three basic switching converter topologies and their inductor current waveforms. The switch position defines the switching variable (control input) u as shown in Fig. 4.3. The defining equations of the system may then be written as

Buck converter:

$$L\frac{di}{dt} = v_g u - v_0$$

$$C\frac{dv_0}{dt} = i - \frac{v_0}{R}$$

Boost converter:

$$L\frac{di}{dt} = v_g - v_0\bar{u}$$

$$C\frac{dv_0}{dt} = i\bar{u} - \frac{v_0}{R}$$

Buck-Boost converter:

$$L\frac{di}{dt} = v_g u + v_0\bar{u}$$

$$C\frac{dv_0}{dt} = -i\bar{u} - \frac{v_0}{R}$$

where $\bar{u} = 1-u$. The systems are time variant and discontinuous. But in the above description all the time variance and the discontinuities have been isolated into the single discontinuous control variable u.

4.2.2 Formulation of Control Problem

The description of all the above converters may be expressed in the following compact form.

$$\dot{x} = Ax + bu + c \tag{4.9}$$

where, for

Buck converter:

$$x = \begin{bmatrix} i \\ v_0 \end{bmatrix} ; A = \begin{bmatrix} 0 & -1/L \\ 1/C & -1/RC \end{bmatrix} ; b = \begin{bmatrix} v_g/L \\ 0 \end{bmatrix} ; c = \begin{bmatrix} 0 \\ 0 \end{bmatrix}$$

Boost converter:

$$x = \begin{bmatrix} i \\ v_0 \end{bmatrix} ; A = \begin{bmatrix} 0 & -1/L \\ 1/C & -1/RC \end{bmatrix} ; b = \begin{bmatrix} v_0/L \\ -i/C \end{bmatrix} ; c = \begin{bmatrix} v_g/L \\ 0 \end{bmatrix}$$

Buck-Boost converter:

$$x = \begin{bmatrix} i \\ v_0 \end{bmatrix} ; A = \begin{bmatrix} 0 & 1/L \\ -1/C & -1/RC \end{bmatrix} ; b = \begin{bmatrix} (v_g - v_0)/L \\ i/C \end{bmatrix} ; c = \begin{bmatrix} 0 \\ 0 \end{bmatrix}$$

The system state vector x and the matrices A,b, and c are all continuous.

In the analysis of dc-to-dc converters, the structure of the converter, and the switching variable as a function of time are known. It is required to find the performance of the converter. In the problem of design of dc-to-dc converters, it is required to select a converter topology, and synthesize the control input u to achieve the desired performance. The analysis and design methods of VSS had already been discussed in great detail in Chapter 3. In the following sections, the theory of VSS is applied to analyze the duty ratio

controlled dc-to-dc converters. The design methods for the application of sliding mode control for the different types of converters are then outlined.

4.3 Analysis of Duty Ratio Controlled Converters

One of the most widely used methods of control of the dc-to-dc converters is by means of the duty ratio d. The equivalent control method described in Chapter 3 can be used to find an equivalent low frequency model for such converters. There are two modes of operation possible under duty ratio control, namely Continuous inductor Current Mode (CCM), and Discontinuous inductor Current Mode (DCM).

4.3.1 Continuous Inductor Current Mode (CCM)

The constant frequency duty ratio controlled dc-to-dc converters in CCM were already introduced in Section 4.1 and shown in Fig. 4.1. They were also described as a VSS in Section 4.2.1, through the switching variable u. The SPDT switch in each of the converters operate at constant frequency. The SPDT switch is in the active position ($u=1$) for a fraction d of the switching period. For the rest of the switching period ($d'T_s$) the SPDT switch is in the nonactive ($u=0$) position. The system description of the various converters, in terms of the switching variable u, are given by Eq. (4.9) in Section 4.2.2. The schematic representation of the duty ratio controlled converters is shown in Fig. 4.4a. The control voltage (v_c) is compared to a constant frequency triangular waveform to generate

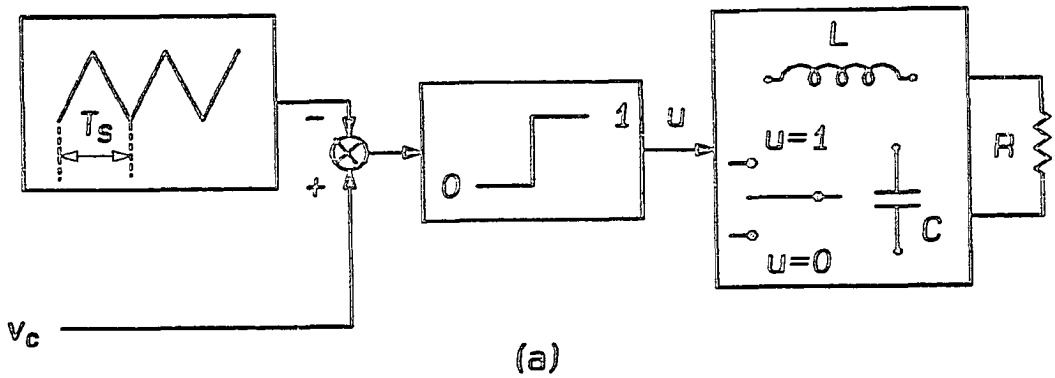

Fig. 4.4a Duty ratio control of switching converters. The control voltage v_c is compared to a constant frequency triangular wave to generate the duty ratio d.

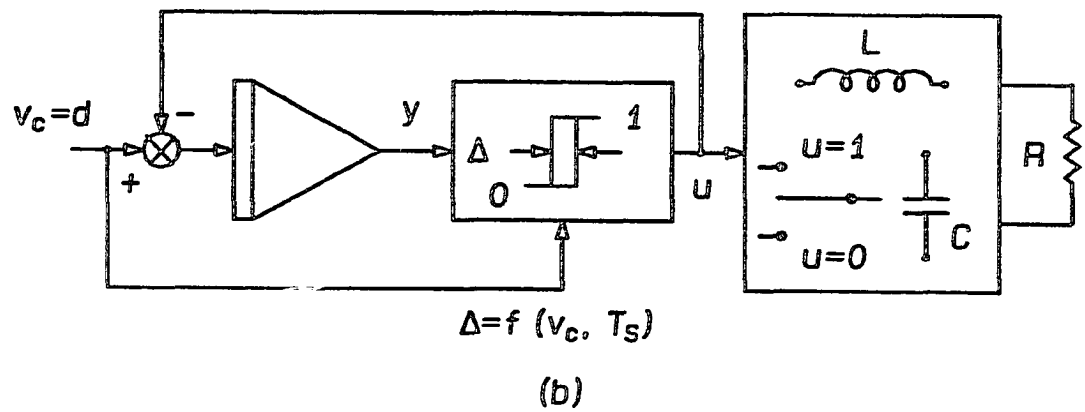

Fig. 4.4b Duty ratio controlled converters as a variable structure system (VSS). The constant frequency triangular wave is replaced by an integrator, and comparator with appropriate feedback. The hysteresis in the comparator is adjusted to obtain constant switching frequency.

the duty ratio d. The same control method is shown by an equivalent scheme in Fig. 4.4b. This equivalent scheme is a mathematical artifice used, in order to be able to apply the principles of sliding mode control for the analysis of duty ratio controlled converters. The equivalent scheme incorporates an integrator and a comparator with hysteresis. The control input is numerically equal to the duty ratio ($0 \leq d = v_c \leq 1$). Suppose that the hysteresis Δ in the comparator is a function of v_c, such that the switching frequency is maintained constant at all duty ratios. It is to be stressed again that the equivalent scheme in Fig. 4.4b is an artificial representation of the constant frequency duty ratio controlled converters, in order to apply the sliding control principles. The dynamic equations of the controller and the converter may now be written as

$$\dot{y} = d - u \tag{4.10}$$

$$\dot{x} = Ax + bu + c \tag{4.11}$$

Equation (4.10) is a scalar equation. Equation (4.11) describes the converter and is of order two. Equations (4.10) and (4.11) may be combined into a single set of a third order system as follows.

$$\begin{bmatrix} \dot{y} \\ \dot{x} \end{bmatrix} = \begin{bmatrix} 0 & 0 \\ 0 & A \end{bmatrix} \begin{bmatrix} y \\ x \end{bmatrix} + \begin{bmatrix} -1 \\ b \end{bmatrix} u + \begin{bmatrix} d \\ c \end{bmatrix} \tag{4.12}$$

The structure-control law is

$$u = \begin{cases} 1 & \text{for } \sigma = y > \Delta \\ 0 & \text{for } \sigma = y < \Delta \end{cases} \tag{4.13}$$

Under ideal sliding mode control, $\sigma = \dot{\sigma} = 0$ and $u_{eq} = d$. The overall

system is of order 3 and the number of control input is 1. As explained in Chapter 3, the equivalent description then is of order 2. By substituting $d = u_{eq}$ in Eq. (4.12) we get an equivalent system description of order 2.

$$\dot{x} = Ax + bd + c \tag{4.14}$$

The above description is exact when the system motion is along the ideal sliding surface ($\Delta = 0$). Finite constant switching frequency implies that $\Delta \neq 0$. As a result the actual system motion consists of nonidealities owing to finite Δ (switching ripple), superimposed on the ideal motion given by Eq. (4.14). When the switching ripple is small, the actual system may be represented by the ideal system within a finite error. This same condition may also be stated as follows: the switching frequency must be sufficiently large compared to the natural frequency of the converter.

Equation (4.14) is in general nonlinear. The only condition imposed so far is that the switching frequency be sufficiently large. Hence Eq. (4.14) may be used to study both the small signal as well as large signal behaviour of the converters. Alternatively Eq. (4.14) may be linearized around the operating point to obtain the transfer function description of the converters. In order to relate the results easily to those obtained by the state space averaging method, Eq. (4.11) may be rewritten as follows.

$$\dot{x} = [A_1 x + b_1 v_g]u + [A_2 x + b_2 v_g](1 - u) \tag{4.15}$$

where A_1, A_2, b_1, b_2 are as defined in Section 4.1.2. Under sliding mode control $u_{eq} = d$ and so Eq. (4.15) reduces to

fn	BUCK CONVERTER	BOOST CONVERTER	BUCK-BOOST CONVERTER
V_0	DV_g	$V_g/(1-D)$	$-V_gD/(1-D)$
I	V_0/R	$V_0/R(1-D)$	$-V_0/R(1-D)$
$\frac{\hat{i}}{\hat{v}_g}$	$\frac{D}{R}\ \frac{1+SCR}{G(S)}$	$\frac{1}{R(1-D)^2}\ \frac{1+SCR}{G(S)}$	$\frac{D}{R(1-D)^2}\ \frac{1+SCR}{G(S)}$
$\frac{\hat{v}_0}{\hat{v}_g}$	$D\ \frac{1}{G(S)}$	$\frac{1}{(1-D)}\ \frac{1}{G(S)}$	$-\frac{D}{(1-D)}\ \frac{1}{G(S)}$
$\frac{\hat{i}}{\hat{d}}$	$\frac{V_0}{RD}\ \frac{1+SCR}{G(S)}$	$\frac{2V_0}{R(1-D)^2}\ \frac{1+SCR/2}{G(S)}$	$\frac{V_0(1+D)}{RD(1-D)^2}\ \frac{1+SCR/(1+D)}{G(S)}$
$\frac{\hat{v}_0}{\hat{d}}$	$\frac{V_0}{D}\ \frac{1}{G(S)}$	$\frac{V_0}{(1-D)}\ \frac{1-SL/R(1-D)^2}{G(S)}$	$\frac{V_0}{D(1-D)}\ \frac{1-SLD/R(1-D)^2}{G(S)}$
$G(S)$	$1+S\frac{L}{R}+S^2LC$	$1+S\frac{L}{R(1-D)^2}+S^2\frac{LC}{(1-D)^2}$	$1+S\frac{L}{R(1-D)^2}+S^2\frac{LC}{(1-D)^2}$

TABLE 4.1 The steady state, and transfer functions of constant frequency duty ratio controlled dc-to-dc converters.

$$\dot{x} = [dA_1 + (1-d)A_2]x + [db_1 + (1-d)b_2]v_g = Ax + b_{v_g} \tag{4.16}$$

Eq. (4.16) is identical to Eq. (4.1) obtained following state space averaging method. Equation (4.16) may be linearized to obtain the small signal transfer functions identical to those obtained (Eq. (4.5) and (4.8)) following the state space averaging method and given in Table 4.1.

4.3.2 Discontinuous Inductor Current Mode (DCM)

Dc-to-dc converters may also be operated in the DCM range of operation. In DCM operation, the inductor current starts from zero in every cycle, goes to zero before the end of the switching period, and restarts from zero at the beginning of the next cycle. Such a mode of operation arises out of the fact that the most inexpensive realization of switches in dc-to-dc converters is by means of unidirectional switches, which are capable of carrying current in only one direction. As a result when the inductor current reaches zero during a part of the switching cycle, the unidirectional switch inhibits reversal of current and blocks. Figure 4.5 shows the basic converters in the DCM range and the corresponding inductor currents. The unidirectional nature of the switch is shown by a diode on the throw arm of the SPDT switches. The dc-to-dc converters in DCM then have three characteristic periods during a cycle – active (u = 1), nonactive (u_2 = 1), and blocking (u' = 1) –. Suppose we define the switching variables as

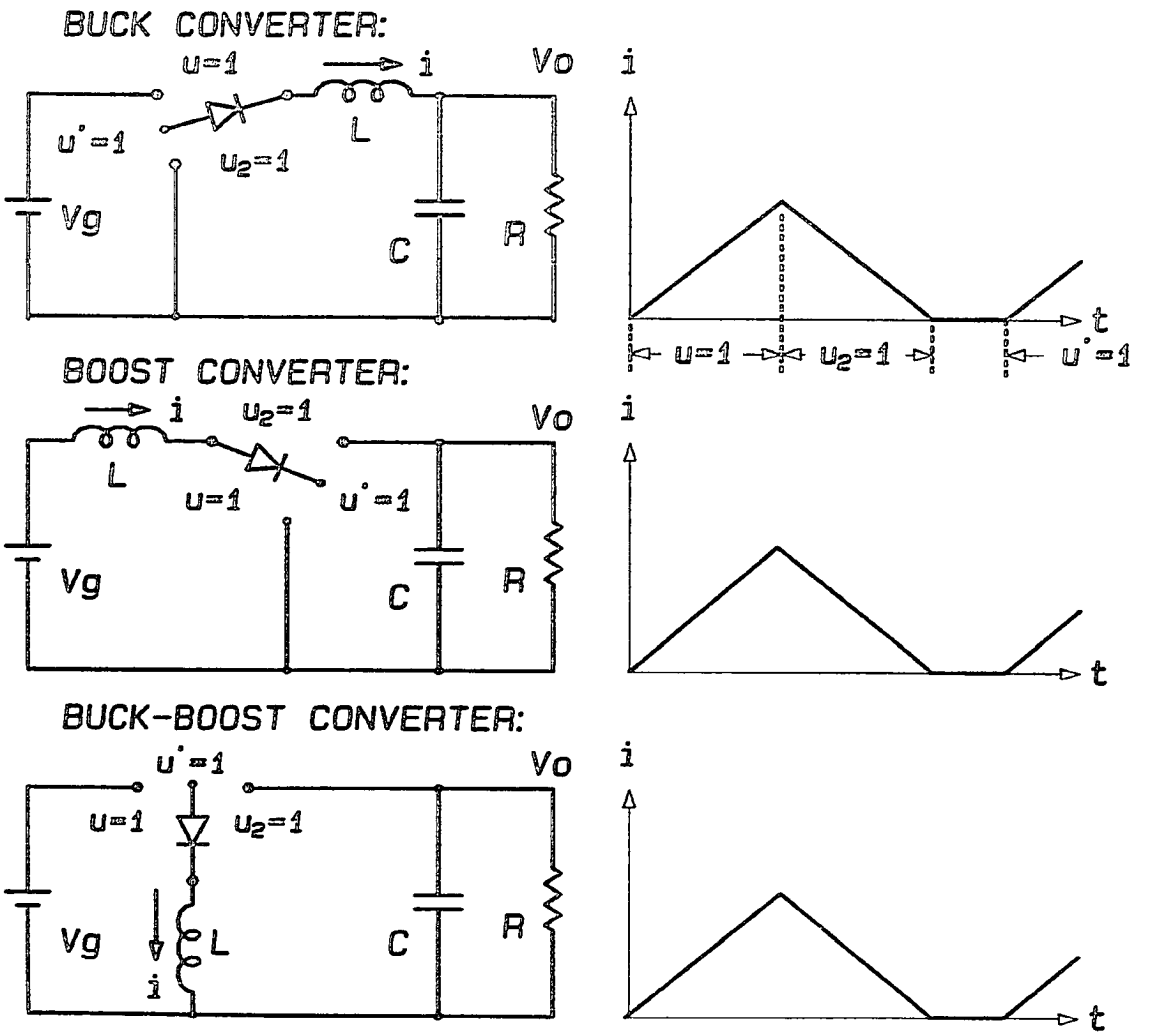

Fig. 4.5 The basic dc-to-dc converters in the Discontinuous Conduction Mode (DCM). The schematic diode in the throw of the SPDT switch indicates the unidirectional nature of the switch. The current in the inductor falls to zero before the end of every cycle.

$$u = \begin{cases} 1 & \text{for} \quad kT_s \le t \le (k+d)T_s \\ 0 & \text{for} \quad (k+d)T_s \le t \le (k+1)T_s \end{cases}$$

$$u_2 = \begin{cases} 0 & \text{for} \quad kT_s \le t \le (k+d)T_s \\ 1 & \text{for} \quad (k+d)T_s \le t \le (k+d+d_2)T_s \\ 0 & \text{for} \quad (k+d+d_2)T_s \le t \le (k+1)T_s \end{cases}$$

$$u' = \begin{cases} 0 & \text{for} \quad kT_s \le t \le \le (k+d+d_2)T_s \\ 1 & \text{for} \quad (k+d+d_2)T_s \le t \le (k+1)T_s \end{cases}$$

$$u + u_2 + u' = 1 \quad \text{for } all \ t$$

The dynamic equations of the system may be written as

$$\dot{x} = A_1 x + b_1 v_g \quad \text{for} \quad u = 1$$
$$\dot{x} = A_2 x + b_2 v_g \quad \text{for} \quad u_2 = 1$$
$$\dot{x} = A_3 x + b_3 v_g \quad \text{for} \quad u' = 1$$

The overall system equations are then given by

$$\dot{x} = [A_1 x + b_1 v_g \quad A_2 x + b_2 v_g \quad A_3 x + b_3 v_g]\underline{u} \tag{4.17}$$

where $\underline{u} = [u \ \ u_2 \ \ u']^T$. The overall system given by Eq. (4.17) is linear with respect to control. The equivalent description is found by replacing the discontinuous switching variables by their average values over a cycle.

$$\dot{x} = [A_1 x + b_1 v_g \quad A_2 x + b_2 v_g \quad A_3 x + b_3 v_g][d \ \ d_2 \ \ d']^T \tag{4.18}$$

The overall dynamic system described by Eq. (4.18) is identical to the system description obtained by the state space averaging method [8]. Although the dynamic equations show up three switching variables d, d_2, d', there is only one independent control input d. The other two input variables d_2 and d' are functions of d, the circuit elements of

the converter and the switching period T_s. The method of obtaining the transfer functions is given in detail in reference [8].

4.3.3 CCM Operation under Variable Switching Frequency

It was seen in Section 4.3.1 that in the case of duty ratio control, the overall system depends on the converter elements and the duty ratio, and independent of the switching frequency; the only restriction on the switching frequency is that it be sufficiently large compared to the natural frequency of the converter. When the switching frequency is constant, state space averaging or the equivalent control method may be used to obtain the transfer function description of the system. This property has been used in the past to independently control two different outputs of a multiple output dc-to-dc converter [9]. When the switching frequency is not constant, duty ratio is not defined and it is not possible to time average the system. However the equivalent control method can very conveniently be used to arrive at the transfer function descriptions. With reference to Fig. 4.4,

$$\dot{y} = v_c - u$$

$$\dot{x} = Ax + bu + c$$

$$\begin{bmatrix} \dot{y} \\ \dot{x} \end{bmatrix} = \begin{bmatrix} 0 & 0 \\ 0 & A \end{bmatrix} \begin{bmatrix} y \\ x \end{bmatrix} + \begin{bmatrix} -1 \\ b \end{bmatrix} u + \begin{bmatrix} v_c \\ c \end{bmatrix} \tag{4.19}$$

The structure-control law is the same as before.

$$u = \begin{cases} 1 & \text{for } \sigma = y > \Delta \\ 0 & \text{for } \sigma = y < \Delta \end{cases} \tag{4.20}$$

fn	BUCK CONVERTER	BOOST CONVERTER	BUCK-BOOST CONVERTER
V_0	$V_c V_g$	$V_g/(1-V_c)$	$-V_g V_c/(1-V_c)$
I	V_0/R	$V_0/R(1-V_c)$	$-V_0/R(1-V_c)$
$\frac{\hat{i}}{\hat{v}_g}$	$\frac{V_0}{RV_g}\ \frac{1+SCR}{G(S)}$	$\frac{V_0^2}{RV_g^2}\ \frac{1+SCR}{G(S)}$	$-\frac{(V_g-V_0)V_0}{RV_g}\ \frac{1+SCR}{G(S)}$
$\frac{\hat{v}_0}{\hat{v}_g}$	$\frac{V_0}{V_g}\ \frac{1}{G(S)}$	$\frac{V_0}{V_g}\ \frac{1}{G(S)}$	$\frac{V_0}{V_g}\ \frac{1}{G(S)}$
$\frac{\hat{i}}{\hat{v}_c}$	$\frac{V_g}{R}\ \frac{1+SCR}{G(S)}$	$\frac{2V_0^3}{RV_g^2}\ \frac{1+SCR/2}{G(S)}$	$\frac{(V_g-V_0)^3}{RV_g^2}\ \frac{1+SCR-V_0/(V_g-V_0)}{G(S)}$
$\frac{\hat{v}_0}{\hat{v}_c}$	$V_g\ \frac{1}{G(S)}$	$\frac{V_0^2}{V_g}\ \frac{1}{G(S)}$	$-\frac{(V_g-V_0)^2}{V_g}\ \frac{1+SLV_0(V_g-V_0)/RV_g^2}{G(S)}$
$G(S)$	$1+S\frac{L}{R}+S^2LC$	$1+S\frac{LV_0^2}{RV_g^2}+S^2LC\frac{V_0^2}{V_g^2}$	$1+S\frac{L(V_g-V_0)^2}{RV_g^2}+S^2\frac{LC(V_g-V_0)^2}{V_g^2}$

TABLE 4.2 The steady state, and transfer functions of variable frequency duty ratio controlled dc-to-dc converters. V_c is the normalized, nondimensional control input.

Just as before, under sliding mode control, $\sigma = \dot{\sigma} = 0$ and $u_{eq} = v_c$. The equivalent system representation is

$$\dot{x} = Ax + bv_c + c \tag{4.21}$$

For convenience, Eq. (4.21) may be restructured as follows where A_1, A_2, b_1, b_2 are all as defined in Section 4.1.2.

$$\dot{x} = [v_c A_1 + (1 - v_c)A_2]x + [v_c b_1 + (1 - v_c)b_2]v_g \tag{4.22}$$

Equation (4.22) is in general nonlinear. x, v_c, v_g may be perturbed to get the steady state solutions and the various transfer functions. The various transfer functions are given in Table 4.2. These are similar to those obtained for constant switching frequency converters and given in Table 4.1. The only difference is that the transfer functions are expressed in terms of the operating voltages and currents instead of the duty ratio. The condition that the switching frequency be sufficiently large still holds.

4.4 Sliding Mode Control of Buck Converter

In Section 4.3, we digressed to apply the equivalent control method to obtain small signal transfer functions of the duty ratio controlled dc-to-dc converters. The purpose of that exercise was to show the usefulness of equivalent control method as an analysis method for programmed switching structures. A more fundamental aspect of VSS is to be able to synthesize the dynamic structure-control law (as against the programmed structure-control law of duty ratio control) to achieve the desired steady state and dynamic

performance of the converter. The steps involved in such a design process are as follows.

i) to relate the steady state and dynamic requirements into an appropriate sliding boundary.

ii) to establish a structure-control law with reference to the selected sliding boundary, such that the conditions of reaching and existence of sliding regime are satisfied.

It was mentioned in Chapter 3 that the above design process is simple when the controllable states of the system (output and its derivatives) are continuous and accessible. Dc-to-dc buck converter satisfies these requirements and is the simplest of all three dc-to-dc converters for the application of sliding mode control. This example was shown briefly in Chapter 3. In the following section, the dc-to-dc buck converter is first taken up for the application of sliding mode voltage control.

4.4.1 Buck Converter in Phase Variable Canonical Form

Figure 4.6 shows the buck converter, its inductor current, and the output voltage under steady state. The VSS description of the buck converter is

$$\dot{x} = Ax + bu \tag{4.23}$$

$$x = \begin{bmatrix} i \\ v_0 \end{bmatrix}; \quad A = \begin{bmatrix} 0 & -1/L \\ 1/C & -1/RC \end{bmatrix}; \quad b = \begin{bmatrix} v_g/L \\ 0 \end{bmatrix}$$

The inductor current i and the output voltage v_0 are both continuous functions. The derivative of the output voltage (dv_0/dt) is

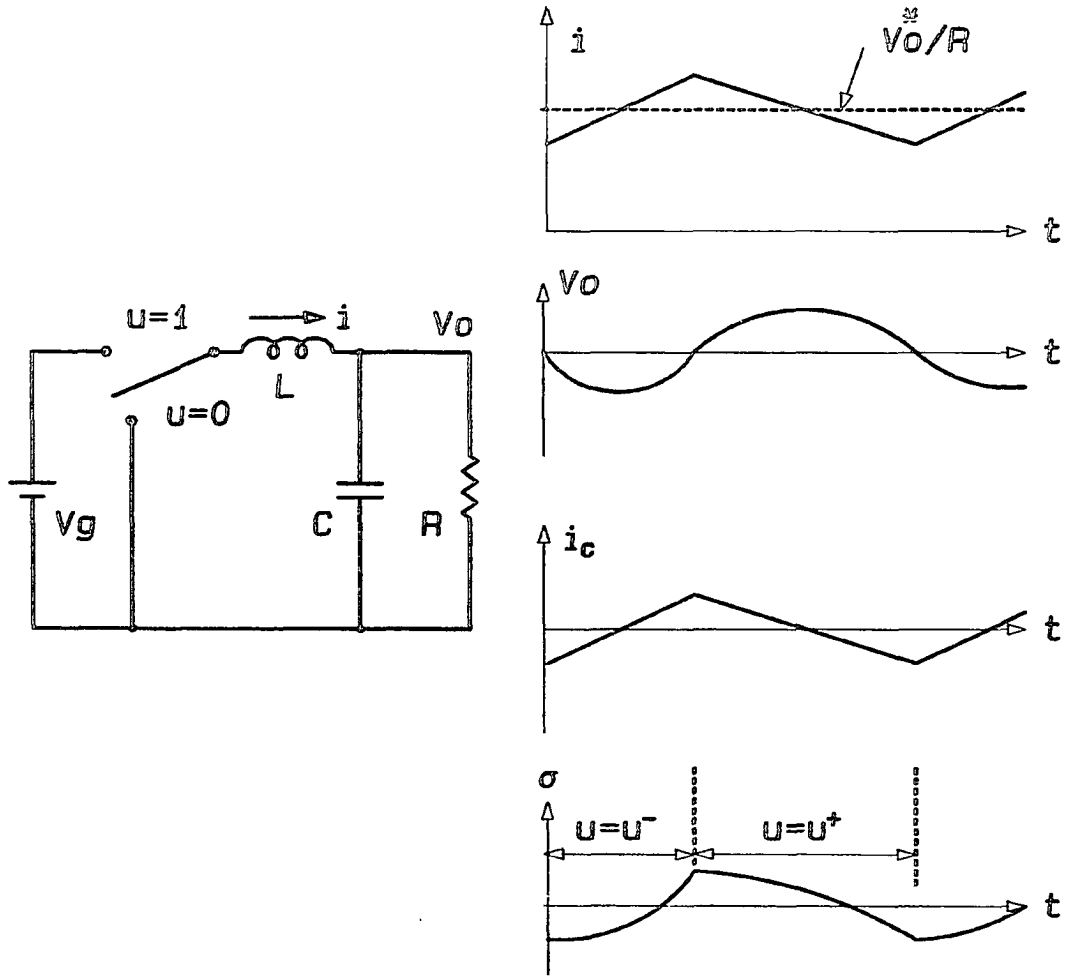

Fig. 4.6 The buck dc-to-dc converter and the various steady state waveforms. The polarity of the switching function σ determines the state of the switch.

proportional to the capacitor current, which is also a continuous function. Let the desired output voltage be V_0^*. Then the output error is defined as $v_0 - V_0^*$. For dc-to-dc buck converters V_0^* is constant, and $V_0^* < v_g$. Equation 4.23 may then be transformed as

$$\dot{y} = A^* y + b^* u + c^* \tag{4.24}$$

$$A^* = \begin{bmatrix} 0 & 1 \\ -\frac{1}{LC} & -\frac{1}{RC} \end{bmatrix}; \quad b^* = \begin{bmatrix} 0 \\ \frac{v_g}{LC} \end{bmatrix};$$

$$y = \begin{bmatrix} v_0 - V_0^* \\ \frac{d(v_0 - V_0^*)}{dt} \end{bmatrix}; \quad c^* = \begin{bmatrix} 0 \\ \frac{-V_0^*}{LC} \end{bmatrix}$$

The dc-to-dc buck converter is a second order system with one control input. Therefore the dynamic response obtainable under sliding mode control is of order 1. The desired steady state and dynamic response may then be expressed as a one dimensional sliding surface (sliding line) in the phase plane. Consider

$$\sigma = (v_0 - V_0^*) + \tau \frac{d(v_0 - V_0^*)}{dt} = 0 = [1 \quad \tau]^T y = gy \tag{4.25}$$

Equation (4.25) describes a stable trajectory in the phase plane with steady state operating point $v_0 = V_0^*$, and first order transient recovery with a time constant τ.

The next step is to select the structure-control law such that the line $\sigma = 0$ is a sliding boundary. The condition for the existence of sliding regime is

$$\lim_{\sigma = 0^+} \dot{\sigma} < 0; \quad \lim_{\sigma = 0^-} \dot{\sigma} > 0$$

Let

$$u = \begin{cases} u^+ & \text{for } \sigma > 0 \\ u^- & \text{for } \sigma < 0 \end{cases}$$

The condition for the existence of sliding regime is

$$gA^{\circ}y + gb^{\circ}u^+ + gc^{\circ} < 0 < gA^{\circ}y + gb^{\circ}u^- + gc^{\circ}$$

Expanding and applying the condition that $dv_0/dt = 0$, we get

$$\begin{aligned} &(1-\frac{\tau}{RC})\,[dv_0/dt]_{u=u^+} + \frac{\tau}{LC}(v_g u^+ - v_0) < 0 \\ &0 < (1-\frac{\tau}{RC})\,[dv_0/dt]_{u=u^-} + \frac{\tau}{LC}(v_g u^- - v_0) \end{aligned} \tag{4.26}$$

From Eq. (4.26) u^+ and u^- are selected as 0 and 1 respectively. The condition for the existence of sliding mode is then $\tau > RC$. The same condition may also be arrived at from the steady state waveforms shown in Fig. 4.6.

$$[\dot{\sigma}]_{u=u^+} < 0 < [\dot{\sigma}]_{u=u^-} \tag{4.27}$$

The next step in the design process is to ensure that starting from anywhere in the phase plane, the system RP will reach the sliding line $\sigma = 0$. Recalling the theorem in Section 3.4 on the sufficient reaching condition, it may be verified from Fig. 4.7 that the sliding line partitions the phase plane into two regions and that the steady state operating point for the control input in each of these regions lies in the opposite region. The switching boundary $\sigma = 0$ then qualifies as a sliding line.

i) $\sigma = 0$ is a stable trajectory satisfying the steady state ($v_0 = V_0^{\circ}$)

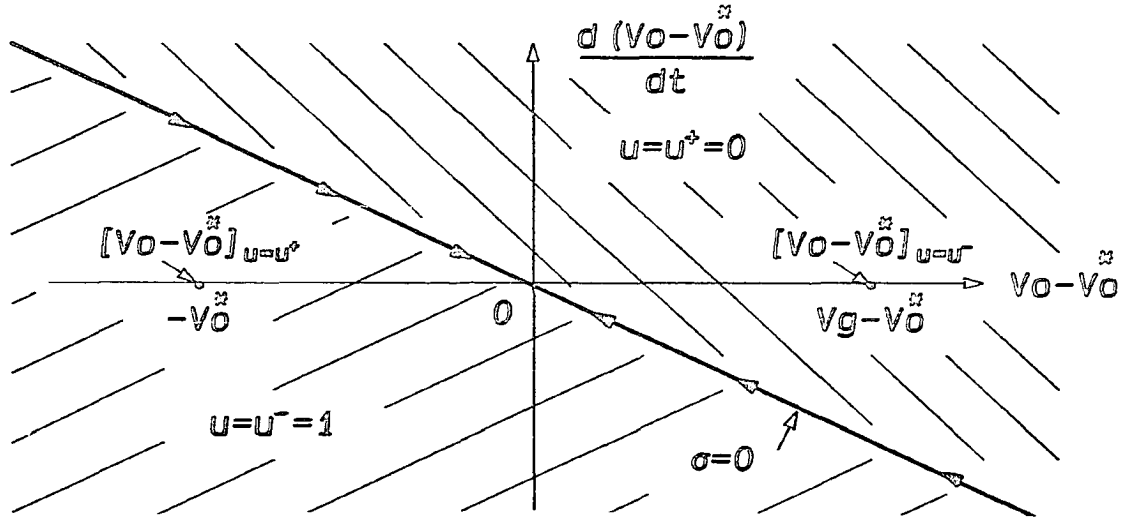

Fig. 4.7 The switching function $\sigma = 0$ is seen in the phase plane. $\sigma = 0$ partitions the phase plane in to two regions ($\sigma < 0$, and $\sigma > 0$). The control input is respectively u^- and u^+ in these two regions.

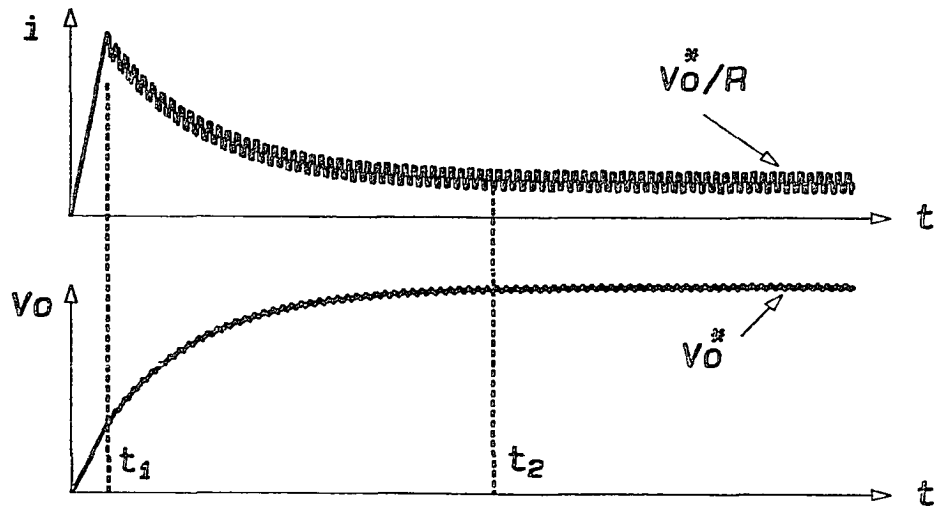

Fig. 4.8 The starting transient in the inductor current i and the output voltage v_0 under sliding mode control. The duration from $t = 0$ to $t = t_1$ is the initial transient in reaching the sliding line $\sigma = 0$. The second part of the transient from $t = t_1$ to $t = t_2$ is the system motion along the sliding line to reach the steady state operating point ($v_0 = V_0^*$).

and dynamic (exponential error recovery with a time constant τ) requirements.

ii) The boundary $\sigma = 0$ is a sliding regime when $u = 1$ for $\sigma < \Delta$ and $u = 0$ for $\sigma > \Delta$. Further, conditions for the existence of the sliding mode are $\tau > RC$ and $v_g > V_0^*$.

iii) Starting from any arbitrary initial condition on the phase plane, the system eventually reaches the sliding line.

4.4.2 Overcurrent Protection

In Fig 4.8 a typical starting transient is shown. It consists of two parts. From time $t = 0$ to $t = t_1$ is the time taken for the system RP to reach the sliding line. From time $t = t_1$ to $t = t_2$ is the time taken to reach the steady state operating point ($v_0 = V_0^*$) along the sliding line. The initial transient time t_1 depends on the system parameters v_g,L,R, and C. The sliding mode transient t_1 to t_2 is exponential with time constant τ and is independent of the system parameters. During the transient, the inductor current i is seen to reach levels much higher than the steady state level. This large transient inrush current is objectionable for two reasons. Firstly it would saturate the inductor magnetic circuit leading to still larger inrush currents. Secondly the electronic SPDT switch in the converter may not be capable of withstanding this large inrush current. It is therefore a healthy practice to limit this inrush current. This feature is easily incorporated under sliding control by the following simple modification of the sliding line.

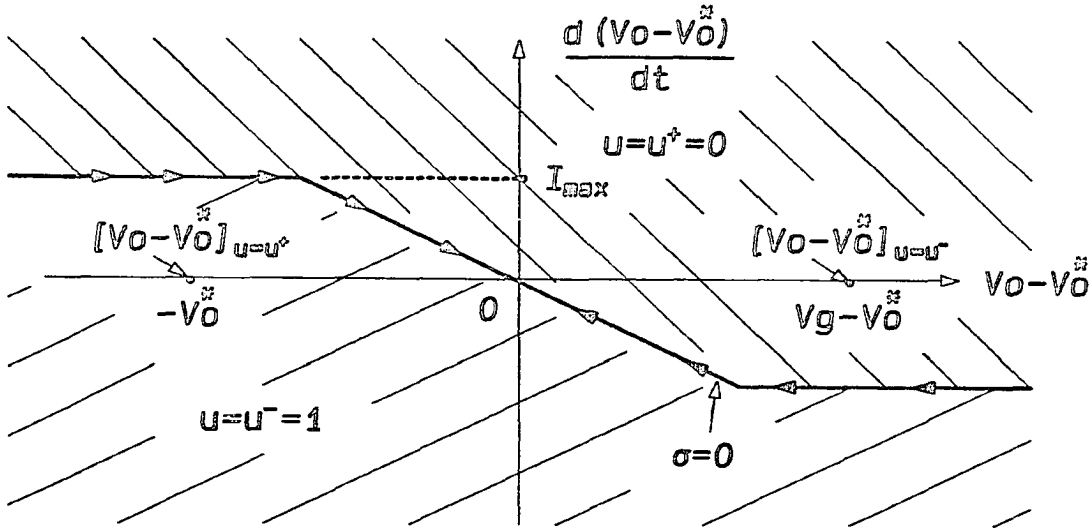

Fig. 4.9 The modified sliding line incorporating overcurrent protection. The sliding line is now limited to I°.

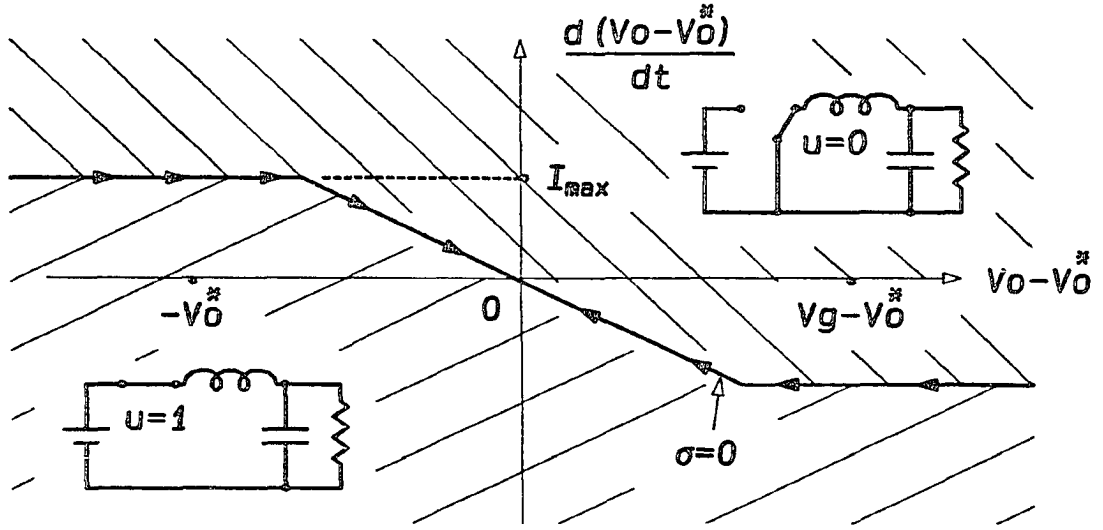

Fig. 4.10 A pictorial representation of the control law for the buck dc-to-dc converter shown on the phase plane.

Figure 4.9 indicates the modified sliding line incorporating the overcurrent protection. The modified sliding line $\sigma^* = 0$ shown in Fig. 4.9 consists of three pieces of straight lines.

$$\sigma^* = \begin{cases} \dfrac{d(v_0 - V_0^*)}{dt} - I_{max} = 0 & \text{for } \dfrac{d(v_0 - V_0^*)}{dt} > I_{max} \\ (v_0 - V_0^*) + \tau \dfrac{d(v_0 - V_0^*)}{dt} = 0 & \text{for } \left| \dfrac{d(v_0 - V_0^*)}{dt} \right| < I_{max} \\ \dfrac{d(v_0 - V_0^*)}{dt} + I_{max} = 0 & \text{for } \dfrac{d(v_0 - V_0^*)}{dt} < -I_{max} \end{cases} \tag{4.28}$$

The modified sliding line also satisfies the reaching condition. This may be seen from the steady state operating points for the two control inputs $u = 1$ and $u = 0$. It was already seen that the existence conditions of sliding regime is satisfied in the middle portion of the sliding line $\sigma^* = 0$. In the current limited region the sliding line may be written as

$$\sigma^* = [0 \quad 1]y - I_{max} = g^* y - I_{max}$$

$$\dot{\sigma}^* = g^* \dot{y}$$

$$-\frac{I_{max}}{RC} + \frac{v_g}{LC}u^+ - \frac{v_0}{LC} < 0 < -\frac{I_{max}}{RC} + \frac{v_g}{LC}u^- - \frac{v_0}{LC} \tag{4.29}$$

When $|I_{max}|$ is sufficiently low, $u^+ = 0$ and $u^- = 1$ satisfy Eq. (4.29). It may also be seen from the orientation of $\sigma^* = 0$ that the overall trajectory along $\sigma^* = 0$ is stable leading to the steady state operating point $v_0 = V_0^*$.

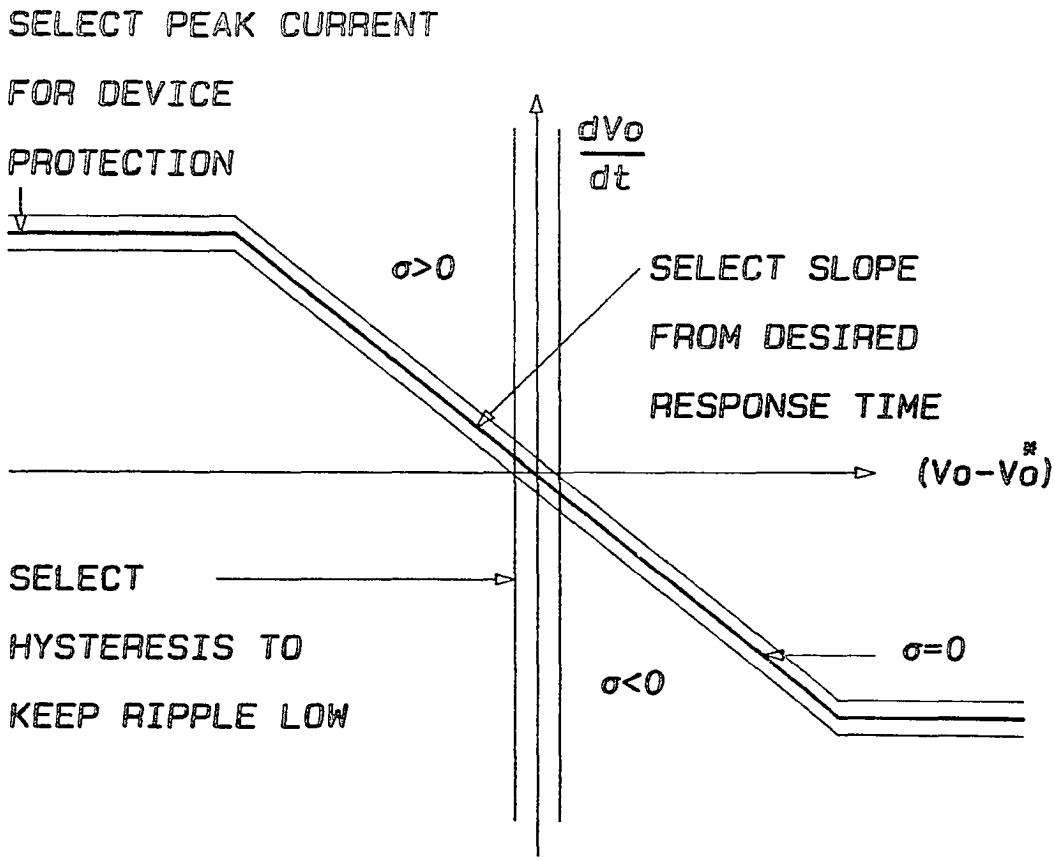

Fig. 4.11 An overall glance of the design criteria used for the sliding mode control of buck dc-to-dc converter.

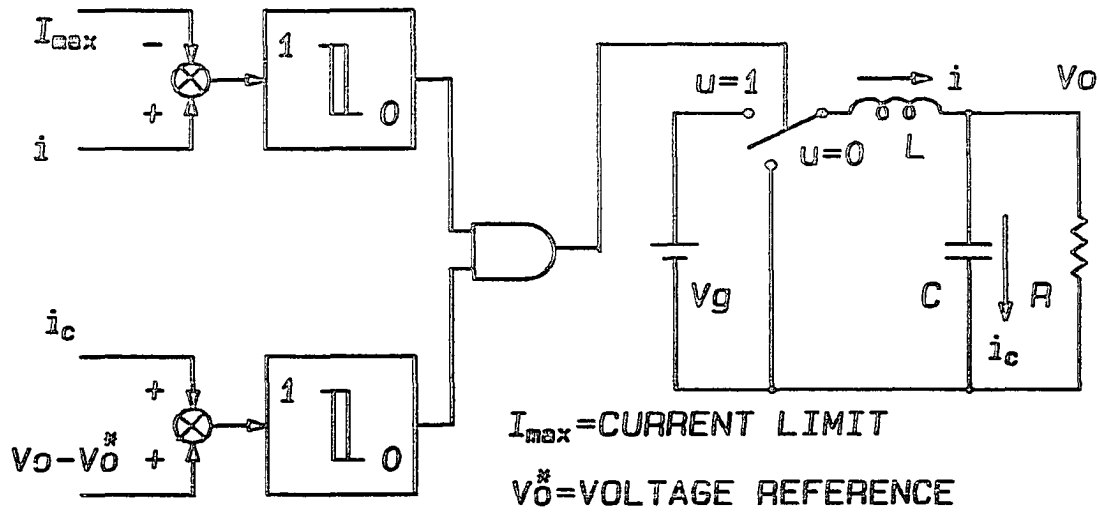

Fig. 4.12 The control schematic of the sliding mode controller for the buck dc-to-dc converter.

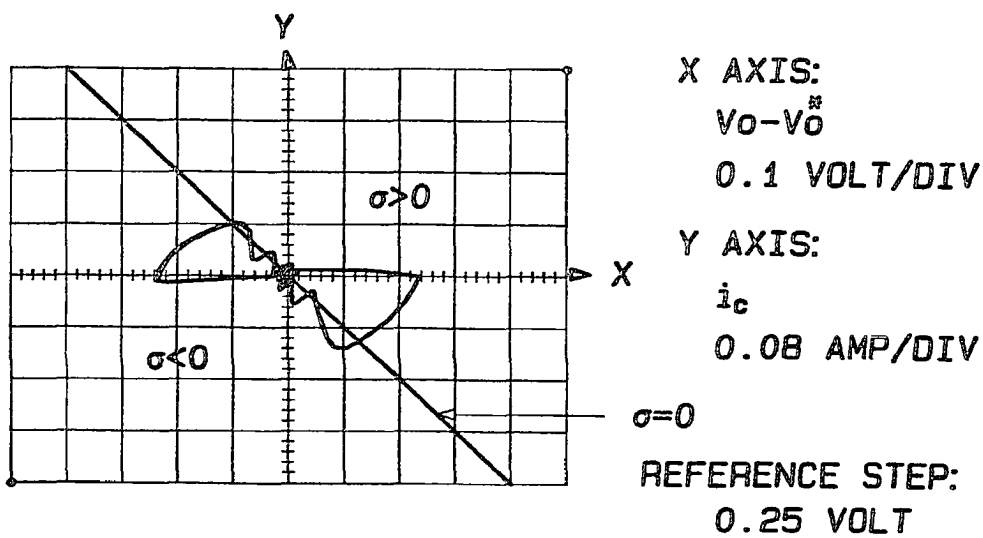

Fig. 4.13 The response of a buck dc-to-dc converter under sliding mode control, for a step change in the reference input, seen on the phase plane.

4.4.3 Design Criterion

The sliding line and the substructures used in the buck converter are shown in Fig. 4.10. The y axis has been reassigned as dv_0/dt. Figure 4.11 indicates the complete design process of the buck converter in the phase plane. Figure 4.12 shows the schematic diagram of a sliding mode voltage controller for the buck dc-to-dc converter. A typical response to step change in reference is shown in Fig. 4.13.

4.4.4 Other Dc-to-dc Converters

The application of sliding mode voltage control, while being straightforward for the buck dc-to-dc converter, is not so simple when applied to the boost and buck-boost converter for the following reasons. Figure 4.14a shows the typical waveforms of a boost dc-to-dc converter. It may be noticed that the derivative of the output voltage (capacitor current to some scale) is discontinuous at the instant of switching. In the presence of parasitic series resistance in the output capacitor, even the output voltage (Fig. 4.14b) is not continuous. As a result the system motion is not continuous when viewed on a phase plane defined as the output voltage and its derivative as the axes. Therefore the same strategy of control used for the buck converter is not applicable to boost, and buck-boost converters. Sliding mode voltage control is possible for the boost and the buck-boost converters, by setting up the sliding line in terms of the output voltage and the inductor current. Before we go on to describe this method and develop the design strategies, it is helpful

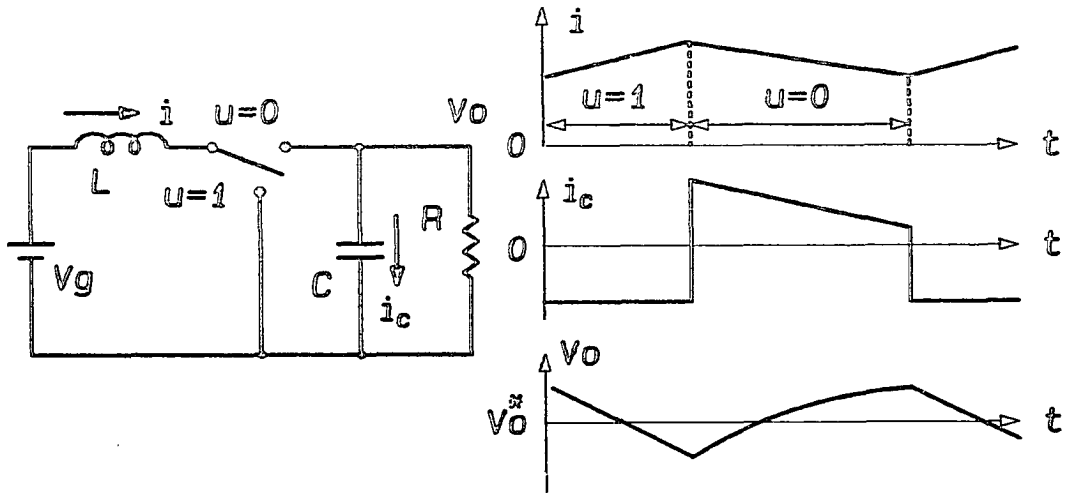

Fig. 4.14a The ideal boost dc-to-dc converter and its steady state waveforms. The capacitor current i_c is seen to be discontinuous.

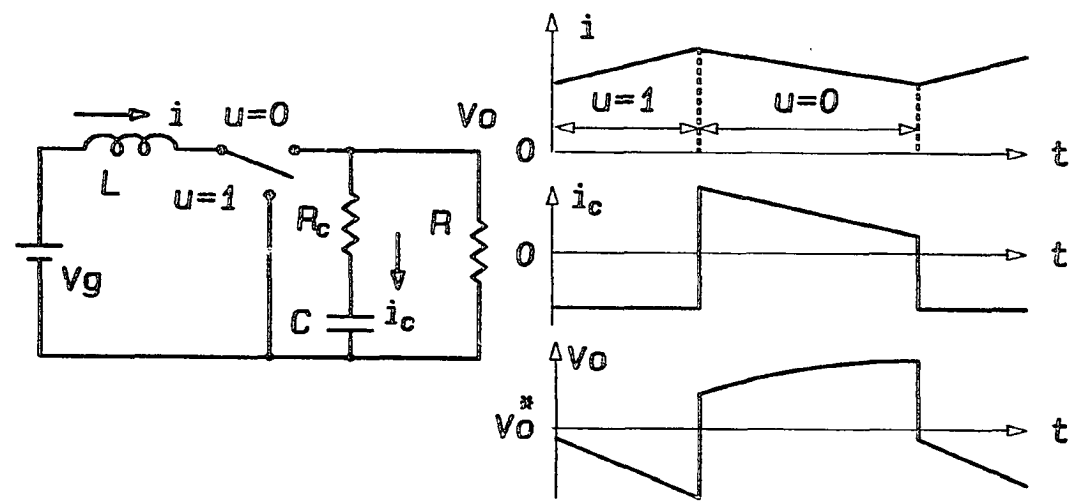

Fig. 4.14b The boost dc-to-dc converter with the Equivalent Series Resistance (ESR) of the capacitor. It is seen that the output voltage as well as the inductor current are discontinuous.

to consider the sliding mode control of the inductor current in dc-to-dc converters. Some of the results obtained from such a control method are used later on to develop a simple voltage control strategy that is applicable to all three dc-to-dc converters.

4.5 Current Programmed Dc-to-dc Converters

Another method of control of dc-to-dc converters is to control the inductor current. In this case, only the control of the inductor current is of interest, and hence all three converters are first order systems and linear with respect to control input. The dynamic equations of the different converters are

Buck Converter:

$$L\frac{di}{dt} = v_g u - v_0$$

Boost Converter:

$$L\frac{di}{dt} = v_g - v_0\bar{u}$$

Buck-boost Converter:

$$L\frac{di}{dt} = v_g u + v_0\bar{u}$$

All the above systems are first order systems ($n = 1$) with one control ($m = 1$). Therefore the sliding surface can be of dimension 0 ($n-m$). Let

$$\sigma = i - I^*$$

$$u = \begin{cases} u^+ & \text{for } \sigma > 0 \\ u^- & \text{for } \sigma < 0 \end{cases}$$

Applying the conditions for the existence of sliding mode, we get

Buck converter:

$$v_g u^+ - v_0 < 0 < v_g u^- - v_0$$
$$u^+ = 0 \; ; \quad u^- = 1 \; ; \quad v_0 < v_g$$

Boost Converter:

$$v_g + v_0 \overline{u}^+ < 0 < v_g + v_0 \overline{u}^-$$
$$u^+ = 0 \; ; \quad u^- = 1 \; ; \quad v_0 > v_g$$

Buck-boost Converter:

$$v_g u^+ + v_0 \overline{u}^+ < 0 < v_g u^- + v_0 \overline{u}^-$$
$$u^+ = 0 \; ; \quad u^- = 1$$

The structure-control law is identical for all three converters.

$$\sigma = i - I^*$$

$$u = \begin{cases} 0 & \text{for } \sigma > 0 \\ 1 & \text{for } \sigma < 0 \end{cases}$$

Phase space description for these first order systems can be graphically shown in one dimension (phase line description). The sliding surface is of dimension zero and is referred to as the sliding point. The structure-control law requires only the output error. The control is effectively a bang-bang control.

Figure 4.15 shows the phase line description of the three dc-to-dc converters. The sliding point is $\sigma = i - I^* = 0$. The substructures active on each half of the phase line are also shown in

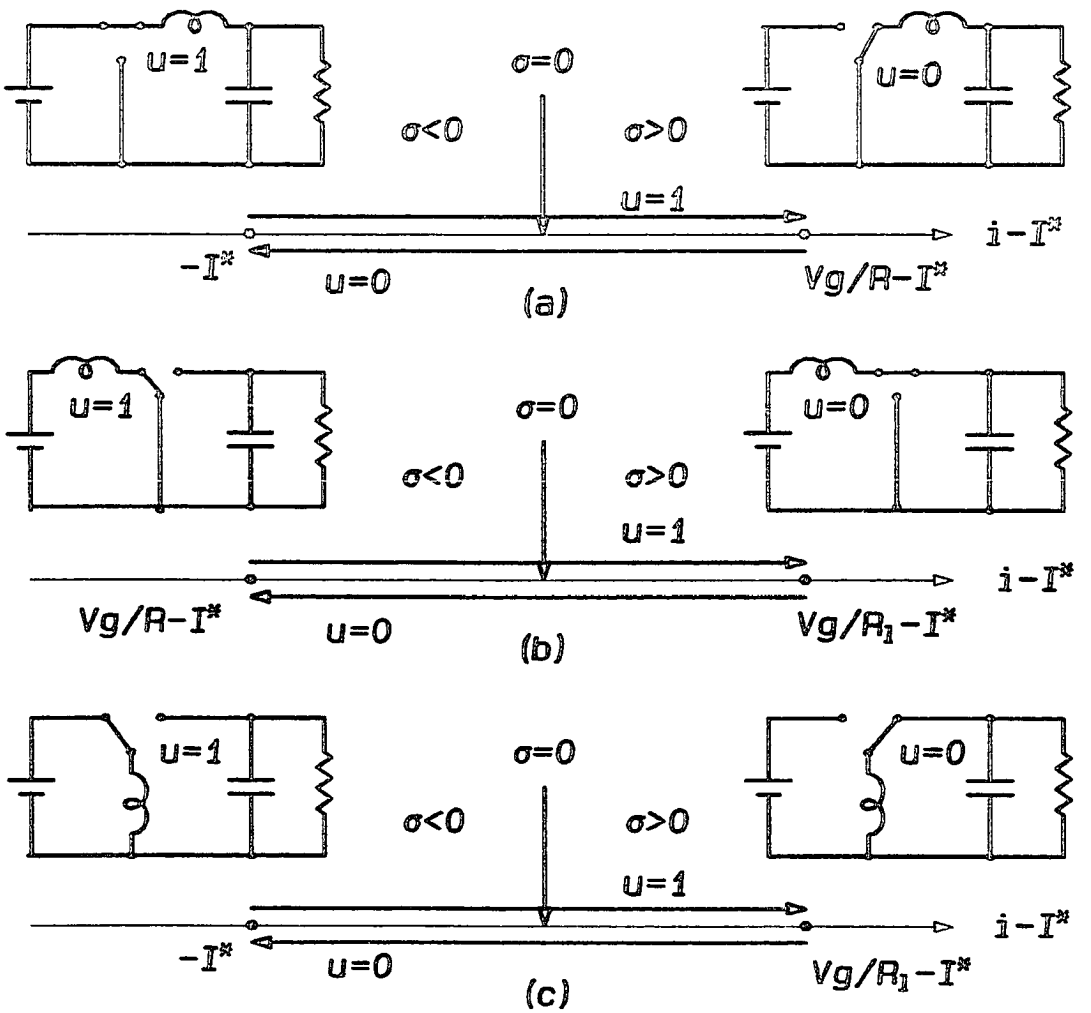

Fig. 4.15 The inductor current control of dc-to-dc converter in the phase space. Under inductor current control all the above converters are first order systems. The phase space is therefore of dimension 1. The sliding surface then reduces to a point $(i - I^*) = 0$. The phase trajectories are straight line. The control law and the effective circuit are also shown.

Fig. 4.15. The steady state operating point for each substructure is seen to be in the other half thus satisfying the reaching conditions.

4.5.1 System Description under Equivalent Control

The method of equivalent control may be used to get an overall description of the current controlled dc-to-dc converters. The method is illustrated here for the boost converter and the results are presented for the other converters.

$$L\frac{di}{dt} = v_g - v_0\bar{u} \tag{4.30}$$

$$C\frac{dv_0}{dt} = i\bar{u} - \frac{v_0}{R} \tag{4.31}$$

From Eq. (4.30)

$$\bar{u}_{eq} = v_g - L\frac{di}{dt}$$

Substitution into Eq. (4.31) yields

$$v_g i = \frac{v_0^2}{R} + \frac{d(Cv_0^2/2)}{dt} + \frac{d(Li^2/2)}{dt}$$

In other words

$$\begin{matrix}\textit{INPUT} \\ \textit{POWER}\end{matrix} = \begin{matrix}\textit{OUTPUT} \\ \textit{POWER}\end{matrix} + \begin{matrix}\textit{RATE OF CHANGE OF} \\ \textit{STORED ENERGY}\end{matrix} \tag{4.32}$$

Equation (4.32) is in general nonlinear between inductor current and output voltage, and is given below for different converters.

Buck Converter:

$$\begin{aligned} v_g i u_{eq} &= \frac{v_0^2}{R} + \frac{d(Cv_0^2/2)}{dt} + \frac{d(Li^2/2)}{dt} \\ u_{eq} &= (v_0 + L\,di/dt)/v_g \end{aligned} \tag{4.33}$$

Boost Converter:

$$v_g i = \frac{v_0^2}{R} + \frac{dCv_0^2/2}{dt} + \frac{dLi^2/2}{dt} \tag{4.34}$$

Buck-boost Converter:

$$v_g i u_{eq} = \frac{v_0^2}{R} + \frac{d(Cv_0^2/2)}{dt} + \frac{d(Li^2/2)}{dt}$$
$$u_{eq} = (-v_0 + L\,di/dt)/(v_g - v_0) \tag{4.35}$$

The above equations may be linearized around the operating point to obtain the following transfer functions between the inductor current and the output voltage.

Buck Converter:

$$\frac{\hat{v}_0(s)}{\hat{i}(s)} = \frac{R}{1+sCR} \tag{4.36}$$

Boost Converter:

$$\frac{\hat{v}_0(s)}{\hat{i}(s)} = \frac{Rv_g}{2V_0^*} \frac{1-sL(V_0^*)^2/Rv_g^2}{1+sCR/2} \tag{4.37}$$

Buck-boost Converter:

$$\frac{\hat{v}_0(s)}{\hat{i}(s)} = \frac{Rv_g}{v_g - 2V_0^*} \frac{1-sLV_0^*(v_g - V_0^*)/Rv_g^2}{1+sCR(v_g - V_0^*)/(v_g - 2V_0^*)} \tag{4.38}$$

These results are identical to the results obtained in Reference [10] following the state space averaging method.

4.5.2 Inductor Current to Output Voltage Transformation

It was mentioned in Section 3.6 that the desirable way of setting up the sliding surface for sliding mode control is by means of output error and its derivatives. The reason for this choice is that the analysis of stability is simple for such a sliding surface. It was also seen in Section 4.4 that such a state assignment is not possible in case of buck and buck-boost converters. It becomes then necessary to set up the sliding surface in terms of suitable continuous physical variables. The inductor current i and the output voltage v_0 are continuous variables and qualify for suitable states in terms of which the sliding surface may be set up. In order to study the stability of the trajectories on such a sliding surface, one has to transform the sliding surface into output error and its derivative. The equivalent system description given by Eqs. (4.33) to (4.35) may be used to obtain this transformation between inductor current and output voltage. The method is illustrated for boost converter and the results are presented for the other converters.

For boost converter, Eq. (4.34) may be manipulated and rewritten as

$$v_0^2 + RCv_0 dv_0/dt = Ri(v_g - L\,di/dt) \tag{4.39}$$

In practical converters in order to obtain good small signal as well as power bandwidth, it is necessary to choose L such that $v_g \gg L\,di/dt$. Then Eq. (4.39) reduces to

$$i = \frac{Cv_0}{v_g}\frac{dv_0}{dt} + \frac{v_0^2}{Rv_g}$$

The above equation gives the relationship between the inductor current and output voltage for boost converter. This relationship is in general nonlinear and is given here for the other converters as well.

Buck Converter:

$$i = C\frac{dv_0}{dt} + \frac{v_0}{R} \tag{4.40}$$

Boost Converter:

$$i = \frac{Cv_0}{v_g}\frac{dv_0}{dt} + \frac{{v_0}^2}{Rv_g} \quad [v_g \gg L\,di/dt] \tag{4.41}$$

Buck-boost Converter:

$$i = C\frac{(v_g - v_0)}{v_g}\frac{dv_0}{dt} + \frac{v_g - v_0}{v_g}\frac{v_0}{R} \quad [v_0 \gg L\,di/dt] \tag{4.42}$$

In the next section sliding mode voltage control of dc-to-dc converters is described where the sliding surface is set up in terms of inductor current and output voltage. The relationship between inductor current and output voltage given by Eqs. (4.40) to (4.42) are then used to analyze the stability of sliding regime.

4.6 Voltage Control of Dc-to-dc Converters

In Section 4.4 the problems associated with the voltage control of boost and buck-boost converters were highlighted. One of the ways of overcoming these problems is to establish an inner loop of sliding mode current controller, and then to design an outer

supervisory loop of voltage controller based on the small signal model of the current controlled converters. The transfer functions given by Eqs. (4.37) and (4.38) are useful for this approach.

An alternative approach is to implement a direct sliding mode voltage controller. The control strategy developed for the buck converter is not applicable in general since the derivative of the output voltage exhibits discontinuity during switching. The alternate approach consists of setting up the sliding surface in terms of some continuous states of the system, and then to relate the resultant dynamics to the desired response. This method is applicable for all three dc-to-dc converters and is illustrated here for the boost converter. The results are then presented for the other converters.

Boost Converter: Example

For the case of boost converter, the sliding line may be set up as usual in terms of some continuous states of the system. The states chosen for this purpose are the errors in the inductor current and the output voltage. Let

$$\sigma = gx = K_v[R_s\hat{i}+\hat{v}_0] = 0$$

$\hat{i}$ and $\hat{v}_0$ are the errors in the inductor current and the output voltage respectively. σ is the weighted sum of the states of the system and $\sigma = 0$ represents a straight line in the phase plane. The inductor current error $\hat{i}$ and the output voltage error $\hat{v}_0$ are the axes of the phase plane. The gain parameters used in setting up the sliding line are K_v and K_vR_s. The gain parameter R_s in practice is the current sensing resistance. The current sensing resistance R_s is

usually orders of magnitude smaller than the load resistance R. The conditions for the existence of sliding mode are derived in a subsequent section. Suppose that sliding mode exists and the system RP is confined to move along the sliding line $\sigma = 0$. K_v does not influence the response. It is significant only as a scale factor of the phase plane. In ideal sliding mode control, switching takes place in an infinitesimal vicinity around the sliding line $\sigma = 0$ and K_v has no significance whatsoever. In real sliding mode control, switching takes place in a finite Δ vicinity around the sliding line and, K_v determines the nominal switching frequency for a given ripple and vice versa.

4.6.1 Stability of Trajectories on the Sliding Line

We now go on to examine whether the trajectories along the sliding line lead to a unique steady state operating point. Define the current and voltage errors by the following relationship.

$$i = I^* + \hat{i}$$
$$v_0 = V_0^* + \hat{v}_0$$

In the boost converter, the relationship between inductor current i and output voltage v_0 was derived in Section 4.5, Eq. (4.41). This relationship may be written in terms of the voltage and current errors as follows.

$$I^* + \hat{i} = \frac{C(V_0^* + \hat{v}_0)}{v_g}\frac{d(V_0^* + \hat{v}_0)}{dt} + \frac{(V_0^* + \hat{v}_0)^2}{Rv_g}$$

Separating the dc and ac components, we get

$$I^* = \frac{V_0^{*2}}{Rv_g} \tag{4.43}$$

$$\hat{i} = \frac{CV_0^*}{v_g}\frac{d\hat{v}_0}{dt} + \frac{2V_0^*}{Rv_g}\hat{v}_0 + \frac{C}{2v_g}\frac{d\hat{v}_0^2}{dt} + \frac{\hat{v}_0^2}{Rv_g} \tag{4.44}$$

Using Eq.(4.44), we may transform the sliding line into

$$\sigma = K_v\left[\hat{v}_0 + \frac{2V_0^*R_s}{Rv_g}\hat{v}_0 + \frac{CV_0^*R_s}{v_g}\frac{d\hat{v}_0}{dt} + \frac{R_s}{Rv_g}\hat{v}_0^2 + \frac{CR_s}{2v_g}\frac{d\hat{v}_0^2}{dt}\right] \tag{4.45}$$

Equation (4.45) may be rearranged and written as

$$\sigma = K_v[a(t)\hat{v}_0 + d\hat{v}_0/dt] \tag{4.46}$$

where,

$$a(t) = 1 + \frac{R_sV_0^*}{Rv_g}[2 + \hat{v}_0/V_0^*]$$

$$b(t) = \frac{CR_sV_0^*}{v_g}[1 + \hat{v}_0/V_0^*]$$

Equation (4.46) is a first order differential equation. The condition for guaranteed stability of response along the sliding line is that both $a(t)$ and $b(t)$ are positive. Or, in other words the relative error $\hat{v}_0/V_0^*$ is less than 1. Alternatively, Eq. (4.46) may be interpreted differently as follows. For large errors, the $\hat{v}_0^2$ terms dominate and the sliding line is determined mainly by $\hat{v}_0^2$ terms; for small errors, $\hat{v}_0$ terms dominate. The response may be thought of as having two parts.

Large signal response:

$$\hat{v}_0^2 + \frac{RC}{2}\frac{d\hat{v}_0^2}{dt} = 0 \tag{4.47}$$

Small signal response:

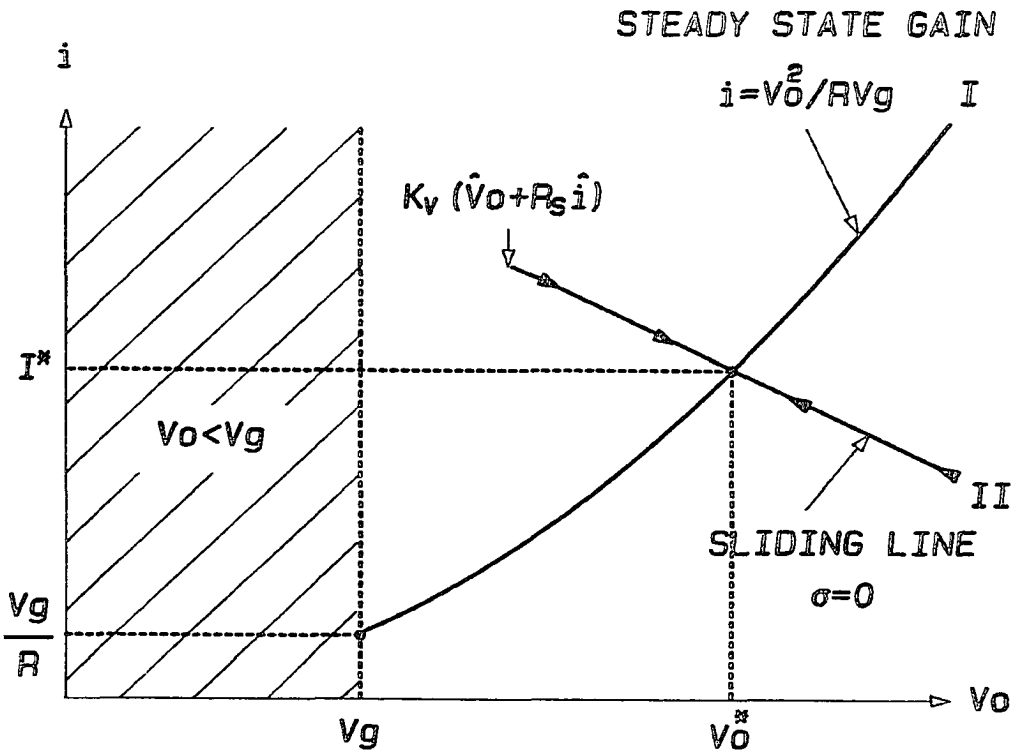

Fig. 4.16 The phase plane of the boost converter with the inductor current and the output voltage as the states of the converter. Line I shows the steady state gain between inductor current i and the output voltage v_0. Line II is the proposed sliding line. Under sliding mode control both the steady state and the sliding condition are satisfied, giving rise to the operating point (V_0^*, I^*).

$$\hat{v}_0 + \frac{2V_0^* R_s}{Rv_g}\hat{v}_0 + \frac{CV_0^* R_s}{v_g}\frac{d\hat{v}_0}{dt} \tag{4.48}$$

The large signal response is a constant current response that is stable, and with a time constant determined by the output circuit elements R and C. The small signal response is decided by the feedback gain (current sensing resistance R_s) and the operating point. The important conclusion is that the system is stable for both large and small signals and the steady state operating point is given by ($v_0 = V_0^*$).

For second order systems, the phase plane representation provides great insight into the system performance. The phase plane representation of the boost converter is shown in Fig. 4.16. The axes are the inductor current and the output voltage. The operating point under sliding mode control has to satisfy two conditions, namely $\sigma = 0$ and the steady state gain $I^* = V_0^{*2}/Rv_g$. Curve I in the phase plane represents the dc gain ($i = v_0^2/Rv_g$). Line II is the sliding line $\sigma = 0$. The sliding line is centered on the operating point with a slope of $-R_s$. The system RP, if confined to move on the sliding line, eventually reaches the steady state operating point (V_0^*, I^*). Before we go on to establish the conditions for the existence and reaching of the sliding mode, overcurrent protection may be introduced similar to the buck converter control. Figure 4.17 shows the modified sliding line in the phase plane incorporating current limit. Again the trajectories on the sliding line converge to the steady state operating point (V_0^*, I^*). Small signal response is unaltered. Large signal response is now a truly constant current response. Having

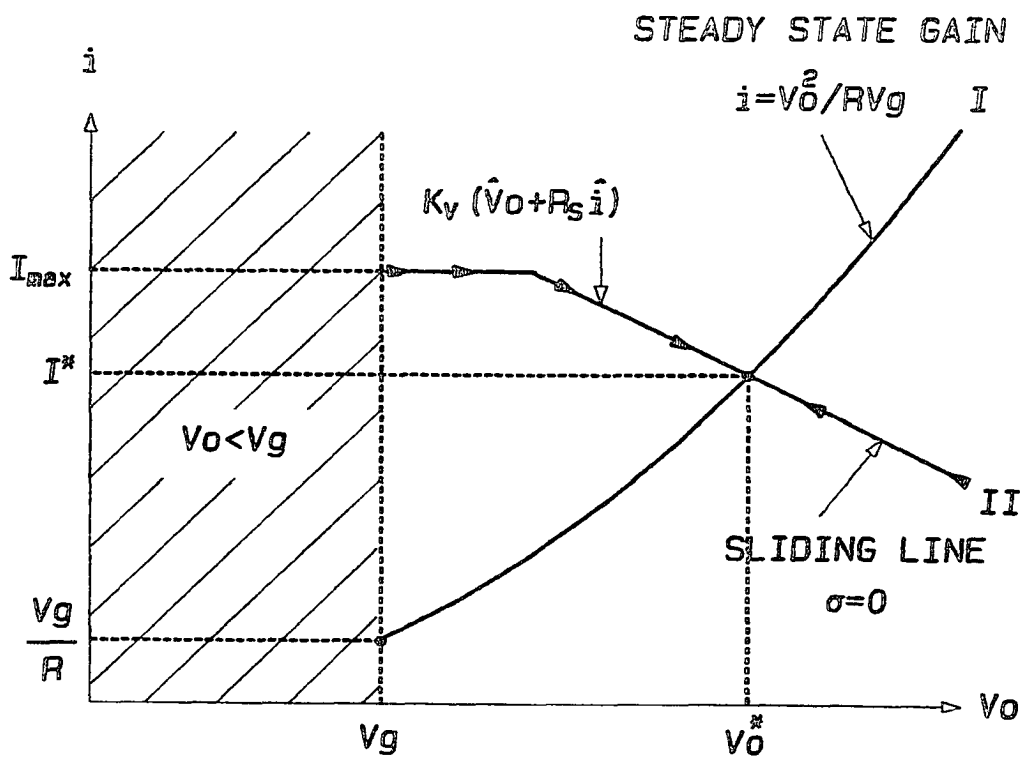

Fig. 4.17 The modified sliding line on the phase plane. The sliding line is clamped to I_{max} providing overcurrent protection to the converter.

established the stability of response along the sliding line, the next step in the design process is to ensure that sliding mode on the chosen sliding line does exist.

4.6.2 Condition for the Existence of Sliding Mode

The structure-control law is the same as in the case of the current controlled dc-to-dc converters.

$$u = \begin{cases} 1 & \text{for } \sigma < 0 \\ 0 & \text{for } \sigma > 0 \end{cases} \qquad (4.49)$$

$$\sigma = K_v[\hat{v}_0 + R_s\hat{i}]$$

Figure 4.18 shows the phase plane, the sliding line, the structure-control law, substructures active in each region of the phase plane, and the steady state operating points for each substructure. The steady state operating point for $u = 0$ is $(v_g, v_g/R)$. The steady state operating point for $u = 1$ is $(v_g/R_l, 0)$, where R_l is the resistance of the inductor L. This has been taken into account as otherwise the inductor current for $u = 1$ tends to ∞ and is not realistic.

The sliding line partitions the phase plane into two regions. The location of the system RP in the phase plane defines the substructure at any instant. The steady state operating point for each of the substructures lies in the opposite region of the phase plane. This property ensures the reaching condition. To find out the existence of sliding mode, we consider the sliding line in two sections denoted in Fig. 4.18 as a, and b. Along section a the operation is under current control. The sliding mode exists under current control

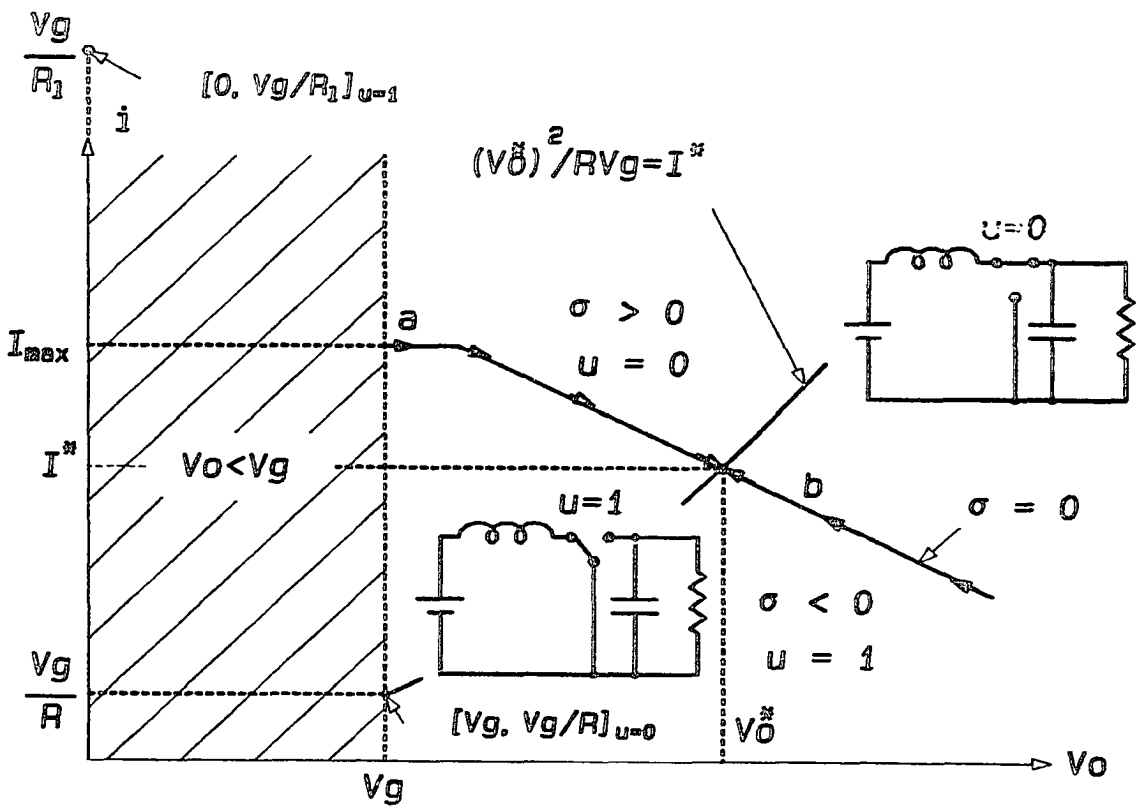

Fig. 4.18 A pictorial representation of the control law for the sliding mode control of the boost dc-to-dc converter. In the hatched region, v_0 is less than v_g and is not a feasible operating region for the boost converter.

when $v_0 > v_g$. This condition was derived in Section 4.5 for the current controlled dc-to-dc converters. We observe then that sliding mode exists along a everywhere except the region shown hatched in Fig. 4.18. This region corresponds to $v_0 < v_g$ and is not feasible region of operation for boost converter. It remains then to find out the conditions for the existence of sliding mode along section b of the sliding line. This is done analytically.

$$\begin{bmatrix} \dot{\hat{i}} \\ \dot{\hat{v}}_0 \end{bmatrix} = \begin{bmatrix} 0 & -\bar{u}/L \\ \bar{u}/C & 1/RC \end{bmatrix} \begin{bmatrix} \hat{i} \\ \hat{v}_0 \end{bmatrix} + \begin{bmatrix} v_g/L \\ 0 \end{bmatrix}$$

$$\sigma = K_v[R_s \quad 1]\,[\hat{i} \quad \hat{v}_0]^T$$

The conditions for the existence of sliding mode are given by

$$[\dot{\sigma}]_{\sigma > 0} < 0$$
$$[\dot{\sigma}]_{\sigma < 0} > 0$$

The above equations may be expanded to give the following inequalities.

$$L < \frac{R_s C(v_0 - v_g)}{I_{max}} \tag{4.50}$$

$$L < \frac{R_s RC v_g}{v_0} \tag{4.51}$$

The value of the circuit inductance must therefore be chosen to satisfy Eqs. (4.50) and (4.51) in order to ensure that sliding mode exists. Equation (4.51) is usually more stringent.

4.6.3 Practical Design Considerations

From Eq. (4.46) it was established that the system stability is always guaranteed, the design may be based on the small signal model. For small signals the relationship between the inductor current error and the output voltage error is linear. Hence the sliding line may be expressed in the frequency domain as well. From Eq. (4.44), for small signals

$$\hat{i}(s) = \frac{2V_0^*}{Rv_g}\hat{v}_0(s) + \frac{CV_0^*}{v_g}s\hat{v}_0(s) \tag{4.52}$$

$\hat{i}$ is defined as the current error. To measure $\hat{i}$, the average value I^* must be subtracted out. This is accomplished by use of a high-pass filter in the inductor current measurement. The simplest form of filter function is a single inverted pole at ω_1. The sliding line in frequency domain is shown here modified to include the high-pass filter for current measurement.

$$\sigma(s) = K_v\left\{\hat{v}_0(s) + \frac{1}{1+\omega_1/s}R_s\hat{i}(s)\right\} \tag{4.53}$$

Equations (4.52) and (4.53) may be combined to obtain

$$\sigma(s) = K_v\frac{1 + \dfrac{2R_sV_0^*}{Rv_g} + \dfrac{\omega_1}{s} + \dfrac{CR_sV_0^*}{v_g}s}{1+\dfrac{\omega_1}{s}}\hat{v}_0(s)$$

$$\approx K_v\frac{1 + \dfrac{\omega_1}{s} + \dfrac{s}{\omega_M}}{1+\dfrac{\omega_1}{s}}\hat{v}_0(s) \tag{4.54}$$

in which the (good) approximation always obtains because the

current sensing resistance R_s is much smaller than the load resistance R, and where

$$\omega_M \triangleq \frac{1}{CR_s}\frac{v_g}{V_0^*} \tag{4.55}$$

In the ideal case in which the current error $\hat{i}$ could be measured without a filter, $\omega_1 = 0$ and Eq. (4.54) reduces to

$$\sigma(s) = K_v\left[1+\frac{s}{\omega_M}\right]\hat{v}_0(s) \tag{4.56}$$

or, in the time-domain as

$$\sigma(t) = K_v\left[\hat{v}_0+\frac{1}{\omega_M}\frac{d\hat{v}_0}{dt}\right] \tag{4.57}$$

Therefore, ω_M is the maximum bandwidth that can be obtained or, in the time-domain, the fastest transient response of the output error is characterized by a time constant $1/\omega_M$ that depends on the system parameters (C, v_0, v_g) and the current sensing resistance (R_s).

In the realistic case of a nonzero filter corner frequency ω_1, Eq. (4.54) may be factored so that

$$\sigma(s) \approx K_v\frac{\left[1+\frac{\omega_1}{s}\right]\left[1+\frac{s}{\omega_M}\right]}{1+\frac{\omega_1}{s}}\hat{v}_0(s)$$

$$= K_v\left[1+\frac{s}{\omega_M}\right]\hat{v}_0(s) \tag{4.58}$$

which is the same ideal result as Eq. (4.56). Therefore, the condition

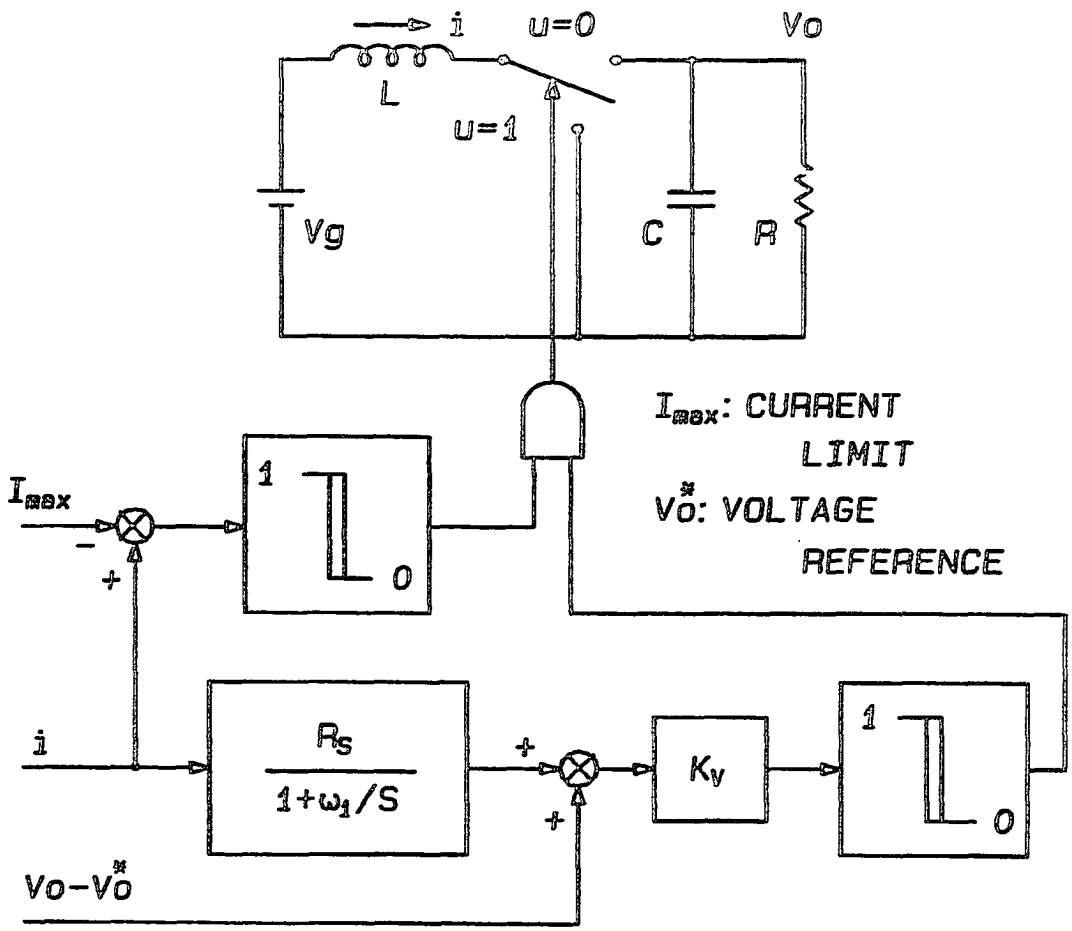

Fig. 4.19 The control schematic of the sliding mode control of boost dc-to-dc converter. A highpass filter is used in the measurement of the inductorcurrent in order to subtract out the steady state current I. The design criterion to obtain maximum bandwidth of the controller is that, the highpass corner is much lower than the maximum obtainable bandwidth.*

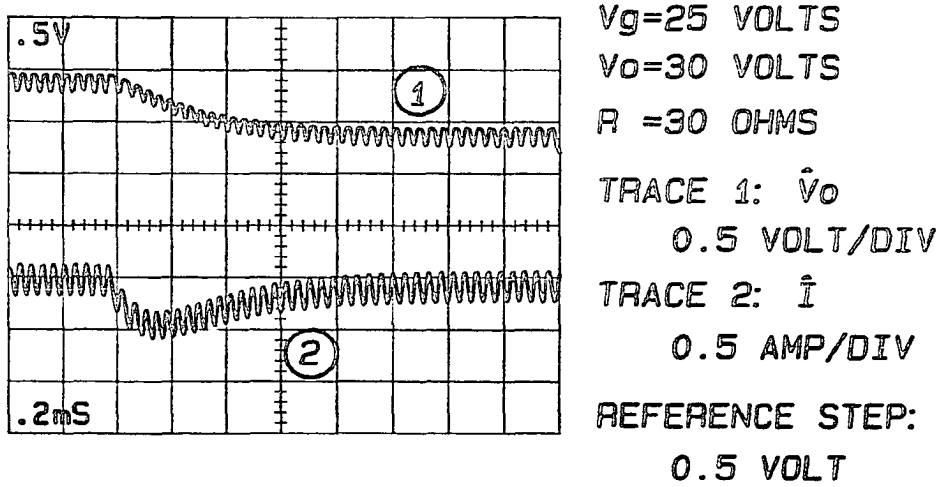

Fig. 4.20 The response of a boost converter to a reference step under sliding mode converter. The response is essentially first order.

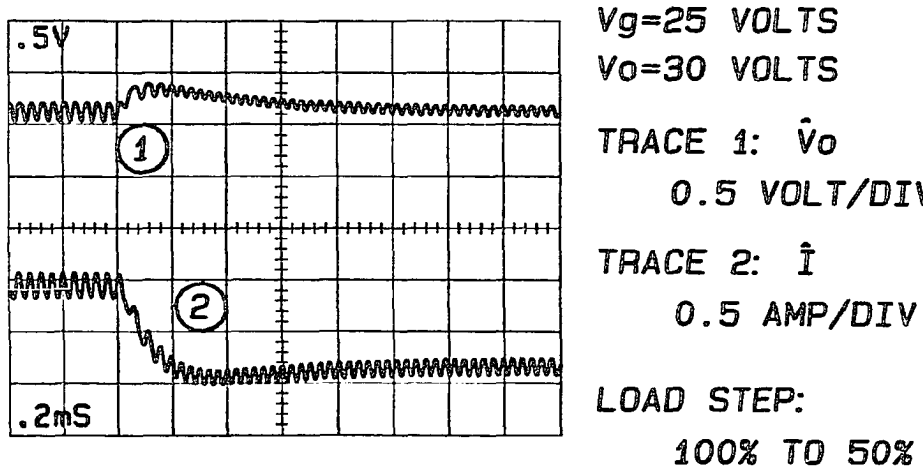

Fig. 4.21 The response of a boost converter to a load step under sliding mode control. The response is essentially first order.

that the factorization be valid, which is $\omega_1 \ll \omega_M$, becomes a design criterion: to retain the maximum bandwidth response, it is neccessary only that the filter corner be chosen much lower than the maximum bandwidth itself.

Figure 4.19 shows the schematic diagram of a sliding mode controller for a boost converter. Figures 4.20 and 4.21 show the response of the converter to a step change in reference and a step change in load, respectively.

4.6.4 Effect of ESR of Output Capacitor

In a practical converter, the output capacitor is not ideal and will have a parasitic Equivalent Series Resistance (ESR). The output voltage therefore will be discontinuous at the switching instants. Figure 4.22 shows the inductor current, output voltage, and the switching function $\sigma(t)$. The switching function σ is seen to have discontinuities. However this does not affect the performance of the sliding mode controller other than decreasing the switching frequency. It will be helpful to use a low-pass filter for measuring the ripple with a corner beyond the switching frequency.

4.6.5 Buck Dc-to-dc Converter

The method of setting up the sliding line in terms of the inductor current and the output voltage as illustrated for the boost converter is applicable to other dc-to-dc converters as well.

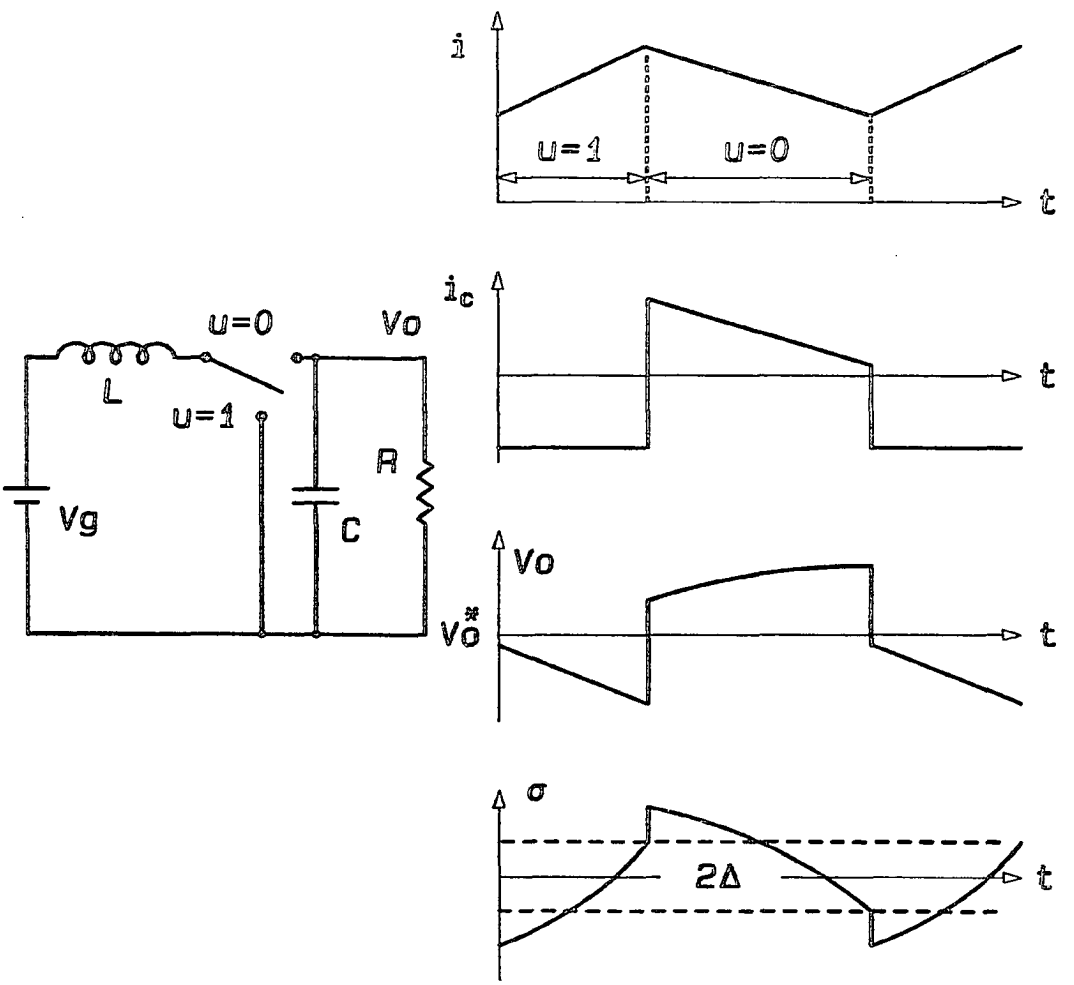

Fig. 4.22 The boost converter with the ESR of the output capacitor and the various steady state waveforms. The switching function σ also exhibits discontinuities. This, however, does not affect the low frequency performance of the converter. The switching frequency is seen to reduce owing to the ESR.

Figure 4.23 shows the phase plane of the buck converter. Also shown are the sliding line, structure control law, substructures active in each region of the phase plane and the steady state operating points for each of the substructures. The steady state operating point (V_0^*, I^*) is the intersection of the sliding line and the dc gain. The sliding line is given by

$$\sigma(s) = \hat{v}_0 + K_v R_s \hat{i}(s) = 0$$

The sliding line transformed to $(\hat{v}_0, d\hat{v}_0/dt)$ is given by

$$\sigma(t) = \hat{v}_0 + K_v R_s C d\hat{v}_0/dt = 0$$

The conditions for the existence of sliding mode are

$$K_v R_s < R$$
$$V_0^* < v_g$$

The maximum obtainable bandwidth is

$$\omega_M = 1/K_v R_s C$$

The practical sliding line is with a high-pass filter for measuring current and is as follows.

$$\sigma^*(s) = (v_0 - V_0^*) + \frac{K_v R_s}{1 + \omega_1/s} i(s) = 0$$

The design criterion is that the current filter corner is much less than the maximum bandwidth ω_M.

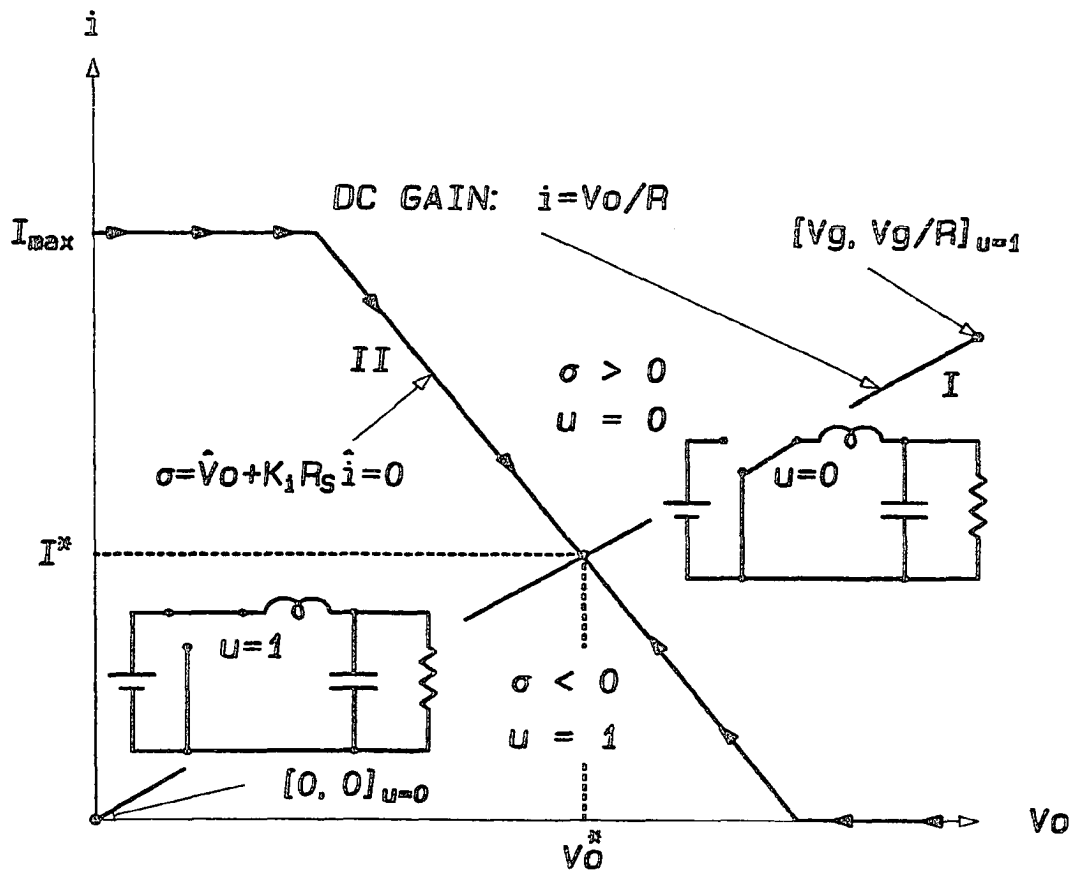

Fig. 4.23 The buck dc-to-dc converter in the phase plane. The sliding line in terms of the inductor current and the output voltage is shown by curve II. Line I is the dc gain between the inductor current and the output voltage. The control law is also shown.

4.6.6 Buck-boost Dc-to-dc Converter

Figure 4.24 shows the phase plane of the buck-boost converter. Also shown are the sliding line, structure-control law, substructures active in each region of the phase plane and the steady state operating points for each of the substructures used. The steady state gain is given by

$$i = -v_0/R + v_0^2/Rv_g$$

The sliding line is given by

$$\sigma(s) = -\hat{v}_0 + K_v R_s \hat{i} = 0$$

The steady state operating point is the intersection of the sliding line and the dc gain. The sliding line transformed to $(\hat{v}_0, d\hat{v}_0/dt)$ axes is

$$\sigma(t) = a(t)\hat{v}_0 + b(t)d\hat{v}_0/dt$$

where

$$a(t) = 1 + \frac{K_v R_s}{R} - \frac{K_v R_s V_0^*}{Rv_g}(2 + \hat{v}_0/V_0^*)$$

$$b(t) = -\frac{K_v R_s C V_0^*}{v_g}\left[1 - \frac{v_g}{V_0^*} + \frac{\hat{v}_0}{V_0^*}\right]$$

The condition for stability of response is $\hat{v}_0/V_0^* < 1$. The maximum obtainable bandwidth is

$$\omega_M \approx \begin{cases} K_v R_s C V_0^*/v_g & \text{for} \quad V_0^* > v_g \\ K_v C R_s & \text{for} \quad V_0^* < v_g \end{cases}$$

The condition for the existence of sliding mode is

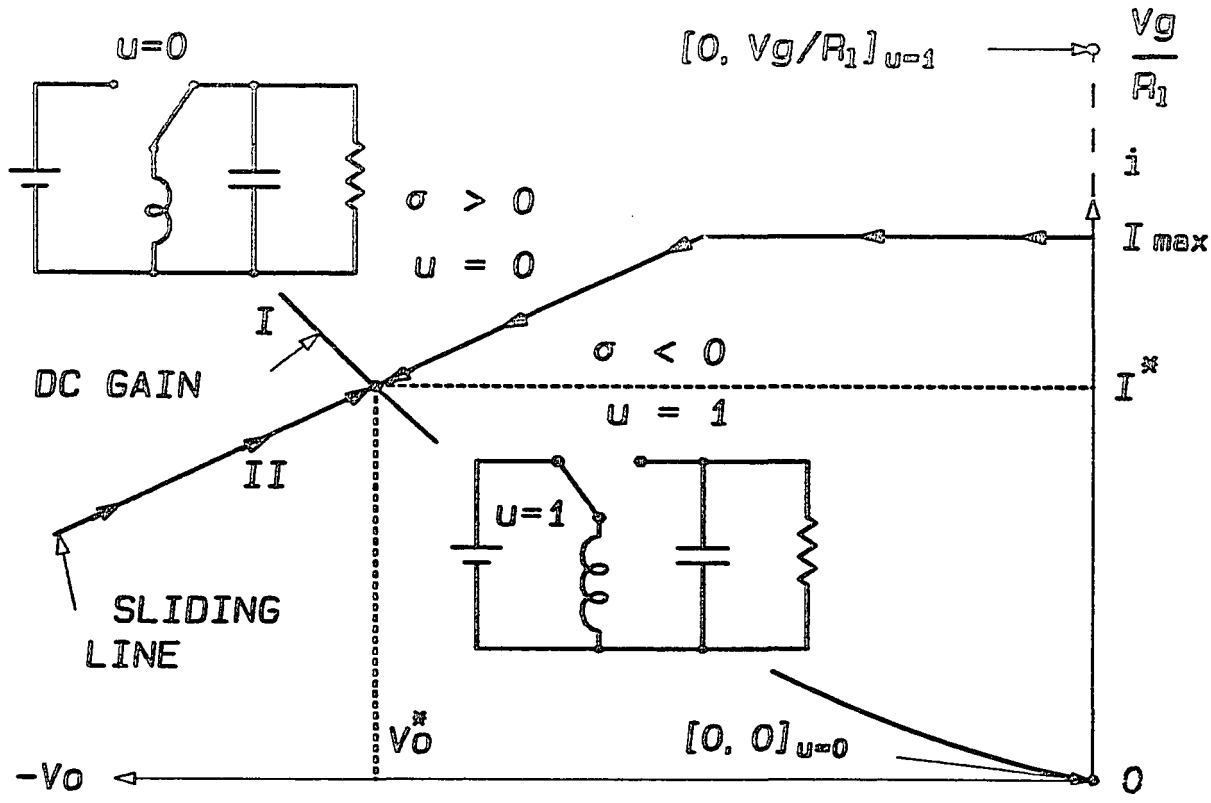

Fig. 4.24 The buck-boost dc-to-dc converter in the phase plane. The sliding line in terms of the inductor current and the output voltage is shown by curve II. Line I is the dc gain between the inductor current and the output voltage. The control law is also shown.

$$L < \min\left\{\frac{K_v R_s C R v_g}{v_0}, \frac{K_v R_s C v_0}{I_{max} + v_0/R}\right\}$$

The practical sliding line incorporating the high-pass filter for measuring the current is

$$\sigma^*(s) = -\hat{v}_0(s) + \frac{K_v R_s}{1 + \omega_1/s}\hat{i}(s) = 0$$

The design criterion for achieving the maximum possible bandwidth is that the current filter corner is much less than the maximum bandwidth ($\omega_1 \ll \omega_M$).

In this section, the method of state space averaging was reviewed as a modelling method of dc-to-dc converters. The theory of VSS and sliding modes were applied to dc-to-dc converters, first as an analysis method and then as a design method for controlling the output voltage of dc-to-dc converters. With sliding mode control it was shown that the overall stability is guaranteed for both small and large signals. With boost converter and buck-boost converter, where the controllable states of the system are discontinuous, alternate method of setting up the sliding surfaces in order to achieve voltage control was illustrated. The response was related to the desired performance, and practical design criteria were derived. Experimental results on a boost converter control were presented to confirm the design process.

CHAPTER 5

GENERAL THEORY OF ELECTRICAL MACHINES

In this chapter the general theory of rotating electrical machines is reviewed. From the general theory [11], the governing equations of different types of electrical machines are derived in such a format as to appreciate their similarity to dc to dc converters, and to apply the sliding mode control principles in order to control different types of electrical machines.

Historically, each type of electrical machine was analyzed as a special case with appropriate simplifying assumptions. This was necessary because the theory of transformations which exposes the unity of all electrical machines was not developed at that time. An example of the type of approach adopted was the stationary, per phase equivalent circuit model of three phase induction motors under the assumptions of i) balanced three phase supply, and ii) symmetrical, balanced and sinuzoidally distributed windings. Such models were simple and adequate for the purpose of steady state performance evaluation. Attention was confined to steady state performance. Unbalanced operation was treated using symmetrical components and the principle of superposition. Appropriate simplifying assumptions were made at the beginning of the analysis; as a result the unifying features of all machines were missed.

In contrast to the above, the general theory regards each and every machine as an assemblage of coils. The performance of any machine is governed by a single voltage equation and a single torque equation. The general theory is concerned exclusively with circuit theory of machines. The machines are treated as black boxes characterized completely by a set of measurements made at the terminals and the shaft. Such a treatment is better appreciated by the control engineer, who is interested in the performance of a system, where the machine is just another component of the total system.

Section 5.1 of this chapter describes the simplest of the rotating machines with two coils and relative motion between the two. Faraday's law and conservation of energy are used to derive the voltage and torque equations.

Section 5.2 describes the fundamental two phase machine. This machine is conceived of as the primitive slip-ring machine, to which all the practical slip-ring machines may be reduced. Section 5.3 describes the action of commutators found in dc machines and presents the basic commutator machine, from which all the practical commutator machines may be derived.

Bulk of the machines used in practice are polyphase machines. Section 5.4 explains the difficulties involved in the analysis of such machines and introduces the mathematical transformations used to simplify the analysis. The properties of these transformations are also presented alongwith the transformations. At this stage the transformations are given purely as a mathematical

artifice. More satisfying physical interpretations to these transformations appear later in Chapter 6.

The application of the various transformations to the general machines, to arrive at the general performance equations are explained in greater detail in Appendix 1. Sections 5.5, 5.6, and 5.7 use the results obtained in Appendix 1 for the general machines to get the performance equations of a separately excited dc motor, a three phase synchronous motor, and a three phase induction motor. Simple electrical equivalent circuits are also given. These equivalent circuits will be used in subsequent chapters to apply sliding mode control to some of these machines.

5.1 Basic Two Winding Machine

In this section the basic two winding machine is analyzed from first principles, using Ohm's law, Faraday's law, and the law of conservation of energy, to arrive at the performance equations. Following the general theory of machines it is possible to analyze the performance of different types of rotating machines in terms of the voltage and torque equations of this basic machine.

The two windings of the basic machine are shown in Fig. 5.1. ϑ is the angle between the axes of the moving coil on the rotor and the stationary coil on the stator. With the rotor moving with an angular velocity of ω_r, ϑ is clearly a function of time.

$$d\vartheta / dt = \omega_r \tag{5.1}$$

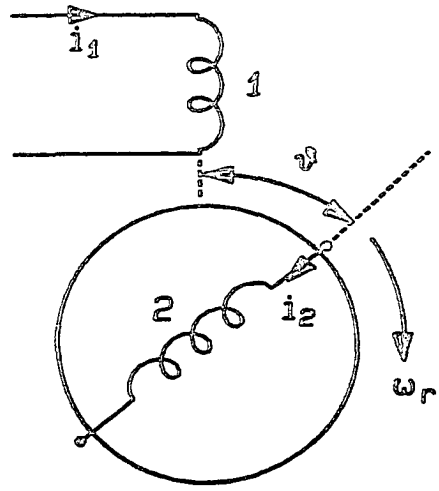

Fig. 5.1 Schematic of the basic two winding machine. The stator carries winding 1. The rotor carries winding 2. The rotor is rotating at an angular velocity of ω.

Applying Kirchoff's law, the voltage equations for the two coils may be written as follows.

$$v_1 = R_1 i_1 + pL_1 i_1 + pM_{12} i_2 \tag{5.2}$$

$$v_2 = R_2 i_2 + pL_2 i_2 + pM_{21} i_1 \tag{5.3}$$

R_1, R_2 are resistances of the two coils. L_1, L_2 are the self inductances of the coils. M_{12}, M_{21} are the mutual inductance between the two coils. p is the differential operator d/dt. The convention followed for the mutual inductances is to associate the first subscript with the voltage and the second subscript with the current. The mutual inductances M_{12} and M_{21} are equal and so the subscripts may be dropped. Equations (5.2) and (5.3), then reduce to

$$v_1 = R_1 i_1 + pL_1 i_1 + pM i_2 \tag{5.4}$$

$$v_2 = R_2 i_2 + pL_2 i_2 + pM i_1 \tag{5.5}$$

In general the various inductances are functions of rotor position and hence functions of time. Equations (5.4) and (5.5) may then be expanded as

$$v_1 = R_1 i_1 + L_1 p i_1 + i_1 p L_1 + M p i_2 + i_2 p M \tag{5.6}$$

$$v_2 = R_2 i_2 + L_2 p i_2 + i_2 p L_2 + M p i_1 + i_1 p M \tag{5.7}$$

Total instantaneous input power is the sum of the input powers into each of the coils and is obtained from Eqs. (5.6) and (5.7).

$$v_1 i_1 + v_2 i_2 = R_1 i_1^2 + R_2 i_2^2 + L_1 i_1 p i_1 + i_1^2 p L_1 + L_2 i_2 p i_2 +$$

$$i_2^2 p L_2 + M i_1 p i_2 + 2 i_1 i_2 p M + M i_2 p i_1 \tag{5.8}$$

Equation (5.8) may be put in the following form, the reason for which will become clear in a while.

$$v_1 i_1 + v_2 i_2 = R_1 i_1^2 + R_2 i_2^2 + p\left(\frac{1}{2} L_1 i_1^2 + \frac{1}{2} L_2 i_2^2 + M i_1 i_2\right) +$$

$$\frac{1}{2} i_1^2 p L_1 + \frac{1}{2} i_2^2 p L_2 + i_1 i_2 p M \tag{5.9}$$

The quantity inside the bracket in Eq. (5.9) is identified as the energy stored in the magnetic field.

The law of conservation of energy may be applied to get the following relationship.

$$\begin{matrix} INPUT \\ POWER \end{matrix} = LOSSES + \begin{matrix} RATE\ OF\ CHANGE\ OF \\ STORED\ ENERGY \end{matrix} + OUTPUT\ POWER \tag{5.10}$$

Now Eqs. (5.9) and (5.10) may be compared to obtain

$$\begin{matrix} OUTPUT \\ POWER \end{matrix} = \frac{1}{2}i_1^2 pL_1 + \frac{1}{2}i_2^2 pL_2 + i_1 i_2 pM \tag{5.11}$$

The power output from the machine is mechanical and is the product of the output torque and the angular velocity of the rotor.

$$OUTPUT\ POWER = Tp\vartheta \tag{5.12}$$

The second performance equation of the machine, namely the torque, is obtained from Eqs. (5.11) and (5.12).

$$T = \frac{1}{2}i_1^2 \frac{dL_1}{d\vartheta} + \frac{1}{2}i_2^2 \frac{dL_2}{d\vartheta} + i_1 i_2 \frac{dM}{d\vartheta} \tag{5.13}$$

Equations (5.4), (5.5), and (5.13) are the fundamental performance equations of the basic two winding machine. They may be put in the following compact matrix form.

$$V = ZI \tag{5.14}$$

$$T = \frac{1}{2}I^T \frac{dL}{d\vartheta} I \tag{5.15}$$

where,

$$V = \begin{bmatrix} v_1 \\ v_2 \end{bmatrix};\quad Z = \begin{bmatrix} R_1 + pL_1 & pM \\ pM & R_2 + pL_2 \end{bmatrix};$$

$$I = \begin{bmatrix} i_1 \\ i_2 \end{bmatrix};\quad L = \begin{bmatrix} L_1 & M \\ M & L_2 \end{bmatrix}$$

The "p" operator present inside the Z matrix warrants caution. It is prudent to consider Eqs. (5.14) and (5.15) as a compact representations of the fundamental performance equations and not as a matrix equation. With the theory of transformations to be

described later, it will be seen that the performance equations of all types of rotating electrical machines may be put in the above form.

5.2 Fundamental Slip-ring Machine

In this section the slip-ring machine is described. It differs from the basic two winding machine described in Section 5.1, in the number of windings on the stator and rotor. The stator carries two windings, orthogonal to each other. So does the rotor. The reason for the selection of the above structure for the fundamental machine is explained below.

The most essential features of all rotating machines are the stator and the rotor. The stator and the rotor carry independent windings. The current in the stator windings produce the stator magneto-motive force (MMF). The current in the rotor windings produce the rotor MMF. The stator MMF and the rotor MMF interact to produce useful torque. The flux distribution in all rotating machines is invariant along the length of the machine. As a result, the magnetic circuit consisting of the stator, rotor and the windings has linear symmetry and reduces to essentially a two-dimensional one. Therefore in any general machine, in order to produce stator and rotor MMF's in any arbitrary direction, it is necessary that such a fundamental machine has at least two non-collinear windings on both the stator and the rotor. If these non-collinear windings are selected to be orthogonal to each other, further simplifications result owing to the fact that the mutual inductances between orthogonal windings are zero. These are the reasons leading to the structure of

the fundamental machine as stated earlier.

Figure 5.2 shows the schematic of the fundamental slip-ring machine. The stator carries two windings A and B, orthogonal to each other. The windings A and B are shown as lumped windings oriented in the direction of their respective MMFs. The rotor carries two lumped windings α and β, orthogonal to each other. Again α and β are shown oriented along their respective MMFs. The voltage equation for the fundamental machine may be written as

$$\begin{bmatrix} v_A \\ v_B \\ v_\alpha \\ v_\beta \end{bmatrix} = \begin{bmatrix} R_A + pL_A & 0 & pM_{A\alpha} & pM_{A\alpha} \\ 0 & R_B + pL_B & pM_{B\alpha} & pM_{B\alpha} \\ pM_{\alpha A} & pM_{\alpha B} & R_\alpha + pL_\alpha & 0 \\ pM_{\beta A} & pM_{\beta B} & 0 & R_\beta + pL_\beta \end{bmatrix} \begin{bmatrix} i_A \\ i_B \\ i_\alpha \\ i_\beta \end{bmatrix} \tag{5.16}$$

Applying the condition that the mutual coupling between the stator and rotor windings are trigonometric functions of the rotor angle ϑ, Eq. (5.16) reduces to

$$\begin{bmatrix} v_A \\ v_B \\ v_\alpha \\ v_\beta \end{bmatrix} = \begin{bmatrix} R_A + pL_A & 0 & Mp\cos\vartheta & Mp\sin\vartheta \\ 0 & R_B + pL_B & -Mp\sin\vartheta & Mp\cos\vartheta \\ Mp\cos\vartheta & -Mp\sin\vartheta & R_\alpha + pL_\alpha & 0 \\ Mp\sin\vartheta & Mp\cos\vartheta & 0 & R_\beta + pL_\beta \end{bmatrix} \begin{bmatrix} i_A \\ i_B \\ i_\alpha \\ i_\beta \end{bmatrix} \tag{5.17}$$

Equation (5.17) is the definining equation for the fundamental slip-ring machine. It is seen that the Z matrix of even this simplified machine is a function of the rotor angle. Furthermore the "p" operator operates on the product of the various currents and the trigonometric functions. The elimination of the rotor angle ϑ from the impedance matrix Z is the central feature of the unified

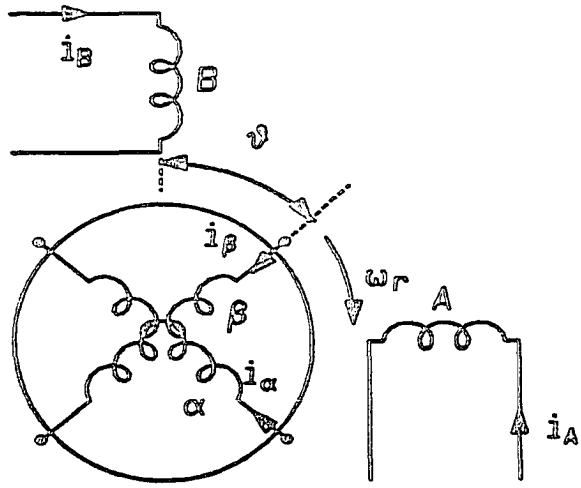

Fig. 5.2 The fundamental slipring machine. The stator carries windings A and B, which are orthogonal to each other. The rotor carries two orthogonal windings α and β. The rotor is rotating with angular velocity ω.

machine theory. These details are explained subsequently in Section 5.4.

5.3 Basic Commutator Machine

In the basic slip-ring machine described in Section 5.2, the rotor MMF is a function of the rotor position when the rotor currents are dc. This physical fact is seen mathematically, in the impedance matrix Z being a function of the rotor angle ϑ. In contrast to this, in the basic commutator machine, the rotor MMF is independent of the rotor angle ϑ. In this section the action of the commutator, leading to the above result is first explained. Then the basic commutator machine is described.

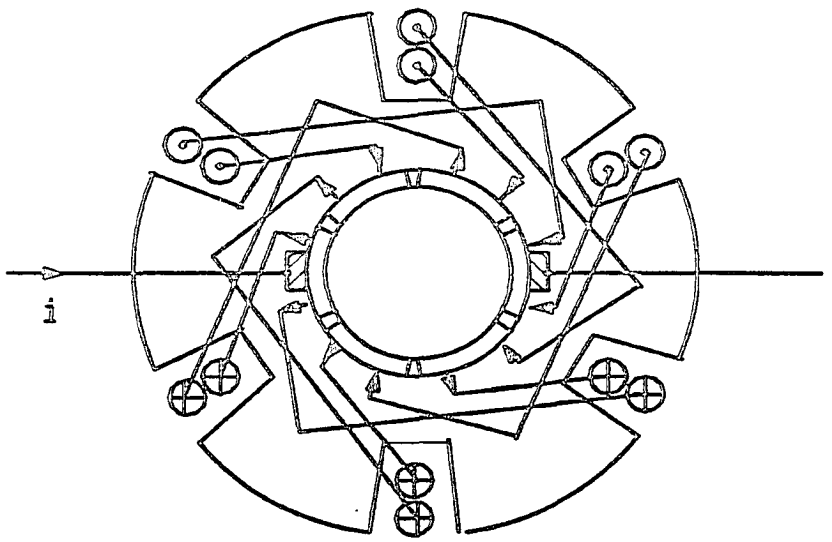

Fig. 5.3 The construction of a commutator rotor. The brushes lead current into the armature through the commutator segments. The commutator segments and the connection to the rotor conductor is such that, the rotor MMF is in line with the brushes and independent of the rotor position.

Figure 5.3 shows the construction of a commutator rotor. The rotor windings, their connection to the commutator segments and the brushes leading current into the rotor coils through the commutator segments are all shown. The direction of currents in the individual rotor coils are also shown. It may be seen that the MMFs produced by the individual windings of the rotor add up to give a nett rotor MMF along the direction of the brushes. The direction of rotor MMF in a commutator fed rotor is therefore, independent of the rotor angle and stays always along the direction of brushes.

Figure 5.4 shows the schematic representation of the commutator rotor. The rotor winding is shown lumped and fixed in direction along the brushes, indicating the fact that the direction of

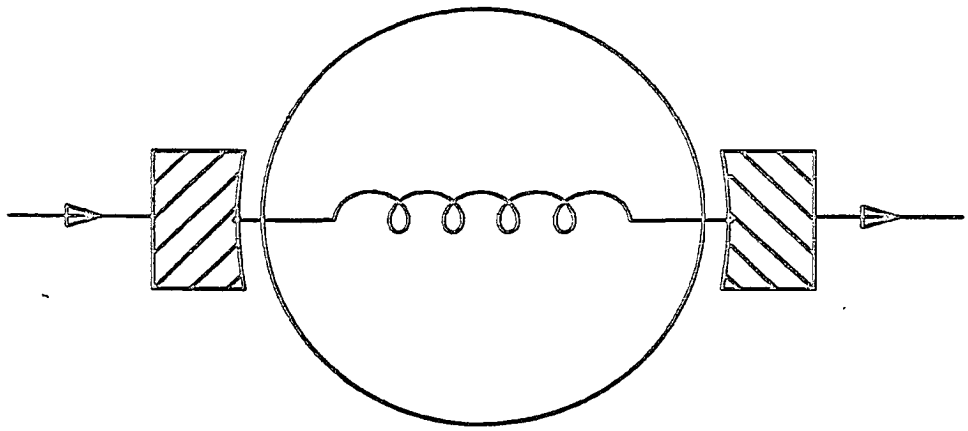

Fig. 5.4 The schematic representation of the commutator rotor. The rotor winding is shown lumped and in line with the brushes to indicate the direction of the rotor MMF.

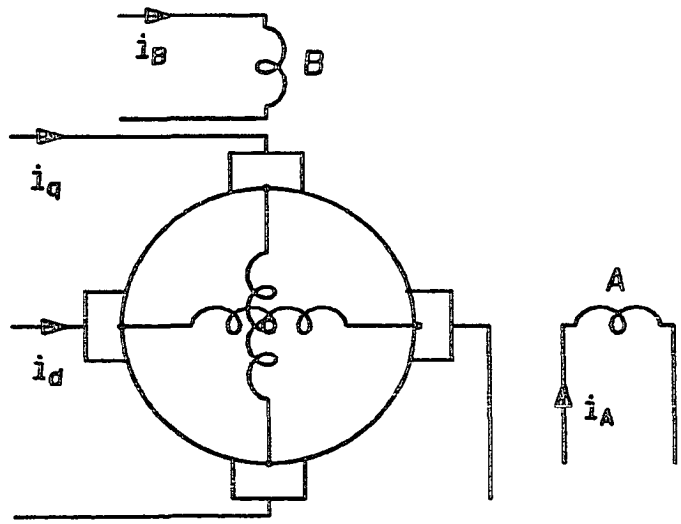

Fig. 5.5 The basic commutator machine. The stator and the rotor each carry two orthogonal windings. The rotor is supplied through commutators and hence the rotor field is independent of the rotor position.

rotor MMF of a commutator rotor is fixed in space along the direction of the brushes.

As had been explained in Section 5.2, the generalized rotor has to carry a minimum of two windings in order to be able to arbitrarily select the direction of rotor MMF in the active plane of the machine. The basic commutator machine, therefore, is conceived with two orthogonal stator windings (just like the stator windings of the fundamental slip-ring machine), and two orthogonal rotor windings supplied through a set of brushes and commutator segments. Figure 5.5 shows the structure of such a basic commutator machine. A and B constitute the orthogonal stator windings. The windings d and q on the rotor are fed through a set of brushes and commutator segments, and are orthogonal to each other. The various windings are shown lumped and oriented along the direction of their respective MMFs.

The unified machine theory consists of applying a series of mathematical transformations, to replace any rotating machine by its equivalent commutator type of machine, the motivation being the impedance matrix of the equivalent commutator machine is independent of the rotor angle, and hence much simpler to analyze. The various transformations that facilitate this process are discussed in the next section.

5.4 Passive Transformations

This section describes the passive transformations that are used to unify the different kinds of rotating electrical machines. These transformations are introduced with the objective of simplifying the analysis of different kinds of rotating machines. In order to appreciate the difficulties involved in solving the general performance equations, a three phase machine is first presented.

Figure 5.6 shows schematic of a three phase slip-ring machine. The stator carries three phase windings R,Y and B. The rotor carries three phase windings r,y and b. Equation (5.18) is the voltage equation for this three phase slip-ring machine, written down from first principles.

$$V = ZI \tag{5.18}$$

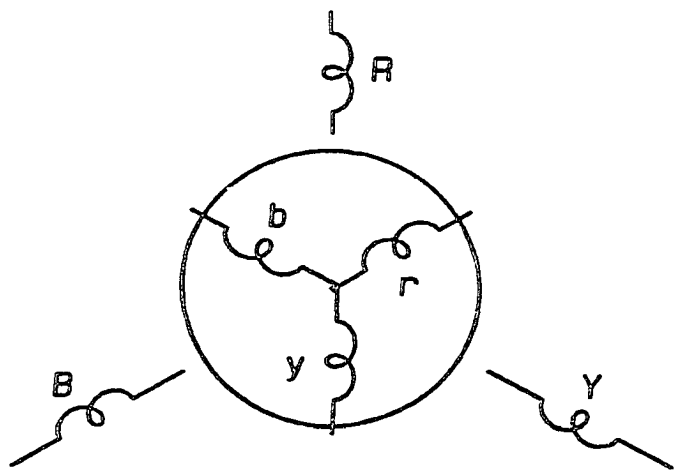

Fig. 5.6 A practical three phase slipring machine. The stator and rotor carry balanced three phase windings.

$$V = [\ v_R \quad v_Y \quad v_B \quad v_r \quad v_y \quad v_b\ ]^T$$

$$I = [\ i_R \quad i_Y \quad i_B \quad i_r \quad i_y \quad i_b\ ]^T$$

$$Z = \begin{bmatrix} R_R+pL_R & pM_{RY} & pM_{RB} & pM_{Rr} & pM_{Ry} & pM_{Rb} \\ pM_{YR} & R_Y+pL_Y & pM_{YB} & pM_{Yr} & pM_{Yy} & pM_{Yb} \\ pM_{BR} & pM_{BY} & R_B+pL_B & pM_{Br} & pM_{By} & pM_{Bb} \\ pM_{rR} & pM_{rY} & pM_{rB} & R_r+pL_r & pM_{ry} & pM_{rb} \\ pM_{yR} & pM_{yY} & pM_{yB} & pM_{yr} & R_y+pL_y & pM_{ry} \\ pM_{bR} & pM_{bY} & pM_{bB} & pM_{br} & pM_{by} & R_b+pL_b \end{bmatrix}$$

The voltage equation consists of six component equations, one for each of the three phase stator and rotor windings. The presence of the differential operator "p" makes this into a system of simultaneous differential equations. The differential operator operates on the products of various mutual inductances and currents, both of which are functions of time. This is so because the mutual inductances between the stator and rotor windings are dependent on the rotor angle and hence on time. The main objective of the passive transformations described next, is to simplify and eliminate the dependence of the above matrix upon the rotor angle ϑ. For the purpose of simplicity this is done in two steps, although it can be accomplished in a single step.

The first step is to apply the phase transformation C_1 to both the rotor and stator windings. The phase transformation C_1 corresponds mathematically to a change of variables. The actual machine voltages and currents are replaced by suitably scaled, more convenient, fictitious voltages and currents. The result of this transformation is to replace the actual three phase machine by its

equivalent fundamental slip-ring machine described in Section 5.2. The phase transformation C_1 considerably simplifies the system equations. However, it does not eliminate the dependence of the impedance matrix upon the rotor angle ϑ. The elimination of the rotor angle ϑ from the impedance matrix is the essence of the generalized machine theory, and is accomplished by the application to the rotor windings of another passive transformation. This second transformation C_2, called the commutator transformation, is a rotor angle dependent transformation. It accomplishes the elimination of the rotor angle from the impedance matrix by replacing the machine variables into yet another set of new variables. In physical terms, the original machine is replaced by its equivalent commutator machine described in Section 5.3.

Although the voltages as well the currents of the machine are transformed into new variables, these individual transformations are not independent of each other, since the power in the transformed description has to be the same as the power in the original description. It is seen below that, when the transformation is unitary, the power invariance condition leads to identical transformation for both voltages and currents. The primed and unprimed system of equations below represent the transformed and original system of equations respectively.

$$V = ZI \tag{5.19}$$

$$V' = Z'I' \tag{5.20}$$

Let

$$V' = C_v V \tag{5.21}$$

$$I' = C_i I \tag{5.22}$$

The convenient form of representing power in matrix form is given by

$$P = V^{*T} I \tag{5.23}$$

where the superscripts $*$ and T represent the transpose and complex conjugate respectively.

$$P' = V'^{*T} I' \tag{5.24}$$

Equating P and P', we get

$$V^{*T} I = V^{*T} C_v^{*T} C_i I \tag{5.25}$$

This leads to

$$C_v^{*T} C_i = I_n \quad \textit{(Identity matrix of order n)} \tag{5.26}$$

$$C_v^{*T} = C_i^{-1} \tag{5.27}$$

When the transformations are real, if C_v and C_i are both identically equal to C, then

$$C^T = C^{-1} \tag{5.28}$$

The phase transformation C_1 and the commutator transformation C_2 both being power invariant transformations, possess the above property.

The phase transformation C_1 and the commutator transformation C_2 are given in Eqs. (5.4.12) and (5.4.13).

$$C_1 = \sqrt{2/3}\begin{bmatrix} 1/\sqrt{2} & 1/\sqrt{2} & 1/\sqrt{2} \\ 1 & -1/2 & -1/2 \\ 0 & \sqrt{3}/2 & -\sqrt{3}/2 \end{bmatrix} \tag{5.29}$$

$$C_2 = \begin{bmatrix} 1 & 0 & 0 \\ 0 & \sin\vartheta & \cos\vartheta \\ 0 & \cos\vartheta & -\sin\vartheta \end{bmatrix} \tag{5.30}$$

The transformed impedance matrix is given by

$$Z' = C^T Z C \tag{5.31}$$

Appendix 1 gives in greater detail how these transformations when applied to the various machines lead to the desired simplifications. From the general equations brought out in Appendix 1, the performance equations and equivalent circuits of a few types of rotating electrical machines are derived in the following sections.

5.5 DC Machine

In this section, the performance equations derived for the general commutator machine in the Appendix 1 are used as a starting point to arrive at the electrical equivalent circuit of a separately excited dc motor drive.

For the general two phase commutator machine the voltage equations (taken from Eq. (A.7) of Appendix 1) are given by

$$\begin{bmatrix} v_A \\ v_B \\ v_d \\ v_q \end{bmatrix} = \begin{bmatrix} R_A + L_A p & 0 & M_A p & 0 \\ 0 & R_B + L_B p & 0 & M_B p \\ M_A p & -M_B \omega_r & R_d + L_d p & -L_q \omega_r \\ M_A \omega_r & M_B p & L_d \omega_r & R_q + L_q p \end{bmatrix} \begin{bmatrix} i_A \\ i_B \\ i_d \\ i_q \end{bmatrix} \tag{5.32}$$

The leading diagonal terms are the voltage drops due to resistances and self inductances. The terms containing Mp terms are the induced voltages due to the mutual coupling and di/dt. These terms are called the transformer voltages. The terms containing ω_r appear only on rotor voltages and are due to rate of change of flux linkage due to rotation. These voltages are termed as rotary voltages or generator voltages.

The various inductance terms may be measured in a physical machine by exciting one winding at a time, and measuring the voltages appearing in the other windings as a result of transformer action and rotation respectively.

The above result for the general machine may now be applied for the particular case of the separately excited dc motor shown in Fig. 5.7. The operation of the dc motor is as follows. The field current i_A in the field winding sets up a field MMF in line with the field winding. The field MMF is stationary in space. The armature current i_q sets up an armature MMF stationary in space and in line with the brushes. The field MMF and the armature MMF are orthoganal to each other. The mechanical torque produced is proportional to the product of the field and the armature MMF's. Comparing Fig. 5.7 with the general machine given in Fig. 5.5, we find that the field winding corresponds to the stator winding A. The armature winding corresponds to the quadrature axis winding q. No

other windings are present. The simplified voltage equations are

$$\begin{bmatrix} v_A \\ v_q \end{bmatrix} = \begin{bmatrix} R_A + L_A p & 0 \\ M_A \omega_r & R_q + L_q p \end{bmatrix} \begin{bmatrix} i_A \\ i_q \end{bmatrix} \tag{5.33}$$

The next performance equation is that of torque. The torque is obtained by applying the conservation of energy. The voltage equation may be separated into resistive drops, induced transformer voltages and rotary voltages.

$$V = RI + LpI + G\omega_r I \tag{5.34}$$

$$R = \begin{bmatrix} R_A & 0 \\ 0 & R_q \end{bmatrix} ; L = \begin{bmatrix} L_A & 0 \\ 0 & L_q \end{bmatrix} ; G = \begin{bmatrix} 0 & M_A \\ 0 & 0 \end{bmatrix}$$

The input power is given by

$$I^T V = I^T RI + I^T LpI + I^T G\omega_r I \tag{5.35}$$

The RHS of Eq.(5.35) gives the power flow through the machine. The first term gives the copper losses. The second term is the rate of change of stored magnetic energy. The last term represents the power that is converted into mechanical output, which is the product of torque and angular velocity of the shaft. The angular velocity ω_r being a scalar, the torque is given by

$$T = I^T GI = M_A i_A i_q \tag{5.36}$$

The torque generated by the machine drives the mechanical system coupled to the motor. The dynamics of the mechanical system is given by

$$M_A i_A i_q = Jd\omega_r / dt + B\omega_r + T_L \tag{5.37}$$

where, J = moment of inertia; B = friction;

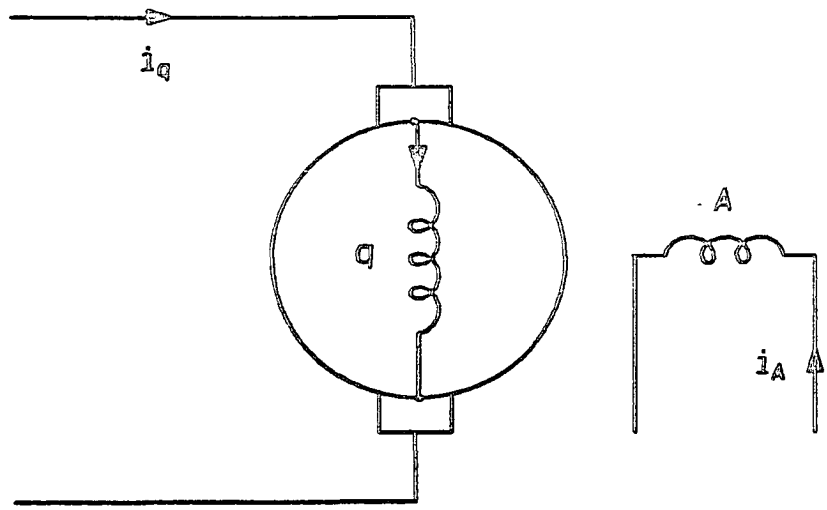

Fig. 5.7 A practical separately excited dc machine. The stator carries the fied winding A. The rotor is supppied through commutator. The stator and the rotor MMF's are orthogonal to each other.

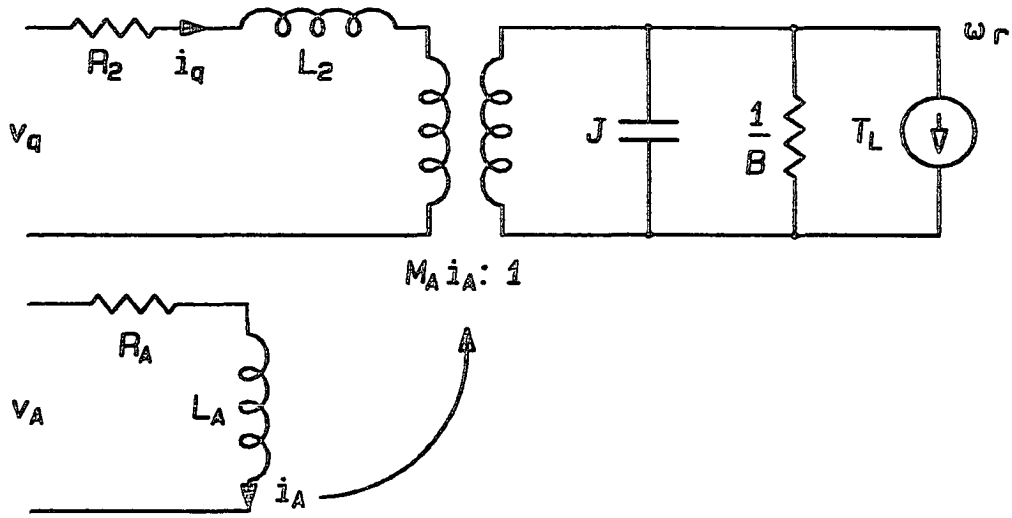

Fig. 5.8 The electrical equivaent circuit of the separately excited dc machine. The mechanical subsystem of the machine is represented by its analog electrical equivalent.

T_L = load torque.

The complete set of electrical and mechanical equations may be put conveniently into the electrical equivalent circuit shown in Fig. 5.8.

5.6 Synchronous Machine

In this section, the performance equations derived for the general slip-ring machine (Fig. A.1) in the Appendix 1 are used as a starting point to arrive at the performance equations and electrical equivalent circuit for the synchronous machine.

The general commutator equivalent of the three phase salient pole machine considered in the Appendix 1 is governed by the (taken from Eq. (A.7) of Appendix 1) following equation.

$$\begin{bmatrix} v_A \\ v_B \\ v_d \\ v_q \end{bmatrix} = \begin{bmatrix} R_A + L_A p & 0 & M_A p & 0 \\ 0 & R_B + L_B p & 0 & M_B p \\ M_A p & -M_B \omega_r & R_d + L_d p & -L_q \omega_r \\ M_A \omega_r & M_B p & L_d \omega_r & R_q + L_q p \end{bmatrix} \begin{bmatrix} i_A \\ i_B \\ i_d \\ i_q \end{bmatrix} \tag{5.38}$$

The various self and mutual inductance terms are fictitious and are related to the original machine parameters by the relationships given in Appendix 1. Alternatively they can also be directly measured if the transformed quantities (v_d, v_q, i_d, i_q) are directly controllable and measurable by appropriate circuits from the physical variables $(v_r, v_y, v_b, i_r, i_y, i_b)$ of the machine.

Now the above results may be applied to the particular case of a three phase synchronous motor drive shown in Fig. 5.9. The rotor carries balanced three phase windings (r, y, b) and excited by

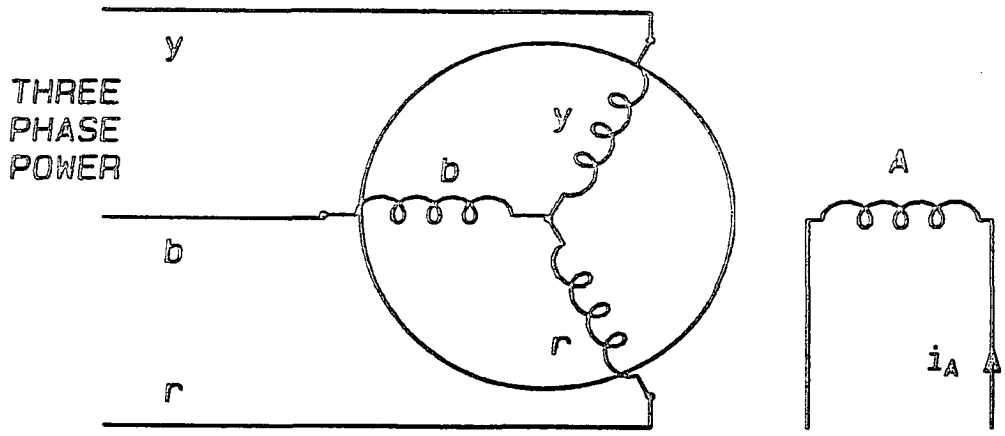

Fig. 5.9 A practical synchronous motor. The armature is supplied three phase power through sliprings. The field is on the stator and is supplied with dc power.

balanced three phase power. The stator carries the field winding A excited by dc. The stator current i_A sets up a stationary MMF in line with the stator winding. The rotor supplied with three phase power at synchronous frequency sets up a rotating MMF, relative to the rotor. Since the rotor is rotating at synchronous speed, the rotor MMF is stationary. The developed torque is proportional to the cross product of the rotor and the stator MMF's. The field winding B of the general machine is absent. Therefore the rows and columns corresponding to winding B may be dropped from Eq. (5.38). The simplified system of equations is given by

$$\begin{bmatrix} v_A \\ v_d \\ v_q \end{bmatrix} = \begin{bmatrix} R_A + L_A p & M_A p & 0 \\ M_A p & R_d + L_d p & -L_q \omega_r \\ M_A \omega_r & L_d \omega_r & R_q + L_q p \end{bmatrix} \begin{bmatrix} i_A \\ i_d \\ i_q \end{bmatrix} \tag{5.39}$$

The voltage equation may be separated as before into resistive drops, induced voltages due to transformer action and induced voltages due to rotation.

$$V = RI + L\underline{p}I + G\omega_r I \tag{5.40}$$

$$R = \begin{bmatrix} R_A & 0 & 0 \\ 0 & R_d & 0 \\ 0 & 0 & R_q \end{bmatrix} ; L = \begin{bmatrix} L_A & 0 & 0 \\ 0 & L_d & 0 \\ 0 & 0 & L_q \end{bmatrix} ; G = \begin{bmatrix} 0 & 0 & 0 \\ 0 & -L_q & 0 \\ M_A & 0 & L_d \end{bmatrix}$$

The input power is given by

$$I^T V = I_T R I + I^T L\underline{p}I + I^T G\omega_r I \tag{5.41}$$

The first two terms of Eq. (5.41) give the copper losses and the rate of change of stored magnetic energy respectively. The last term gives the mechanical output power. The output torque is given by

$$T = I^T G I = M_A i_A i_q + (L_d - L_q) i_d i_q \tag{5.42}$$

The torque is made up of two parts. The first part ($M_A i_A i_q$) is the torque due to stator excitation. The second part $(L_d - L_q) i_d i_q$ is independent of the stator excitation and is due to the saliency of the pole structure. This part of the torque is called the reluctance torque. Reluctance torque is absent in non-salient pole ($L_d = L_q$) machines.

The mechanical system equation is identical to those given for dc machine in Section 5.5.

$$T = Jd\omega_r / dt + B\omega_r + T_L \tag{5.43}$$

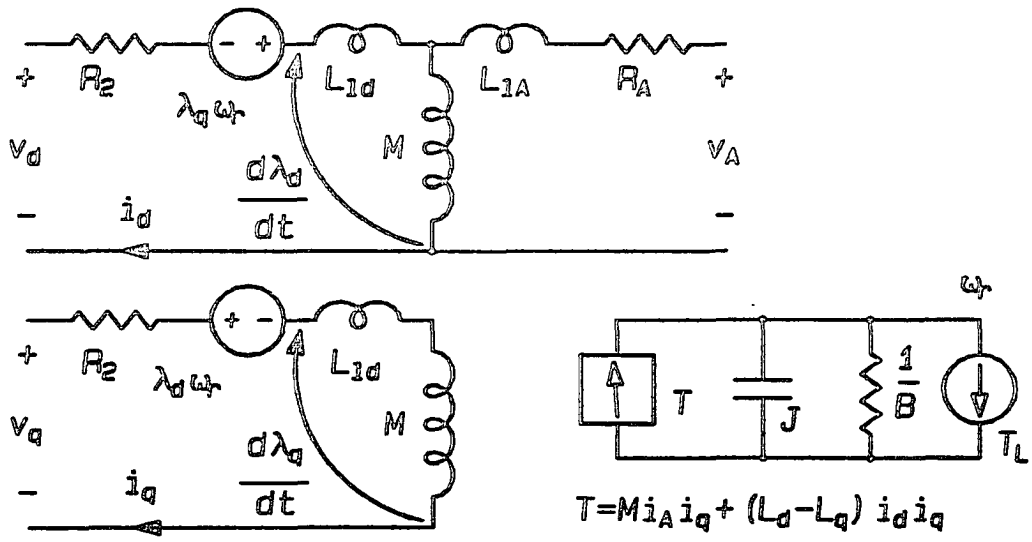

Fig. 5.10 The electrical equivalent circuit of a synchronous machine. The mechanical subsystem of the machine is represented by its electrical analog.

Equation (5.39) though compact and adequate mathematically, does not give an elegant equivalent circuit. For this purpose the various self inductances in Eq. (5.39) may be written as the sum of respective leakage inductances and mutual inductances as given below.

$$\begin{bmatrix} v_A \\ v_d \\ v_q \end{bmatrix} = \begin{bmatrix} R_A + (M + L_{lA})p & Mp & 0 \\ Mp & R_d + (M + L_{ld})p & -(M + L_{lq})\omega_r \\ M\omega_r & (M + L_{ld})\omega_r & R_q + (M + L_{lq})p \end{bmatrix} \begin{bmatrix} i_A \\ i_d \\ i_q \end{bmatrix} \tag{5.44}$$

From Eq. (5.44), the equivalent circuit readily follows and is given in Fig. 5.10. The flux linkages in the d and q axes are named λ_d and λ_q respectively.

$$\lambda_d = L_d i_d + M i_A \tag{5.45}$$

$$\lambda_q = L_q i_q \tag{5.46}$$

5.7 Induction Motor

From the voltage equations obtained from the Appendix 1 for the induction machine, we go on in this section to arrive at an electrical equivalent circuit for the induction motor. The voltage equations for the induction motor referred to a rotating orthogonal reference frame (rotating at $d\varphi/dt$) is given by (taken from Eq. (A.10))

$$\begin{bmatrix} v_{d1} \\ v_{q1} \\ v_{d2} \\ v_{q2} \end{bmatrix} = \begin{bmatrix} R_1 + L_1 p & -L_1 p\varphi & Mp & -Mp\varphi \\ L_1 p\varphi & R_1 + L_1 p & Mp\varphi & Mp \\ Mp & -Mp(\varphi - \vartheta_r) & R_2 + L_2 p & -L_2 p(\varphi - \vartheta_r) \\ Mp(\varphi - \vartheta_r) & Mp & L_2 p(\varphi - \vartheta_r) & R_2 + L_2 p \end{bmatrix} \begin{bmatrix} i_{d1} \\ i_{q1} \\ i_{d2} \\ i_{q2} \end{bmatrix} \tag{5.47}$$

The convenient reference frame to choose is $d\varphi/dt = \omega_e$, the electrical frequency of the three phase supply. Under this case all the transformed quantities are dc quantities. Further, the various self inductance terms may be decomposed into leakage and mutual inductances to arrive at an elegant equivalent circuit.

$$L_1 = M + L_{l1}$$
$$L_2 = M + L_{l2}$$

The power relationship is given by

$$I^T V = I_T R I + I^T L p I + I^T G \omega_r I \tag{5.48}$$

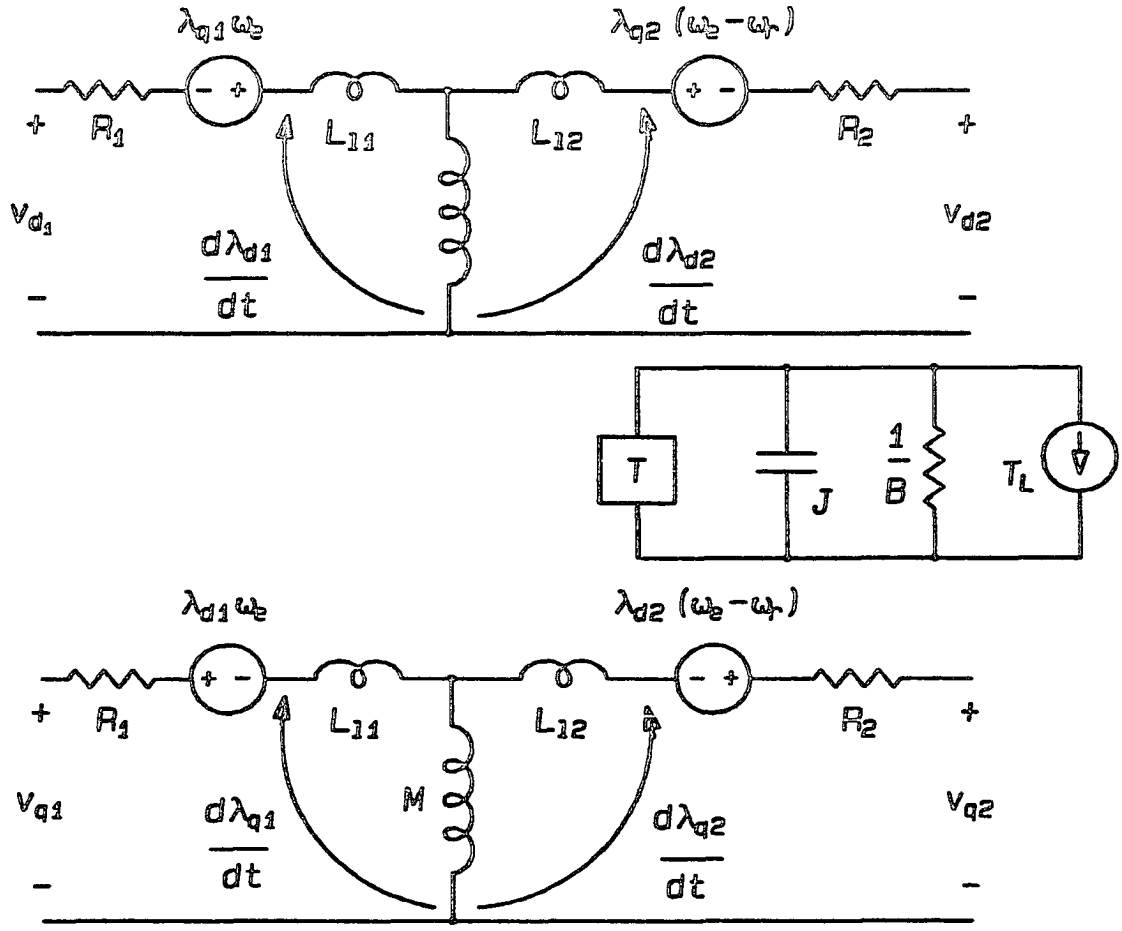

Fig. 5.11 The electrical equivalent circuit of an induction motor. The mechanical subsystem of the machine is represented by its electrical analog.

$$T = M(i_{q1}i_{d2} - i_{q2}i_{d1}) \tag{5.49}$$

The mechanical system of equation is as before given by

$$T = Jd\omega_r / dt + B\omega_r + T_L \tag{5.50}$$

From Eqs. (5.47) and (5.50), the overall electrical equivalent circuit for the induction motor drive is given by Fig. 5.11.

CHAPTER 6

CONTROL OF ELECTRICAL DRIVES

Electrical drive systems provide a convenient means of operation of industrial machinery. The high reliability and great versatility of electrical drives have resulted in their widespread application. A frequent requirement of industrial drives is the capacity for efficient control of mechanical quantities of torque, speed etc. The function of power conversion and power conditioning (torque control, speed control) can be combined together. The mechanical counterparts of power conditioners (such as gear trains, clutches, etc.) do not enjoy this advantage.

In Chapter 5, the general theory of electrical machines was reviewed. The operation of different types of machines was outlined and the performance equations derived.

DC motors had occupied a wide spectrum of applications for variable speed drives, because of their simplicity and versatility of control. The simplicity is obtained owing to the typical mechanical construction of the DC machine. The mechanical commutator in the DC machine and the brush orientation leading current into the armature enables orthogonality between the magnetomotive force (MMF) produced by the armature current and the main excitation MMF. As a result, for any given excitation to the DC machine, the

armature voltage determines operating speed and the armature MMF determines the developed torque. Under constant excitation, the DC motor is essentially a linear system resulting in the simplicity of control.

On the other hand the presence of commutator and brushes contribute to the wear and tear, and the consequent maintenance overheads of the drive. These disadvantages have led to the application of AC machines, which are robust in construction, for variable speed applications [12].

Polyphase synchronous and asynchronous motors, when supplied from a constant frequency, polyphase bus, operate at fixed speed (synchronous motors) or nearly fixed speed (asynchronous motors). They may be operated at variable speed when supplied from a variable frequency source. Conversion of power to polyphase variable frequency system became viable with high speed solid-state switches, opening up the application of AC motors for variable speed applications. Different converter topologies such as voltage fed inverter, current fed inverter, etc., are being used for the purpose. Different modulation techniques such as pulse width modulation (PWM), pulse amplitude modulation (PAM), etc., are used to control the amplitude of the output voltage and to minimize the hormonic content of the output polyphase power.

From the point of view of the motor being controlled different mathematical descriptions (voltage fed machine, current fed machine, stationary refernce frame, rotating reference frame, etc.) exist giving rise to different control options such as current fed

operation, constant volts/hertz operation, etc. More recently, the rotating reference frame description of the machine and the vector control or the field oriented control is being very successfully applied for superior dynamic performance of the a.c. drive [13].

One common feature among all the above control methods is that there is a converter (switching power processor) with its characteristic control loop (phase control, quasi-square wave control, PWM, etc.) and dynamics; and there is a motor (synchronous or asynchronous) with its static and dynamic characteristics. The two are then combined together to develop an overall model. Suitable feedback techniques are then employed to achieve the control objective such as speed control, position control, etc.

In contrast to the above, the theory of variable structure systems and the concept of sliding mode control may be used on the power processor and the motor together to develop a control strategy that is integrated to the final control objective namely speed control, position control, etc.

In this chapter, the principle of sliding mode control is applied for the speed control of dc motors and brushless dc (BLDC) motors. Useful criteria are developed for the design of speed controllers for these machines. The design methods are then verified from experimental results.

The dc motor drive controlled by a switching converters is described in Section 6.1. The method of control is described through the phase plane description of the dc motor. It will be noticed that the speed control of the dc motor is mathematically analogous to the

voltage control of the buck dc-to-dc converter described in Chapter 4. The design inequalities are derived for the existence of sliding mode control. Practical considerations are highlighted and the practical design criteria along with the experimental results are presented.

Measurement of speed in drive applications is usually done with a tachogenerator, which is one of the expensive components in the control loop. For low cost drives, an interesting application of sliding mode control is the estimation of speed from the electrical quantities of the drive. Section 6.2 describes such a speed estimator for a dc motor along with experimental results.

The performance equations and the operation of the synchronous motor were given in Chapter 5. The BLDC motor is a special case of the synchronous motor. Section 6.3 describes the BLDC motor and the simplified equivalent circuit of the BLDC motor. Current controlled operation and speed controlled operation are both discussed along with the respective control strategies.

The field oriented control developed in Section 6.3 requires the physical variables (phase currents) of the motor to be transformed to rotating reference frame ($d-q$ axes) variables. Section 6.4 describes the practical aspects of hardware associated with the transformations. Practical design criteria are developed to relate to the dynamic performance of the drive. Results on current-controlled operation and speed-controlled operation are then presented.

The practical design of field oriented control explained in Section 6.4, though mathematically exotic, is quite inexpensive to realize using digital circuit blocks. However further simplifications leading to more economy is feasible for certain applications. Section 6.5 explains simplified approximate realizations of the transformations. Experimental results are presented showing that the difference in performance after the simplifications is imperceptible.

6.1 Dc Motor Drive

Figure 6.1 shows the chopper-driven dc motor. The electrical equivalent circuit of the drive under constant excitation together with the power converter is shown in Fig. 6.2. The electrical equivalent circuit represents a completely electrical analog of the electromechanical system consisting of the motor and its mechanical load. The transformer shown in Fig. 6.2 represents the electromechanical torque conversion taking place in the motor. The secondary side current in the electrical equivalent circuit is analogous to the torque generated in the motor. The moment of inertia and the friction of the load appear as analogous capacitance and conductance in parallel in the equivalent circuit. The constant current load and the output voltage are analogs of the load torque and the shaft speed respectively. It will be noticed that the speed control of the constant excitation dc motor and the voltage control of the buck dc-to-dc converter are analogous problems. The performance equations of the drive given by Eqs. (5.33) and (5.37) in Chapter 5 for general dc motors are given here for the case of the

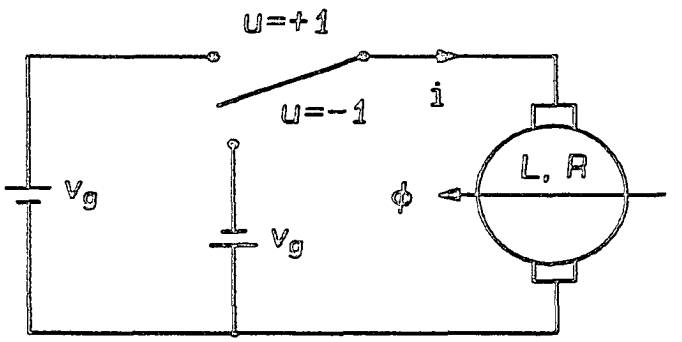

ϕ= AIR GAP FLUX
L= ARMATURE INDUCTANCE
R= ARMATURE RESISTANCE
J= INERTIA
B= FRICTION
T_L= LOAD TORQUE
ω= SHAFT SPEED

$$Ldi/dt + Ri + K_E\omega = v_g u$$

$$Jd\omega/dt + B\omega + T_L = K_T i$$

Fig. 6.1 Chopper-driven dc motor – definition of terms and defining equations under constant excitation.

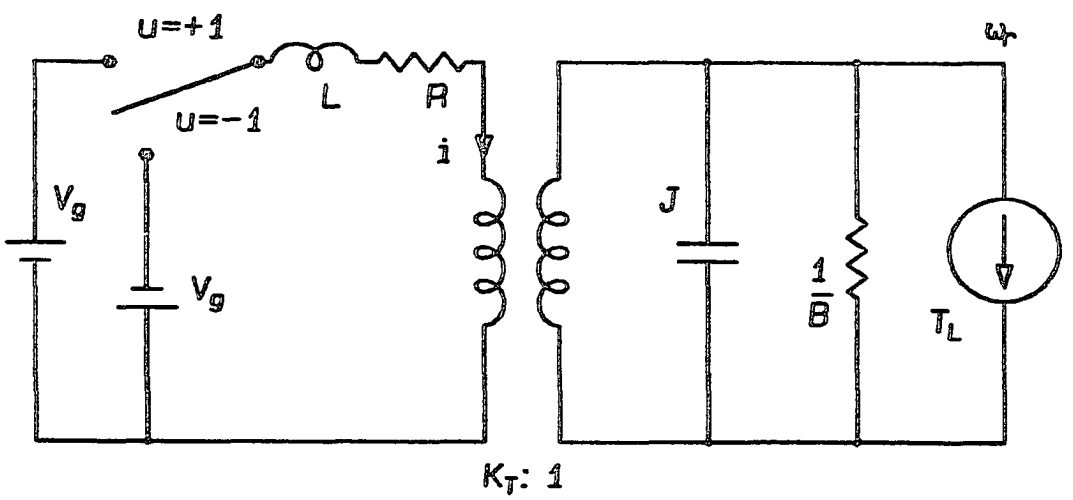

Fig. 6.2 The electrical equivalent circuit of the chopper-driven dc motor. The system structure is analogous to the buck dc-to-dc converter with the speed of the motor being analogous to the output voltage of the buck dc-to-dc converter.

constant excited dc motor.

$$L\frac{di}{dt} + Ri + K_E\omega = v_g u \tag{6.1}$$

$$J\frac{d\omega}{dt} + B\omega + T_L = K_T i \tag{6.2}$$

where,

L = Armature inductance; R = Armature resistance;

K_E = Back emf constant; ω = Angular velocity of rotor;

T_L = Load torque; K_T = Motor torque constant;

i = Armature current; v_g = Source voltage;

J = Moment of inertia of load;

B = Friction coefficient of load;

u = Discontinuous control, ±1.

The torque constant K_T and the back emf constant K_E are numerically equal in MKSA system of units. The above description is valid at all times. The control input u is the only discontinuous variable and takes on the value of either +1 or -1 depending on the switch position. The impressed voltage to the armature is correspondingly positive or negative leading to the possibility of bidirectional speed control. After some manipulation, the system Eqs. (6.1) and (6.2) may be put in the following form:

$$\dot{x} = A^* x + b^* u + c^* \tag{6.3}$$

where,

$$A^* = \begin{bmatrix} 0 & 1 \\ -\frac{K_T K_E}{JL}\left[1+\frac{BR}{K_T K_E}\right] & -\left(\frac{R}{L}+\frac{B}{J}\right) \end{bmatrix} \quad ; \quad b^* = \begin{bmatrix} 0 \\ \frac{K_T v_g}{JL} \end{bmatrix}$$

$$x = \begin{bmatrix} \omega-\omega^* \\ \frac{d(\omega-\omega^*)}{dt} \end{bmatrix} \quad ; \quad c^* = \begin{bmatrix} 0 \\ \frac{-R(T_L+B\omega^*)-K_T K_E \omega^*}{JL} \end{bmatrix}$$

and ω^* is the desired speed. Again it may be noticed that the system representation in Eq. (6.3) is identical in form to the buck dc-to-dc converter given in Chapter 4, Eq. (4.24). The system states have been assigned as the output speed error and its derivative, so that the desired operating point is given by the state vector $x = 0$. The control problem now reduces to establishing a switching strategy to select an appropriate u at any instant of time to meet the dynamic requirements of the system.

We recall that the system order being 2 ($n = 2$), and the number of control inputs being 1 ($m = 1$), it is possible to achieve under sliding control an overall response of order 1 ($n-m = 1$). Suppose that it is desired to achieve a response of zero steady-state error and a stable first-order transient response with a time constant of τ. These requirements are translated into a sliding boundary in the state space given by the following differential equation:

$$(\omega-\omega^*)+\tau\frac{d(\omega-\omega^*)}{dt} = 0 \qquad (6.4)$$

In matrix form Eq. (6.4) may be expressed as

$$\sigma = gx = 0; \quad g = [1 \quad \tau] \tag{6.5}$$

σ is a weighted sum of the states of the system and $\sigma = 0$ may be visualized as a line in the two-dimensional state space. Having related the steady state and the dynamic requirements into a suitable switching boundary, the next step is to establish the conditions for the existence of sliding mode along the chosen switching boundary. The general existence conditions are

$$\lim_{\sigma>0} \dot{\sigma} < 0, \quad \text{and} \quad \lim_{\sigma<0} \dot{\sigma} > 0 \tag{6.6}$$

Let the control inputs be,

$$u = \begin{cases} u^+ & \text{for } \sigma > 0 \\ u^- & \text{for } \sigma < 0 \end{cases} \tag{6.7}$$

Equation (6.6) now yields

$$\dot{\sigma} = \begin{cases} GA^*X + GB^*u^+ + GT^* & \text{for} \quad \sigma > 0 \\ GA^*X + GB^*u^- + GT^* & \text{for} \quad \sigma < 0 \end{cases}$$

$$GBu^+ < -GAX - GT < GBu^- \tag{6.8}$$

The control input is now chosen as

$$u^+ = -1 \quad \text{and} \quad u^- = +1 \tag{6.9}$$

For the selected control inputs, Eq. (6.8) reduces to

$$-\frac{\tau K_T V_g}{JL} \leq \frac{\tau K_T}{JL}\left\{K_E\omega + \frac{R(B\omega + T_L)}{K_T}\right\}$$

$$+\tau\frac{d(\omega-\omega^*)}{dt}\left(\frac{R}{L}+\frac{B}{J}-\frac{1}{\tau}\right) \leq \frac{\tau K_T V_g}{JL} \tag{6.10}$$

Equation (6.10) may be interpreted as follows. The dc quantities in

Eq. (6.10) give the condition on the direction of average motion of the system which is

$$\left|v_g\right| \geq \left|I^{\circ}R\right| + \left|K_E\omega^{\circ}\right| \tag{6.11}$$

where

ω° = steady-state desired speed.

I° = steady-state armature current at desired speed and load.

The time varying quantities in Eq. (6.10) (terms containing $d(\omega-\omega^{\circ})/dt$.) give the condition on the motion of the system in between switchings, which is

$$\frac{1}{\tau} \leq \frac{R}{L} + \frac{B}{J} \tag{6.12}$$

Equation (6.12) gives the condition on the best transient response obtainable. For machines whose electrical and mechanical time constants are well separated ($B/J << R/L$) one may say that the best transient response time constant achievable is the same as the electrical time constant of the motor. Such a design would result in large inrush of armature current during transients. In practice the rated armature current of the motor must not be exceeded. Therefore the rated armature current limits the rate of speed correction (acceleration or deceleration) during transients resulting in a response time which is usually higher than that given by Eq. (6.12).

6.1.1 Dc Motor Drive in the Phase Plane

The relevant steps in designing a sliding mode speed controller for the dc motor drive was seen in the previous section. It is worthwhile to briefly see the same aspects related in a graphical way through the phase plane description of the dc motor drive.

Figure 6.3. shows the phase plane description of the sliding mode speed controller for the dc motor. The axes of the phase plane are assigned as speed error and its derivative. The sliding line $\sigma = 0$ shown in Fig. 6.3 consists of three sections. The central portion of the sliding line is the same as explained in the last section. For large errors the sliding line is shaped such that the maximum acceleration and deceleration are limited thereby incorporating overcurrent protection to the drive. The control inputs, namely the switch position and the applicable equivalent circuits, are also shown in Fig. 6.3 corresponding to the two regions in the phase plane. The steady state operating points for each control inputs are also shown. It may be noticed that the dc motor drive and the buck dc-to-dc converter, being analogous systems, both lead to identical phase plane descriptions.

In order to be able to directly extend this concept of control later on to the BLDC motor, it is worthwhile to understand the switching decision ($u = +1$ *or* $u = -1$) qualitatively. This is necessary because the switching converter for driving the polyphase motor has three pairs of switches corresponding to the three phases of the motor. Accordingly at any instant three switch positions are to be determined. To enable this the switch inputs

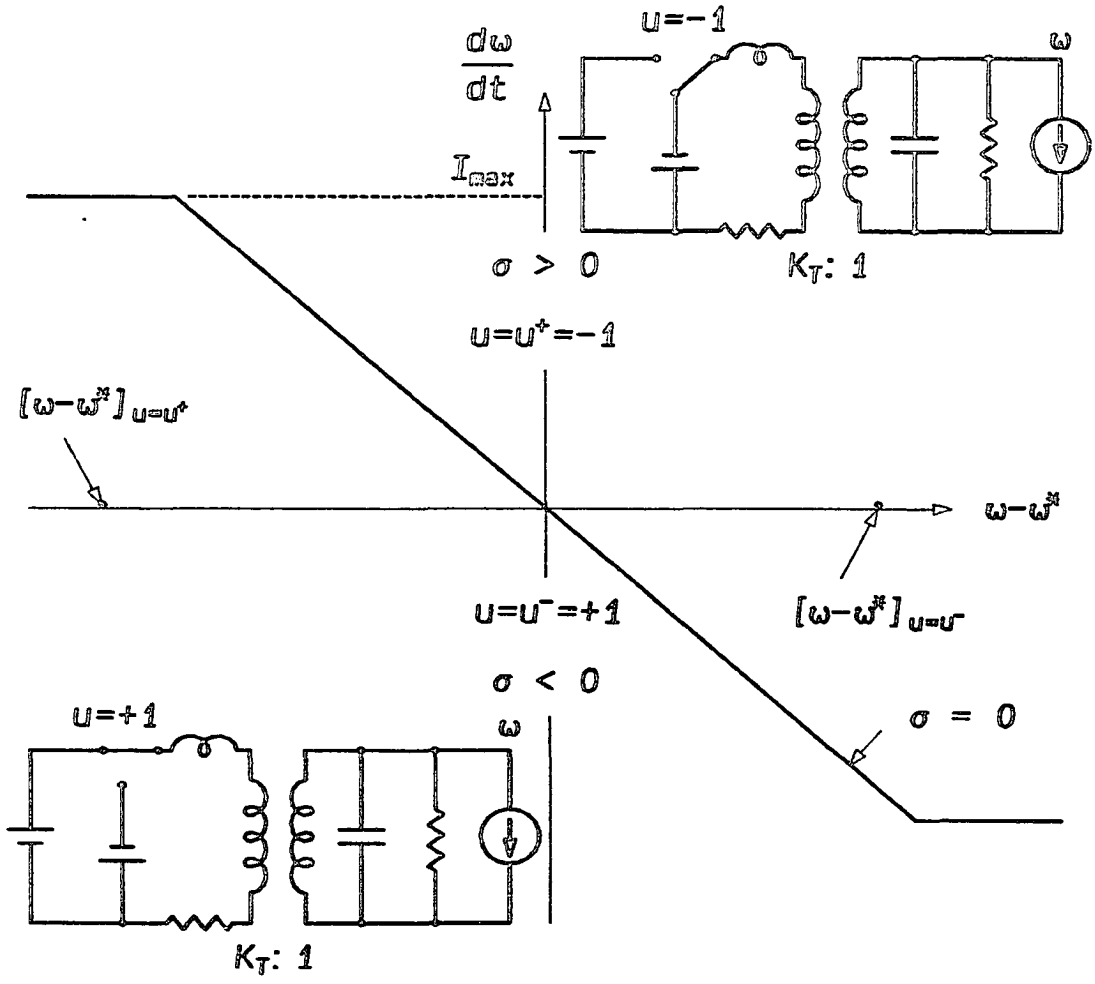

Fig. 6.3 Chopper-driven dc motor in the phase plane. The sliding line partitions the phase plane in two halves. The control and motor equivalent circuit in each half is shown. The steady state operating point for each of the control inputs $u = u^+$ and $u = u^-$ are also shown.

($u = +1$ *or* $u = -1$) may be qualitatively stated as "accelerate" ($u = +1$) and "decelerate" ($u = -1$). Later on these qualitative switch input commands "accelerate" and "decelerate" will be related through a look-up table to the three phase switch inputs, when applied to BLDC motor control.

6.1.2 Practical Design Considerations

The sliding mode speed controller for the dc motor drive was explained in its simplest form in the foregoing sections. The control law is extremely simple. To realize the control law given by Eq. (6.9), it is necessary to find out the location of the system RP in the phase plane with reference to the sliding boundary $\sigma = 0$. This involves the measurement of the switching function σ which is a weighted sum of the speed error and acceleration. Speed may be conveniently measure by means of a tachogenerator. We recall that in the analogous problem of dc-to-dc converter the derivative of the output voltage was available as the current through the output capacitor current. In the dc motor drive the derivative of output speed is not physically accessible. Therefore the alternative method of setting up the sliding line in terms of the output speed and armature current (analogous to output voltage and inductor current in the buck dc-to-dc converter) is used. In the following sections sliding mode control and linear control theory are combined in order to set up a practical sliding line and then to relate the response to the desired response.

The sliding line is set up in terms of armature current error and the output speed error.

$$\sigma(t) = (\omega - \omega^*) + R_s \hat{i} \tag{6.13}$$

$\hat{i}$ is the armature current error, and ω^* is the desired operating speed. R_s is the design parameter and is usually the current measuring resistance. When the friction is low and the load torque is constant or slowly varying, Eq. (6.2) may be approximated as

$$K_T \hat{i} = J\frac{d\omega}{dt} \tag{6.14}$$

The sliding line equation being a linear differential equation, one may represent the same in frequency domain as well.

$$\sigma(s) = (\omega - \omega^*) + R_s \hat{i}(s) \tag{6.15}$$

Under sliding mode control $\sigma = 0$. Substitution of Eq. (6.14) into Eq. (6.15) yields an overall response of

$$\omega(s) = \frac{\omega^*(s)}{1 + s\, JR_s / K_T} \tag{6.16}$$

We do get a resultant first order response. However unlike real sliding mode control, now the response time is a function of the design parameter R_s and the motor parameters J and K_T as well as ($\tau = JR_s / K_T$).

In Eq. (6.15) the sliding line is set up as a linear combination of the speed error and the current error. To measure the current error, the steady state current (I^*) will have to be subtracted out of the armature current. The simplest way to realize this is by means of a high-pass filter. Further, speed measurement

from tachogenerator also requires filtering due to the commutator noice present in the tachogenerator output. Therefore in practice, the sliding line is set up incorporating suitable prefilters. Equation (6.17) gives the practical sliding line in the frequency domain.

$$\sigma^*(s) = \frac{1+\omega_2/s}{1+\omega_1/s}\omega - \frac{\omega_1/s}{1+\omega_1/s}\omega^* + \frac{R_s}{1+\omega_1/s}\hat{i}(s) = 0 \qquad (6.17)$$

The current measurement circuit has an inverted pole. Speed signals are also measured with the same inverted pole. Inverted zeroes have been added to the speed signals in order not to lose their steady state values. Equation (6.17) may be put in the following form for convenience.

$$\sigma^*(s) = \frac{1+\tau_2 s}{1+\tau_1 s}\omega - \frac{1}{1+\tau_1 s}\omega^* + \frac{\tau_1 s R_s}{1+\tau_1 s}\hat{i}(s) = 0 \qquad (6.18)$$

Under sliding mode control $\sigma^*(s)$ is maintained to be zero, leading to the following closed loop response.

$$\omega(s) = \frac{\omega^*(s)}{1+s/Q\omega_0+s^2/\omega_0^2} \qquad (6.19)$$

$$\omega_0^2 = K_T/JR_s\tau_1$$
$$Q = 1/\omega_0\tau_2$$

The response as seen by Eq. (6.19) is a second order response,and provides suitable design criterion. τ_1 is the current filtering time constant and is chosen higher than the electrical time constant of the motor. The current gain R_s is selected to obtain the desired response time. The inverted zero frequency ($1/\tau_2$) of speed measurement is chosen to obtain the desired damping.

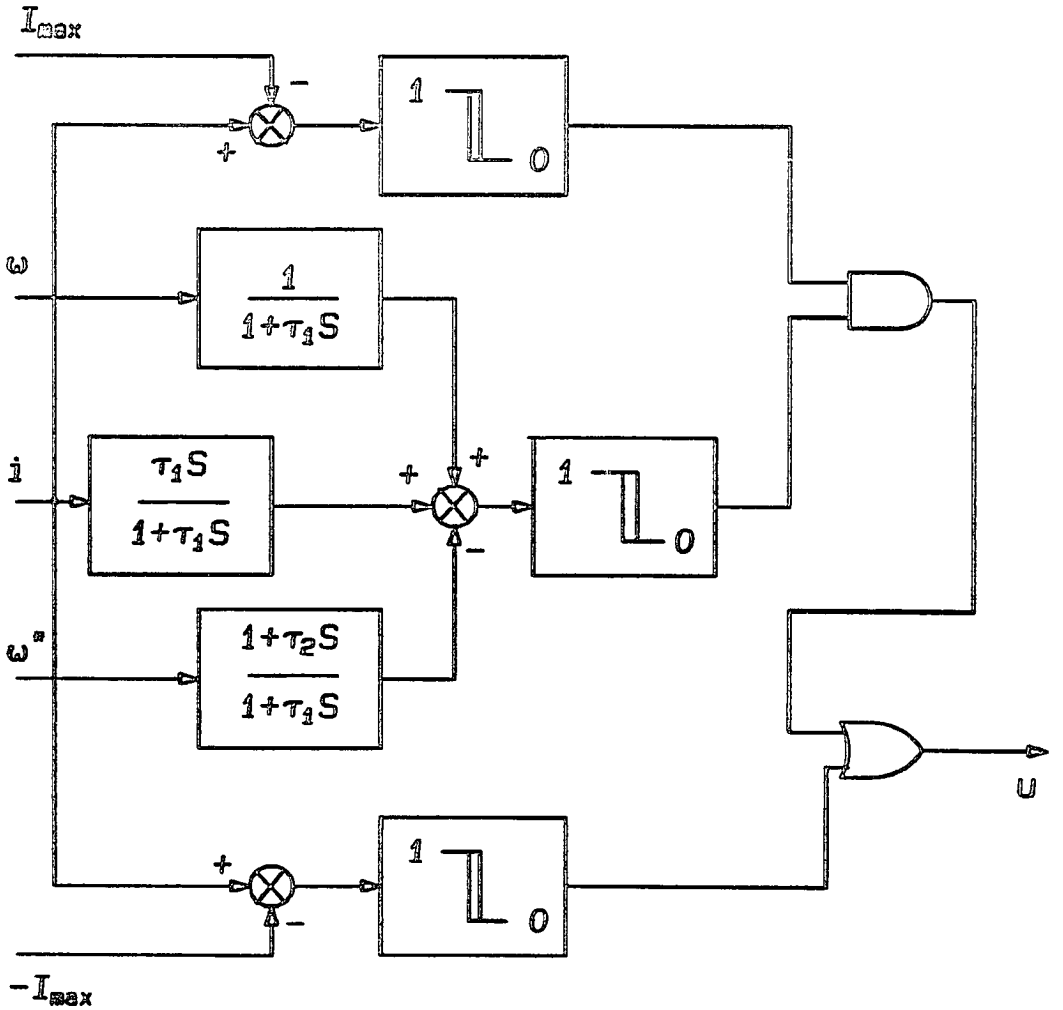

Fig. 6.4 Sliding mode controller for the chopper-driven dc motor. The sliding line is made up of a linear combination of the speed error and the armature current with appropriate prefilters. Overriding overcurrent protection is also incorporated.

The circuit schematic of the speed controller is shown in Fig. 6.4. The circuit was tested with a dc machine with the following parameters.

K_T = 0.09 Nw.m/amp; J = 6.45E-4 Nw.m sec^2/rad;

B = 7.11E-4 Nw.m sec/rad; R = 3.83 ohms;

L = 3.94 mH.

The current filtering time constant (τ_1) is chosen as 10 ms – in between the electrical time constant(1 ms) and mechanical time constant(0.9 s) of the motor. The current gain (R_s) and the speed prefilter time constant τ_2 are chosen to achieve the desired response time and adequate damping respectively.

Figures (6.5) and (6.6) show the starting transient of the dc motor drive for two different compensator designs.

6.2 Estimation of Speed Using Sliding Mode

In this section, the principle of sliding mode control is applied to estimate motor speed. This is of special interest in position control servos where the speed feedback is necessary only for achieving the dynamic properties of the drive, and the steady state accuracy is determined by a primary position sensor feedback.

Conventionally the speed estimation is done by an analog controller as shown in Fig. 6.7, with motor current and voltage as feedback signals. From Fig. 6.7,

$$y(s) = \frac{K}{(R+K)} \frac{v(s)-Ri(s)-sLi(s)}{1+sL/(R+K)} \tag{6.20}$$

i = Armature current; v = Armature voltage;

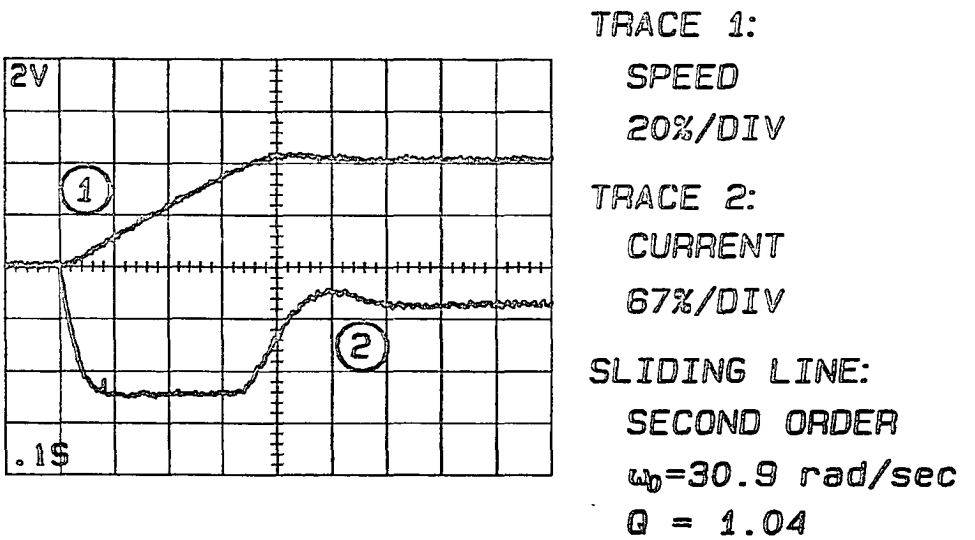

Fig. 6.5 Starting transient of the chopper-driven dc motor with sliding mode controller. The initial constant acceleration region corresponds to current limited region of operation.

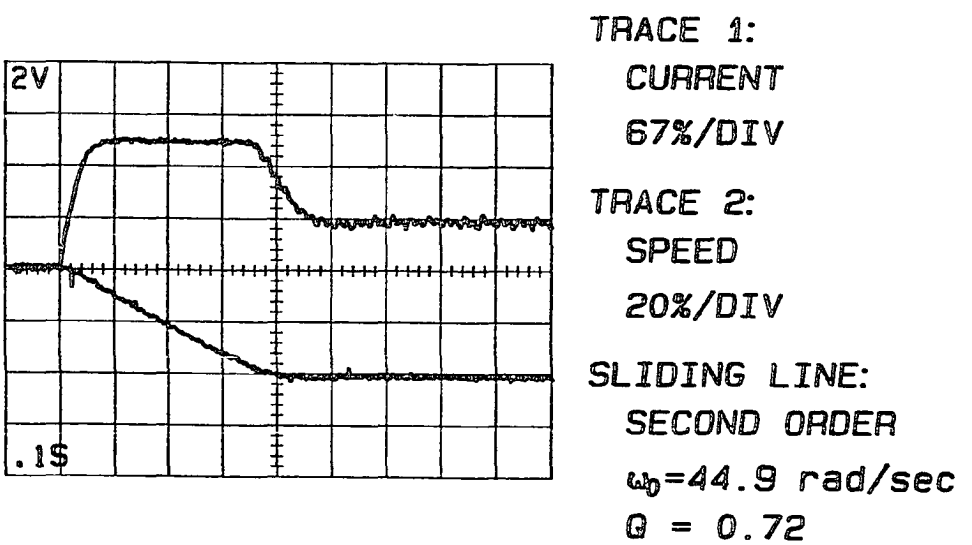

Fig. 6.6 Starting transient of the chopper-driven dc motor with sliding mode controller. The initial constant acceleration region corresponds to current limited region of operation.

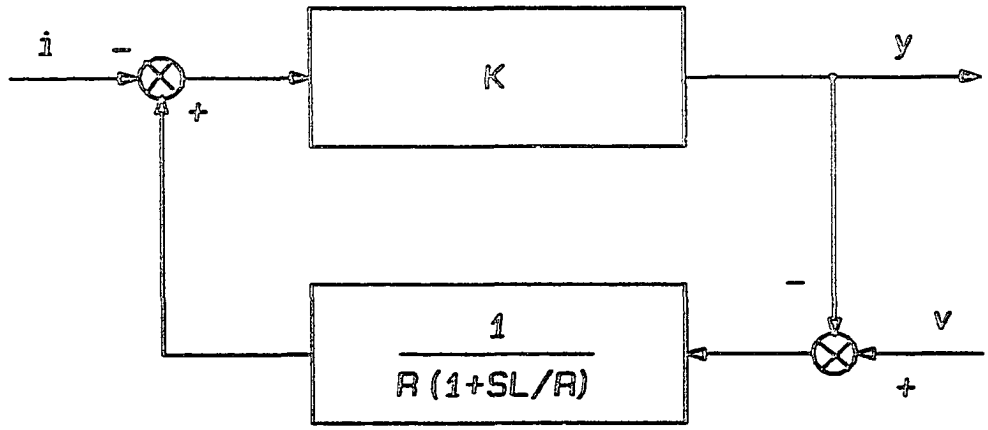

Fig. 6.7 Continuous control speed estimator. The dynamic block is the model of the motor. The compensator gain K determines the accuracy of the estimated speed y.

R = Armature resistance; L = Armature inductance;

K = Compensator gain; y = Output speed signal.

Usually the electrical frequency (R/L) of the motor is much higher than the desired bandwidth of the estimator. Further if the compensator gain K is chosen large ($K>>R$) Eq. (6.20) reduces to

$$y(s) \approx v(s) - Ri(s) - sLi(s) = K_E\omega \tag{6.21}$$

The closeness of this approximation depends on K; the higher the compensator gain, the better is the accuracy of the estimated speed.

As an alternative to the above, it is possible to build such an estimator based on sliding control. Consider the electrical subsystem of the machine

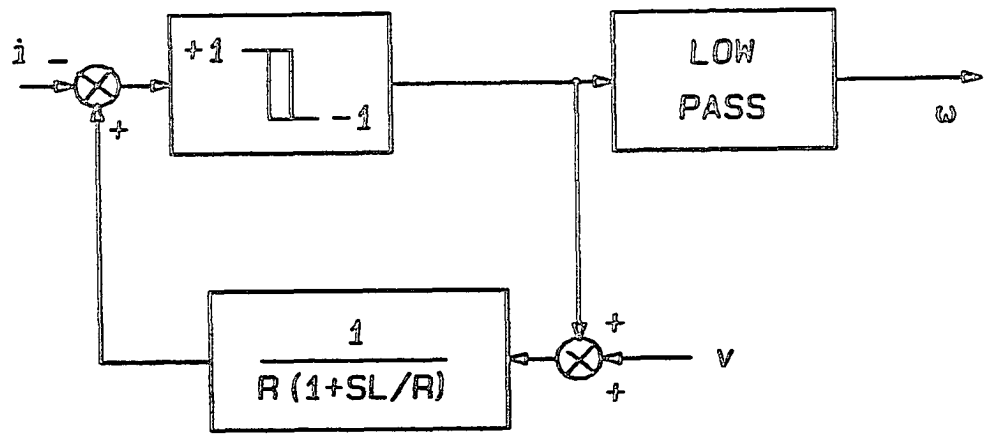

Fig. 6.8 Sliding mode speed estimator. The dynamic block is the model of the motor. The comparator with hysteresis makes up the sliding controller. The low pass filter measures the averaged speed signal.

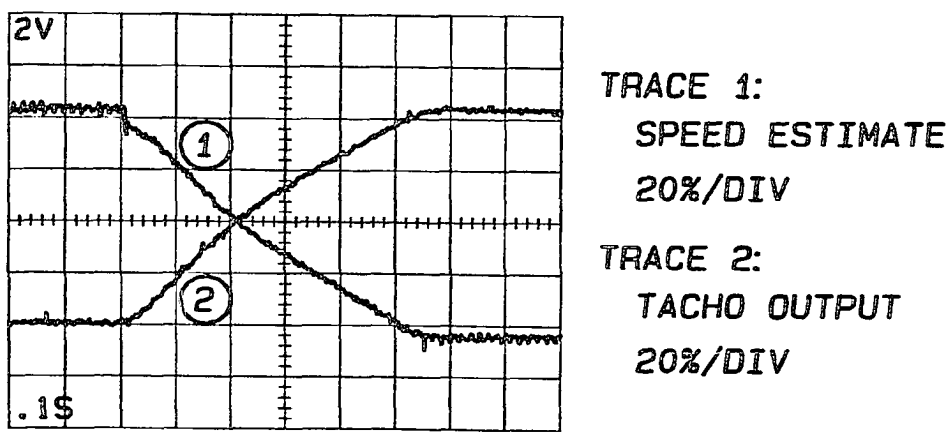

Fig. 6.9 The speed estimate (trace 2) and the speed measured through a tachogenerator (trace 1) are compared. Speed estimate is shown inverted for ease of comparison.

$$L\frac{di}{dt}+Ri+K_E\omega = v \tag{6.22}$$

We may construct a model of the motor given by,

$$L\frac{di_m}{dt}+Ri_m+v_g u = v \tag{6.23}$$

If the current (i_m) in the model is made equal to the current (i) in the motor, then comparison of Eqs. (6.22) and (6.23) shows that $v_g u$ equals the motor back emf, which may be used as a speed signal. Equation (6.23) is the model of the motor. The objective is to control the current in the model (i_m) equal to the current in the motor, by means of the control input u. This is a first order system with one control. The sliding mode control effectively reduces to a bang-bang control:

$$\sigma = i_m - i \tag{6.24}$$

$$u = \begin{cases} +1 & \text{for } \sigma > 0 \\ -1 & \text{for } \sigma < 0 \end{cases} \tag{6.25}$$

It may be verified that the sliding condition given by Eq. (6) is satisfied when $v_g > v + RI_{\max}$. The average value of the discontinuous signal $v_g u$ equals the back emf and proportional to the speed. Figure 6.8 shows the sliding mode speed estimator. It may be pointed out here that the ideal sliding mode speed estimator and the ideal analog speed estimator are the same (zero hysteresis and infinite compensator gain respectively). Figure 6.9 compares the speed estimator output with the tachogenerator output.

6.3 Brushless Dc Motor Drive

In Chapter 5, the operation and performance equations of the synchronous motor were outlined. The BLDC motor is a special case of a synchronous motor drive. In this section, the BLDC motor equivalent circuit is derived following the transformations explained in Chapter 5, and Appendix 1. In Appendix 1, the transformations were treated simply as mathematical artifices employed to simplify the mathematical description of different machines. In this Section the transformations on the permanent magnet synchronous motor (BLDC motor) leading to the rotating reference frame equivalent DC motor description are interpreted physically at every step. The system equations are written down directly in each reference frame, and the description in different reference frames are related to each other using some physical criterion. The reason to follow this method is that the mathematical transformations explained in Chapter 5, and Appendix 1 are firmly anchored to physical interpretations and the inter-relationship between the physical constants of the machine in different frames of reference is more readily apparent.

The principle of sliding mode control is then applied for the speed control of BLDC motor. Practical design criteria are then developed and experimental results presented.

6.3.1 Permanent Magnet Synchronous Motor

Figure 6.10 shows the construction of the permanent magnet synchronous motor. The rotor is without saliency and carries surface mounted permanent magnets providing the rotor MMF. The stator carries symmetrically distributed three phase windings. The stator is excited with balanced three phase power. The three phase currents in the stator windings produce stator MMF which is rotating in the airspace of the machine at the same speed (synchronous speed) as the electrical frequency of the stator power supply. The interaction of the stator MMF and the rotor MMF produce the torque. Average torque exists only when the rotor speed is the synchronous speed. Compared with the generic synchronous motor explained in Chapter 5, the following differences in the case of the permanent magnet synchronous motor may be noticed. The armature is on the

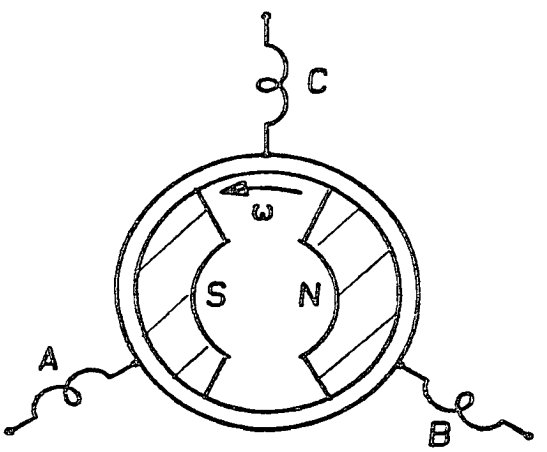

Fig. 6.10 Construction of a permanent magnet synchronous motor. The stator carries balanced three phase windings. The excitation is provided by permanent magnets fixed on the periphery of the rotor.

stator. The excitation field is on the rotor. The excitation MMF is fixed, and provided by permanent magnets mounted on the surface of the rotor.

6.3.2 Brushless Dc Motor

It was mentioned that the synchronous motor has net average torque only when the rotor speed is the same as the synchronous speed of the three phase power supplied to the armature. The brushless dc operation of a synchronous motor is obtained in the following manner. The power supplied to the armature is related to the physical position of the excitation field in the airspace of the machine such that the synchronous speed of the ac power fed to the armature at all times equals the rotor speed. Due to this closed loop relationship between the rotor speed and the armature power frequency, the motor runs in synchronism at all speeds and net average torque exists at all speeds.

6.3.3 Performance Equations of BLDC motor

In this section, the various transformations leading to the transformation of the permanent magnet synchronous motor into the equivalent $d-q$ axes machine are applied to obtain the performance equations of the BLDC motor. Figure 6.11 shows the essential construction of the permanent magnet synchronous motor. The physical structure of the rotor is represented by the innermost circle. The rotor carries the permanent magnets providing constant field excitation. The rotor MMF in the absence of stator currents sets

up an airgap flux of φ_d. The outermost annular ring in Fig. 6.11 represents the physical structure of the stator. The stator phase windings A,B and C are shown schematically to coincide with the direction in which the respective MMF's are oriented. The intermediate annular rings in Fig. 6.11 represent fictitious structures which are helpful in stepping through the various transformations and are explained as we go along.

The defining equations of the machine are in three parts. First is the electrical subsystem definiton relating the electrical quantities of the machine. The definition of the electrical subsystem depends on the chosen frame of reference. The second part is the electromagnetic subsystem of the machine indicating the mechanism of torque generation. The electrical quantities in the torque relationship again depend on the chosen frame of reference. The last part is the mechanical subsystem relating the break-up of the generated torque into load, friction and inertia. The selection of a frame of reference is to simplify the definition of the electrical subsystem and does not change the definition of the mechanical subsystem.

The definition of the mechanical subsystem is independent of the frame of reference and is given by

$$J\frac{d\omega}{dt}+B\omega+T_L = T_g \tag{6.26}$$

where the quantities J,B,T_L and ω are as defined earlier in Section 6.1 and T_g is the generated torque.

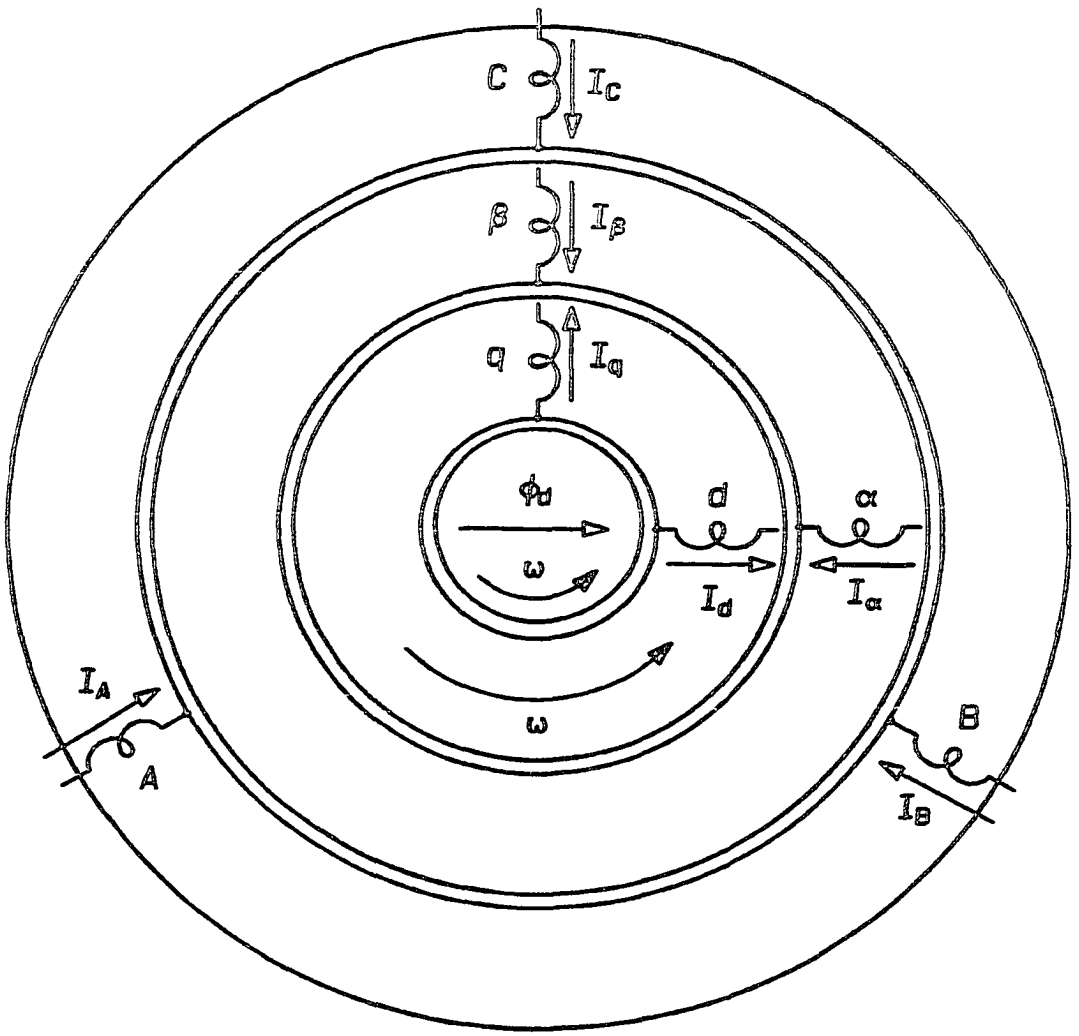

Fig. 6.11 A,B,C to α, β to d, q transformations. The outermost annular ring and the innermost circle represent the physical stator and the physical rotor respectively. The second annular ring from outside represents a fictitious equivalent two phase rotor which when excited by appropriate two phase currents would result in the same machine performance. The third annular ring from outside represents a fictitious two phase equivalent "rotor", which when carrying dc currents (I_d, and I_q) results in the same performance as the original machine.

The electrical subsystem equations are dependent on the frame of reference. In the physical stationary reference frame (stator represented by the outermost circle and the rotor represented by the innermost circle in Fig. 6.11), the stator electrical circuit equations may be written from first principles as below.

$$R_A I_A + L_{AA}\frac{dI_A}{dt} + L_{AB}\frac{dI_B}{dt} + L_{AC}\frac{dI_C}{dt} + \frac{d\psi_{Ad}}{dt} = V_A \tag{6.27}$$

$$L_{BA}\frac{dI_A}{dt} + R_B I_B + L_{BB}\frac{dI_B}{dt} + L_{BC}\frac{dI_C}{dt} + \frac{d\psi_{Bd}}{dt} = V_B \tag{6.28}$$

$$L_{CA}\frac{dI_A}{dt} + L_{CB}\frac{dI_B}{dt} + R_C I_C + L_{CC}\frac{dI_C}{dt} + \frac{d\psi_{Cd}}{dt} = V_C \tag{6.29}$$

where

L_{XX} = self inductance of phase windings;

R_X = resistance of phase windings;

L_{XY} = mutual inductance between phase windings X and Y;

ψ_{Xd} = flux linkage to winding X due to rotor flux φ_d;

V_X = phase voltage; I_X = phase current.

Under the assumption of symmetrical balanced 3 phase windings, without neutral conductor and sinuzoidal flux distribution,

$$R_A = R_B = R_C = R \; ; \quad L_{AA} = L_{BB} = L_{CC} = L_S \; ;$$

$$L_{AB} = L_{BA} = L_{BC} = L_{CB} = L_{CA} = L_{AC} = -L_M \; ;$$

$$I_A + I_B + I_C = 0$$

Notice that L_{XY} is defined with a negative coefficient due to the selection of the current directions in Fig. 6.11. Equations (6.27),(6.28) and (6.29) may then be simplified as

$$\begin{aligned} RI_A + (L_S + L_M)\frac{dI_A}{dt} + \frac{d\psi_{Ad}}{dt} &= V_A \\ RI_B + (L_S + L_M)\frac{dI_B}{dt} + \frac{d\psi_{Bd}}{dt} &= V_B \\ RI_C + (L_S + L_M)\frac{dI_C}{dt} + \frac{d\psi_{Cd}}{dt} &= V_C \end{aligned} \tag{6.30}$$

The generated torque is the sum of the torques due to the interaction between the rotor MMF and each of the stator phase current MMF's. The generated torque due to each of the stator phase currents depends on the rotor position. The total torque is given by

$$T_g = K\varphi_d\left\{I_A \sin(330° + \omega t) + I_B \sin(150° + \omega t) + I_C \sin(90° + \omega t)\right\} \tag{6.31}$$

where K is a proportionality constant with proper dimensions and ωt is the instantaneous angular position of the rotor. Equation (6.31) may be further simplified as

$$T_g = K\varphi_d\left\{(-I_A/2 - I_B/2 + I_C)\cos\ \omega t + (\sqrt{3}I_A/2 - \sqrt{3}I_B/2)\sin\ \omega t\right\} \tag{6.32}$$

In Eq. (6.30) the rotor position is implicit through the terms ψ_{Xd}. In Eq. (6.32) the rotor position is explicit. Equations (6.30) and (6.32) define the electrical and the electromagnetic subsystems in the physical stator reference frame. The electrical quantities appearing

in these equations are the same as what can be measured in the stator circuit.

The currents in the stator phase windings of the motor produce an MMF in the active plane of the motor, which interacting with the rotor MMF in the same plane produces the required torque. This stator MMF may very well be produced by an equivalent stator with two phase orthogonal windings carrying two phase ac currents. The first step in simplifying the system equations is to transform the stationary reference frame three phase stator equations (Eqs. (6.30) and (6.32)) to an equivalent stationary reference frame, two phase stator equations.

The second annular ring from outside in Fig. 6.11 represents this fictitious stator with two phase windings on it (α and β) as shown. Again from first principles the circuit equations and torque equation may be written down as below.

$$R^*I_\alpha + L^*\frac{dI_\alpha}{dt} + \frac{d\psi_{\alpha d}}{dt} = V_\alpha$$

$$R^*I_\beta + L^*\frac{dI_\beta}{dt} + \frac{d\psi_{\beta d}}{dt} = V_\beta \qquad (6.33)$$

$$T_g = K\varphi_d(I_\beta \cos \omega t - I_\alpha \sin \omega t) \qquad (6.34)$$

The subscripted quantities represent the fictitious two phase stator electrical quantities. The machine constants in the equivalent fictitious two phase system are shown with asterisks. Their relationship to the original machine constants is yet to be established.

The next step is to find the relationship between the A,B,C system and the α,β systems. To do this we invoke the condition that the torque developed in both the systems are equal. Comparing Eqs. (6.32) and (6.34), we get

$$I_\alpha = -\sqrt{3}I_A/2 + \sqrt{3}I_B/2$$
$$I_\beta = -I_A/2 - I_B/2 + I_C \qquad (6.35)$$

From Eqs. (6.35) and (6.30), we get

$$R^* = R \;\; ; \;\; L^* = L_S + L_M$$
$$V_\alpha = -\sqrt{3}V_A/2 + \sqrt{3}V_B/2$$
$$V_\beta = -V_A/2 - V_B/2 + V_C$$
$$\psi_{\alpha d} = -\sqrt{3}\psi_{Ad}/2 + \sqrt{3}\psi_{Bd}/2$$
$$\psi_{\beta d} = -\psi_{Ad}/2 - \psi_{Bd}/2 + \psi_{Cd} \qquad (6.36)$$

Now the system equations in the two phase stationary reference frame (α,β axes) may be written as

$$RI_\alpha + (L_S + L_M)\frac{dI_\alpha}{dt} + \frac{d\psi_{\alpha d}}{dt} = V_\alpha$$
$$RI_\beta + (L_S + L_M)\frac{dI_\beta}{dt} + \frac{d\psi_{\beta d}}{dt} = V_\beta \qquad (6.37)$$

$$T_g = K\varphi_d(I_\beta \cos\omega t - I_\alpha \sin\omega t) \qquad (6.38)$$

Notice that the system equations are still functions of rotor position. Just as before the rotor position is implicit in Eq. (6.37) and explicit in Eq. (6.38). The electrical quantities appearing in Eqs. (6.37) and (6.38) are fictitious quantities in the sense that they are not accessible at any point in the actual machine.

Polyphase currents in the stator at synchronous frequency produce an MMF rotating in the machine airspace in synchronism with the rotor MMF. The interaction between these stator and rotor MMF's produce the required torque. The rotating stator MMF may very well be produced by an equivalent set of windings rotating in space at synchronous speed but carrying dc currents. The next step in simplifying the system equations is to transform the system Eqs. (6.37) and (6.38) in the two phase stationary reference frame into a two phase frame of reference rotating in space at synchronous frequency.

The third annular ring from outside in Fig. 6.11 represents this fictitious rotating structure carrying dc currents (I_d and I_q) in the two phase windings (d and q windings). The electrical circuit equations and the torque equation may be directly written as

$$R^{*}I_d + L^{*}\frac{dI_d}{dt} + K_d\omega = V_d$$

$$R^{*}I_q + L^{*}\frac{dI_q}{dt} + K_q\omega = V_q \qquad (6.39)$$

$$T_g = -K\varphi_d I_q \qquad (6.40)$$

Notice that apart from resistive and inductive drops, the phase windings also have speed voltage term because the d,q windings are rotating in space. The machine parameters are shown with asterisks, because their relationship to the original machine parameters are yet to be established. We now invoke the condition that the MMF's produced by the d,q windings are the same as those produced by the α,β windings and the generated torque in both the systems are equal.

Comparing Eqs. (6.38) and (6.40), we get

$$I_q = I_\alpha \sin \omega t - I_\beta \cos \omega t \tag{6.41}$$

Equating d axis MMF's, we get

$$I_d = -I_\alpha \cos \omega t - I_\beta \sin \omega t \tag{6.42}$$

From Eqs. (6.41) and (6.42), the inverse relationship is also obtained.

$$\begin{aligned} I_\alpha &= -I_d \cos \omega t + I_q \sin \omega t \\ I_\beta &= -I_d \sin \omega t - I_q \cos \omega t \end{aligned} \tag{6.43}$$

Further, assumption of sinusoidal flux distribution leads to

$$\begin{aligned} \psi_{\alpha d} &= -\psi_d \cos \omega t \\ \psi_{\beta d} &= -\psi_d \sin \omega t \end{aligned} \tag{6.44}$$

where ψ_d is the maximum flux linkage due to rotor flux to stator (α,β) windings. Substitution of Eqs. (6.43) and (6.44) into Eqs. (6.37) and (6.38) leads to

$$\begin{aligned} &RI_d + (L_S + L_M)\frac{dI_d}{dt} - (L_S + L_M) I_q \omega = V_d \\ &RI_q + (L_S + L_M)\frac{dI_q}{dt} + (L_S + L_M) I_d \omega + \psi_d \omega = V_q \end{aligned} \tag{6.45}$$

$$T_g = -K \varphi_d I_q \tag{6.46}$$

Equations (6.45) and (6.46) describe the system in synchronously rotating frame of reference. As expected the electrical quantities in Eqs. (6.45) and (6.46) are all dc quantities. They are independent of rotor position. Again the electrical quantities as expressed in Eqs. (6.45) and (6.46) are fictitious in the sense that they are not directly accessible at any point in the actual machine.

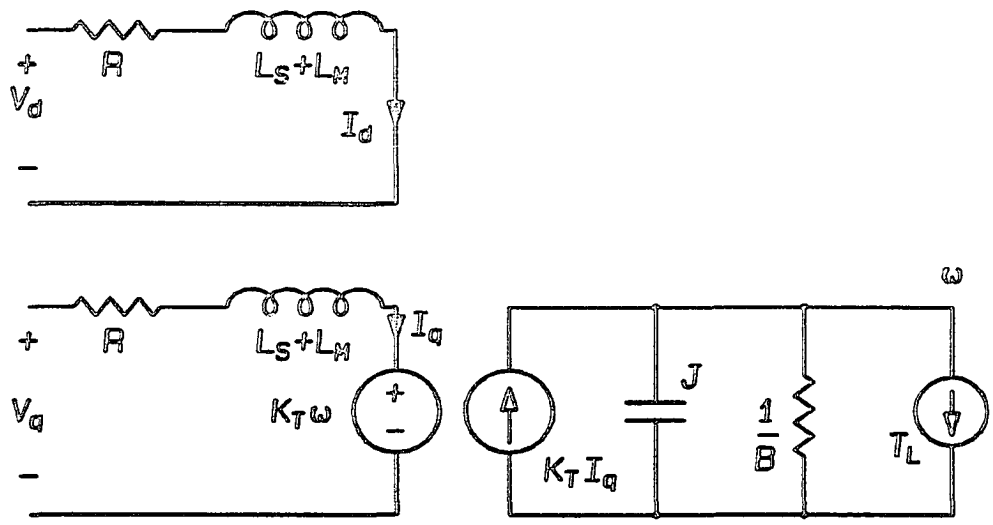

Fig. 6.12 The electrical equivalent circuit of the permanent magnet synchronous machine in the synchronously rotating (d,q) reference frame. The voltages (V_d,V_q) and the currents (I_d,I_q) are dc quantities.

In the case of permanent magnet synchronous motor the effective airgap between the rotor and stator is large, on account of the fact that the relative permeability (μ_r) of the permanent magnet material is nearly unity. As a result the cross coupling terms ($(L_S+L_M)\omega I_q \ll V_d, (L_S+L_M)\omega I_d \ll \varphi_d\omega$) in Eq. (6.45) are negligible, leading to the following approximations.

$$V_d \approx RI_d + (L_S+L_M)\frac{dI_d}{dt}$$

$$V_q \approx RI_q + (L_S+L_M)\frac{dI_q}{dt} + K_E\omega \qquad (6.47)$$

$$T_g = K_T I_q \qquad (6.48)$$

The constants ψ_d and $-K\varphi_d$ have been replaced in the Eqs. (6.47) and (6.48) by the more familiar back emf constant K_E and the torque

constant K_T. The system of Eqs. (6.26), (6.47) and (6.48) may be more conveniently represented by the equivalent circuit shown in Fig. 6.12.

6.3.4 Control Strategy of BLDC Motor Drive

The BLDC motor drive consists of a switching converter and a permanent magnet synchronous motor. The converter is controlled in such a way as to provide ac power to the armature at synchronous frequency at all operating speeds. Or, equivalently, the armature MMF at all speeds is maintained at a fixed phase angle with respect to the excitation MMF. The BLDC motor drive consisting of the synchronous motor and the switching converter is shown in Fig. 6.13. First current-fed operation of the BLDC motor is developed. Speed regulation under sliding mode control is explained in a subsequent section.

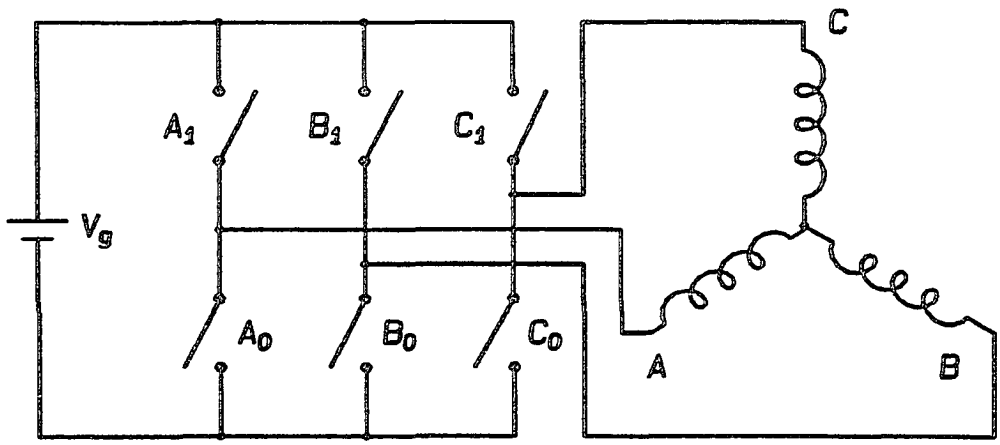

Fig. 6.13 Power circuit of the BLDC motor. The switches are synchronized to the rotor position and are the electronic counterpart of the mechanical commutator in the dc motor.

In the d–q frame of reference, the rotor MMF is constant in magnitude and oriented along the d axis fixed to the rotor. The stator MMF along the q axis determines the instantaneous torque ($T = \varphi_d I_q$). The stator MMF along the d axis does not contribute to the developed torque. The operating principle of the BLDC motor in the d–q frame of reference may be stated as follows. The current I_d, which does not contribute to useful torque is maintained zero at all times. The current I_q, which is responsible for the developed torque, is maintained at such a magnitude and polarity as to develop the desired torque. The control strategy of the current fed BLDC motor is then to achieve $I_d = 0$ and $I_q = I_q^*$, where I_q^* is the desired q axis current. The equivalent circuit of the current fed BLDC motor is shown in Fig. 6.14.

The essence of the control problem of the current fed BLDC motor drive is to relate the requirements of the d–q axes currents ($I_d = 0$ and $I_q = I_q^*$) into a suitable switching strategy for the three switches in the converter. This is done best in the following graphical manner. Figure 6.15 shows the active plane of the machine. The rotor is shown frozen at an angular position of 15°. The orientation of the d axis is fixed on the rotor and coincides with the rotor MMF direction. The orientation of the q axis is also fixed on the rotor and normal to the d axis. The directed arrows in Fig. 6.15 represent the direction of the steady state stator MMF's for the different switch positions shown alongside. For example, switch inputs (A_1,B_1,C_0) produces a steady state MMF vertically upwards in the active plane of the motor. For the rotor position (15°) shown in

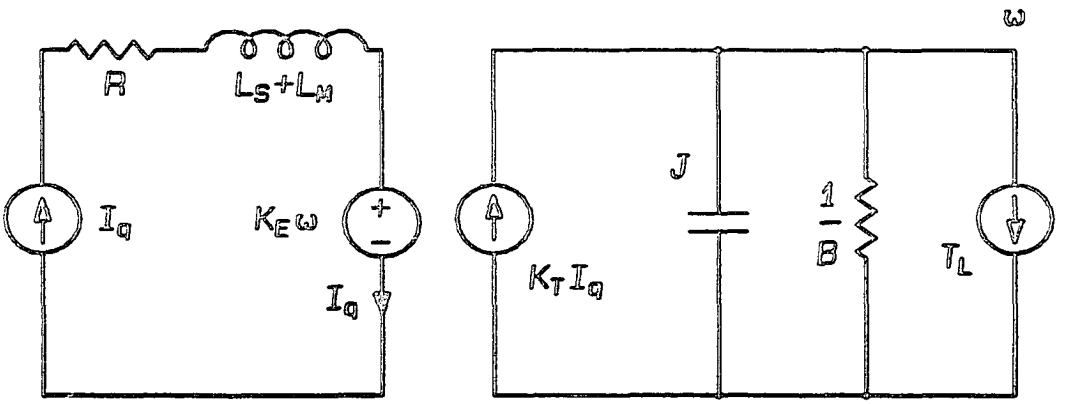

Fig. 6.14 Equivalent circuit of the current fed BLDC motor (with I_d = 0). The mechanical system consisting of the inertia (J), friction (B), and the load torque (T_L) is represented by their electrical analog.

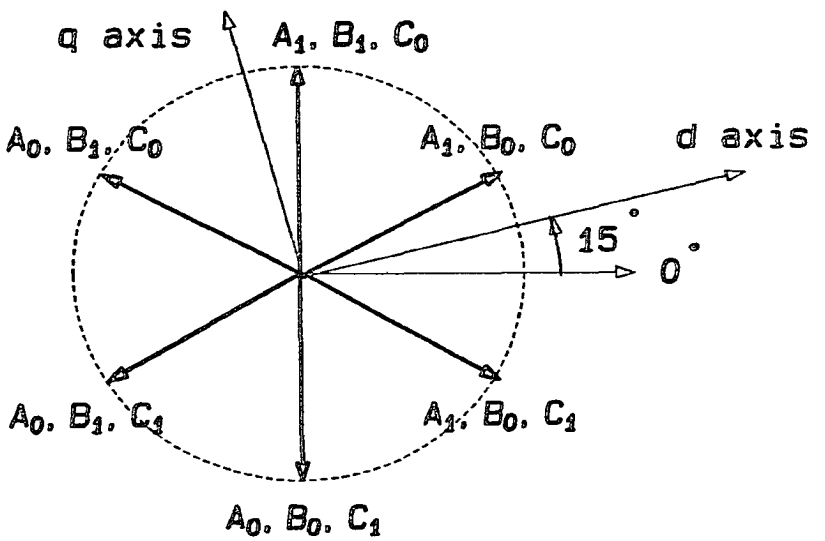

Fig. 6.15 Steady state armature MMF for the various inverter switch positions. The directed arrows show the steady state armature MMF in the active plane of the motor for the six possible switch inputs. The orientation of the d,q axes are shown frozen in space corresponding to the rotor at 15°.

Fig. 6.15, the switch inputs (A_1,B_1,C_0) produce a steady state stator MMF corresponding to some positive I_d and some positive I_q. In a similar way the switch inputs (A_0,B_0,C_1) produce a stator MMF corresponding to some negative I_d and some negative I_q; switch inputs (A_0,B_1,C_0) produce a steady state stator MMF corresponding to some negative I_d and some positive I_q; switch inputs (A_1,B_0,C_1) produce a steady state stator MMF corresponding to some positive I_d and some negative I_q. This above resolution of steady state MMF's due to different switch inputs into equivalent d and q axes currents is valid in the range of rotor position $0 < \omega t < 60°$. Table 6.1 shows the interpretation of steady state MMF's in terms of I_d and I_q and the validity of this interpretation in terms of the rotor position ωt.

Switch Position	Direction of MMF		Range of ωt
	d axis	q axis	
A_1,B_1,C_0	$+I_d$	$+I_q$	$0° < \omega t < 60°$
A_0,B_1,C_0	$-I_d$	$+I_q$	$0° < \omega t < 60°$
A_0,B_1,C_1	$-I_d$	$-I_q$	$-30° < \omega t < +30°$
A_0,B_0,C_1	$-I_d$	$-I_q$	$0° < \omega t < 60°$
A_1,B_0,C_1	$+I_d$	$-I_q$	$0° < \omega t < 60°$
A_1,B_0,C_1	$+I_d$	$+I_q$	$-30° < \omega t < +30°$

TABLE 6.1 Steady state stator MMF's for different switching inputs and their interpretation in the synchronously rotating (d,q) reference frame. As we are interpreting a stationary quantity (steady state stator MMF) in a rotating reference frame the interpretation is valid only in a limited range of rotor position. The last column indicates this limitation.

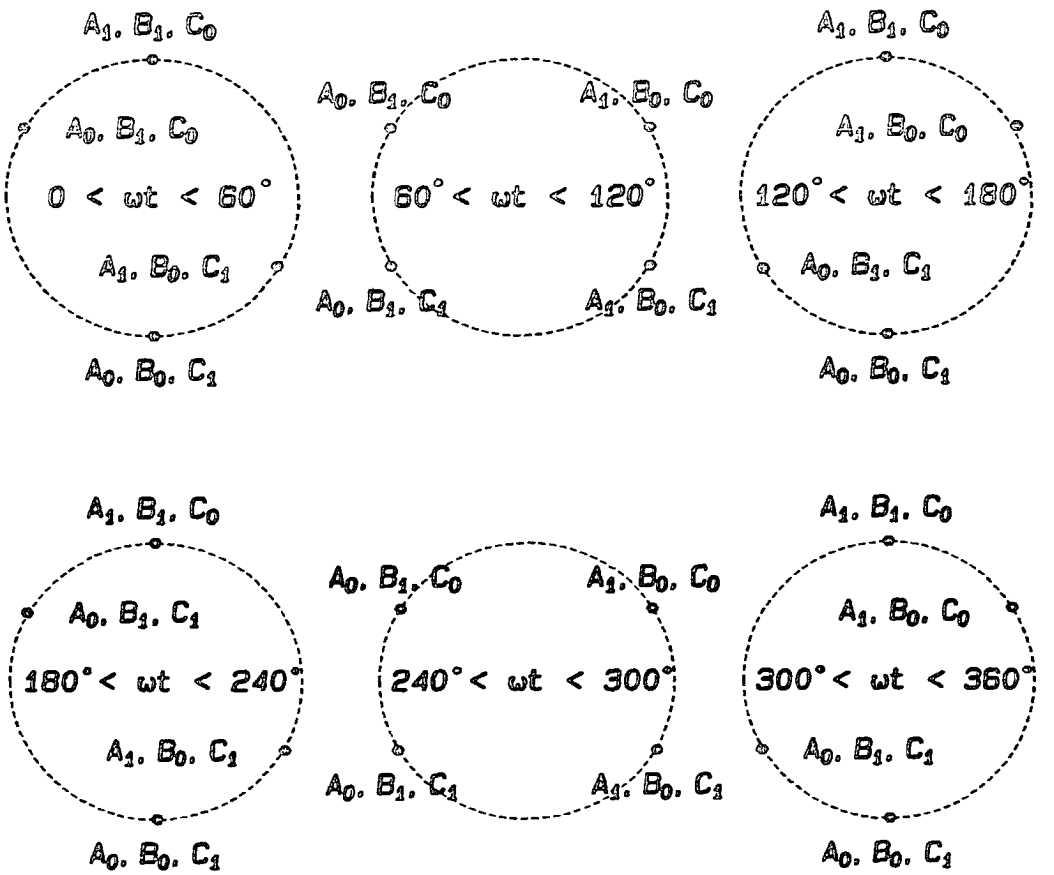

Fig. 6.16 Sufficient control inputs for each 60° wide sectors of the rotor position. The requirement of having to control independently only two quantities I_d and I_q with three independent switches (A,B,C) results in the availability of more than sufficient control options. Notice that only four switch inputs of all the possible switch inputs are used in each sector.

We need to relate the requirements of I_d and I_q to the three switch positions at any instant. There are two variables (I_d and I_q) to be controlled with three switch inputs indicating an extra degree of freedom. This extra choice available is also seen in Table 6.1. However we may select a set of control inputs capable of achieving $\pm I_d$ and $\pm I_q$ and with a consistent range of ωt in which they are applicable. These are (A_1,B_1,C_0),(A_0,B_1,C_0),(A_0,B_0,C_1) and (A_1,B_0,C_1) in the range of rotor position $0 < \omega t < 60°$. Therefore in the range of $0° < \omega t < 60°$, the above four control inputs combination is sufficient to obtain the required correction (increasing or decreasing) in both I_d and I_q. Figure 6.16 shows the control input combinations used in each of the 60° wide sectors in the active plane in which the rotor MMF is oriented.

The strategy of control is to determine the error in the instantaneous value of the currents I_d and I_q and to select the appropriate switch inputs (A,B,C) depending on this error. In each of the six sectors shown in Fig. 6.16 the instantaneous value of I_d and I_q enables one to select an appropriate power circuit switch positions. For example, in the sector $0°<\omega t<60°$, if the value of I_d and I_q are higher than their desired values (I_d^* and I_q^*), the converter is switched to (A_0,B_0,C_1). If I_d is less than I_d^* and I_q is higher than I_q^*, then the converter is switched to (A_1,B_0,C_1) and so on. Rotor position (ωt) and the phase currents (I_A,I_B,I_C) of the motor are sensed. By using the transformations given in Section 6.2.3, they are converted into I_d and I_q. I_d is checked for zero value. I_q is checked for the desired value I_q^*. From these inputs and the sector in which

Sector	$I_d > 0$?	$I_q > I_q^*$?	Switch Inputs		
			A	*B*	*C*
$0° < \omega t < 60°$	0	0	1	1	0
	0	1	1	0	1
	1	0	0	1	0
	1	1	0	0	1
$60° < \omega t < 120°$	0	0	0	1	0
	0	1	1	0	0
	1	0	0	1	1
	1	1	1	0	1
$120° < \omega t < 180°$	0	0	0	1	1
	0	1	1	1	0
	1	0	0	0	1
	1	1	1	0	0
$180° < \omega t < 240°$	0	0	0	0	1
	0	1	0	1	0
	1	0	1	0	1
	1	1	1	1	0
$240° < \omega t < 300°$	0	0	1	0	1
	0	1	0	1	1
	1	0	1	0	0
	1	1	0	1	0
$300° < \omega t < 360°$	0	0	1	0	0
	0	1	0	0	1
	1	0	1	1	0
	1	1	0	1	1

TABLE 6.2 Look-up table relating the input quantities – rotor MMF sector, d axis current ($I_d > 0$?) and the q axis current ($I_q > I_q^*$?) – directly into the necessary control action in terms of the inverter switch positions (A,B,C).

the rotor MMF lies at any instant, the power circuit switch inputs are selected. Table 6.2 is a look-up table for this purpose.

6.3.5 Current Fed BLDC Motor Drive and Test Results

The above control strategy was implemented on a 1/2 hp BLDC motor. Figure 6.17 shows the block diagram of the hardware to compute I_d and I_q. The Hall-effect current sensors generate analog signals proportional to the phase currents (I_A,I_B, and I_C) of the motor. An incremental encoder drives the up/down counter to produce digital shaft position signal (ωt). The $ABC-\alpha\beta$ transformation block realizes the Eq. (6.35). It takes in analog phase current signals (I_A,I_B, and I_C) to produce the analog two phase current signals (I_α and I_β). Two Eproms store the trigonometric functions cos ωt and sin ωt, and are addressed by the digital shaft position signal. Multiplying D/A converters realize Eqs. (6.41) and (6.42) to produce the analog direct

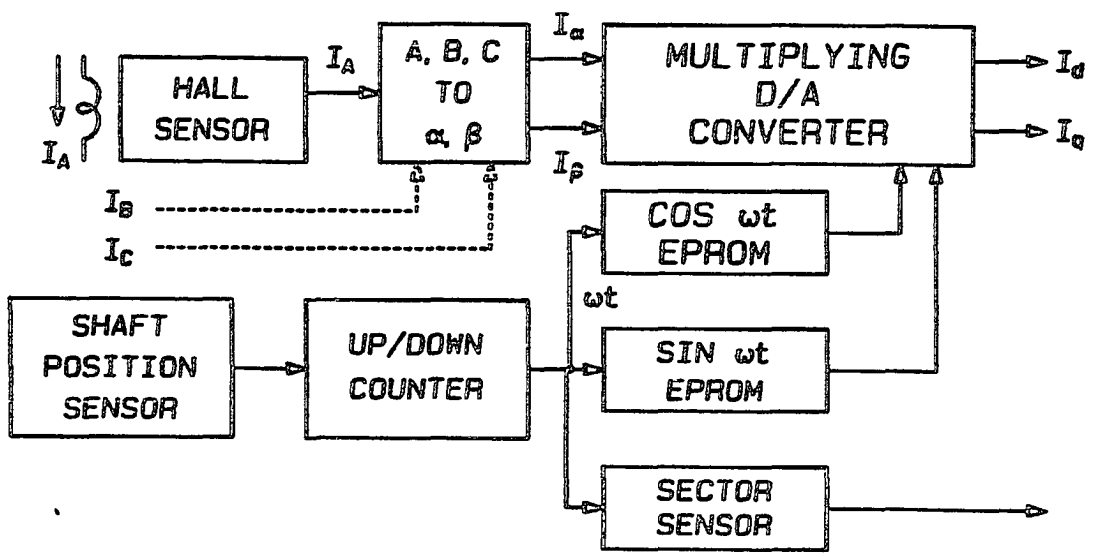

Fig. 6.17 Hardware for computing the direct axis and the quadrature axis currents I_d and I_q.

and quadrature axes current signals.

Figure 6.18 shows the block diagram of the current-fed BLDC motor. The two comparators sense the polarity of the error in the direct axis current I_d and the quadrature axis current I_q. The sector sensor is realized with an Eprom. It senses the 60° wide sector in which the rotor MMF is oriented at any instant. From these inputs the look-up table selects the switch input for the three phase input switches. The content of the look-up table is the same as given in Table 6.2.

Figure 6.19a shows the phase currents I_A and I_B. Figure 6.19b shows the transformed two phase currents I_α and I_β.

Under current control the overall system (I_q vs ω) is a first order system whose time constant is the same as the mechanical time constant (J/B) of the motor. Figure 6.20 shows the step change

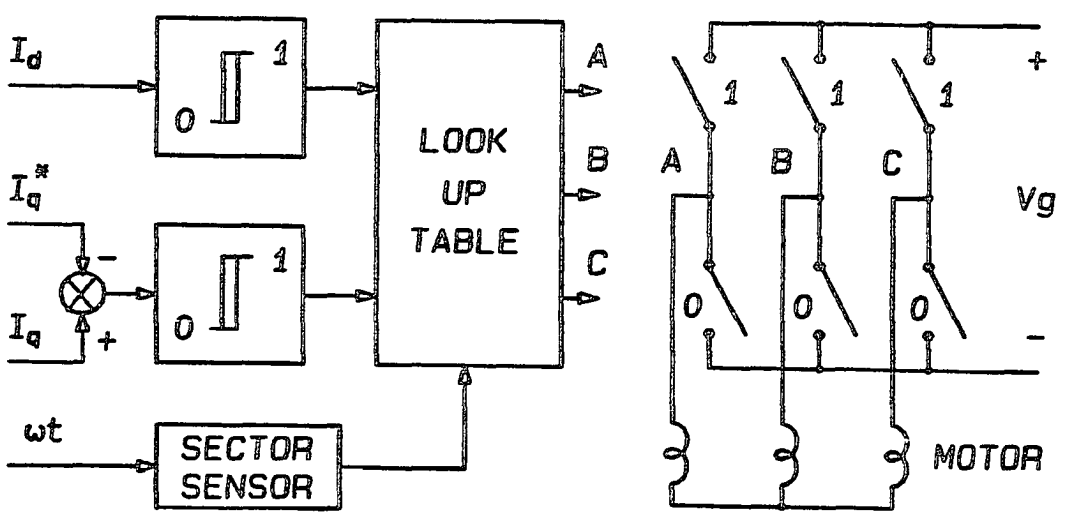

Fig. 6.18 Block diagram of the current-fed BLDC motor drive. The switch inputs u_A,u_B,andu_C are stored in a lookup table as a function of the errors in the direct and quadrature axes currents and the sector of the rotor MMF.

in I_q and the consequent response in speed. This test is useful in determining the motor parameters. The time constant of the speed response gives the mechanical time constant (J/B) of the motor. The slope of the speed response ($d\omega/dt$) as the speed passes through zero speed is a measure of the load inertia ($K_T I_q/J$). With a dynamometer load the torque generated per ampere of I_q (K_T) may be measured. From this test all the mechanical parameters of the motor may be experimentally determined.

Figure 6.21 shows the block diagram of the current fed BLDC motor drive. The quadrature axis current (I_q) and the speed (ω) are both continuous signals. The shaft speed (ω) is related to the quadrature axis current (I_q) by a first order dynamics. Simple linear feedback compensators may be used to design an overall speed controller. In the following section the alternative approach of a

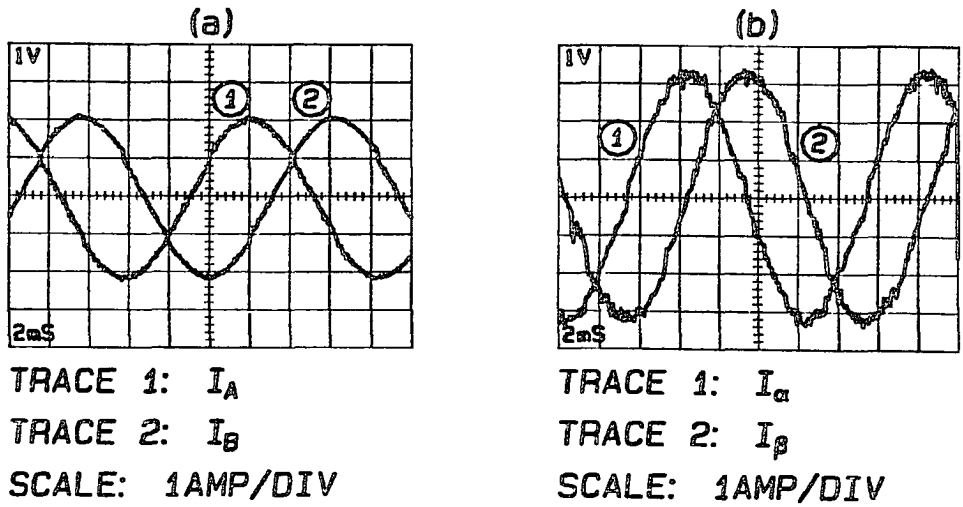

Fig. 6.19 Current waveforms of the current controlled BLDC motor. The physical stator currents I_A,andI_B (a) and the transformed two phase currents I_α and I_β (b).

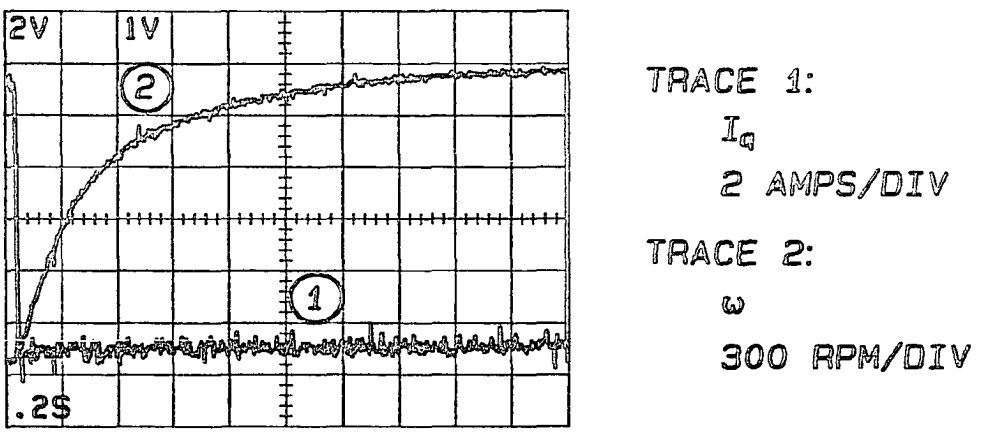

Fig. 6.20 The response in speed of the current fed BLDC motor for step change in the torque producing current I_q. The electrical time constant of the motor being low, the response in current is almost instantaneous. The speed response is exponential with a time constant equal to the mechanical time constant of the drive.

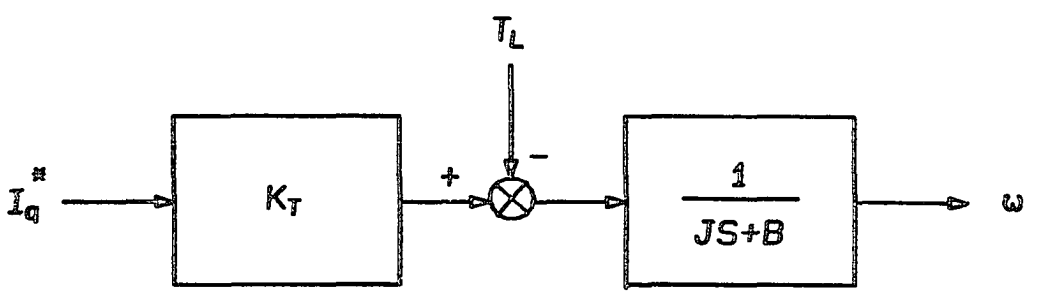

Fig. 6.21 Block diagram model of the current fed BLDC motor drive. The system is linear and first order between I_q^* and ω.

sliding mode speed controller is given.

6.4 Sliding Mode Speed Controller

The BLDC motor drive may be represented by the front end converter and the rotating reference frame equivalent circuit of the motor as shown in Fig. 6.22. The control problem is to select an appropriate control strategy for the switches in the front end converter in order to achieve the dynamic and steady state speed response requirements for the drive. Recalling from the case of DC motor speed control discussed in Section 6.1, the response requirements may be put in the following form.

$$\sigma_q = (\omega - \omega^*) + \tau \frac{d(\omega - \omega^*)}{dt} = 0 \tag{6.49}$$

The extra condition required to be satisfied for orthogonality between stator and rotor MMF's is that

$$\sigma_d = I_d = 0 \tag{6.50}$$

The value of σ_q at any instant (again recalling from Section 6.1) helps decide the need to "accelerate" or "decelerate" the motor. The need for acceleration or deceleration determines the polarity of I_q desired. From Eq. (6.46) it is seen that increasing I_q decelerates the motor and decreasing I_q accelerates the motor. The value of σ_d at any instant determines the corrective action desired in I_d. Given the value of σ_d, σ_q and the sector of the rotor MMF at any instant a look-up table may be constructed to relate these conditions to the desired switch input. Table 6.3 is the look-up table for this purpose. Table 6.3 is identical in its content to Table 6.2 used for current

Sector	$\sigma_d > 0$?	$\sigma_q < \sigma_q^*$?	Switch Inputs		
			A	*B*	*C*
$0° < \omega t < 60°$	0	0	1	1	0
	0	1	1	0	1
	1	0	0	1	0
	1	1	0	0	1
$60° < \omega t < 120°$	0	0	0	1	0
	0	1	1	0	0
	1	0	0	1	1
	1	1	1	0	1
$120° < \omega t < 180°$	0	0	0	1	1
	0	1	1	1	0
	1	0	0	0	1
	1	1	1	0	0
$180° < \omega t < 240°$	0	0	0	0	1
	0	1	0	1	0
	1	0	1	0	1
	1	1	1	1	0
$240° < \omega t < 300°$	0	0	1	0	1
	0	1	0	1	1
	1	0	1	0	0
	1	1	0	1	0
$300° < \omega t < 360°$	0	0	1	0	0
	0	1	0	0	1
	1	0	1	1	0
	1	1	0	1	1

TABLE 6.3 Look-up table relating the input quantities – rotor MMF sector, d axis sliding line ($\sigma_d > 0$?) and the q axis sliding line ($\sigma_q > 0$?) – directly into the necessary control action in terms of the inverter switch positions (A,B,C).

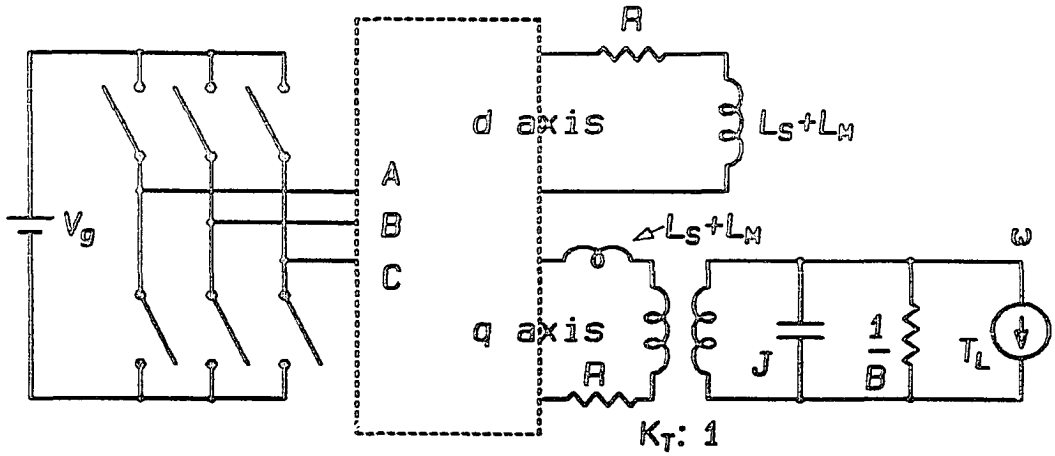

Fig. 6.22 The complete schematic diagram of the BLDC motor drive. The electrical and the electromechanical subsystems of the drive are given in the synchronously rotating (d,q) reference frame.

controlled BLDC motor. The difference is in the q axis control decision. This difference is due to the fact that positive I_q produces negative torque and negative I_q produces positive torque.

6.4.1 Practical Design Considerations

The control strategy indicated above requires the output speed error and its derivative to be measured in order to evaluate σ_q at any instant. In the motor, the speed derivative is not directly accessible for measurement. Therefore the sliding line has to be modified in practice with certain approximations as was done for dc motor drives explained in Section 6.1.

Under the assumption that friction is low and that the load torque is constant or slowly varying, the mechanical system equation given by Eq. (6.26) may be approximated as

$$-K_T\hat{I}_q = J\frac{d\omega}{dt} \tag{6.51}$$

The switching boundary σ_q may be set up in terms of the q axis current error $\hat{I}_q$ and the speed error $(\omega-\omega^*)$.

$$\sigma_q(t) = (\omega-\omega^*)-R_s\hat{I}_q \tag{6.52}$$

R_s is a design parameter and is usually the current measuring resistance. The sliding line equation being a linear differential equation, one may represent the same in frequency domain as well.

$$\sigma_q(s) = (\omega-\omega^*) - R_s\hat{I}_q \tag{6.53}$$

Under sliding mode control, since $\sigma_q^*(s)$ is maintained to be zero, the resultant closed loop transfer function of the system is given by

$$\omega(s) = \frac{\omega^*(s)}{1+s\,JR_s/K_T} \tag{6.54}$$

Notice that unlike real sliding mode control, now the response time is a function of the design parameter R_s as well as the motor parameters J and K_T.

In Eq. (6.53) the sliding line is shown as the weighted sum of the speed error and the current error $\hat{I}_q$. To measure current error $\hat{I}_q$, the steady state value I_q^* will have to be subtracted out from the current I_q. The simplest way to realize this function is by means of a high-pass filter. Further, speed measurement from tachogenerators also require filtering due to the commutation noise in the

tachogenerator output. Therefore in practice, the sliding line is set up incorporating suitable prefilters. Equation (6.55) gives the practical sliding line in the frequency domain.

$$\sigma^*(s) = g\frac{1+\omega_2/s}{1+\omega_1/s}\omega - g\frac{\omega_1/s}{1+\omega_1/s}\omega^* - \frac{1}{1+\omega_1/s}I_q(s) = 0 \qquad (6.55)$$

The current measurement circuit has an inverted pole. Speed signals are also measured with the same inverted pole. In order not to loose the steady state speed information inverted zeroes also have been added to the speed measurement. Equation (6.55) may be put in the following form for convenience.

$$\sigma^*(s) = g_1\frac{1+\tau_2 s}{1+\tau_1 s}\omega - g_1\frac{1}{1+\tau_1 s}\omega^* - \frac{\tau_1 s}{1+\tau_1 s}I_q(s) = 0 \qquad (6.56)$$

Under sliding mode control $\sigma^*(s)$ is maintained to be zero, leading to the following closed loop response.

$$\omega(s) = \frac{\omega^*(s)}{1+s/Q\omega_0+s^2/\omega_0^2} \qquad (6.57)$$

$$\omega_0^2 = K_T g_1/J\tau_1$$
$$Q = 1/\omega_0\tau_2$$

The response as seen by Eq. (6.57) is a second order response, and provides the design criterion. τ_1 is the current filtering time constant and is chosen higher than the electrical time constant of the motor. The speed gain g_1 is selected to obtain the desired response time. The inverted zero frequency $(1/\tau_2)$ of speed measurement is chosen to obtain the desired damping.

Equation (6.57) may be modified as follows to obtain certain practical advantages.

$$g_1\frac{1+\tau_2 s}{1+\tau_1 s}\omega - g_1\frac{1}{1+\tau_1 s}\omega^* + \frac{1}{1+\tau_1 s}I_q(s) = I_q(s) \tag{6.58}$$

In the case of current controlled drive, the response in the current is almost instantaneous due to the fact that the electrical time constant of the motor is quite low. And since we have chosen the various filter time constants higher than the electrical time constant of the motor, the term $I_q(s)$ on the RHS of Eq. (6.58) may be replaced by $I_q^*(s)$ giving rise to the following equation.

$$-g_1\frac{1}{1+\tau_1 s}\omega^* + g_1\frac{1+\tau_2 s}{1+\tau_1 s}\omega + \frac{1}{1+\tau_1 s}I_q(s) = I_q^*(s) \tag{6.59}$$

Equation (6.59) is in such a form as to be added on conveniently to a current controlled BLDC motor. Another added advantage is that overcurrent protection can be simply added by incorporating limits on this current reference signal.

The practical implementation of the speed controller is shown in Fig. 6.23. The two comparators sense the polarity of the error σ_d and σ_q respectively. The switch inputs for the three phase switches are obtained from the look-up table. The contents of the look-up table are given in Table 6.3.

Figures 6.24 and 6.25 show the response in speed error and I_q for step speed reversal for two different compensator designs.

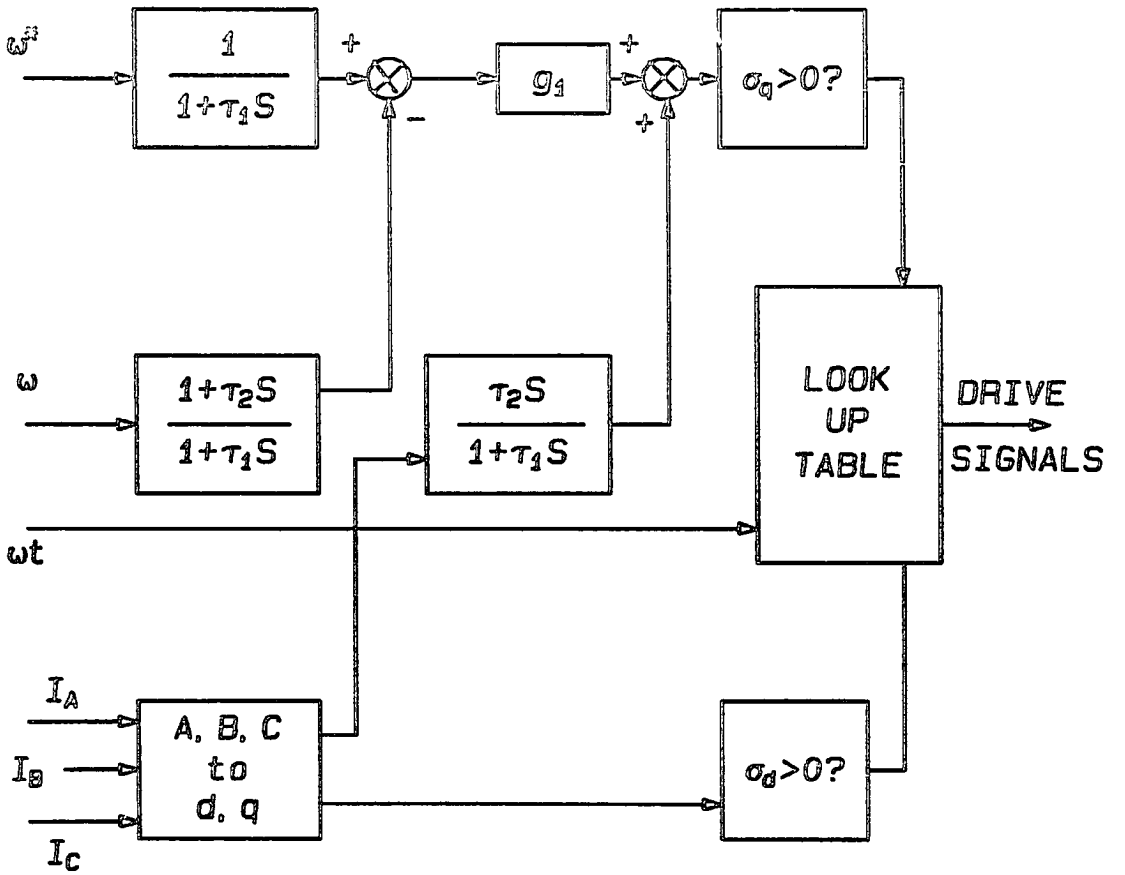

Fig. 6.23 The sliding mode speed controller. Unlike the real sliding mode control using the speed error and its derivative as the feedback variables, the modified sliding mode controller uses the speed error and the q axis current as the feedback variables. Appropriate prefilters have been added to facilitate measurement. The state of the system (σ_d and σ_q) at any instant and the sector in which the rotor MMF lies at any instant are used to look up into a table to decide the necessary control action.

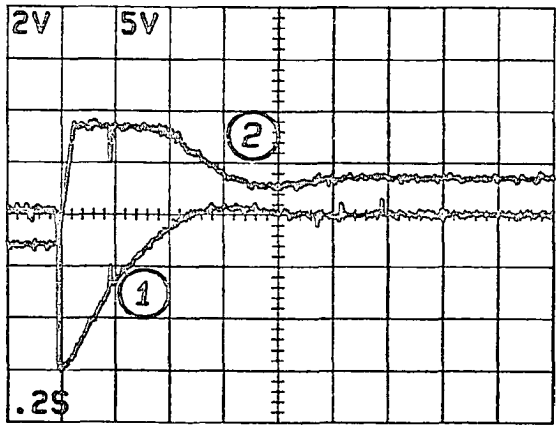

TRACE 1:
SPEED ERROR
600 RPM/DIV

TRACE 2:
CURRENT I_q
5 AMPS/DIV

SLIDING LINE:
SECOND ORDER
ω_0=10.8 rad/sec
Q = 1.2

Fig. 6.24 The response to step speed reversal command of a BLDC motor drive with sliding mode controller. The control design in this case is an underdamped second order response.

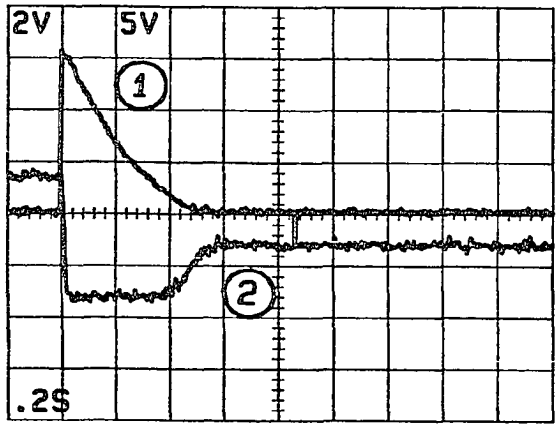

TRACE 1:
SPEED ERROR
600 RPM/DIV

TRACE 2:
CURRENT I_q
5 AMPS/DIV

SLIDING LINE:
SECOND ORDER
ω_0=20.6 rad/sec
Q = 0.61

Fig. 6.25 The response to step speed reversal command of a BLDC motor drive with sliding mode controller. The control design in this case is an overdamped second order response.

6.5 SOME MORE PRACTICAL ASPECTS

From performance point of view the BLDC motor is seen to equal the dc motor drive. The electronic hardware is more complex because reconstruction of the rotating reference frame currents I_d and I_q calls for position sensor of good resolution, multipliers, etc. With digital memory chips and D/A converters, the multipliers can be realized inexpensively. The position sensor is still one of the high cost components of the system.

In this section some simplifications in the hardware for certain applications are outlined. Possible solution to overcome the disadvantages incurred due to the above simplifications is identified in the design of the motor.

From Section 6.3, we may write the relationship between the $d-q$ axes currents and the phase currents as below.

$$\begin{bmatrix} I_d \\ I_q \end{bmatrix} = \begin{bmatrix} -\cos \omega t & \sin \omega t \\ -\sin \omega t & -\cos \omega t \end{bmatrix} \begin{bmatrix} -\sqrt{3}/2 & \sqrt{3}/2 & 0 \\ -1/2 & -1/2 & 1 \end{bmatrix} \begin{bmatrix} I_A \\ I_B \\ I_B \end{bmatrix} \tag{6.60}$$

When we desire sinusoidal currents in the windings, the above transformations have to be realized with good accuracy of the trigonometric terms involved in Eq. (6.60). Granting that non-sinusoidal phase currents are tolerable, the trigonometric terms in the above transformations may be replaced by the average values of their end values in each of the 60° wide sectors of the rotor MMF position. For example, considering the $0° < \omega t < 60°$ sector, the end values of the currents I_d and I_q are given by the following equations.

$$\begin{bmatrix} I_d \\ I_q \end{bmatrix}_{\omega t=0^\circ} = \begin{bmatrix} -1 & 0 \\ 0 & -1 \end{bmatrix} \begin{bmatrix} -\sqrt{3}/2 & \sqrt{3}/2 & 0 \\ -1/2 & -1/2 & 1 \end{bmatrix} \begin{bmatrix} I_A \\ I_B \\ I_B \end{bmatrix} \tag{6.61}$$

$$\begin{bmatrix} I_d \\ I_q \end{bmatrix}_{\omega t=60^\circ} = \begin{bmatrix} -1/2 & -\sqrt{3}/2 \\ \sqrt{3}/2 & -1/2 \end{bmatrix} \begin{bmatrix} -\sqrt{3}/2 & \sqrt{3}/2 & 0 \\ -1/2 & -1/2 & 1 \end{bmatrix} \begin{bmatrix} I_A \\ I_B \\ I_B \end{bmatrix} \tag{6.62}$$

Taking the average of Eqs. (6.61) and (6.62) we may write for the sector $0^\circ < \omega t < 60^\circ$

$$\begin{bmatrix} I_d \\ I_q \end{bmatrix}_{0^\circ<\omega t<60^\circ} = \begin{bmatrix} \frac{3\sqrt{3}}{4} I_A \\ \frac{3}{4}(I_B - I_C) \end{bmatrix} \tag{6.63}$$

Further simplification is possible since under sliding control I_d is zero. Then it follows that

$$\begin{bmatrix} I_d \\ I_q \end{bmatrix}_{0^\circ<\omega t<60^\circ} = \begin{bmatrix} \frac{3\sqrt{3}}{4} I_A \\ \frac{3}{2} I_B \end{bmatrix} \tag{6.64}$$

Using the above idea we may piece together the currents I_d and I_q from the appropriate phase currents in each of the sectors. The piece-wise relationship between the currents I_d and I_q and the phase currents is given in Table 6.4.

Figure 6.26 shows the block diagram of the hardware needed to compute I_d and I_q approximately according to Table 6.4. Comparing with Fig. 6.22, we see that reconstructing the currents I_d and I_q using Table 6.4 requires only a sector sensor (much less expensive than a high resolution position sensor) and analog

Sector	I_d	I_q
$0° < \omega t < 60°$	$\frac{+3\sqrt{3}}{4} I_A$	$\frac{3}{2} I_B$
$60° < \omega t < 120°$	$\frac{-3\sqrt{3}}{4} I_C$	$\frac{3}{2} I_B$
$120° < \omega t < 180°$	$\frac{+3\sqrt{3}}{4} I_B$	$\frac{3}{2} I_C$
$180° < \omega t < 240°$	$\frac{-3\sqrt{3}}{4} I_A$	$\frac{3}{2} I_C$
$240° < \omega t < 300°$	$\frac{+3\sqrt{3}}{4} I_C$	$\frac{3}{2} I_A$
$300° < \omega t < 360°$	$\frac{-3\sqrt{3}}{4} I_B$	$\frac{3}{2} I_A$

TABLE 6.4 Appoximate relationship between the d,q axes currents and the three phase motor currents. From this relationship I_d and I_q may be appoximately pieced together from the phase currents with the use of only sector sensors and analog switches instead of position sensors and multipliers.

switches instead of multipliers. Considerable simplification is possible by following the above method of generating I_d and I_q. For good many applications the difference in performance because of the above changes is imperceptible. Figure 6.27a shows the phase currents under such a control. Figure 6.27b shows the currents I_α and I_β; Figure 6.28 gives the response in speed error and I_q for step reversal in speed command under such a control.

It may be seen that the phase current waveforms are quasi-square wave. As a result the generated torque will be pulsating causing difficulties at very low speeds. This problem exists only if the motor has a sinusoidal distribution of flux. However if the motor can be built with trapezoidal distribution of flux the low speed

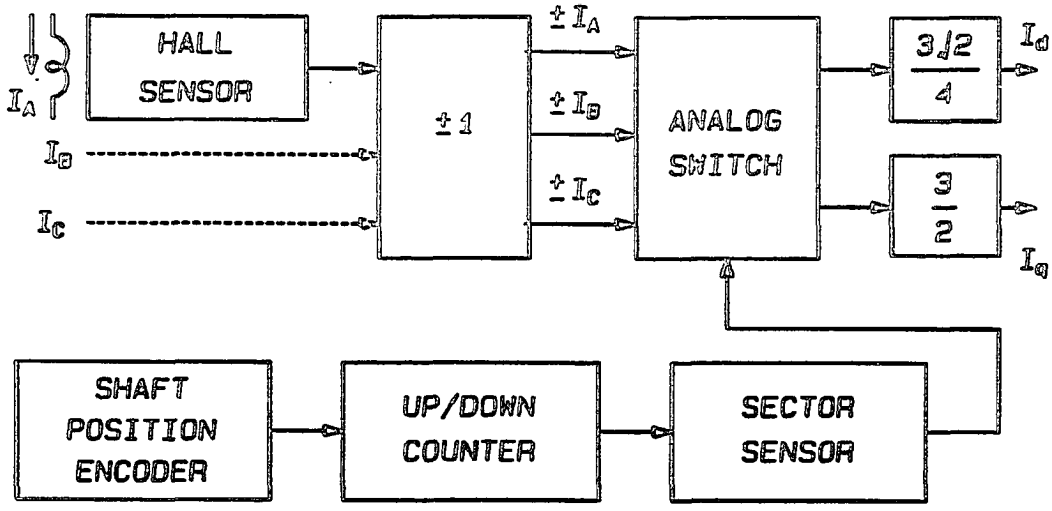

Fig. 6.26 Hardware for the approximate computation of the direct and quadrature axes currents according to Table 6.4.

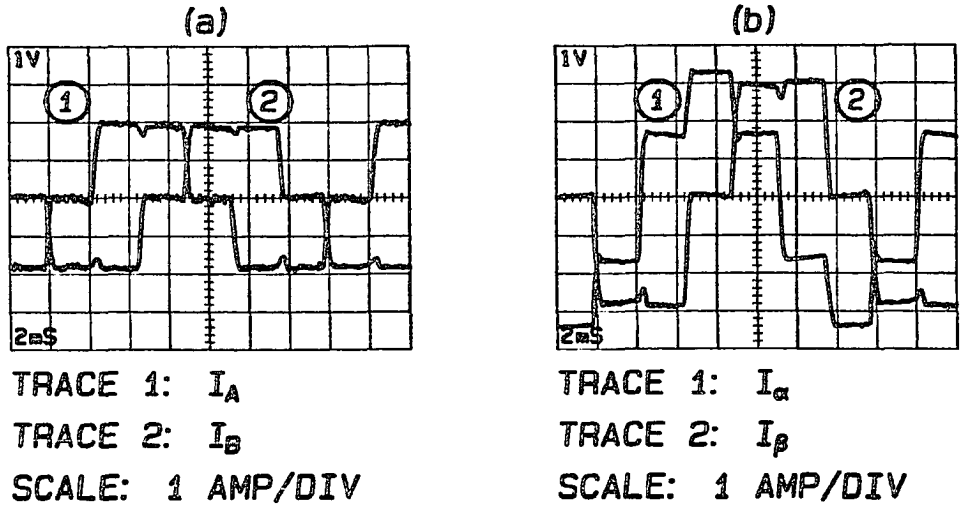

Fig. 6.27 Three phase current waveforms (a) and the equivalent two phase current waveforms (b) when the approximation given in Table 6.4 is used to measure I_d and I_q. This approximation leads to the well known quasi-square wave control of the motor.

performance can be considerably improved.

In this Chapter the application of sliding mode control for the speed regulation of dc motor and BLDC motor were explained. Linear control theory and sliding mode control were combined to obtain suitable design criteria for speed regulators. Experimental results were presented to verify the design procedure.

The BLDC motor drive performance equals the dc motor drive. In view of the robustness of the motor the BLDC motor provides an attractive option for variable speed applications. With high speed switches the motor may be designed with higher number

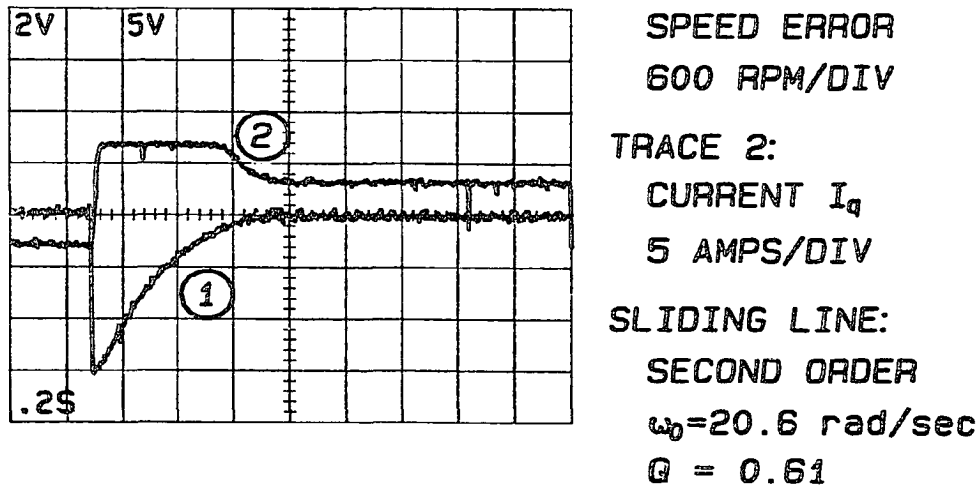

Fig. 6.28 The response to step speed reversal command when piece-wise approximation is used to evaluate the I_d and I_q. The response is practically indistinguishable from the one given in Fig. 6.25 where the more accurate trigonometric transformations are used to evaluate I_d and I_q.

of poles for operation at higher synchronous frequency resulting in higher power density for the motor. With trapezoidal flux distribution further simplification in the electronic hardware is possible.

CHAPTER 7

EXTENSION TO SYNCHRONOUS MOTOR DRIVE

In Chapter 5, it was indicated that the various machines lead qualitatively to identical description. Such a description, when expressed in an appropriate reference frame, also turns out to be time invariant thus simplifying the analysis. In Chapter 6, the concept of sliding mode control was applied to the dc motor drive and the BLDC motor drive. The design criteria were also found to be identical in both cases. The same method of control is applicable to synchronous motor drives as well. The field oriented control of induction motors following the principles of sliding mode control is similar, but not in the scope of this thesis.

In this chapter, we set forth a discussion on the sliding mode speed control of synchronous motor drives and the scope of steady state efficiency optimization applied to synchronous motor drives.

7.1 Synchronous Motor Drives

From Chapter 5, we have the defining equations of the synchronous

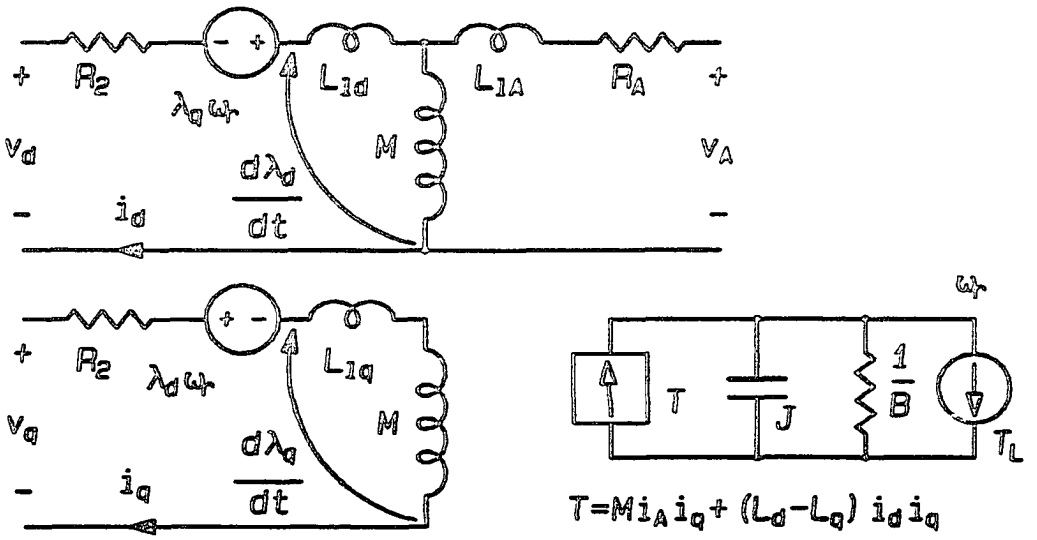

Fig. 7.1 The electrical equivalent circuit of the synchronous motor.

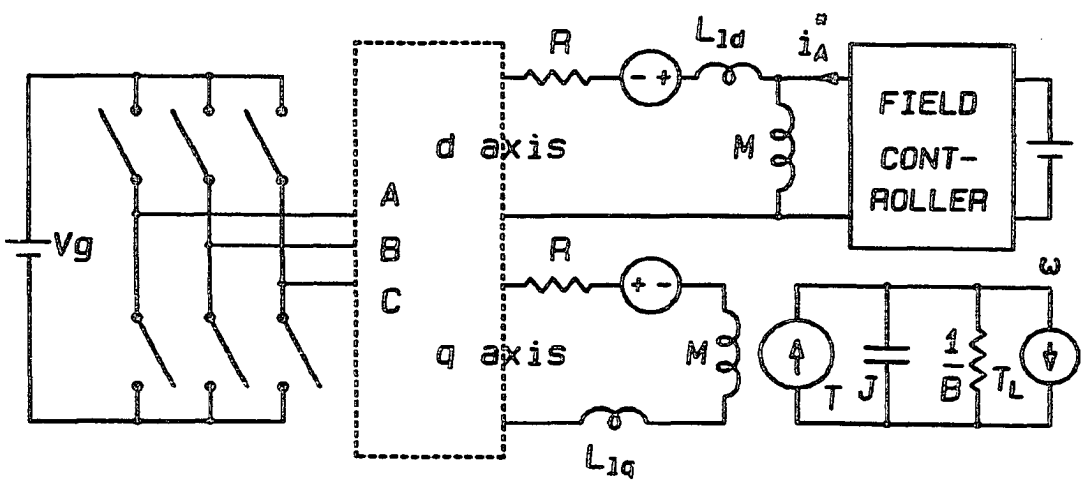

Fig. 7.2 The complete control and power circuit schematic of a synchronous motor drive.

motor.

$$\begin{bmatrix} v_A \\ v_d \\ v_q \end{bmatrix} = \begin{bmatrix} R_A + (M + L_{lA})p & Mp & 0 \\ Mp & R_d + (M + L_{ld})p & -(M + L_{lq})\omega \\ M\omega & (M + L_{ld})\omega & R_q + (M + L_{lq})p \end{bmatrix} \begin{bmatrix} i_A \\ i_d \\ i_q \end{bmatrix} \tag{7.1}$$

$$T = Mi_A i_q + (L_d - L_q) i_d i_q \tag{7.2}$$

The equivalent circuit of the synchronous motor follows readily from Eqs (7.1) and (7.2) and is shown in Fig. 7.1. The q axis equivalent circuit is identical to that of the BLDC motor. The d axis circuit involves the excitation circuit as well as the armature circuit. When we apply the sliding control principles of speed control of synchronous motors, the armature control circuit is identical to the control circuit of the BLDC motor. The extra control circuit required is the excitation controller. This can be very conveniently realized as a constant current controller. The overall control scheme is shown in Fig. 7.2. The armature controller is identical to the controller described in Chapter 6, for the BLDC motor. The field controller is a constant current controller whose purpose is to maintain the excitation in the machine constant corresponding to I^*_A. The machine excitation may be set to a fixed nominal value. Then the performance of the overall drive will be identical to that obtained for the BLDC motor. In the follwing section we see how the excitation may be independently controlled to achieve optimum efficiency under different operating loads.

7.2 Losses in the Motor

For the synchronous motor, under steady state operation, with reference to Fig. 7.2, we may identify the losses in the motor. Under steady state operation, $i_d = 0$, $i_q = I_q^\circ$, and $i_A = I_A^\circ$. The following are then the steady state losses.

i) There are no iron or copper losses in the d axis armature circuit. This is because the d axis current and consequently the d axis armature MMF are zero.

ii) There is a component of copper loss in the d axis excitation circuit equal to $I^*_A{}^2 R_A$. There are no hysterisis or eddy current losses in the excitation circuit, since the excitation MMF is dc.

iii) The q axis armature circuit experiences both copper losses and iron losses. The q axis armature copper losses are $I^*_q{}^2 R_q$, and the q axis iron losses are proportional to the q axis MMF.

Under steady state then the losses are

$$LOSSES = I^*_q{}^2 R_q + I^*_A{}^2 R_A + f(I^*_q) \tag{7.3}$$

where $f(I^*_q)$ is the iron losses and is a nonlineaar monotonic function of I^*_q. Further under steady state, the load torque is constant and hence $I^*_q = T^*/MI^*_q$. Therefore the losses may be written as

$$LOSSES = K_1/I^*_A{}^2 + K_2 I^*_A{}^2 + f_1(I^*_A) \tag{7.4}$$

K_1 and K_2 are suitable constants. From Eq. (7.4), we see that the losses are high at either end of excitation conditions. A minimum value of losses exist for a specific value of I^*_A for any specific steady state operating condition.

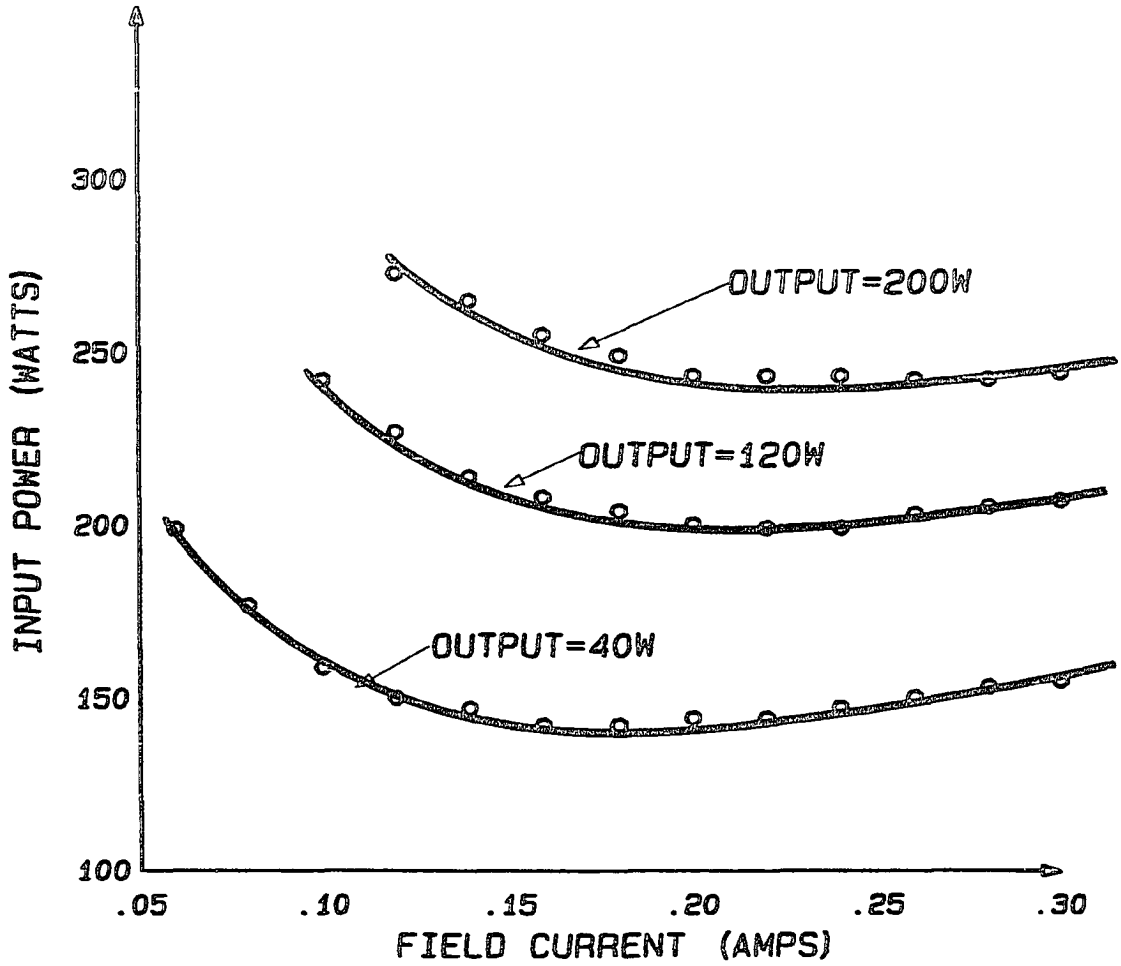

Fig. 7.3 The Input power vs excitation curves for a dc motor under different output load conditions. For every load condition, there is a certain excitation level which results in minimum input power and maximum overall efficiency. From the argument given in the text, the losses or a synchronous motor are also similar.

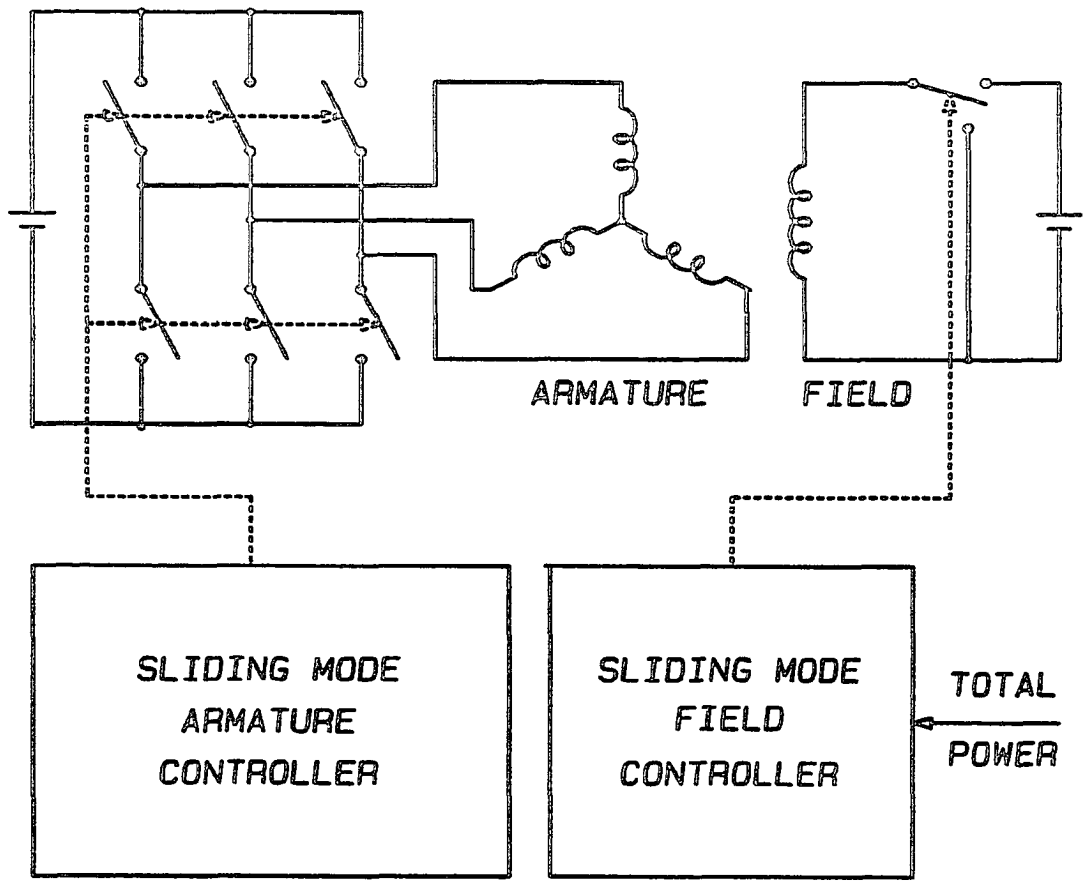

Fig. 7.4 The synchronous motor drive under sliding mode control. The armature control is identical to the control of BLDC motor. In a synchronous motor, since the excitation is also controllable, a sliding mode field controller may be added as shown in order to select the excitation level to obtain maximum operating efficiency.

The loss breakup given by Eq. (7.4) for the synchronous motor holds good equally well for a separately excited dc motor as well. It is more convenient to verify this on a dc motor. A test was performed on a dc motor to evaluate the input power for constant output power under different conditions of excitation. Figure 7.3 shows the result of this test, on a 1/3 hp motor for loads of 40W, 120W, and 200W for different excitation, plotted. It is seen that the minimum loss condition is obtained under different excitation conditions for different loads. This criterion may be therefore used to select the excitation level I^*_A of the drive. The selection of the proper I^*_A for any operating condition is a single input scalar optimization problem and had been described in Chapter 3, Section 3.9. Figure 7.4 shows the schematic diagram of a complete controller for a synchronous motor drive. The speed controller is a sliding mode field oriented controller and is identical to the one explained in Chapter 6. The field controller is a current controller and incorporates loss optimization as explained in Section 3.9.

CHAPTER 8

CONCLUSION

The theory of variable structure systems and its counterpart of sliding mode control have been applied to the analysis and design problems of switched mode power converters. The result is an elegant analysis method and an integrated design approach to the control of switched mode power converters. In contrast to the conventional, small signal, frequency domain approach, the sliding mode control is a time domain method and results in stable control for both small and large signals. The control is less sensitive to system parameters compared to conventional frequency domain design techniques such as loop shaping. The phase plane description turns out to be a powerful graphical aid to the design process in the case of second order systems.

In the case of motor drives, sliding mode control integrates the design objectives of the drive to the control strategy of the power converter, with resultant simplicity of controller hardware. The method of sliding mode control is also shown to be applicable to state estimation problems.

Sliding mode control is a time domain design method and results in a globally stable system under all operating conditions. Conventional wisdom of phase margin and gain margin are therefore

not applicable to such systems. The concept of loop gain would still be applicable. An area that requires to be addressed in future would be to relate the sliding surface to the loop gain of the classical control.

The advantage of reduced sensitivity to system parameters and external excitation in sliding mode control is derived from the fact that the system operates free running. The switching frequency is therefore not constant. This is an area that requires to be addressed in order to increase the acceptability of sliding mode control.

REFERENCES

[1] R. D. Middlebrook, and Slobodan Ćuk, *Advances in Switched Mode Power Conversion*, Vol I,II, and III., TESLAco, Pasadena, Second Edition, 1983.

[2] Utkin.V.I., *Sliding Modes and their Application in Variable Structure Systems*, MIR, Moscow; (English Translation,1978).

[3] R. D. Middlebrook, and Slobodan Ćuk, "A General Unified Approach to Modelling Switched Converter Power Stages," IEEE Power Electronics Specialists Conference, 1976 Record, pp 18-34, (IEEE Publication 76 CH 1084-3 AES).

[4] Khai D. Ngo, "Topology and Analysis in PWM Inversion, Rectification, and Cycloconversion," Ph.D. Thesis, California Institute of Technology, Department of Electrical Engineering, Pasadena, California, May 1984.

[5] U. Itkis, *Control Systems of Variable Structure Systems*, John Wiley, Newyork, 1976.

[6] A. Netushil, ed., *Theory of Automatic Control*, Mir, Moscow, (English Translation, 1978).

[7] D. G. Luenberger, "Observing the State of a Linear System," IEEE Transactions on Military Electronics, Vol MIL-8, No. 2, pp 74-80, April 1964.

[8] R. D. Middlebrook, and Slobodan Ćuk, "A General Unified Approach to Modelling Dc-to-Dc Converters in Discontinuous Conduction Mode," IEEE Power Electronics Specialists Conference, 1977 Record, pp 36-57, (IEEE Publication 77 CH 1213-8 AES).

[9] Abraham Dauhajre, and R. D. Middlebrook, "Simple PWM-FM Control for an Independently Regulated Dual Output Converter," Proceedings of Powercon 10, Tenth International Solidstate Power Electronics Conference, pp D3-1 to D3-8, March 1983.

[10] Shi-Ping Hsu, Art Brown, Loman Rensink, and R. D. Middlebrook, "Modelling and Analysis of Switching Dc-to-Dc converters in Constant Frequency Current Programmed Mode," IEEE Power Electronics Specialists Conference, 1979 Record, pp 284-301, (IEEE Publication 79 CH 1461-3 AES).

[11] C. V. Jones, *The Unified Theory of Electrical Machines*, Plenum Press, Newyork, 1967.

[12] B. K. Bose, ed., *Adjustable Speed Ac Drive Systems*, IEEE Press, 1981.

[13] F. Blaschke, "The Principle of Field Orientation as Applied to the New Transvektor Closedloop Control System for Rotating Field Machines," Siemens Review, Vol 34, pp 217-220, May 1972.

[14] Faruk Bilalović, Osman Music´ and Asif Sabanović, "Buck Converter Regulator Operating in the Sliding Mode," Proc. Seventh International PCI'83 Conference, pp. 331-340.

[15] Okyak Kanak.M, Fumio Harashima and Seiji Kondo, "Microprocessor Controlled Position Control System with a Sliding Mode," ETG Conf. Microelectronics in Power electronics and Electrical drives, 1982, pp. 273-279.

[16] Fumio Harashima, Hideki Hoshomoto and Seiji Kondo, "Mosfet Converter Fed Position Servo System with Sliding Mode Control," IEEE Power Electronics Specialists Conference, 1983 record, pp. 73-79 (IEEE Publication 83CH-1877-0).

APPENDIX 1

TRANSFORMATIONS USED IN GENERAL MACHINE THEORY

In this section, the performance equations of practical electrical machines are derived from first principles using the transformations outlined in Section 5.4. At first a general salient pole machine is considered. This will lead to the performance equations of the synchronous machine and the dc machine at appropriate stages. The three phase induction machine, which is a uniform airgap machine, is considered later.

A1.1 Salient Pole Machine

The general salient pole machine shown in Fig. A.1 consists of a salient pole stator carrying orhogonal windings A and B. The round rotor without saliency carries the three phase balanced windings r,y and b. The system of equations for this general machine is derived first. Appropriate equations are picked up from here in Chapter 6 to arrive at the electrical equivalent circuits of particular types of machines.

The voltage equations for the windings in Fig. A.1 are

$$V = ZI = \begin{bmatrix} V_1 \\ V_2 \end{bmatrix} = \begin{bmatrix} Z_{11} & Z_{12} \\ Z_{21} & Z_{22} \end{bmatrix} \begin{bmatrix} I_1 \\ I_2 \end{bmatrix} \tag{A.1}$$

The equations are put into compound matrix form for convenience. The subscripts 1 and 2 refer to the stator and the rotor respectively.

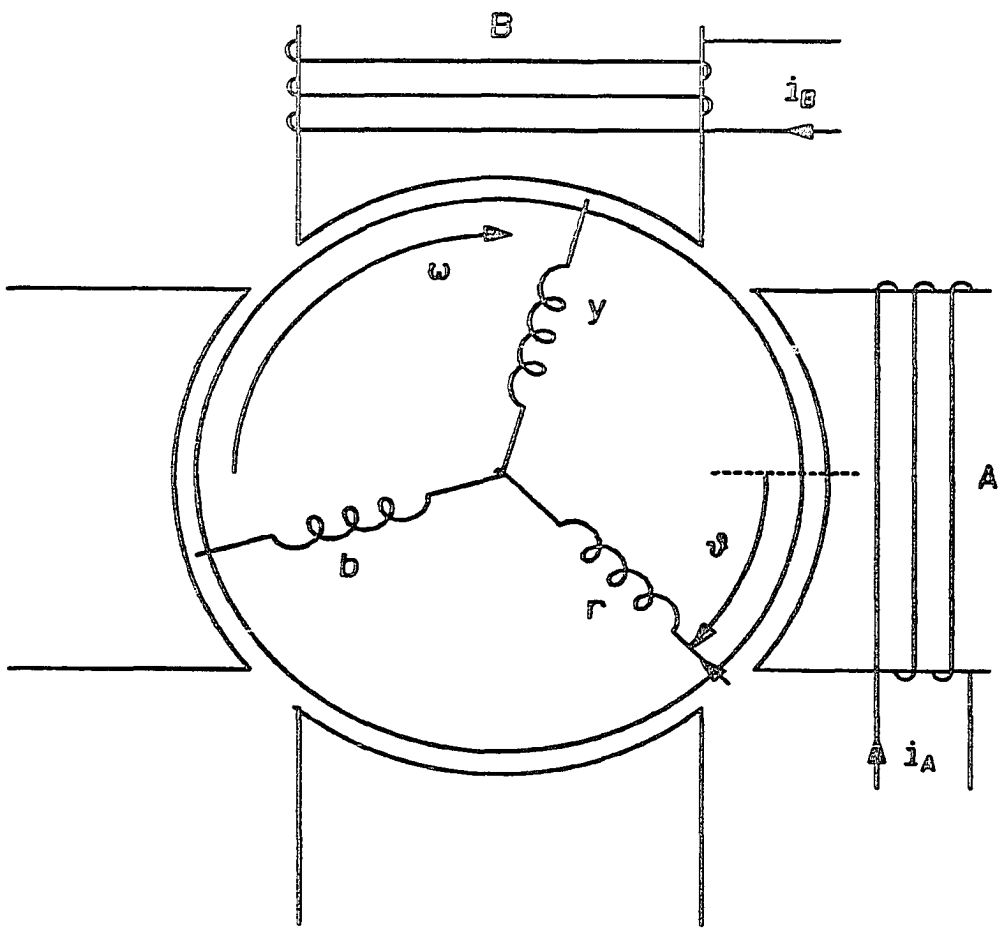

Fig. A.1 A general salient pole machine with a three phase rotor.

$$V_1 = \begin{bmatrix} v_A \\ v_B \end{bmatrix} ; \quad I_1 = \begin{bmatrix} i_A \\ i_B \end{bmatrix} ; \quad Z_{11} = \begin{bmatrix} R_A + pL_A & 0 \\ 0 & R_B + pL_B \end{bmatrix}$$

$$V_2 = [\ v_r \quad v_y \quad v_b\ ]^T ; \quad I_2 = [\ i_r \quad i_y \quad i_b\ ]^T ;$$

$$Z_{12} = [Z_{21}]^T = \begin{bmatrix} pM_{Ar} & pM_{Ay} & pM_{Ab} \\ pM_{Br} & pM_{By} & pM_{Bb} \end{bmatrix}$$

$$Z_{22} = \begin{bmatrix} R_r + pL_r & pM_{ry} & pM_{rb} \\ pM_{yr} & R_y + pL_y & pM_{yb} \\ pM_{br} & pM_{by} & R_b + pL_b \end{bmatrix}$$

The machine being salient pole, all the inductances except L_A and L_B are functions of the rotor angle ϑ.

$$M_{Ar} = \bar{M}_A \cos \vartheta \qquad M_{Br} = -\bar{M}_B \sin \vartheta$$
$$M_{Ay} = \bar{M}_A \cos \vartheta_2 \qquad M_{By} = -\bar{M}_B \sin \vartheta_2$$
$$M_{Ab} = \bar{M}_A \cos \vartheta_1 \qquad M_{Bb} = -\bar{M}_B \sin \vartheta_1$$

$$\vartheta_1 = \vartheta + 120°$$
$$\vartheta_2 = \vartheta + 240°$$

Rotor self inductance is maximum when $\vartheta = 0$, and minimum when $\vartheta = 90°$. Using the truncated Fourier series to approximate the self and mutual inductances, we get

$$L_r = \bar{L}_a + \bar{L}_b \cos 2\vartheta \qquad M_{yb} = M_{by} = \bar{M}_a + \bar{M}_b \cos 2\vartheta$$
$$L_y = \bar{L}_a + \bar{L}_b \cos 2\vartheta_2 \qquad M_{br} = M_{rb} = \bar{M}_a + \bar{M}_b \cos 2\vartheta_2$$
$$L_b = \bar{L}_a + \bar{L}_b \cos 2\vartheta_1 \qquad M_{ry} = M_{yr} = \bar{M}_a + \bar{M}_b \cos 2\vartheta_1$$

The first step in simplifying the above system is to apply the phase transformation C_p described in Section 5.4 to the rotor part of the system.

$$\begin{bmatrix} V \\ I \end{bmatrix} = C_p \begin{Bmatrix} V' \\ I' \end{Bmatrix} ; \qquad C_p = \begin{bmatrix} I & 0 \\ 0 & C_1 \end{bmatrix}$$

$$C_1 = \sqrt{2/3} \begin{bmatrix} 1/\sqrt{2} & 1 & 0 \\ 1/\sqrt{2} & -1/2 & \sqrt{3}/2 \\ 1/\sqrt{2} & -1/2 & -\sqrt{3}/2 \end{bmatrix}$$

The transformed system is given by

$$V' = Z'I' ; \qquad Z' = C_p{}^T Z C_p \tag{A.2}$$

Knowing the original impedance matrix Z and the transformation C_p, the new impedance matrix Z' is computed.

$$\begin{bmatrix} Z'_{11} & Z'_{12} \\ Z'_{21} & Z'_{22} \end{bmatrix} = \begin{bmatrix} I & 0 \\ 0 & C_1{}^T \end{bmatrix} \begin{bmatrix} Z_{11} & Z_{12} \\ Z_{21} & Z_{22} \end{bmatrix} \begin{bmatrix} I & 0 \\ 0 & C_1 \end{bmatrix}$$

$$\begin{bmatrix} Z'_{11} & Z'_{12} \\ Z'_{21} & Z'_{22} \end{bmatrix} = \begin{bmatrix} Z_{11} & Z_{12}C_1 \\ C_1{}^T Z_{21} & C_1{}^T Z_{22} C_1 \end{bmatrix} \tag{A.3}$$

Expanding the RHS of Eq. A.1.03, we get

$$Z'_{11} = Z_{11} = \begin{bmatrix} R_A + L_A p & 0 \\ 0 & R_B + L_B p \end{bmatrix}$$

$$Z'_{12} = Z_{12}C_1 = \begin{bmatrix} 0 & M_A \cos\vartheta & M_A \sin\vartheta \\ 0 & -M_B \sin\vartheta & M_B \cos\vartheta \end{bmatrix}$$

$$M_A = \sqrt{3/2}\,\bar{M}_A ; \qquad M_B = \sqrt{3/2}\,\bar{M}_B$$

$$Z'_{21} = C_1{}^T Z_{21} = Z'_{12}{}^T$$

$$Z'_{22} = \begin{bmatrix} R_2 + L_0 p & pL_{0b}\cos 2\vartheta & -pL_{0b}\sin 2\vartheta \\ pL_{0b}\cos 2\vartheta & R_2 + p(L_a + L_b \cos 2\vartheta) & pL_b \sin 2\vartheta \\ -pL_{0b}\sin 2\vartheta & pL_b \sin 2\vartheta & R_2 + p(L_a - L_b \cos 2\vartheta) \end{bmatrix}$$

$$R_2 = R_r = R_y = R_b; \quad L_0 = \bar{L}_a + 2\bar{M}_a; \quad L_b = \bar{L}_b/2 + \bar{M}_b;$$

$$L_{0b} = (\bar{L}_b - \bar{M}_b)/\sqrt{2}; \quad L_a = (\bar{L}_a - \bar{M}_a)$$

Some more simplifications on the system order are now possible. With balanced supply and without neutral conductor in the three phase system,

$$v_0 = \frac{1}{\sqrt{2}}(v_r + v_y + v_b) = 0$$

$$i_0 = \frac{1}{\sqrt{2}}(i_r + i_y + i_b) = 0$$

Therefore the rows and columns corresponding to v_0 and i_0 from Eq. (A.2) may be dropped and the transformed system of equations is given by

$$V' = Z'I' \tag{A.4}$$

$$V' = [\, v_A \quad v_B \quad v_\alpha \quad v_\beta \,]^T; \quad I' = [\, i_A \quad i_B \quad i_\alpha \quad i_\beta \,]^T$$

$$Z' = \begin{bmatrix} R_A + L_A p & 0 & M_A \cos\vartheta & M_A \sin\vartheta \\ 0 & R_B + L_B p & -M_B \sin\vartheta & M_B \cos\cos\vartheta \\ M_A \cos\vartheta & -M_B \sin\vartheta & R_2 + p\,(L_a + L_b \cos 2\vartheta) & p L_b \sin 2\vartheta \\ M_A \sin\vartheta & M_B \cos\vartheta & p L_b \sin 2\vartheta & R_2 + p\,(L_a - L_b \cos 2\vartheta) \end{bmatrix}$$

Physically these equations correspond to the two phase equivalent of the original machine shown in Fig. A.2. The Eq. (A.4) differs from the Eq. (5.16) given in Section 5.2 owing to the saliency of the rotor. Equation (A.4) is more general and leads to Eq. (5.16) when there is no saliency ($L_b = 0$) in the machine.

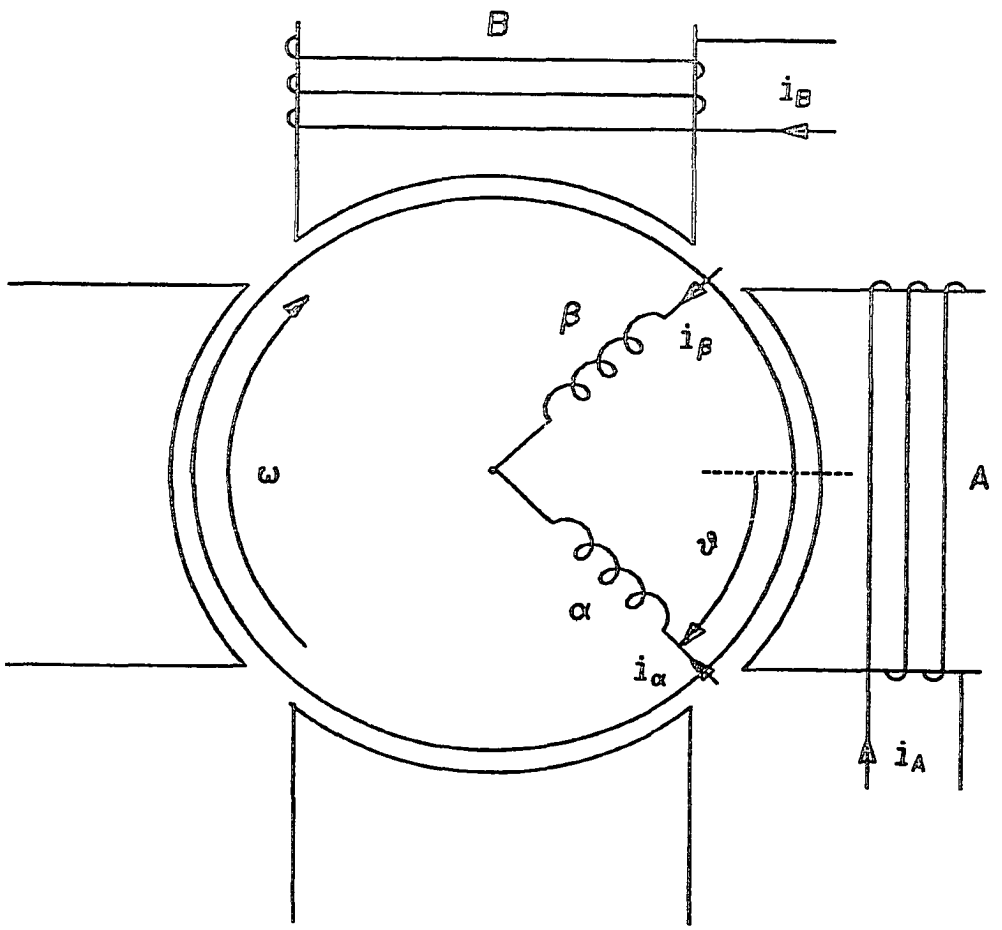

Fig. A.2 A salient pole machine with a two phase rotor. All three phase machines are reducible to this fundamental two phase configuration.

The Eq. (A.4) may be put in the compound matrix form, the suffixes 1 and 2 referring to the stator and rotor respectively.

$$\begin{bmatrix} V_1 \\ V_2 \end{bmatrix} = \begin{bmatrix} Z'_{11} & Z'_{12} \\ Z'_{21} & Z'_{22} \end{bmatrix} \begin{bmatrix} I_1 \\ I_2 \end{bmatrix}$$

The next simplifying step is to apply the commutator transformation C_c described in Section 6.4 to the rotor variables.

$$\begin{bmatrix} V \\ I \end{bmatrix} = C_c \begin{bmatrix} V^\circ \\ I^\circ \end{bmatrix}; \qquad C_c = \begin{bmatrix} I & 0 \\ 0 & C_2 \end{bmatrix}$$

$$C_2 = \begin{bmatrix} \cos\vartheta & -\sin\vartheta \\ \sin\vartheta & \cos\vartheta \end{bmatrix}$$

The transformed system of equations is given by

$$V^\circ = Z^\circ I^\circ ; \qquad Z^\circ = C_c{}^T Z' C_c \tag{A.5}$$

The new impedance matrix Z° is now computed.

$$\begin{bmatrix} Z^\circ_{11} & Z^\circ_{12} \\ Z^\circ_{21} & Z^\circ_{22} \end{bmatrix} = \begin{bmatrix} Z'_{11} & C_2{}^T Z'_{12} \\ Z'_{21} C_2 & C_2{}^T Z'_{22} C_2 \end{bmatrix} \tag{A.6}$$

Expanding the RHS of Eq.A.1.06, we get

$$Z^\circ_{11} = Z'_{11} = \begin{bmatrix} R_A + L_A p & 0 \\ 0 & R_B + L_B p \end{bmatrix}$$

$$Z^\circ_{12} = Z'_{12} C_2 = \begin{bmatrix} M_A p & 0 \\ 0 & M_B p \end{bmatrix}$$

Caution is required in evaluating Z°_{21} and Z°_{22}. The "p" operator occurs as intermediate terms and must be considered along with the following current terms to avoid errors.

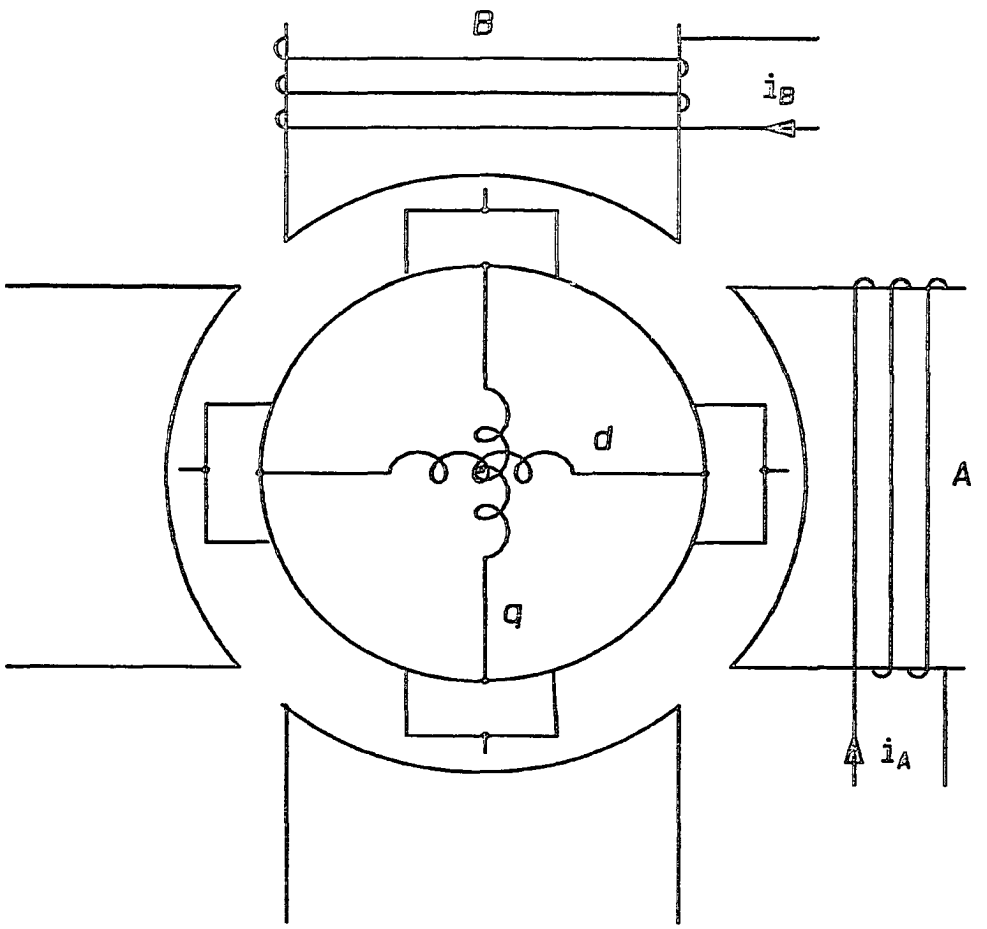

Fig. A.3 A salient pole machine with a two phase commutator fed rotor. All types of electrical machines are derivable from this general configuration.

$$Z^{\circ}_{21}I^{\circ} = C_2^{T}Z'_{21}I' = \begin{bmatrix} \cos\vartheta & \sin\vartheta \\ -\sin\vartheta & \cos\vartheta \end{bmatrix} \begin{bmatrix} M_A p\cos\vartheta & -M_B p\sin\vartheta \\ M_A p\sin\vartheta & M_B p\cos\vartheta \end{bmatrix} \begin{bmatrix} i_A \\ i_B \end{bmatrix}$$

The "p" operator applies to the product of the trigonometric term and the following current term. Expanding and then dropping the post-multiplying current terms, we get

$$Z^{\circ}_{21} = \begin{bmatrix} M_A p & -M_B\omega_r \\ M_A\omega_r & M_B p \end{bmatrix}; \qquad Z^{\circ}_{22} = \begin{bmatrix} R_2 + L_d p & -L_q\omega_r \\ L_d\omega_r & R_2 + L_q p \end{bmatrix}$$

$$L_d = L_a + L_b \; ; \quad L_q = L_a - L_b$$

The complete set of equations is given by

$$\begin{bmatrix} v_A \\ v_B \\ v_d \\ v_q \end{bmatrix} = \begin{bmatrix} R_A + L_A p & 0 & M_A p & 0 \\ 0 & R_B + L_B p & 0 & M_B p \\ M_A p & -M_B\omega_r & R_2 + L_d p & -L_q\omega_r \\ M_A\omega_r & M_B p & L_d\omega_r & R_2 + L_q p \end{bmatrix} \begin{bmatrix} i_A \\ i_B \\ i_d \\ i_q \end{bmatrix} \qquad \text{(A.7)}$$

Equation (A.7) corresponds to the equivalent two phase commutator machine described in Section 5.3 and shown in Fig. A.3. This equation is used in Sections 5.5 and 5.6 to arrive at the equivalent circuits of dc motor and synchronous motor drives. The next machine structure considered here is the uniform airgap, three phase slip-ring machine in order to derive the performance equations of an induction motor.

A1.2 Round Rotor Machine

Figure A.4a shows the round rotor induction motor with three phase windings on the rotor and stator. The voltage equations for the various windings are given in Eq. (A.7). For convenience, they are put in the following compound matrix form, the suffixes 1 and 2 representing the stator and rotor variables respectively.

$$V = ZI = \begin{bmatrix} V_1 \\ V_2 \end{bmatrix} = \begin{bmatrix} Z_{11} & Z_{12} \\ Z_{21} & Z_{22} \end{bmatrix} \begin{bmatrix} I_1 \\ I_2 \end{bmatrix} \tag{A.8}$$

$$V_1 = [\ v_R \quad v_Y \quad v_B\ ]^T \ ; \ I_1 = [\ i_R \quad i_Y \quad i_B]^T$$

$$V_2 = [\ v_r \quad v_y \quad v_b\ ]^T \ ; \ I_2 = [\ i_r \quad i_y \quad i_b]^T$$

$$Z_{11} = \begin{bmatrix} R_1+\bar{L}_1p & -\bar{M}_1p & -\bar{M}_1p \\ -\bar{M}_1p & R_1+\bar{L}_1p & -\bar{M}_1p \\ -\bar{M}_1p & -\bar{M}_1p & R_1+\bar{L}_1p \end{bmatrix}$$

$$Z_{22} = \begin{bmatrix} R_2+\bar{L}_2p & -\bar{M}_2p & -\bar{M}_2p \\ -\bar{M}_2p & R_2+\bar{L}_2p & -\bar{M}_2p \\ -\bar{M}_2p & -\bar{M}_2p & R_2+\bar{L}_2p \end{bmatrix}$$

$$Z_{12} = [Z_{21}]^T = \begin{bmatrix} \bar{M}p\cos\vartheta & \bar{M}p\cos\vartheta_1 & \bar{M}p\cos\vartheta_2 \\ \bar{M}p\cos\vartheta_2 & \bar{M}p\cos\vartheta & \bar{M}p\cos\vartheta_1 \\ \bar{M}p\cos\vartheta_1 & \bar{M}p\cos\vartheta_2 & \bar{M}p\cos\vartheta \end{bmatrix}$$

$$\vartheta_1 = \vartheta + 120^\circ$$
$$\vartheta_2 = \vartheta + 240^\circ$$

The first step in simplification is to apply the phase transformation C_p and convert the above system into its two phase equivalent system.

$$\begin{bmatrix} V \\ I \end{bmatrix} = C_p \begin{bmatrix} V' \\ I' \end{bmatrix} ; \quad C_p = \begin{bmatrix} C_1 & 0 \\ 0 & C_1 \end{bmatrix}$$

$$C_1 = \sqrt{2/3} \begin{bmatrix} 1/\sqrt{2} & 1 & 0 \\ 1/\sqrt{2} & -1/2 & \sqrt{3}/2 \\ 1/\sqrt{2} & -1/2 & -\sqrt{3}/2 \end{bmatrix}$$

The transformed system is given by

$$V' = Z'I' = \begin{bmatrix} V'_1 \\ V'_2 \end{bmatrix} = \begin{bmatrix} Z'_{11} & Z'_{12} \\ Z'_{21} & Z'_{22} \end{bmatrix} \begin{bmatrix} I'_1 \\ I'_2 \end{bmatrix} \tag{A.9}$$

$$V'_1 = [\ v_{01} \quad v_{\alpha 1} \quad v_{\beta 1}\ ]^T \ ; \quad V'_2 = [\ v_{02} \quad v_{\alpha 2} \quad v_{\beta 2}\ ]^T$$

$$I'_1 = [\ i_{01} \quad i_{\alpha 1} \quad i_{\beta 1}\ ]^T \ ; \quad I'_2 = [\ i_{02} \quad i_{\alpha 2} \quad i_{\beta 2}\ ]^T$$

$$Z'_{11} = \begin{bmatrix} R_1 + L_{01}p & 0 & 0 \\ 0 & R_1 + L_1 p & 0 \\ 0 & 0 & R_1 + L_1 p \end{bmatrix}$$

$$Z'_{22} = \begin{bmatrix} R_2 + L_{02}p & 0 & 0 \\ 0 & R_2 + L_2 p & 0 \\ 0 & 0 & R_2 + L_2 p \end{bmatrix}$$

$$Z'_{12} = [Z'_{21}]^T = \begin{bmatrix} 0 & 0 & 0 \\ 0 & Mp\cos\vartheta & -Mp\sin\vartheta \\ 0 & Mp\sin\vartheta & Mp\cos\vartheta \end{bmatrix}$$

$$L_{01} = \bar{L}_1 - 2\bar{M}_1 \ ; \quad M = (3/2)\bar{M} \ ; \quad L_1 = \bar{L}_1 + \bar{M}_1 \ ; \quad L_2 = \bar{L}_2 + \bar{M}_2$$

Under the assumption of balanced three wire supply, the rows and columns corresponding to v_{01}, v_{02}, i_{01}, and i_{02} may be dropped and the

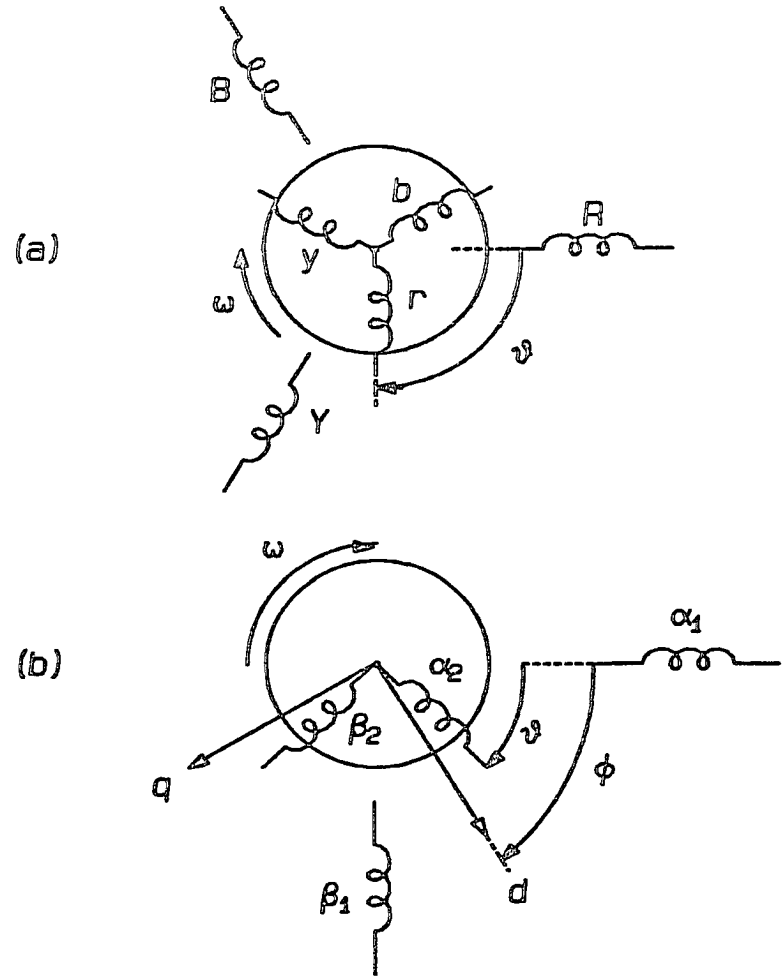

Fig. A.4 Practical nonsalient pole three phase machine (a), and its equivalent two phase configuration. The d and q axes shown in (b) are the rotating reference frame. By suitable choice of the angular velocity of the rotating reference frame, substantial simplification of the mathematical representation of the machine is possible.

system order reduces.

$$\begin{bmatrix} v_{\alpha 1} \\ v_{\beta 1} \\ v_{\alpha 2} \\ v_{\beta 2} \end{bmatrix} = \begin{bmatrix} R_1 + L_1 p & 0 & Mp\cos\vartheta & -Mp\sin\vartheta \\ 0 & R_1 + L_1 p & Mp\sin\vartheta & Mp\cos\vartheta \\ Mp\cos\vartheta & Mp\sin\vartheta & R_2 + L_2 p & 0 \\ -Mp\sin\vartheta & Mp\cos\vartheta & 0 & R_2 + L_2 p \end{bmatrix} \begin{bmatrix} i_{\alpha 1} \\ i_{\beta 1} \\ i_{\alpha 2} \\ i_{\beta 2} \end{bmatrix} \tag{A.10}$$

The next step in the simplification of the system is to choose a reference axis rotating at an arbitrary speed $\omega_e = d\varphi / dt$ indicated by the axes d,q in Fig. A.4b, and transform the two phase voltages and currents to this new reference axes. This is the commutator transformation given by C_c.

$$\begin{bmatrix} V \\ I \end{bmatrix} = C^c \begin{bmatrix} V^c \\ I^c \end{bmatrix} ; \quad C_c = \begin{bmatrix} C_{21} & 0 \\ 0 & C_{22} \end{bmatrix}$$

$$C_{21} = \begin{bmatrix} \cos\varphi & -\sin\varphi \\ \sin\varphi & \cos\varphi \end{bmatrix} ; \quad C_{22} = \begin{bmatrix} \cos(\varphi - \vartheta) & -\sin(\varphi - \vartheta) \\ \sin(\varphi - \vartheta) & \cos(\varphi - \vartheta) \end{bmatrix}$$

After carrying out all the transformations, the new set of voltage equation is given by,

$$\begin{bmatrix} v_{d1} \\ v_{q1} \\ v_{d2} \\ v_{q2} \end{bmatrix} = \begin{bmatrix} R_1 + L_1 p & -L_1\omega_e & Mp & -M\omega_e \\ L_1\omega_e & R_1 + L_1 p & M\omega_e & Mp \\ Mp & -M(\omega_e - \omega_r) & R_2 + L_2 p & -L_2(\omega_e - \omega_r) \\ M(\omega_e - \omega_r) & Mp & L_2(\omega_e - \omega_r) & R_2 + L_2 p \end{bmatrix} \begin{bmatrix} i_{d1} \\ i_{q1} \\ i_{d2} \\ i_{q2} \end{bmatrix} \tag{A.11}$$

In the transformed reference frame the various inductances turn out to be constants. Due to the relative motion between the reference axes and the various windings, rotary voltages now appear on both the rotor and the stator windings. Equation (A.11) is used in

Section 5.7 to arrive at the equivalent circuit of the induction motor.